EXPERIMENTAL INVESTIGATION OF ENHANCED EARTH ELECTRODE SYSTEMS UNDER HIGH FREQUENCY AND TRANSIENT CONDITIONS

SALAH MOUSA

BSc, MSc (Electrical Engineering)

Thesis submitted to Cardiff University in candidature for the degree of PhD

2014

School of Engineering

Cardiff University, Cardiff

ABSTRACT

This thesis is primarily concerned with experimental tests and computer simulations to determine the high frequency and transient performance of earth electrode systems. The work has involved an extensive review of published literature, theoretical and analytical investigations of earth electrode systems.

The experimental investigations on earth electrodes were carried out an outdoor site prior to electrode testing the test site soil resistivity were undertaken. Specifically, the soil resistivity was obtained at the location of the vertical test rod. In order to obtain better understanding of the soil stratification, fourteen profiles of soil resistivity were measured at the field site. From the measurements 2D soil models were constructed to visualise both horizontal and vertical resistivity variation.

High frequency and impulse characteristics of vertical test rods up to 6m length and horizontal electrodes up to 88m buried in a non-uniform soil outdoor test site were tested. DC, AC and impulse test results show that increasing the length of electrode reduces the earthing resistance but not impedance. It was shown that, the earth resistance/impedance is constant over a low frequency range, while higher or lower impedance values are observed in the high-frequency range due to inductive or capacitive effects, depending on the length of earth electrode.

Improved high- frequency and transient response of earth rods was determined experimentally by connecting horizontal electrode enhancements in star or cross formation at the top of vertical rods. Using these additional enhancements, a reduction in both resistance and impedance has been demonstrated.

The addition of horizontal enhancements to the vertical rod can reduce the earth potential rise (EPR) by approximately 70% and 48% for 1.2m and 6m rods respectively.

Voltage and current distributions of earth electrode systems under low/high frequency and impulse conditions, for different lengths of vertical rods with horizontal electrode enhancements and along a horizontal electrode with and without insulated conductor, were investigated experimentally and verified by computer simulation. In the case of the of the rods with an added ‘4-cross’ horizontal conductor enhancement, it was shown that the rods carry the majority of the current at low frequency, but this proportion decreases significantly as frequency increases The field test results show that current distribution in earth conductor systems is significantly different under high-frequency and impulse energisation compared with power frequency conditions. Close agreement was obtained between the measured and computed current and voltage

High voltage tests in the ground around the vertical electrodes were investigated experimentally. It was observed that when a sufficiently high current magnitude is injected through vertical electrodes, a significant reduction in the impulse resistance by increase in current with a sudden fall of voltage is observed which is called soil ionisation. Such phenomenon does not occur when the vertical electrodes with horizontal enhancements is tested, where the current through all earth electrodes is small.

PUBLICATIONS

1. **S. Mousa**, N. Harid, H. Griffiths, and A. Haddad: ‘‘High Frequency Performance of A Vertical Electrode’’, 3th UHVnet Colloquium, Winchester, UK, January 18th-19th 2011.

2. **S. Mousa**, N. Harid, H. Griffiths, and A. Haddad: ‘‘Experimental Investigation on High-Frequency and Transient Performance of a Vertical Earth Electrode’’ 46th International Universities Power Engineering Conference (UPEC), Soest, Germany, September 5-8, 2011. (*Awarded Best Conference Paper*)

3. **S. Mousa**, H. Griffiths, N. Harid, and A. Haddad: ‘‘Experimental Investigation of High Frequency and Transient Performance of Earth Rod Systems’’ 44th International Conference on Lightning Protection (ICLP), Vienna, Austria, 2-7 September 2012.

4. **S. Mousa,** H. Griffiths, N. Harid and A. Haddad: ‘‘Current Distribution under High Frequency and Transient Conditions in Earth Electrode Systems’’ International Conference on High Voltage Engineering and Application (ICHVE), Shanghai, China, 17-20 September 2012.

5. **S. Mousa,** H. Griffiths, N. Harid and A. Haddad: ‘‘Experimental Investigation of High Frequency and Transient Performance of Earth Rod Systems’’, Electrical Power Systems Research (EPSR), Available online 8 April 2014, (http://www.sciencedirect.com/science/article/pii/S0378779614001199)

6. D. Clark**, S. Mousa**, H. Griffiths, N. Harid and A. Haddad: ‘‘Lightning Performance Analysis of Different Length Rod Ground Electrodes’’, 6th International Conference on Grounding and Earthing (GROUND’2014), May 12-16, Manaus (Amazon Region), Brazil, abstract accepted.

DECLARATION

This work has not previously been accepted in substance for any degree and is not concurrently submitted in candidature for any degree.

Signed ……. (candidate) Date ….....

STATEMENT 1

This thesis is being submitted in partial fulfilment of the requirements for the degree of PhD

Signed ……. (candidate) Date ….....

STATEMENT 2

This thesis is the result of my own work/investigation, except where otherwise stated. Other sources are acknowledged by explicit references.

Signed ……. (candidate) Date ….....

STATEMENT 3

I hereby give consent for my thesis, if accepted, to be available for photocopying and for inter-library loan, and for the title and summary to be made available to outside organisations.

Signed ……. (candidate) Date ….....

STATEMENT 4

I hereby give consent for my thesis, if accepted, to be available for photocopying and for inter-library loans after expiry of a bar on access previously approved by the Graduate Development Committee.

Signed ……. (candidate) Date ….....

ACKNOWLEDGEMENTS

First and above all, I praise Allah, the almighty for providing me this opportunity and granting me the capability to proceed successfully.

I would like to extend my heartfelt gratitude to my supervisors, Prof. A. Haddad and Dr. H. Griffiths for their vital guidance and inspiration the duration of this research.

Special thanks to Dr. Noureddine Harid for his advice and supervision during the field experiments of this thesis.

I would like to express my sincere thanks to Dr. David Clark for his co-operation in the experiments and simulations.

I am most grateful to staff members of the research office for always being so helpful and friendly: Chress, Adyern and

The input, support and of the following within the high voltage group has been invaluable: Mohamed Ahmeda, Ahmed El Maghairbi, Muhammad Saufi Karmarudin, Fabian Moore, Ronald Atuhairwe, Alseddig Elzowawi, Shuaib Braini and Christopher Stone.

I wish to express my love and gratitude to my beloved family; ‘‘my mother’’, ‘‘my father’’ and ‘‘my wife’’. Thanks as well to Allah for his gifts; my beloved kids ‘‘Mohamed’’, ‘‘Ahmed’’, ‘‘Lyth’’ and ‘‘Iyad’’

Last but not least, I would like to thank my brothers and my sisters, for their continued love, moral support and prayers.

TABLE OF CONTENTS

CHAPTER SEVEN: HIGH CURRENT IMPULSE CHARACTERSTICS OF ENHANCED ELECTRODE SYSTEMS

CHAPTER ONE: INTRODUCTION

1.1 Introduction

Earthing systems are designed to dissipate high magnitude fault current to earth and provide safety to persons working in or living near power system installations. It is also necessary that earthing systems are designed with low-magnitude earth impedance so that the high magnitude and fast transient surges are dissipated to earth. High voltage distribution and transmission systems are protected from lightning, and effective protection requires a good connection to earth. In high voltage substations, buried earth grids, vertical rods and horizontal electrodes are used in combination to provide a low impedance connection to earth.

Investigations of the earthing systems under high frequency and transient behaviour experimentally and theoretically studies were conducted in the first half of the twentieth century, which is summarized by Sunde, Towne and other researchers [1.1]. In spite of the large amount of work that has been devoted to this subject, there is still no consensus on how to apply present knowledge to the design of actual earthing for better high frequency and transient performance.

1.2 Earthing System Functions and Components

Although earthing systems are designed primarily to provide protection under power frequency earth fault conditions, they are also required to conduct satisfactorily under fast-front surges so that the power system can be protected against excessive voltages. The characteristics of an earthing system under these conditions are very different from those under power frequency and, therefore, the design of earthing systems to perform satisfactory under such conditions is more difficult. This is due to that of the

behaviour of high frequency has more significant influence on inductive and capacitive effects. In contrast to the power frequency response (50Hz), at high frequency the inductance of a small earthing system, such a rod, has a significant effect and the effective length of such systems can be very small.

Earth electrodes generally comprise solid copper conductors, buried below the equipment to be protected. Earthing system components include vertical earth electrode, horizontal electrodes or a combination of both. In larger substations, earth electrodes are arranged in the form of a buried grid occupying the entire area under where the equipment is installed.

In case of transient currents, the standard EA TS 41-24 [1.2] recommends the installation of a ‘‘high frequency earth electrode’’, usually a vertical earth electrode. The phrase ‘‘high frequency earth electrode’’ proposes that the role of the earth rod is to disperse to earth the high frequency components of the transient. In reality, every single part of the earthing system may play a role in the dispersion of both power frequency and transient currents.

1.3 National and International Standards for Earthing Design

There are a number of UK and international standards that provide guidelines concerning earthing system design under transient conditions. A recommendation common to all the standards is that the earth connection between substation equipment involved in the dissipation of surges and the buried earth electrode system should be of low resistance and reactance, and to obtain this, it should be as short and as straight as possible [1.2]. In addition, the standards provide a number of methods to improve earthing performance under surge conditions. In substations, local ‘high frequency electrode’ earth electrodes in the form of earth rods are recommended to be placed

directly under the item of plant to be earthed [1.2]. In rocky areas where a rod electrode cannot be installed easily, it is recommended that two or four radial horizontal 10m electrodes are used instead. However, this standard also recommends that the 'high frequency earth electrode' earth be bonded to the main earth grid [1.2]. IEEE Std. 80-2000 [1.3] discusses and outlines important aims of earthing systems including measurement and testing of earthing impedance, earthing design and methods for installing the earth electrodes, and useful investigations on soil resistivity. However, this is restricted to power frequency performance under earth faults.

The main applications of the earth electrodes such as the vertical rods are to improve power frequency performance when the rods applied at the perimeter of grid. Also, it is recommended that rods are applied at point where high-frequency and transient current will be discharged into ground [1.2]. In addition, horizontal earth electrodes are commonly used to enhance earthing systems located in areas with high soil resistivity, to reduce overall earth impedance; for example, to interconnect adjacent earthing grids or the individual earthing systems of turbines on wind farms [1.3]. Furthermore, there are outdoor transmission substation earthing grids which can encompass large areas reaching more than 30,000 m^2, while indoor substations are more compact with smaller earth grids.

For surge arresters, BS 7430 [1.4] and EA TS 41-24 [1.2] recommend that the earth connection should be located as close as possible to the equipment being protected. EN 62305-3 standards [1.5] recommends that the whole earth termination network for the structure should have a resistance of less than 10Ω.

1.4 Modeling and Measurement of High Frequency and Transient Performance

The majority of testes have been carried out on simple electrodes. The theoretical studies have sought to establish suitable models to describe the observed experimental behaviour of these simple electrodes and have been extended to describe earth grid and grid-rod combination.

Computer based earth analysis techniques are used to verify measurements in the field and in the laboratory, and also contribute to a better understanding of the earthing system behaviour under high frequency and transient performance. Earthing systems are also required to dissipate high frequency currents, such as those generated by lightning strikes. Many authors have investigated the high frequency and transient behaviour of earthing systems from experimental [1.6-1.10] and computational [1.11-1.16] points of view. The impedance of earth electrode systems can be determined using equivalent circuit models or field theory based techniques. Lumped parameter models are commonly used to describe the low frequency performance of simple earth electrodes. At high frequency, the distributed parameter model can provide a more accurate solution for simple earth electrode configurations such as rods and horizontal earth electrodes [1.15, 1.16-1.18]. Field theory techniques can provide advantages over a circuit-based approach in that they can be used to analyse complex and arbitrarily oriented buried earth conductor systems such as transmission substation earthing systems.

Many studies [1.19-1.25] of soil breakdown around earth electrodes under high current magnitudes were conducted to introduce a better understanding of soil conduction under these conditions. These studies involved laboratory, field tests and computer models. These investigations showed that a reduction in earth resistance occurs at high

current magnitudes. However, details about the conduction process that causes soil ionisation behaviour under high magnitude at field test sites are not well understood.

1.5 Safety Considerations

The earth potential rise (EPR) of the substation when the fault current flows through its earthing systems must be limited to an acceptable value so that it can protect the people who are working inside the substation from touching conductive material, such as the fence of the substation. There are limits placed on the permissible EPR of an earthing system as reported in International Telecommunication Union ITU-T [1.26]. These limits are:

- 650V for sites fed from high reliability lines where faults are rare and cleared quickly (200ms maximum).
- 430V for sites fed from lines having standard protection.

The voltage difference between the earth surface potential experienced by an operator bridging a 1m distance, without touching any earthed structure, is referred to step voltage [1.3].

The touch voltage is the voltage difference between the earth potential rise at the metal and the earth surface potential where a person is standing at a normal maximum reach (1m) from the earthed structure. Most earthing standards provide the worst case of step and touch voltage scenarios where the current density and, hence, the potential gradient are the highest at the corners of earth grids.

Step voltages are usually considered less hazardous than touch voltages. This is because the human body can tolerate higher currents for a path from foot to foot than current from hand to feet which passes through the chest, and the step voltage is less

than the prospective touch voltage, as described in IEC 479-1 [1.27]. As given by IEEE 80-2000[1.3], the minimum and maximum step voltages according to soil resistivity values of 500Ωm and 4500Ωm are 1162V and 6082V, respectively (100ms maximum). However, at the same conditions the touch voltages are 469.5V and 1743.8V respectively.

Many standards [1.2-1.5, 1.28-1.30] provide safe step and touch voltage thresholds applicable to persons who are working within and around the substation. The thresholds are found from tolerable current magnitude and duration, and using assumed magnitudes of the human body impedance.

1.6 Aims and objective

The aims and objectives of this thesis are as follows:

- To review published studies of earthing systems under variable frequency and transient conditions, and to develop a good understanding of the behaviour of earth electrode systems when subjected to high impulse currents (Chapter 2),
- To analyse the test results of soil resistivity surveys obtained at the University's earthing test site, and to extract 2D resistivity plots (Chapter 3),
- To develop a novel technique to improve high frequency and transient performance of earth rods (Chapters 4 and 5),
- To investigate the current distribution in the individual conductive paths of electrode systems. DC/low frequency test results are compared with those obtained under high frequency and fast rise-time impulse energisations, permitting detailed evaluation of the effectiveness of the electrode enhancements (Chapter 6),

- To conduct high voltage impulse tests on vertical rods, both with and without horizontal enhancements, and to examine non-linear behaviour or the earth resistance for large impulse current magnitudes (Chapter 7).

1.7 Contribution of Thesis

The investigations conducted in this work have led to the following contributions:

1. An extensive critical review of earthing systems performance under high frequency and transient conditions was carried out, and identified that a case for investigation of enhancements to horizontal and vertical earth electrodes.

2. Better characterisation of soil resistivity at the Llanrumney field test site.

3. The behaviour of earth electrode systems when subject to low/high-frequency currents up to 10MHz was investigated experimentally and using computer models. Experimental evidence is shown for inductive and capacitive effects in earthing systems.

4. A new technique to improve the high-frequency and transient performance of earth electrode systems by using additional horizontal electrode enhancements to the vertical electrode. Good agreement was obtained between the experimental results and simulations.

5. A comprehensive analytical and experimental analysis of the current distribution under high frequency/transient conditions was compared with that at power frequency. Two specific earthing arrangements are the subject of this study: (i) a vertical rods with horizontal electrode enhancements and (ii) a horizontal electrode with a parallel insulated interconnected conductor. Experimental studies of these

systems are presented and, by analysing the current distribution, the contribution of the additional conductors is clarified.

6. In addition, an improved understanding the phenomenon of soil ionisation for vertical rods with and without horizontal enhancements was established.

1.8 Thesis Layout

The thesis is divided into eight chapters. References are numbered in square brackets and correspond to a full list at the end of the thesis. The content of each main chapter is summarised as follows.

Chapter 2: Performance of Earth Electrodes under High Frequency and Transient Conditions: Review of Previous Work

An extensive review of published studies on the high frequency and transient analysis of earthing systems is presented in this chapter. The review based on field tests, laboratory measurements and computational methods. The work on characterisation of the non-linear behaviour is also reviewed. It is shown in most published investigations that the behaviour of vertical electrodes of different lengths with and without horizontal enhancements under low/high-frequency and impulse performance at test site, have not yet been investigated.

Chapter 3: Long Term Soil Resistivity Analysis at Llanrumney Field Site

A comprehensive soil resistivity survey for long term data at Cardiff University facilities is conducted. Measurements were carried out using two different instruments. The soil resistivity at the location of the test earth electrodes before installation is measured, and the soil resistivity layer is estimated for use in computer simulations.

Chapter 4: Low Voltage Variable Frequency Characterisation of Proposed Enhanced Earth Electrode Systems

In this chapter, an experimental investigation on the high-frequency response of vertical earth is described. Rods of different lengths are installed at the Cardiff University outdoor earthing test facility. The tests were carried out for a range of frequencies between DC and 10 MHz using variable-frequency AC current sources. The variations of the measured earth impedance with frequency are determined for characterising the frequency behaviour of the tested earth electrodes. The experimental results are compared with computation results using different models. The new proposal suggests the use of horizontal enhancement electrodes (star/cross-shaped) with various lengths of vertical earth electrode to decrease the earthing impedance at low frequency, and to reduce the inductive effect at high frequency.

Chapter 5: Proposed Enhanced Earth Electrode Systems under Impulse Energisation

This chapter describes the experimental tests on various lengths of vertical electrodes with and without proposer horizontal enhancements using a similar experimental arrangements and test circuits as adopted in Chapter 4. Low magnitude impulse current with variable magnitude and shape was injected into the vertical earth electrode with and without horizontal enhancements. The impulse impedance was measured and simulated as a function of the injected impulse rise time. The effect of an additional above ground conductor with different lengths of the bare horizontal electrode is also conducted at Cardiff University earthing test facilities. The analysed measurement results are then compared with computer simulations.

Chapter6: Improved Voltage and Current Distributions in Enhanced Earth Electrode Systems

The measurement results of the voltage and current distributions of different lengths of vertical earth electrodes with horizontal enhancements under low/high-frequency and transient performance are performed. For each electrode system, both variable frequency and impulse tests were carried out. The current work focuses on current distribution in the individual component paths in the electrode systems. Also, the current distributions at each segment of the 88m horizontal earth electrode with and without above-ground insulated conductor under low/high-frequency and transient conditions are investigated. The tests are extended to consider the effect of impulse rise-time on current distribution. The percentage of current dissipation of the horizontal electrode with an additional conductor was calculated, and compared with simulation results.

Chapter7: High Current Impulse Characteristics of Enhanced Electrode Systems

This chapter involves investigation of earthing characteristics of a vertical earth electrode under high impulse current. In this section, a wireless measurement system was described. A high impulse current is injected into the vertical rods, and the impulse resistances were determined as a function of current magnitude. The soil ionisation phenomenon around the vertical rod was demonstrated on the recorded voltage and current traces. The effect of an additional 8-point star to the vertical rods was also investigated, and the results were compared with previous research work.

Chapter Eight: gives the overall conclusions and suggestions are proposed for future work.

CHAPTER TWO: PERFORMANCE OF EARTH ELECTRODES UNDER HIGH FREQUENCY AND TRANSIENT CONDITIONS: REVIEW OF PREVIOUS WORK

2.1 Introduction

Work to investigate the characteristics of the transient performance of earthing systems began at the start of the last century. Early work concentrated on the performance of earthing systems through experiments and simulations using circuit models for simple earth electrode systems such as vertical earth electrodes and horizontal electrodes. These simple earth electrodes are widely used today in earthing systems and in lightning protection systems either as main earth electrodes or as reinforcing electrodes to help reduce the earth impedance and improve the system's high frequency and transient performance. The most significant outcomes of these studies resulted in an improvement in the design of earthing systems subjected to power frequency faults and fast transient currents. The most recent work analysing the performance of an earthing system subjected to impulse currents has used computer simulation packages which enable investigation of complex earthing systems configurations.

This chapter provides a review of work describing the behaviour of earth electrodes under variable frequency and impulse performance. A review of quantitative studies performed by previous authors is carried out to obtain further understanding of the phenomenon of soil breakdown under high impulse currents. Finally, the effects of length and area are considered.

2.2 Soil Resistivity

Soil resistivity is a measure of how much the soil resists the flow of electrical current. It is a main factor in earthing designs that rely on passing current through the earth's

surface. Understanding soil resistivity and how it changes with depth in the soil is very important for designing the earthing system of an electrical power substation, or for specifying lightning conductors. A wide range of typical soil resistivity values have been reported in the literature.

2.2.1 Typical Resistivites for Various Soil Types

Soil resistivity values vary widely, depending on the type of ground, for instance, silt on riversides may have a resistivity value around 1.5Ωm, while dry sand or granite in mountainous country may have values higher than 10,000Ωm, but the range typically encountered in earthing system design varies from about 10Ωm in clays to 1000Ωm in granites [2.1, 2.2]. It is found that earth resistivity varies from 0.01 to 1Ωm for sea water, and up to 10^9Ωm for sandstone [2.3].

2.2.2 Measuring and Modelling of Soil Resistivity

It is very important to find an accurate soil resistivity model as a basis for designing an earthing system, and there are a lot of different methods and extensive sources of information available. Methods, such as geological maps, borehole data, seismic testing [2.4, 2.5] and ground penetrating radar, are beneficial for determining physical boundaries in the soil. The measured value of soil resistivity is referred to as the apparent resistivity that is used in the calculation of the soil model, and is not the actual value of resistivity. There are some electrical techniques to investigate soil resistivity, the most common of which is the Wenner method and its variants [2.6, 2.7, 2.8, 2.9]. The Wenner method uses four electrodes arranged in a straight line and all four electrodes are moved after each reading, with the spacing between each adjacent pair remaining the same [2.3]. If the electrode spacing is increased, then the average soil resistivity is measured to a greater depth. If the average resistivity increases as the

electrode spacing increases, there is a region of soil that has resistivity at a greater depth. Apparent resistivity curves obtained from the measurements may indicate complex soil structures of many layers. It may become more complicated to establish a simple soil model for earthing system applications when the soil structure increases in complexity. A simpler method can be used to achieve an effective equivalent value of soil resistivity from the apparent resistivity data as described in [2.7, 2.10, 2.11, 2.12].

2.3 Methods to Reduce Earthing Resistance

Due to the complex structure of soil layers, the measured earthing resistance of electrodes buried into the earth directly may not reach the earthing resistance required. Therefore, common methods used to lower earthing resistance can be classified into physical reduction and chemical reduction techniques.

2.3.1 Soil Treatment to Reduce an Electrode's Earth Resistance

A high earthing resistance value may adversely affect the operation of protection equipment within power substations. Various methods have been used to reduce the earth resistance of the earthing system [2.13-2.21]. Sunde, in his book [2.1], described the effect of chemical treatment on the soil. He suggested that if the resistance of earth containing one or more earth rods is to be reduced, it may be useful to use chemical treatment such as salt instead of adding more rods to reduce the resistivity, especially where the resistivity is very high. However, he paid attention to the property of the salt, which has a tendency to be absorbed by the earth so that the reduction in earth resistance may not continue for many years. IEEE Std [2.3] described the utilisation of this phenomenon as an advantage, for instance use of sodium chloride, magnesium etc. to increase the conductivity of the soil surrounding the earth electrodes, but this

technique may not be permitted by government legislation because of possible pollution to surrounding areas. Further, the salt must be renewed periodically.

2.3.2 Use of Reinforced Concrete to Reduce Earth Resistance

This method is useful for medium and high resistivity soils because just one metallic electrode encased in concrete would give a lower earth resistance than a similar electrode installed directly in the earth. However, the earth resistance might be increased after years due to corrosion of the concrete reinforcing bar material [2.22].

2.4 Measuring and Modelling of Earth Electrodes under Impulse Conditions

A number of impulse studies on soils have been carried out in the field and laboratory [2.23-2.43]. The investigations were classified according to the type of earth electrode: vertical rods, horizontal electrodes and the mesh electrodes.

2.4.1 Vertical Earth Electrode

In 1928, Towne [2.23] conducted measurements to investigate the characterisation of the impulse behaviour of vertical electrodes used to earth lightning arresters. Galvanised iron pipes up to 6.1m in length and 21.3mm in diameter buried in loose gravel soil were used. Discharge current magnitudes of up to 1500A with rise-times between 20μs and 30μs were applied. It was shown that when the impulse current was injected into the rod, the resistance fell from 24Ω (measured at 60Hz) to 17Ω. This was due to arcing in the soil surrounding the electrode, and this was confirmed visually. The ′impulse resistance′ was defined as the ratio of the measured voltage to current at any instant. In 1941, Bellaschi [2.24] presented the fundamentals of the impulse data on the actual driven rods under injection of high impulse currents. The performance of earthing systems under power frequency fault conditions had been

improved by installing parallel vertical electrodes and suitably treating the soil with common salt. Experiments were conducted on four steel rods of one-inch diameter (25.4mm), which were installed in natural soil and up to 9ft (2.7m) length with earth resistance magnitudes between 30Ω and 40Ω at 60Hz. 2000 to 8000A impulse current values were applied in these measurements with rise-time values of 6μs and 13μs. Bellaschi neglected the effect of inductance and capacitance when he defined impulse resistance as the ratio between voltage peak value to current peak value, in which he agrees with Towne [2.23]. These measurements however, might include inductive effects. The impulse resistance was found to decrease with current magnitudes and to have lower values lower than the 60Hz earth resistance, which was attributed to the soil ionisation process. He summarised his work through the characteristic curve that contains the ratio of impulse to 60Hz resistance shown in Figure 2.1.

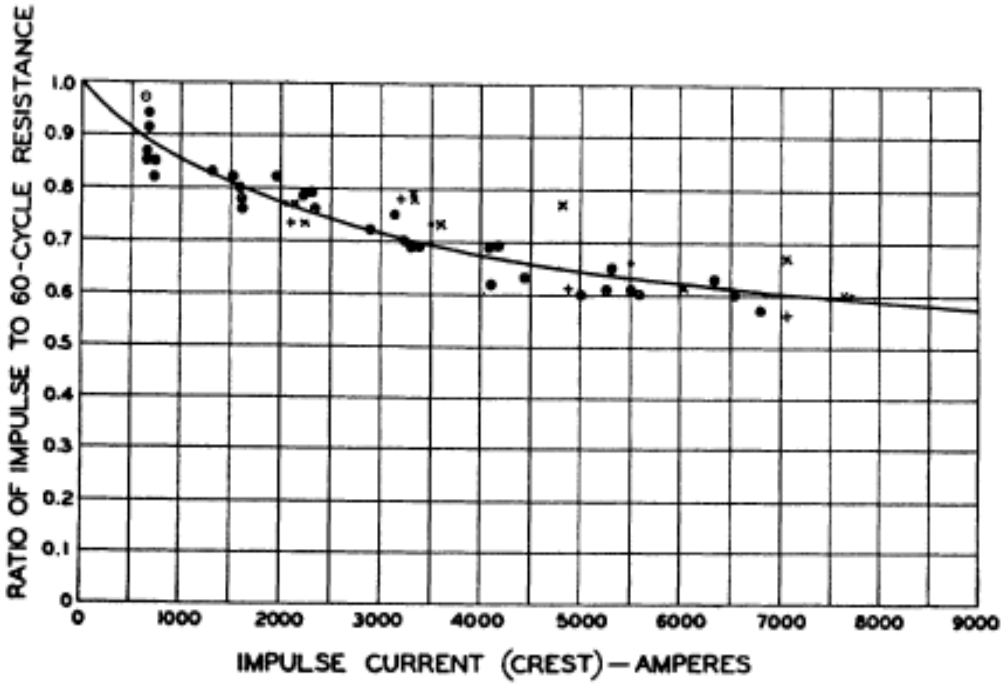

Figure 2.1: Characteristics of driven grounds (reproduced from reference [2.24])

Bellaschi, in his subsequent paper [2.25], added experimental work with 12 earth-driven electrodes in the field, seven rods were located in clay soil with earth resistance

values between 10Ω and 40Ω. Another two driven rods were installed in naturally dry and gravelly soil and one in sand, and their earth resistance measured from 60Ω to 220Ω. The remaining two driven rods were installed in soil that contained mixture of clay and stone and with 60Hz measured resistance values from 25Ω to 190Ω. The rods were buried into the earth at depths ranging from 2.44m (8ft) to 9.144m (30ft). The impulse current value, a range of 400 to 15,500A with various rise-times of 20/50μs, 8/125μs and 25/65μs, were applied. It was found that the degree of reduction of impulse resistance, which is calculated by the ratio of impulse resistance to 60-cycle resistance, is dependent on the properties of soil and electrode arrangement but independent of the current rise-time. A similar result was obtained by Vainer [2.26], who found also that the reduction in resistance under high impulse currents depended on AC earth resistance. In these experiments, impulse voltages of 1.5 and 0.8MV were applied to vertical rods of 10m to 140m in length. Here, Vainer defined the impulse impedance as the ratio of crest voltage to the corresponding current at crest voltage. It was confirmed that there is a small reduction of impulse impedance for an electrode of lower AC earth resistance, which is similar to Bellaschi's results [2.25].

Liew and Darvenzia [2.27] conducted experiments on 0.61m (2ft) long vertical rods with a diameter of 12.7mm and 25.4mm buried in soil and a 152.4mm-diameter buried under the surface of the soil with a range of resistivities from 5,000Ωcm to 31,000Ωcm. A current impulse value in the range of up to 20kA with different rise-times between 10μs and 54μs was applied. The impulse resistance was presented as the instantaneous ratio of voltage to current as time varied. Figure 2.2 shows this dynamic model which has three stages: (a) constant soil resistivity in all directions called the 'no ionisation zone'; (c) the current density exceeds the critical current density value J_c ,and the soil resistivity decreases exponentially and is constrained by a

magnitude defined as ‘ionisation time constant’; (b) if the current density has a value greater than the critical value then the soil recovers to the initial value in an exponential manner. A reduction of impulse resistance with increasing current magnitudes was obtained, and was attributed to soil ionisation. It was found that the reduction of impulse resistance depended on the characteristics of the soil and lower breakdown gradients. Moreover, individual vertical rods exhibited a greater reduction than multiple rods due to the current density around the rods being higher, therefore, to a great extent, ionisation was shown to reduce the localised resistivity of the soil. It was found from tests at 100kA impulse current injected value that the impulse resistance decreased significantly, and more than in the case of 15kA injected current. The authors showed that the impulse resistance of the vertical electrodes was dependent on impulse current rise-times which contradicted the results found by Bellaschi et al. [2.25], who concluded that the impulse resistance is independent of the current rise-times. Dick and Holliday [2.28] carried out tests on metal earth rods of different dimensions, under high impulse and alternating currents. The results showed that, under high impulse current, the earth resistance decreased for all tests, which is attributed to the soil ionisation process. From experimental field results, it was found that the characteristics of the soil would become non-linear when subjected to high impulse current magnitudes. It was also found that the degree of soil conduction non-linearity is dependent on the DC earth resistance value. High voltage tests were conducted on a concrete pole with soil resistivity of about 170Ωm behaviour by Sekioka et al. [2.29] to examine the soil ionisation. High impulse currents of several tens of kA were injected into a concrete pole. The impulse impedance of the pole was determined as the ratio of V_{peak} to I_{peak}. The impulse pole impedance was found to reduce with increasing current magnitude due to the soil ionisation process, as shown in Figure 2.3.

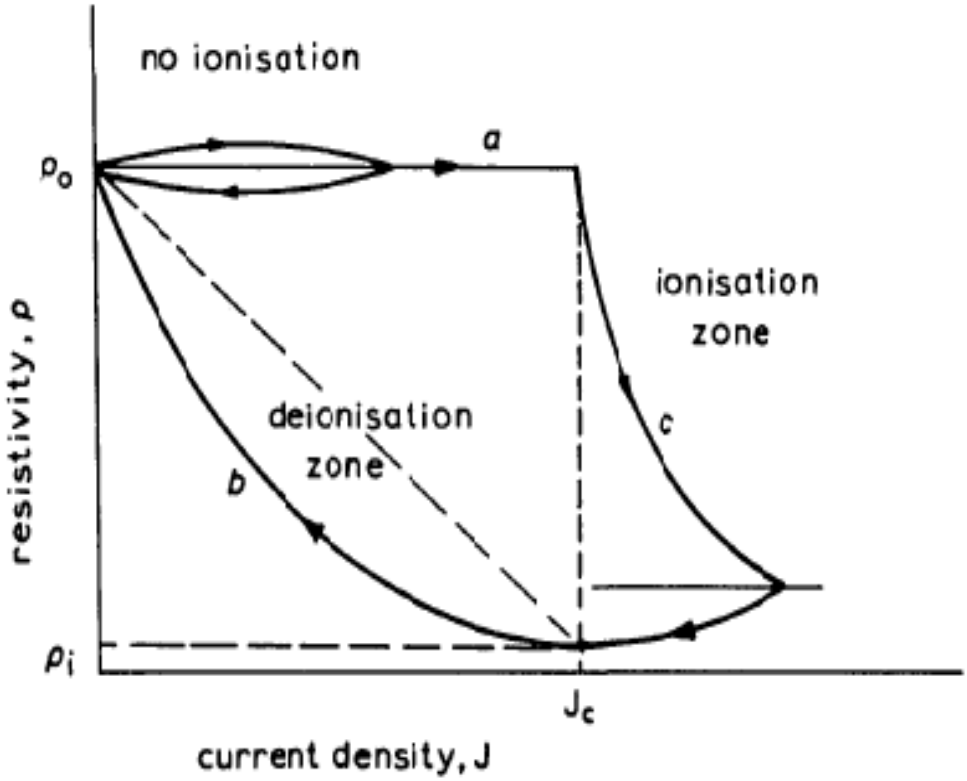

Figure 2.2: Soil ionisation process (reproduced from reference [2.27])

Almeida et al. [2.30] conducted tests on a 0.6m vertical rod with a radius of 0.075m and installed into sand/gravel soil. An impulse current value of 3.5kA with an impulse shape of 5/16.5μs was injected into a single vertical rod. Figure 2.4 shows the new proposed model of impulse resistance. It was observed that at the time of ionisation, the soil resistivity decreased due to high current density. The results showed that the resistance of electrodes reduced according to the ionisation region, as suggested by Liew and Darveniza [2.27].

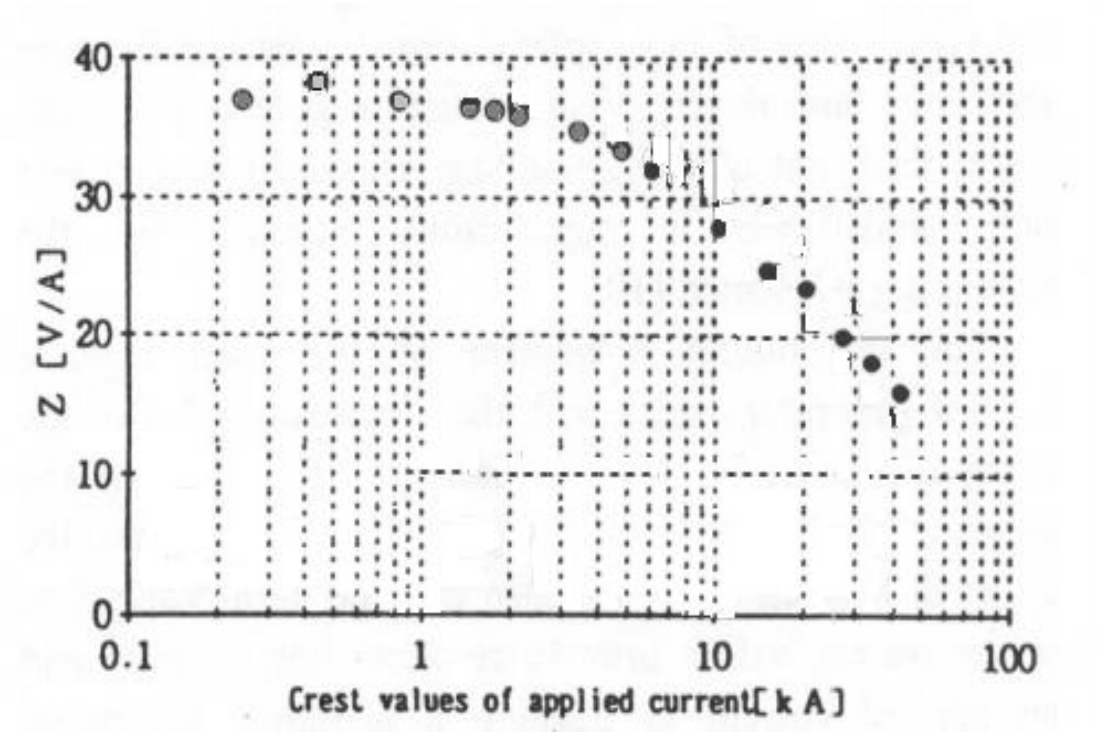

Figure 2.3: Impulse impedance as function of current (reproduced from reference [2.29])

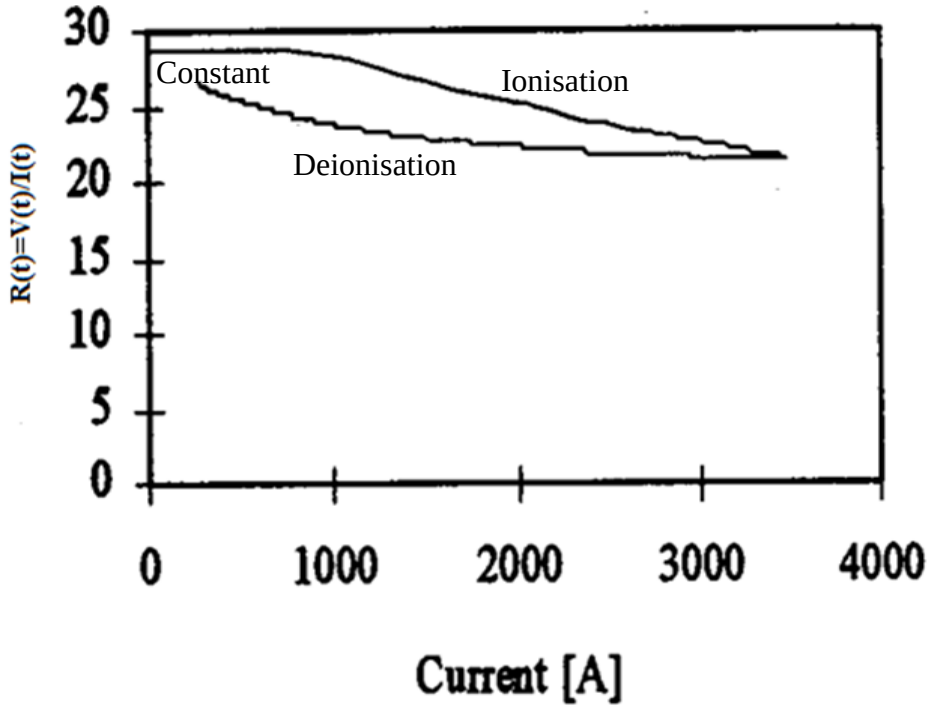

Figure 2.4: Impulse resistance vs. of current (reproduced from reference [2.30])

2.4.2 Horizontal Earth Electrodes

Bewley [2.31] carried out tests on two parallel counterpoises of lengths 281m and 465m .An impulse current magnitude of 900A with a rise time of 2μs was applied. The initial value of the transient impedance was 100Ω, and it fell very quickly to a value of 9Ω. It was observed that a counterpoise of over 91.4m (300ft) in length gave little further benefit, but that using an additional parallel counterpoise would be useful. In addition, no soil ionisation was obtained, which might be due to the low impulse current value. Bewley continued his work [2.32] and conducted more experiments on counterpoises to verify his calculation model. The high voltage impulse values of 15kV and 90kV with a rise-time of 0.5μs was applied on 61m, 152m and 282m counterpoises. In common with his previous paper, it was observed that the transient impedance reduced rapidly from the initial surge impedance to the leakage resistance, consistent with the findings of [2.31].

Gupta et al. [2.33] provided an empirical formula for the impulse impedance of substation earth grids. Here, the impulse impedance defined as the ratio of the voltage peak measured at the injection point to the peak value of the current injection. However, as we know the peak value of the voltage does not always occur at the same time as the peak value of the current due to mainly inductive effects. The authors mention that the impulse impedance depends on factors such as the shape of the earth grid, the distance between electrodes, the point of injection, the magnitude and wave shape of the injected impulse current, and the characteristics of the soil. Tests on 16 mesh square grids of copper wire in a 6m hemispherical tank were conducted, and found that when the current was injected at the centre point, the impulse impedance value was much lower than the injection at the corner. It was concluded that the effect of soil ionisation was very small when using an earthing grid and could be neglected.

In a subsequent paper by Gupta et al. [2.34], the work was extended to investigate rectangular earthing grids. The results showed that for the same area of a square and rectangle, the impulse resistance for the rectangle is higher than that of the square.

The soil characteristics of horizontal electrodes at field measurements have been carried out by Sonoda et al. [2.35]. Injected currents up to 30kA and impulse voltage up to 3MV were used for testing two dimensional square grids; (i) $10m^2$ and (ii) $20m^2$, and two horizontal earth electrodes of lengths 5m and 20m. The results have shown that both horizontal electrodes showed strong current dependency which is attributed to the soil ionisation process, as shown in Figure 2.5a. However, the impulse resistance remained almost constant for all current values for grid (ii) for both injections points of applied currents (corner and centre injections) as shown in Figure 2.5b. Yanqing et al. [2.36] presented a model to investigate the transient characteristics of earthing grids under impulse currents. An earthing grid of $20\times20m^2$ was used as a study case, buried at 0.8m depth in a soil resistivity value of 500Ωm and permittivity of $\varepsilon_r=9$. Impulse currents up to 10kA with a 2.6/50μs wave shape were injected into the corner and centre locations of the earthing grid. From their results, the characteristics of the impulse resistance were found to depend on the parameters of the earthing grid, the waveform and the magnitude of the current and injection location. The results were shown that the impulse resistance exhibited a higher value for current injection at the corner of the grid than for injection at the grid centre, which is in agreement with Gupta [2.35]. This was thought to be due to the effect of the inductance of the earthing conductor, which obstructs the impulse current to flow in other directions in the case of a corner injection point, but, at the centre injection point, the earthing conductor has a small inductive effect.

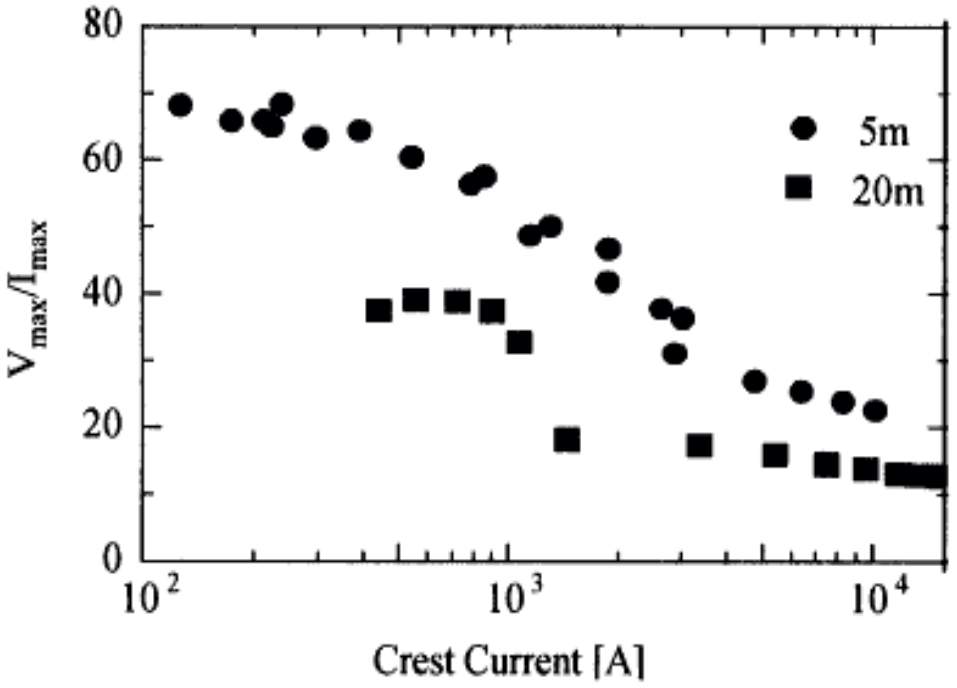

a) Horizontal electrodes

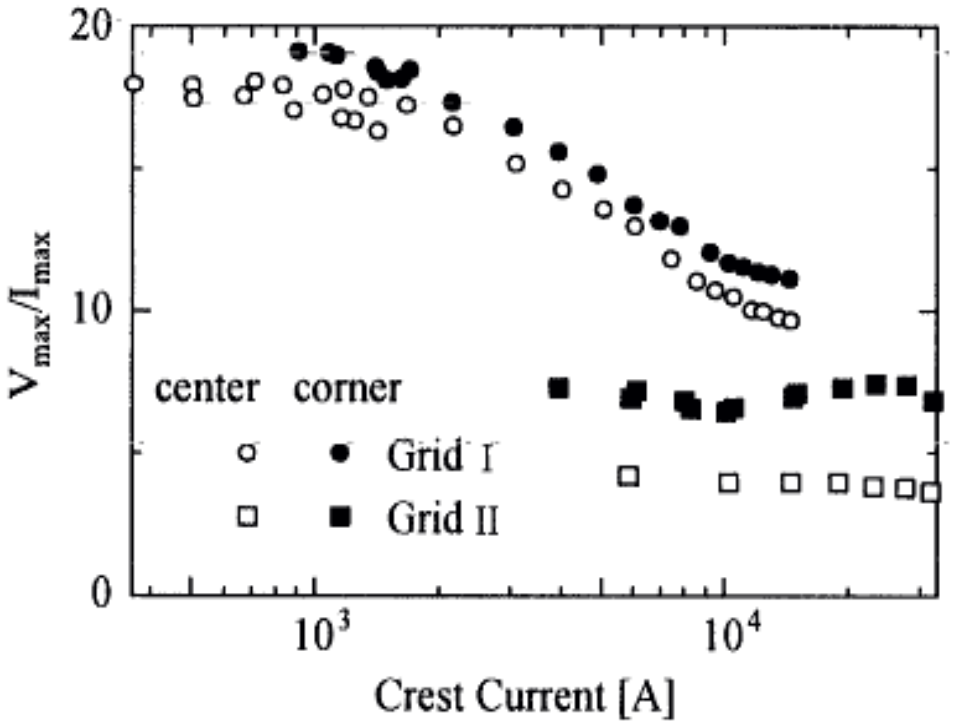

b) Earthing grid

Figure 2.5: Current dependency of earthing resistance (reproduced from reference [2.35])

2.4.3 Comparative Investigations

Ottle et al. [2.37] conducted impulse measurements on vertical and horizontal earth electrodes buried in two soil conditions (dry and wet). The applied impulses had voltage magnitudes up to 250kV and current magnitudes up to 5kA peak and a rise time of 10 μs. The impulse resistance was calculated as the ratio of voltage to current and as a function of time. At higher currents, the impulse resistance reduced for all conditions which can be described by thermal and ionisation processes of the soil conduction processes. Geri et al. [2.38] carried out experiments on two earth electrode configurations; a 1m steel vertical rod and a 5m steel wire horizontal electrode were buried in soil of uniform resistivity. An impulse current value of up to 30kA with a rise-time of 2.5μs was applied in these tests. He defined the impulse resistance as the ratio between the peak value of voltage and the peak value of current. It was found from the measurements that when the impulse current was increased from 5kA to 30kA, the impulse resistance decreased from 17.6Ω to 8.1Ω for a rod, and from 10Ω to 6.9Ω for a wire.

Sekioka et al. [2.39] carried out tests on different types of earth electrode, which included an 8.1m concrete pile, a 17m single vertical electrode and grounding net with dimensions of $34 \times 24.8 m^2$. The earth resistance measured for each electrode was 38.5Ω, 71.7Ω and 3.2Ω respectively. In their experiments, the authors applied 40kA impulses with a rise-time of a few microseconds. The impulse resistance was taken as the ratio of the peak value of the voltage to the peak value of the current. The earthing resistance of the concrete pile and a single rod decreased with increasing current magnitudes, which means that the earthing resistance was completely dependent on the peak value of the current. However, the earthing resistance of the ground net was almost constant due to its large surface area, as shown in Figure 2.6.

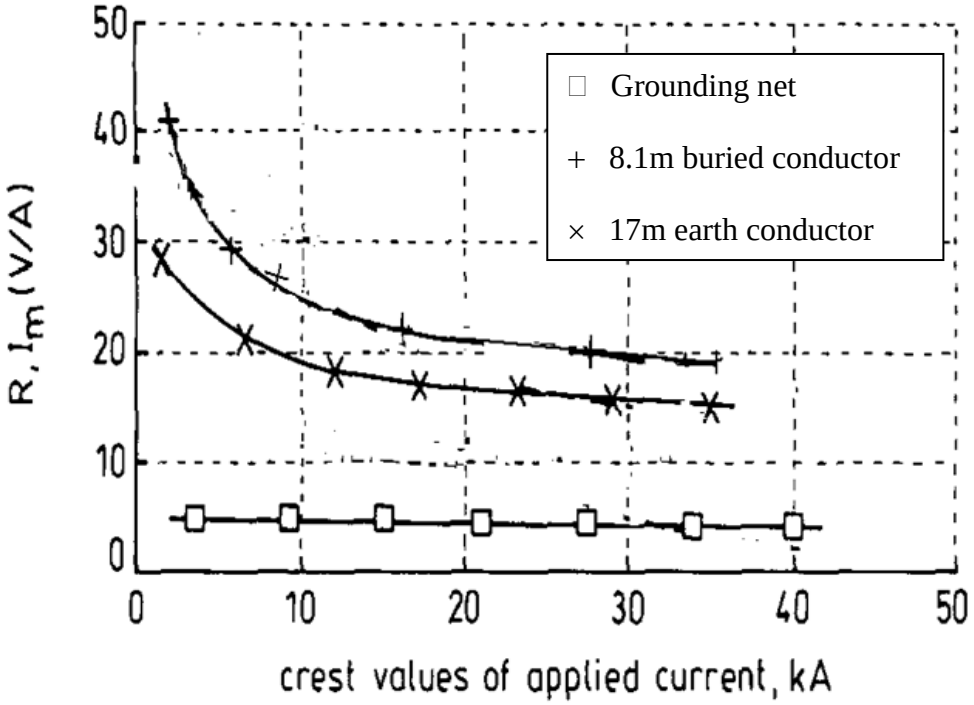

Figure 2.6: Earthing resistance vs. the peak of injected current value (reproduced from reference [2.39])

Vander et al. [2.40] described the impulse behaviour of four different earth electrodes of 5m vertical earth rod, 5 to 20m horizontal earth rods and a $100\times100m^2$ grid electrode with four meshes by using an electromagnetic-field analysis program (CDEGS) [2.41]. The current magnitude of 1A was injected into each arrangement. Their study of the 5m earth rod showed that the transient earth potential rise (TEPR) increases with increasing soil resistivity but decreases with increasing permittivity in soils with significant resistivity values. The horizontal rod exhibited inductive behaviour in low resistivity soils, and in the medium to high range of resistivity, the 20m horizontal rod was seen to exhibit lower TEPR than the 5m horizontal and vertical rods. This variation is presented in the graph shown in Figure 2.7 for the same impulse shapes and soil properties.

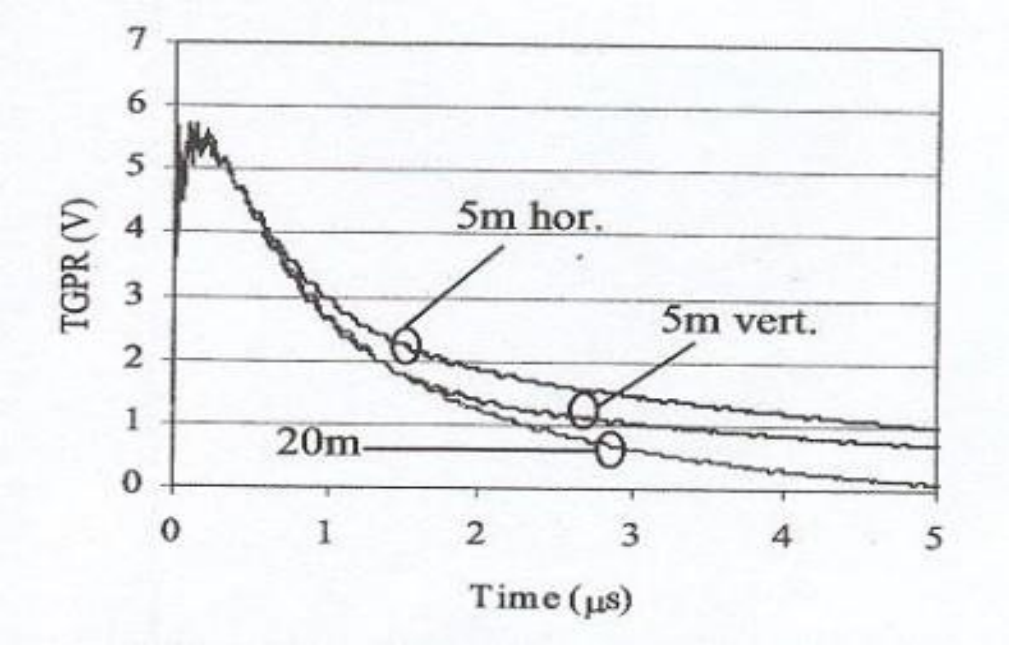

Figure 2.7: The comparison of TGPR for 5m and 20m horizontal rods (reproduced from reference [2.40])

2.4.4 Hemispherical Test Geometry

Berger [2.42] carried out tests on a hemispherical pit of 2.5m in diameter, was half buried in the soil in a hemispherical tank. Tests were conducted on various sizes of electrodes and different type of soils. 3.8kA to 11.4kA peak impulse currents with rise-times between 3μs to 30μs were applied in these tests. At high current magnitudes, for rise-times less than 3μs on the current front, a linear v-i curve was obtained and the impulse resistance magnitudes were similar to the earth resistance measured at 60Hz.Figure 2.8 shows the impulse resistance as a function of time for different current magnitudes where the higher reduction in the resistance observed with higher current magnitude. Petropoulos [2.43] used a similar hemispherical model. The behaviour of earth resistance under high impulse currents was concentrated. Iron electrodes buried at about 20mm depth were used and he found that the resistance started falling when the current is increasing and fell rapidly when the breakdown

occurred. In addition, the results showed that when the length of spikes is increased, the impulse resistance decreased.

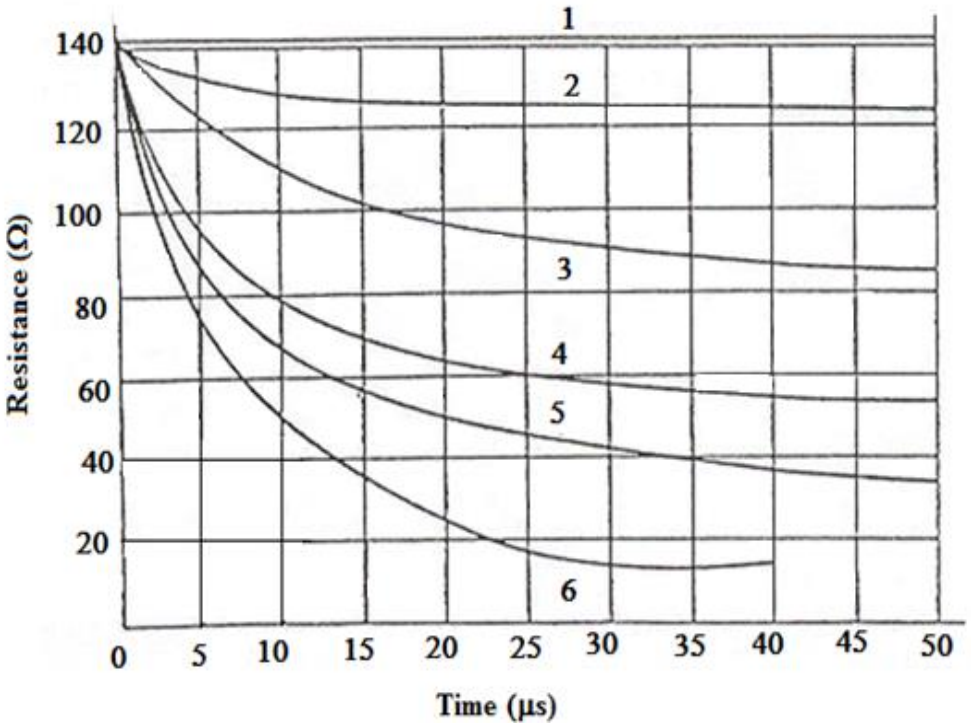

1, imax=250A **2, imax=560A** **3, imax=975A**

4, imax=1800A **5, imax=2400A** **6, imax=5300A**

Figure 2.8: Impulse resistance vs. time at different peak current values (reproduced from reference [2.42])

2.5 Measurement and Simulation of Earth Electrodes under High Frequency

Brourg et al. [2.44] conducted an experimental study on short electrodes (<4m) buried in high resistivity soil and found that there was a reduction in earth impedance magnitude with a frequency of up to 1MHz. In the same investigation, experiments on a 32m rod showed that the earth impedance is constant at low frequency range up to a threshold frequency, above which the earthing impedance increased sharply. Grcev

[2.45] investigated the main parameters that can govern the high-frequency behaviour of long earth rods in high soil resistivity, and also compared his experimental results with Brourg's results [2.44]. He conducted experiments on different lengths of vertical electrode in the range of 2m to 32m. The soil resistivity surrounding the rods had a value of 1Ωm after covering the rods with low soil resistivity material (LRM), while the resistivity of the surrounding soil was measured at 1,300Ωm. The results confirmed the conclusions in [2.44] that, in the soil with poor conductivity, the impedance of earth rods is purely resistive up to 10 kHz, becoming capacitive at high frequencies for rods shorter than about 8m, and inductive for long vertical electrodes. It was recommended that if the current is injected at the midpoint of the earth electrode, high frequency performance can be improved as shown in Figure 2.9. Choi et al. [2.46] carried out tests on a medium-sized grid ($27\times9m^2$). The results showed a reduction in impedance over the range dc to 200 kHz, attributed to capacitive effects in a high resistivity medium. Visacro et al. [2.47] simulated the frequency response of a buried horizontal earth electrode systems. The results showed that the earth impedance reduced with frequency and then increased above a particular frequency related to electrode length.

In another study, Nekhoul et al. [2.48] presented FEM modelling on 2m to 8m vertical electrodes, and predicted a significant reduction of impedance with frequency up to a threshold value in the frequency range 10 kHz to 100 kHz. The threshold frequency at which the impedance started to rise again was calculated. It was observed that the frequency threshold reduced as the length of the electrode increased, indicating an increase in self-inductance with length.

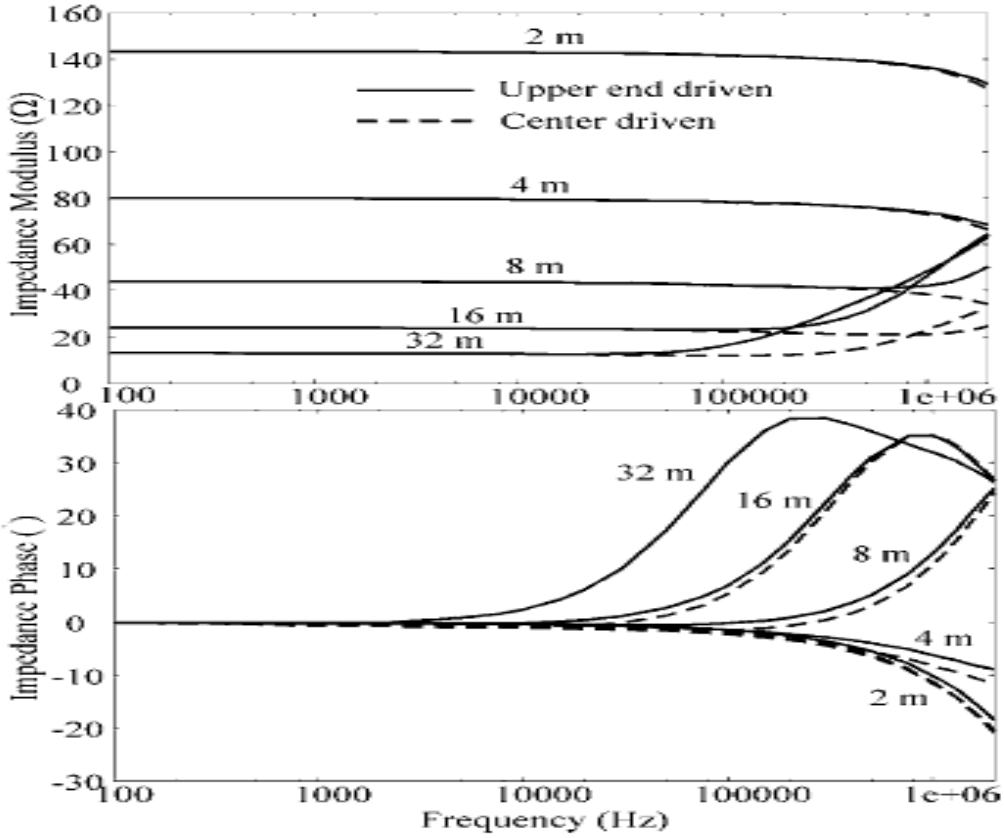

Figure 2.9: Frequency response of earth rods in soil with ρ=300Ωm (reproduced from reference [2.45])

Papalexopoulos et al. [2.49] developed a new model in which a simple system of aerial and buried conductors was used, and the analytical studies of numerous earthing systems were performed. A conductor buried in the soil was used and divided it into N small segments; when the current flows in these segments it induces a voltage. At high frequency, the reactance of the earthing system is very influential and cannot be neglected, while at 60Hz the resistance is roughly equal to the DC resistance. Davies et al. [2.50] have undertaken extensive analysis of the high frequency behaviour of vertical earthing electrodes. Frequencies of 50Hz, 100kHz, 1MHz and 10MHz were chosen, and the effects of soil resistivity, rod radius and rod length were studied. Using earthing software [2.41], the results of the distributed and lumped parameters with the simulation results for different current injection points were compared. The length and radius of the vertical rod were 5m and 7mm respectively, the soil was assumed to be

homogenous with a resistivity of 100Ωm, and that the relative permittivity and permeability were taken to be unity. The authors state that the inductance of the rod has much effect, and appears at high frequency above 1MHz but, above 10MHz, the phase angle is affected by the capacitive behaviour. The permittivity, thus, affects the impedance only at high frequencies. Zedan et al. [2.51] studied the frequency response of rod, horizontal and grid earth electrodes at 10MHz using the same program in [2.41]. The effective length of the vertical and horizontal earth rods was calculated. For the horizontal earth electrode, the inductive effect appears at specific frequencies, and is also related to the resistivity of the soil. The authors observed a resonance effect above 1MHz. Grcev et al. [2.52] compared simple equivalent circuits to electromagnetic field theory (EMF). 3m and 30m lengths of vertical electrode with 30Ωm and 300Ωm soil resistivity were computed by lumped circuit model, distributed parameter circuit model and EMF. The radius of the rod modelled was 1.25cm, and the soil permittivity was 10. The computer simulation showed that the RLC and the lumped parameter model overestimate the earth rod impedance, particularly at high frequency, compared with the EMF model which gave much better results while the distributed parameter model was found to overestimate to a lesser degree. To reduce these overestimations, the authors suggest using the EMF model at high frequency. Figure 2.10 shows the comparison between the computed results for '*the harmonic impedance*' of 3m and 30m rods. Llovera et al. [2.53] carried out tests on a hemispherical electrode in the laboratory, buried in soils with a range of resistivities, and a 1m vertical electrode with a diameter of 1.5cm. The authors connected seven rods, of length 2m and diameter of 1.5cm in diameter arranged in a circular configuration leaving the studied rod (a 1m long and 1.5cm in diameter copper rod) in the centre of the distribution. The distance between the studied rod and each of the

other rods was 10m. The measurement results showed capacitive behaviour for both low soil resistivity (281Ωm) and high soil resistivity (1900Ωm) up to 1MHz. However, when the frequency was increased to 10MHz, the inductive effect was dominant for high soil resistivity. This was thought to be due to the inductance of the connection cables. Figure 2.11 shows the effect of adding auxiliary vertical rods on the earthing impedance. These measurements showed that adding rods reduced the inductance of the connection cables and increased the capacitance between the studied rod and the additional rods, which improved the earthing impedance at high frequency. Griffiths [2.54] presented the variation of impedance magnitude at various frequencies for a 100m horizontal earth electrode. The impedance magnitude of horizontal electrode was found to increase above a particular frequency for low soil resistivities. When the soil resistivity is high, there is resonance in the response for frequencies above 1MHz, and the impedance decreases above a particular frequency. Choi et al. [2.55] carried out tests on a 40m horizontal electrode with a radius of 0.28cm. High conductivity powdered carbon was mixed with the soil at one end of the counterpoise to study the earthing impedance. The dissipating current rates were measured when the current was injected at both ends of the counterpoise buried in a ground with two-layered soil resistivity. The authors measured the earth resistance arising from current injection at both ends of the 10m-long electrode, yielding values of 45.5Ω and 21.6Ω. The results showed that the earthing impedance of the horizontal electrode is related to the current dissipation. In addition, the results also showed that the earth impedance at the low resistivity location (current injection point 2) was lower than the earth impedance at the high resistivity end (current injection point 1) for both the low and high frequency ranges, as shown in Figure 2.12. Alipio et al. [2.56] presented the effect of frequency dependence on soil parameters. A horizontal earth electrode with lengths ranging from

5m to 90m and a radius of 7mm was used, buried at a depth of 0.5m in soils of low and high resistivity (300Ωm and 3kΩm). For the simulation, a Hybrid Electromagnetic Model (HEM) was used for low and high frequencies up to 1MHz, and for computing the impulse response. Figure 2.13 shows the measurement results for the frequency responses of the 30m horizontal earth electrode. At low frequency, the earthing impedance was frequency-independent and equal to the low frequency resistance for both resistivities. However, at high frequency the results showed that for both low and high soil resistivity, the frequency dependence of soil parameters caused a reduction in earthing impedance due to capacitive effects. Recently, Griffiths et al. [2.57] presented a numerical simulation for the frequency dependence of the earth impedance of a rod, horizontal and grid electrodes in the range DC to 10MHz, and for a wide range of resistivities of 10Ωm-10kΩm using CDEGS software [2.41]. Equations to calculate the upturn frequency, downturn frequency and frequency of oscillations in high resistivity media were also derived. The 5m vertical rod, 100m horizontal earth electrode, $100\times100m^2$ and the number of meshes was 2×2 for earth grid electrode and all connecting conductors selected in this investigation were assumed to be of cylindrical copper construction with 1cm radius. The simulation results showed that inductive effects were dominant for all earth electrodes above a particular frequency, termed the upturn frequency, which is related to soil resistivity. In high soil resistivity the authors expected a reduction in earth impedance, above a particular downturn frequency due to capacitive effects.

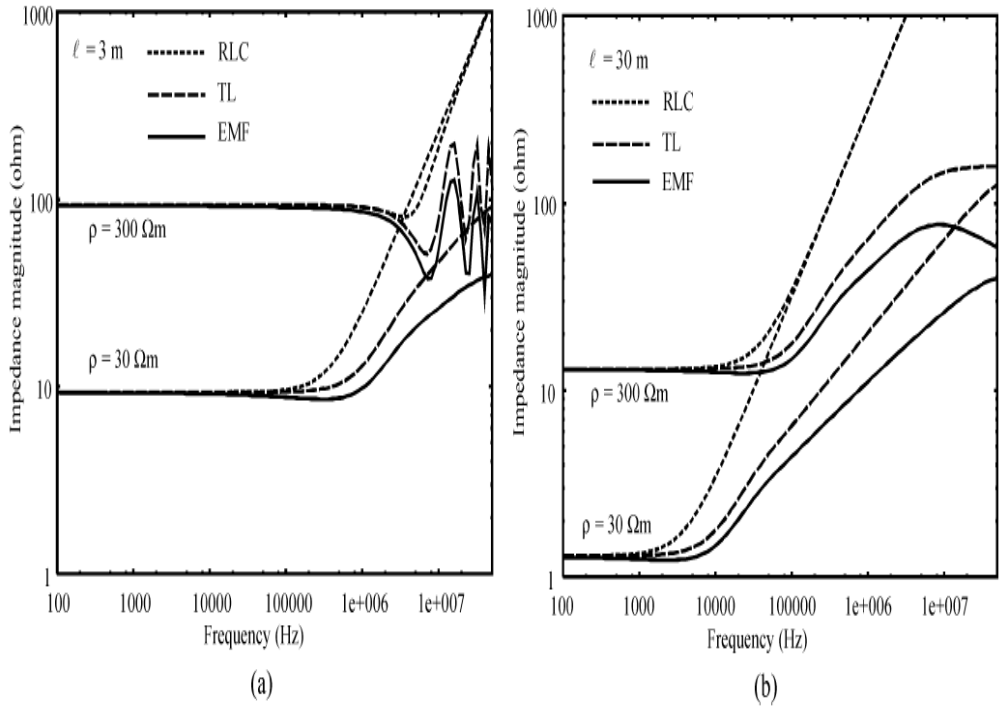

Figure 2.10: High frequency response of vertical electrodes: (a) l=3m, (b) l=30m (reproduced from reference [2.52])

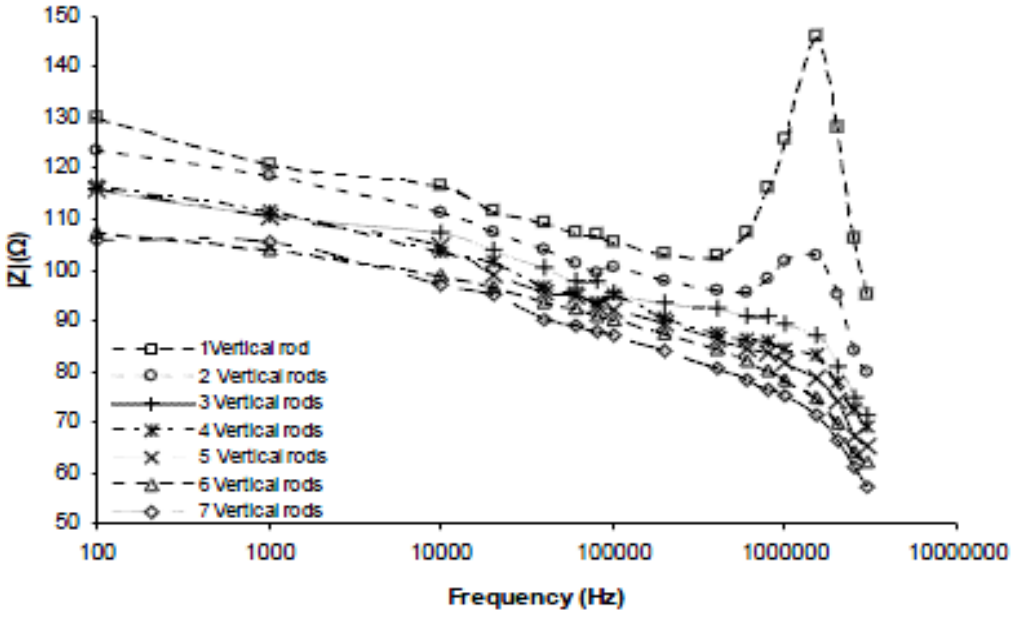

Figure 2.11: Effect of increasing the number of rods on the impedance modulus (reproduced from reference [2.53])

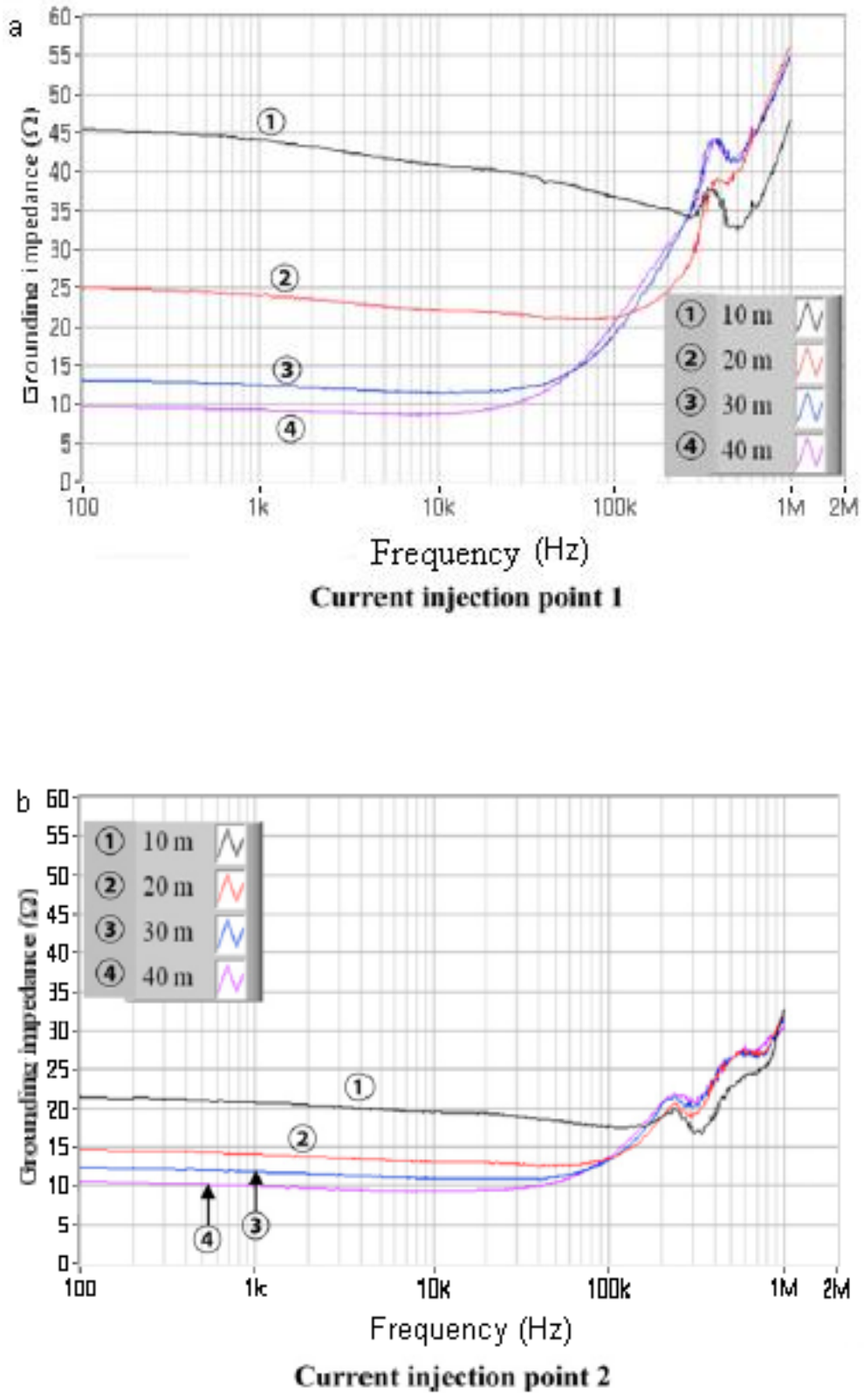

Figure 2.12: Frequency response of a 40m horizontal electrode buried in the two-layered soils (reproduced from reference [2.55])

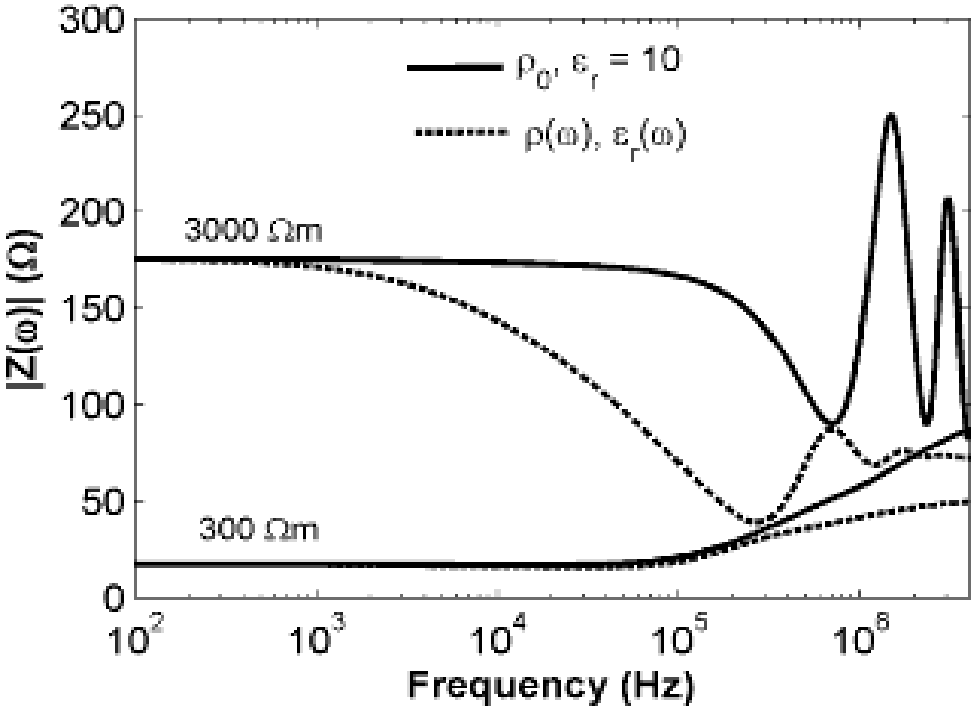

Figure 2.13: Frequency response for a 30m horizontal electrode (reproduced from reference [2.56])

2.6 Effective Length of Horizontal Earth Electrode

The effective length of earthing horizontal electrodes under lightning fast transient is very important when the earthing system is being designed. Many investigations into effective length have been published [2.58-2.65]. The effective length of a single buried horizontal electrode is that from the point of injected current to the point at which the voltage approaches 3% of its value at current entrance point [2.58]. Lorentzou et al. [2.59] presented another definition, which is the length above which no further reduction in the earthing impedance of a horizontal electrode is noticed, when the length of the electrode exceeds a certain value. In addition, '*the maximum transient voltage at injection point will not decrease any more, when the length of the conductor exceeds a certain value* 'was defined by Liu et al. [2.60].

Mazzeti et al. [2.61] conducted investigations of horizontal electrodes placed in soil having a resistivity of 30Ωm with the injected current having a waveshape of 25/100μs. The results showed that when the soil has low resistivity, a voltage drop occurs along the conductor due to the effect of inductance. Therefore, a certain effective length of conductor can be defined which governs current dispersion into the soil. They also found that the effective length of a horizontal electrode increases with increasing resistivity.

A new formula to calculate the effective area of grid electrode with current injected at the corner or centre location was obtained by Gupta and Thapar [2.33]. Their formula for determining the effective length of a horizontal earth electrode is:

$$L_{effective\ length} = k(\rho\tau)^{0.5} \qquad (2.1)$$

Where L is the length of conductor in meters, ρ is the soil resistivity in (Ωm), and τ is the rise-time of the impulse of injected current in second. The coefficient k is in $(m/\Omega.sec)^{0.5}$, and is 1.4 for a horizontal electrode fed at one end while it is 1.55 when the current is injected into the middle of the conductor.

In another study by Munshi et al. [2.62], the authors used an analytical model of a horizontal electrode based on an equivalent transmission line. No significant benefit could be obtained by increasing the length of a horizontal electrode beyond the effective length. Lorentzou et al. [2.59] carried out simulations on a horizontal electrode under high impulse current of 31kA with a rise-time of 8/20μs. The results showed that the voltage peak per unit of peak injected current decreases when the length of electrode increases until it approaches a constant value at the electrode's

'effective length'. Griffiths et al. [2.63] studied the effective length using the distributed parameter model of earth electrodes over a range of frequencies 1MHz to 10MHz. They concluded that the electrode impedance decreases with an increase in the length of electrode until it reaches the characteristic impedance at the effective length.

The effect of the length of horizontal earth electrodes under high impulse current was simulated, and a new formula to calculate the effective length proposed by Chonghui et al. [2.64]. Using lumped parameters, they simulated a horizontal electrode with radius of 10mm, buried at a depth of 0.8m in soil of resistivity of 100Ωm and relative permittivity of 9. The impulse current had up to 50kA injected value with a rise-time of 2.6/50 μs. The simulation showed that the impulse earthing resistance reduces with the increasing length of the horizontal electrode, reaching a constant value when the length of electrode reaches a certain value, and this was thought to be due to the inductive effect of the earthing conductor increase with the increment of the conductor length, which gives rise to non-uniform current leakage along the conductor.

Griffiths et al. [2.65] conducted extensive computer simulations using a distributed parameter model and computer mode (CDEGS) to calculate the impedance of earth horizontal electrodes of different lengths in a range of frequencies up to 10MHz and resistivity values of 10Ωm to 10kΩm. They presented a new simple analytical equation to determine the effective length of horizontal electrodes. Elmghairbi et al. [2.66, 267] proposed a new technique for increasing this effective length for horizontal electrodes. Extensive tests were carried out under impulse conditions on an 88m horizontal electrode having cross-sectional area of 50mm^2, buried to a depth of 30cm. The aim of this technique was to connect an additional insulated conductor with a bare underground horizontal electrode at points along its length. The effective length of the

electrode was determined from the curves of impulse resistance. The results showed that a reduction in the impulse resistance of 22% was obtained in the case of the addition of a parallel-insulated conductor, representing an increase in the electrode's effective length.

2.7 Effective Area of Earth Grid

To obtain a reduction in the earth impedance of a grid electrode, the area of the grid is increased. However, this area has a limiting value, termed the 'effective area', beyond which no further reduction in earth grid impedance can be attained. Gupta and Thapar [2.33] reach this conclusion, and present a formula to determine the effective radius of an earth grid.

$$r_e = k(\rho T)^{0.5} \qquad (2.2)$$

Where r_e is in meters, k is the coefficient factor in $(m/\Omega.sec)^{0.5}$, and is (1.45-0.05s for centre fed, 0.6-0.025s for corner fed), ρ is soil resistivity in (Ωm), T is the impulse rise-time in second and s is the distance between grid conductors in meter.

They showed that the effective area for centre injection is higher than that for corner injection due to the increased inductance of the current path.

Grcev [2.68] conducted investigations on the effective area in which an electromagnetic field approach was used. Different sizes of area were selected ranging from $100\times100m^2$ to $120\times120m^2$. Impulse currents of fast rise-time were injected into the earthing grid electrode. The author found from the results that the effective area of earth grid as constrained to less than $20\times20m^2$ for fast impulse rise-time and corner injection point. It was observed that under high frequency and fast-front impulse

injection, significant reduction in earth grid impedance cannot be achieved when the area of earth grid exceeds the effective area. Grcev presented in his recent paper [2.69] a new formula to determine the effective area of the earthing grid. He reported that the formula suggested by [2.33] would be valid only for slow rise-time because the fast impulse has high frequency content. Grcev's formula is:

$$a_{eff} = k.exp[0.84(\rho T)^{0.22}] \qquad (2.3)$$

Where: α_{eff} is in meter, k=1 for centre fed or 0.5 for corner fed current, ρ is soil resistivity (Ωm) and T is the impulse rise-time and is in second.

Figure 2.14 shows a comparison of different formula results [2.33, 2.64, 2.69] for the effective area. It shows similar trends but gives quite substantial differences, which may be attributed to the difference in definitions of effective area.

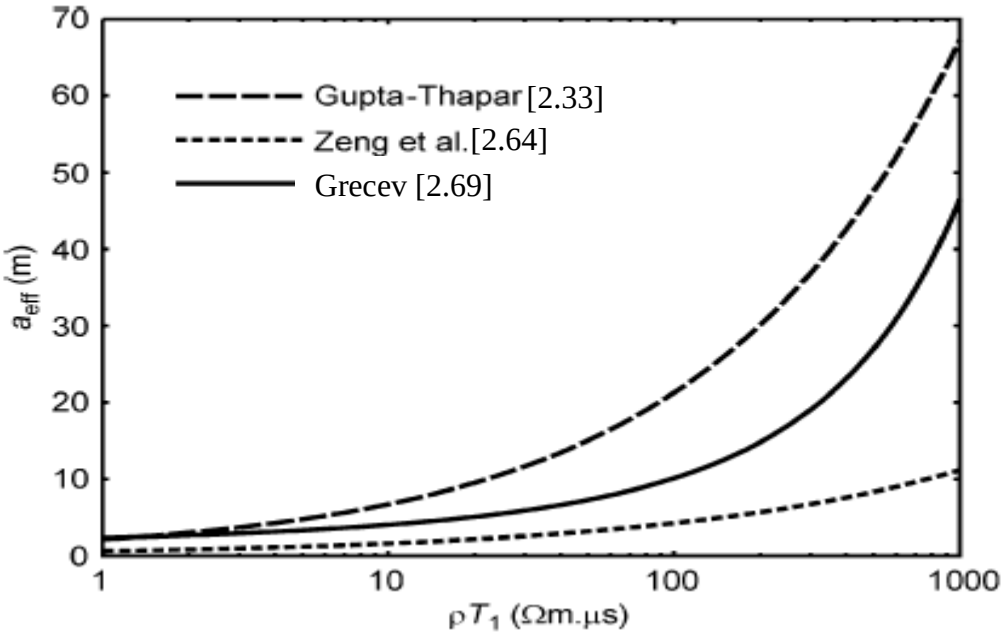

Figure 2.14: Comparison between different formulas for calculation of the effective area of a grid electrode (reproduced from reference [2.69])

2.8 Current Distribution of Earth Electrode Systems

Xishan et al. [2.70] carried out tests on an earthing grid in water under laboratory condition, in order to measure current distributions in the vicinity of the electrode. The grid had an area of $0.3\times0.3m^2$ and the number of meshes was 2×2. Current magnitudes up to 100mA were injected into the earthing electrodes. The results showed that the current distributions in the earth grid electrode were near symmetrical, while the current flowing into the vertical rods was dependent on the value of their resistances.

Tao et al. [2.71] carried out tests to investigate the current distribution in earthing electrodes with various structures under impulse conditions. Measurements were conducted inside a 5m-diameter hemispherical sand pond. A range of high impulse current transients with various magnitudes, and a fixed rise-time of 8/20μs, were injected into a single horizontal electrode, a vertical electrode, and a cross and star-shaped electrode. The results showed that the current distribution at points in the same electrode is not symmetrical, and that the current magnitude in the conductor reduces with the distance from the injection point and near to zero at the end of the electrode.

Ahmeda et al. [2.72] conducted experiments on a 88.5m counterpoise with a cross-sectional area of $0.2cm^2$ and buried to a depth of 30cm. A current impulse of 5.41A with wave shape 5.8/16μs was applied, and the voltage and current measured at different points along the horizontal electrode. The authors found that the reduction in current peak value was not uniform, as obtained by [2.71].

In addition, a time delay was observed on the voltage and current waveforms measured at different points, and this was attributed to the travel time of the surge throughout the length of the electrode. Most of the current injected was dissipated near to the injection

point, and the proportion was found to be independent of the magnitude of the injected current.

Choi et al. [2.73] tested a horizontal earth electrode of 40m length and 3mm diameter buried in a two-layer soil structure at a depth of 0.5m. The authors divided the length of the 40m horizontal electrode into four sections, each section 10m long. The soil was mixed with high conductivity powdered carbon at one end of the horizontal electrode, defined as point 2, while the high soil-resistivity end is defined as point 1. An impulse current with waveshape 2.4/81.9μs was injected into the 40m horizontal electrode. It was observed that for fast impulse rise-time, the behaviour of the earthing impedance was inductive, while the slow rise-time presented a resistive behaviour. The results showed that the majority of the injected current was dissipated near to the injection point, which is consistent with the result of [2.72], and the current was more easily dissipated into the sections with low soil resistivity (point 2), than those in the sections with a high soil resistivity (point 1).

A subsequent paper [2.74], reported a series of current distribution tests on a 50m horizontal earth electrode with the same specifications as in [2.73]. Impulse currents with rise-times of 4μs and 39μs were applied. It was observed from the measurements that the current dispersion into the soil in the case of the slow rise-time was dependent on the soil resistivity, and the majority of the injected current was dissipated near the injection point, as shown in Figure 2.15.

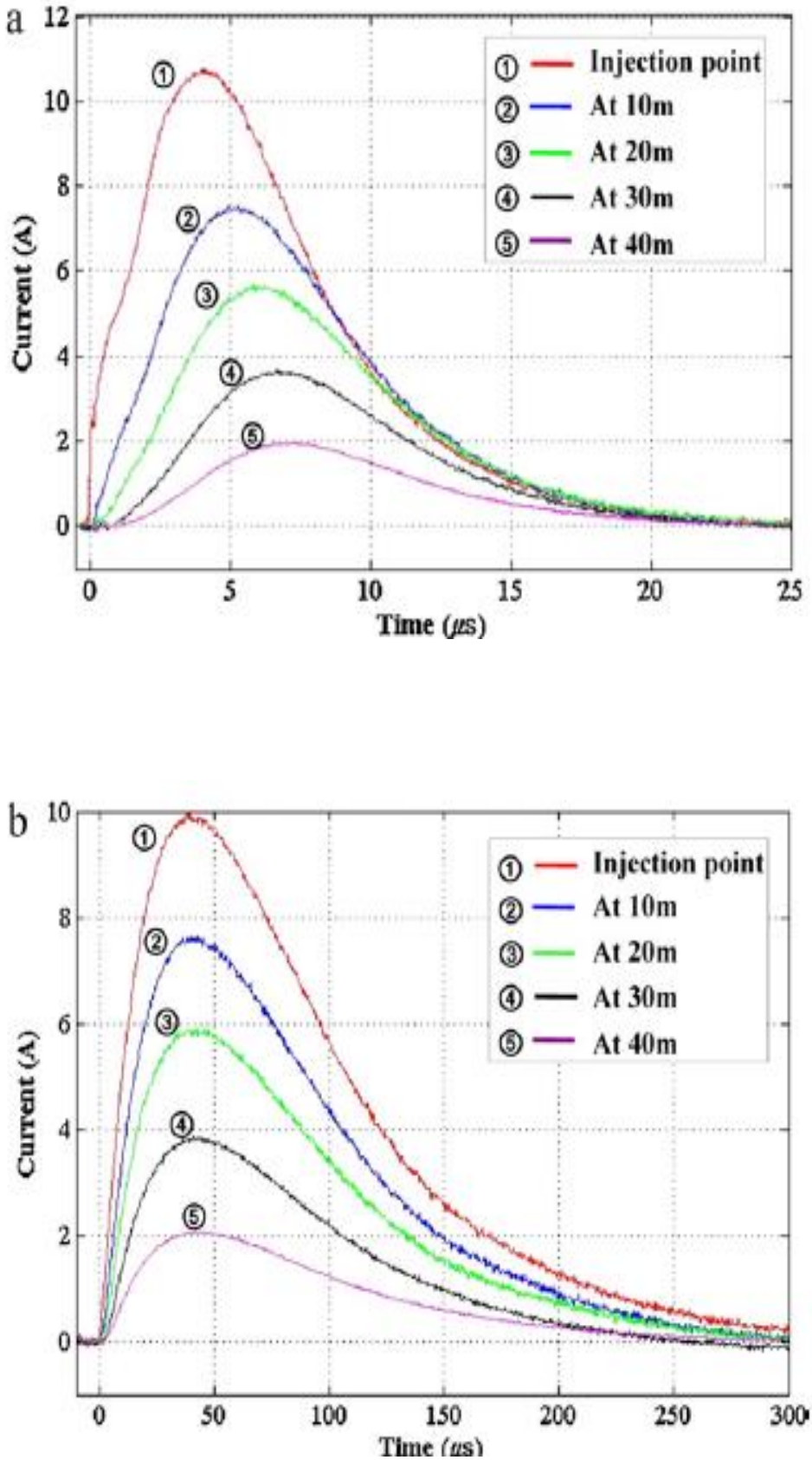

Figure 2.15: Current distribution waveforms for a 50m horizontal earth electrode: a) rise-time = 4μs, b) rise-time = 39μs (reproduced from reference [2.74])

2.9 Conclusions

In this chapter, an extensive review of high frequency and transient performance of earth electrodes has been undertaken. Published field tests, laboratory tests and computational work since the 1920s have been investigated. Special emphasis has been given to the high frequency and transient performance of earthing systems, including vertical, horizontal and grid earth electrodes, and the voltage and current distributions of earth electrode systems. In addition, studies have attempted to investigate the behaviour of earth electrodes using different approaches. Work has included high-voltage measurements, both in the laboratory and on electrodes installed in the field.

Most of the work reviewed presents the results of simulating high frequency and transient conditions using computer software. However, very little has been published on field tests at high frequency up to 10MHz. This aspect will, therefore, be the main thread of experimental work and simulation techniques presented in this thesis.

Many researchers have investigated the high frequency and transient performance of vertical earth electrodes. In this thesis, an improvement in the low/high frequency and impulse performance of vertical earth electrodes using horizontal enhancements is proposed and the results are reported, for rods buried in non-homogenous soil of low resistivity (Chapter 4, 5).

To date, there has been no publication of a comprehensive or detailed method for measuring detailed current distribution in earth electrode systems in the field. Accordingly, Chapter 6 will measure and simulate the voltage and current distributions for different earth electrode structures under low/high frequency and transient conditions. The aim here is to understand more clearly the role of enhancing the electrodes and their contribution to improve both low and high frequency performance.

Non-linear soil behaviour under high current magnitudes have been investigated by many researchers, and they found that the impulse resistance decreases when increasing the current magnitude but with dependence on the factors such as soil resistivity, area of earth electrode and current magnitude. However, no detailed studied to examine different length rods with horizontal enhancements at the same location were investigated.

CHAPTER THREE: LONG TERM SOIL RESISTIVITY ANALYSIS AT LLANRUMNEY FIELD SITE

3.1 Introduction

Given that the earth electrode resistance is proportional to the resistivity of the soil in which it is buried; soil resistivity tests are a very important first stage in the design of earthing installations. Therefore, accurate modelling of soil resistivity is an important prerequisite for predicting the performance of a particular earthing system in designing a new system. The most reliable means of getting the soil resistivity investigation is by conducting soil resistivity measurements around the location of the earthing systems prior to installation.

Soil resistivity is principally affected by the type of soil (clay, shale, etc.), moisture content, electrolytes content (minerals and dissolved salts) and temperature [3.1]. Soil resistivity will, therefore, exhibit seasonal variation.

In this chapter, the results of a long term investigation of the soil resistivity over a number of years [2002- 2003] and [2008- 2011] at four locations at the Cardiff University earthing test site at Llanrmuney are analysed**.** The results in this thesis from 2002 to 2003 and from 2008 to 2009 are the work of previous researchers, and results from 2010 to 2011 were obtained by the candidate. The tests were carried out at the test site using two different instruments: (i) Megger DET 2/2; (ii) the ABEM Terrameter and difference between readings obtained from the two meters are investigated. The effect of seasonal variation of the soil resistivity is included, and a soil resistivity survey at the location of test electrodes is also investigated. Finally, 2D soil resistivity inversion at selected locations is performed, so that the degree of reliability of the resistivity imaging was increased.

3.2 Factors Influencing Soil Resistivity

The earthing of an electrical system requires electrical connection to the general mass of earth [3.2]. The resistivity of the soil depends on many factors such as temperature, grain size distribution and packing of soil and concentration of dissolved salts in the contained water, and has a significant effect on an earthing system's performance [3.1]. Examples of typical soil resistivity ranges for various soil types are shown in Table 3.1 [3.2]. The values are given for normal to high rainfall conditions (greater than 500mm per year).

Table 3.1: Examples of soil resistivity (Ωm)[3.2]

Type of soil	Typical resistivity range (Ω.m)
Clay	5-20
Marls	10-30
Porous limestone	30-100
Porous sandstone	30-300
Quartzities, compact and crystalline limestone	100-1000
Clay slates, saltey shales and granite	300-3000
Igneous rock	1000 upwards

3.3 Review of Soil Resistivity Measurement Techniques

Measuring the resistivity of the soil gives details about its physical structure which may be used in the model. The simplest soil model assumes a single homogenous layer of infinite depth. This single layer representation is usually considered to be overly simplistic, as per standard [3.3], and a more realistic representation is suggested by increasing the number of layers as shown in Figure 3.1.

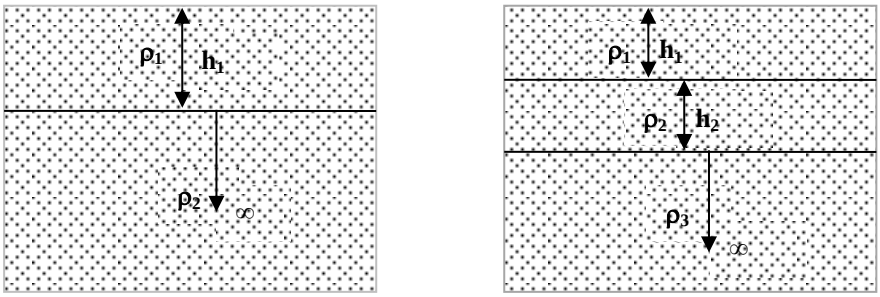

Figure 3.1: Two and three soil layer model representations

Generally, the top layer has a higher resistivity than the bottom layers due to increasing water content with depth. For a substation, the upper layer can often be assumed to have a high resistivity due the use of stone chippings on the surface [3.4]. Soil resistivity measurement generally involves injecting a current into the general mass of the earth and measurement of the surface potential at specific locations in the immediate vicinity of the injection point. The classical methods as proposed by Frank Wenner in 1915 [3.5] are still widely used today [3.1].

3.3.1 Wenner Configuration

The Wenner configuration is the most commonly used test method to investigate the resistivity of soil [3.6]. The Wenner configuration is depicted in Figure 3.2. Four vertical electrodes are driven into the ground, equally spaced along a straight line. A current is circulated between outer two electrodes ′C1′ and ′C2′ , producing a potential on the surface ′V′ which is measured between the inner two electrodes ′P1′ and ′P2′. The Wenner configuration is characterised by an equal spacing between all of the electrodes, that is termed the ‘Wenner spacing’, ‘a’.

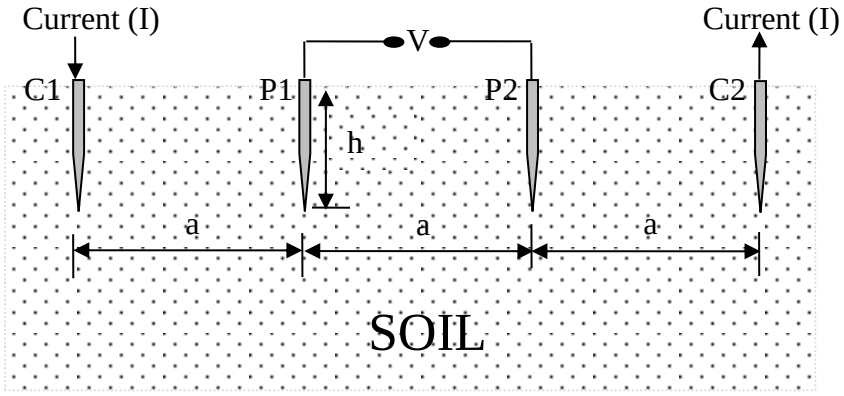

Figure 3.2: The Wenner configuration

From these electrode configurations C1, P1, C2, and P2, the soil resistivity can be calculated from Equation (3.1) [3.5]:

$$\rho = \frac{4\pi aR}{1+\frac{2a}{\sqrt{a^2+h^2}}-\frac{2a}{\sqrt{4a^2+4h^2}}} \qquad (3.1)$$

Where:

ρ: is the apparent soil resistivity (Ω.m)

R: is ratio of measured voltage to injected current

a: is the distance between electrodes

h: is the depth of electrode

The distance between electrodes, a, is generally much greater than the driven depth, h. To measure the resistivity of the soil at different depths, the distance between electrodes, a, is increased and the measurements repeated. Therefore, the apparent

resistivity as function of the distance between two electrodes, a, which provides an indication of the change in soil resistivity of the earth as a function of depth. The advantage of the four electrode technique arises from the separate current and potential circuits. This allows potential drop in the potential circuit due to electrode contact and lead resistance to be eliminated. Therefore, the voltage difference measured at the voltmeter terminals is equal to that on the soil surface between the potential electrodes (neglecting any induced effects) [3.5].The ratio of the potential difference divided by the current passed, provides the measured resistance.

3.4 Description of Test Site and Locations of Resistivity Surveys

The first location at the university test site is shown in Figure 3.4, showing the survey lines from the first round of tests using the MEGGER DET2/2 tester (2002) [3.7]. Seven lines perpendicular to the line route (orthogonal lines) were selected to the right of the tower (labelled R_1 to $R_{7)}$, and eight lines to the left (labelled L_1 to $L_{8)}$. The lateral spacing between these lines was fixed at 10m. A further nine (labelled H_1 to $H_{9)}$ lines were chosen at 20m intervals in a direction parallel to the transmission line route. The adopted survey line lengths were 180m for the Megger DET 2/2 and 240m for the ABEM Terrameter system. Figure 3.5 shows the satellite image of a second location of resistivity tests in Llanrumney in 2009. Figure 3.6 shows the location of soil resistivity measurement for a third round of tests (2009-2010). The fourth test location for soil resistivity measurement is shown in Figure 3.7 (2010-2011), with an area of $240\times65m^2$. Fourteen profiles were selected with 5m separation between profiles to investigate the soil resistivity An ABEM Terrameter SAS 1000 [3.8] and associated LUND imaging system earth tester were used. 2D resistivity inversion software [3.9] was then used to analyse the measured data. Post-test analysis enabled 2-D map of the subsurface soil resistivity to be obtained.

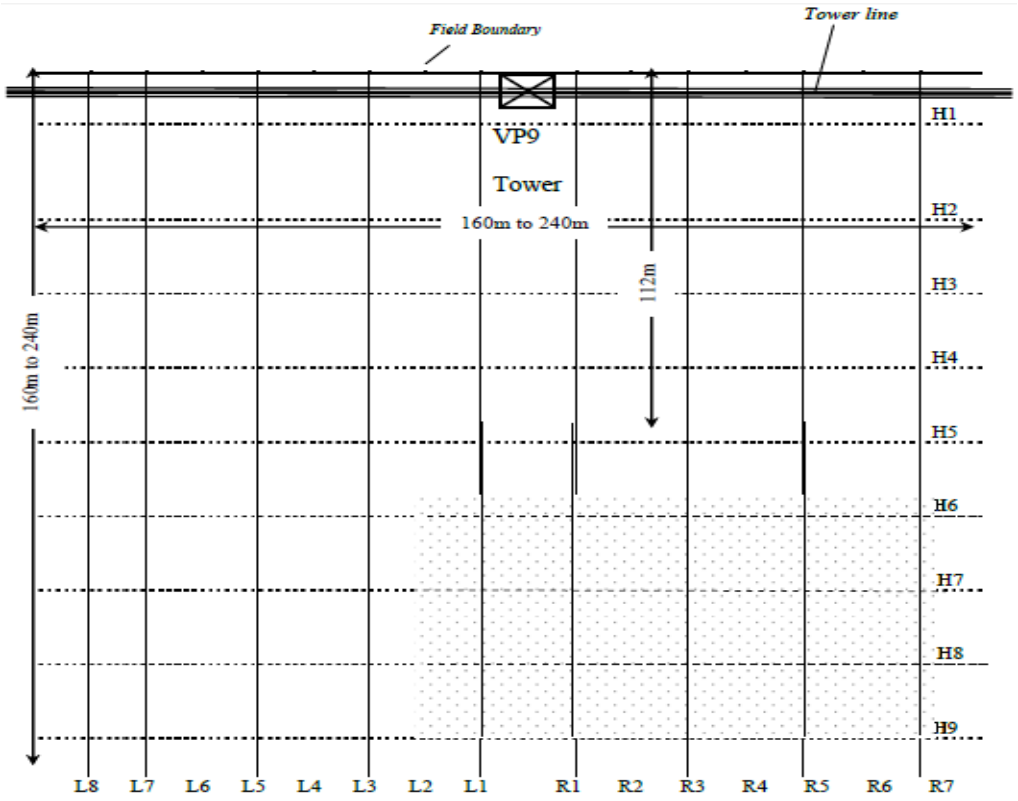

Figure 3.4: Diagram showing lines used for soil resistivity survey for location 1 (2002) (reproduced from reference [3.7])

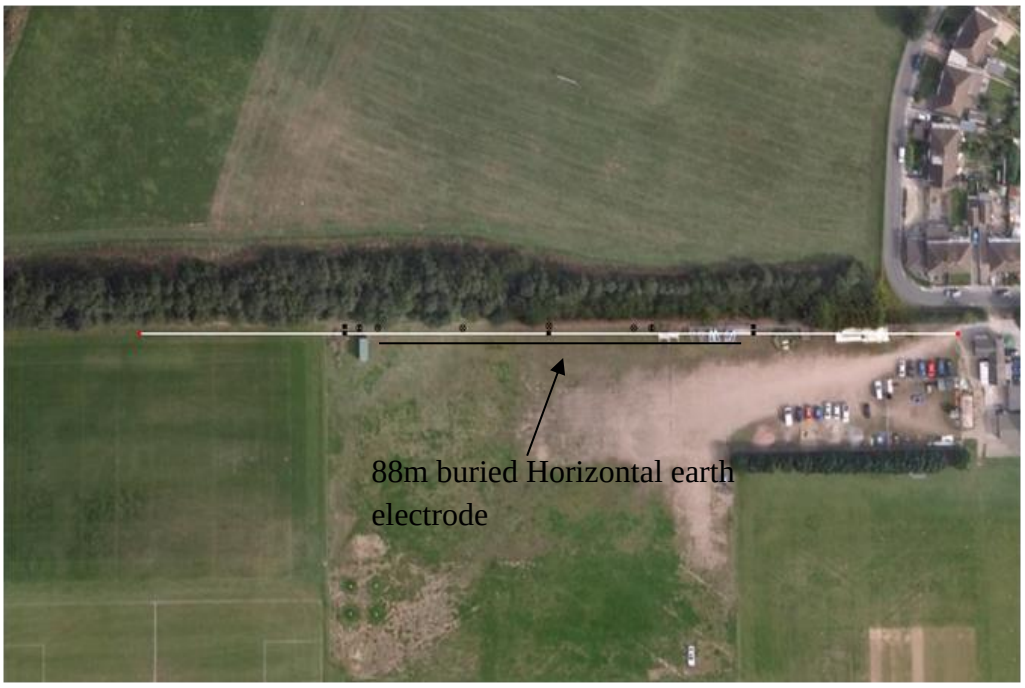

Figure 3.5: Satellite image of measurement location 2

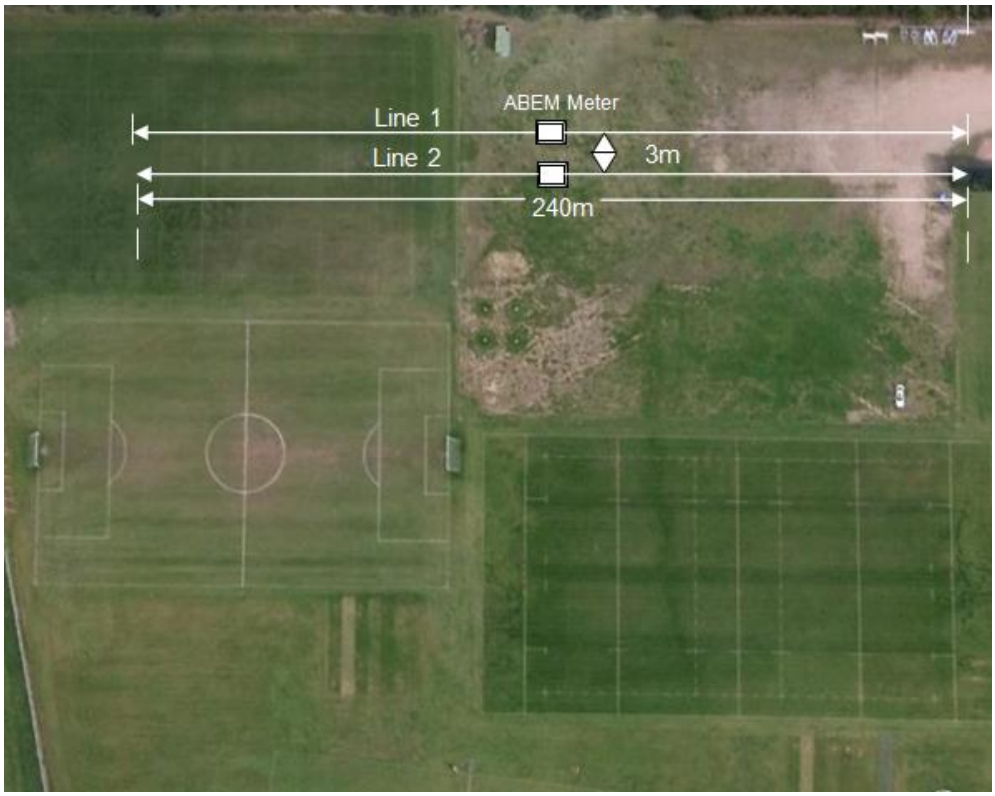

Figure 3.6: Satellite image of measurement location 3 at Llanrumney field site.

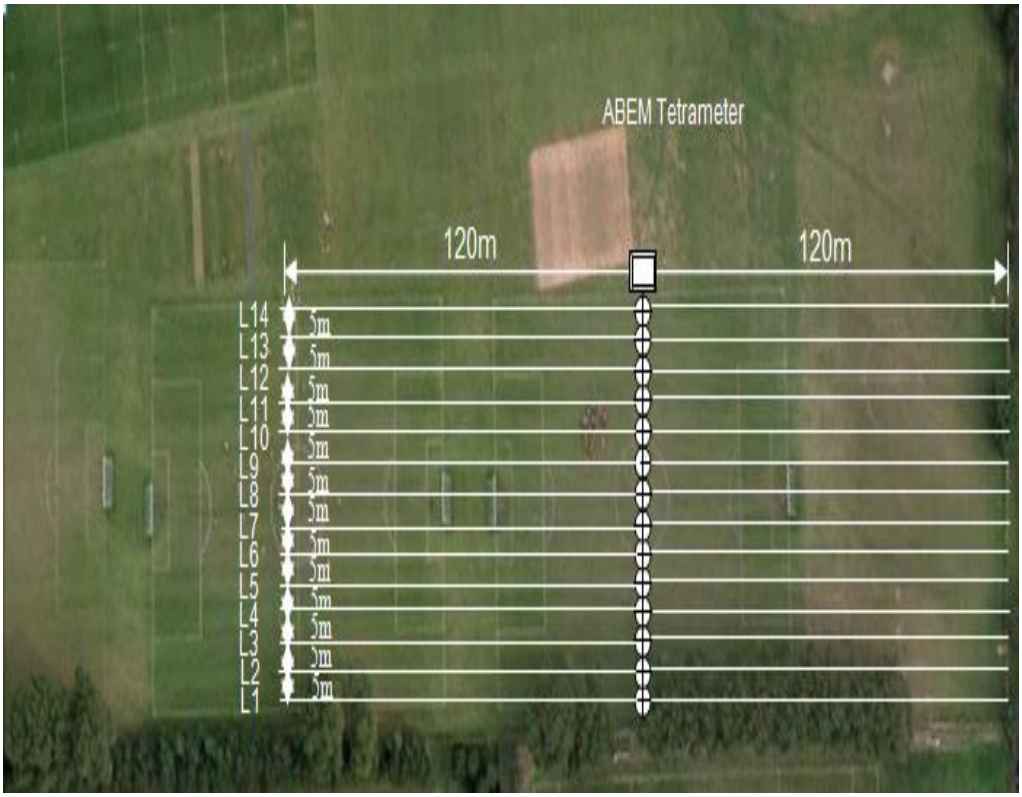

Figure 3.7: Satellite image of measurement location 4 at Llanrumney fields

3.5 Description of Test Instruments and Electrode Setup

This section describes the two instruments used for measuring the soil resistivity at the test site; the Megger Det 2/2 and the Lund/ Abem SAS 1000 Terrameter.

3.5.1 Megger Det 2/2 Earth Tester

The MEGGER DET 2/2 is a switched d.c. test instrument, manufactured specifically for field testing. It can measure earth resistances ranging from 10mΩ to 20kΩ with a resolution of 1mΩ [3.10]. The instrument can also deliver a maximum current of 50mA, at different frequencies between 108Hz and 150Hz with a default frequency of 128Hz. The current is injected between the two current terminals C_1 and C_2, and the potential difference measured between two potential terminals P_1 and P_2. Two multi-core cable reels of 100m each and a switch box allowed long and short Wenner spacings to be achieved for a given line without the need to change electrode positions [3.10].

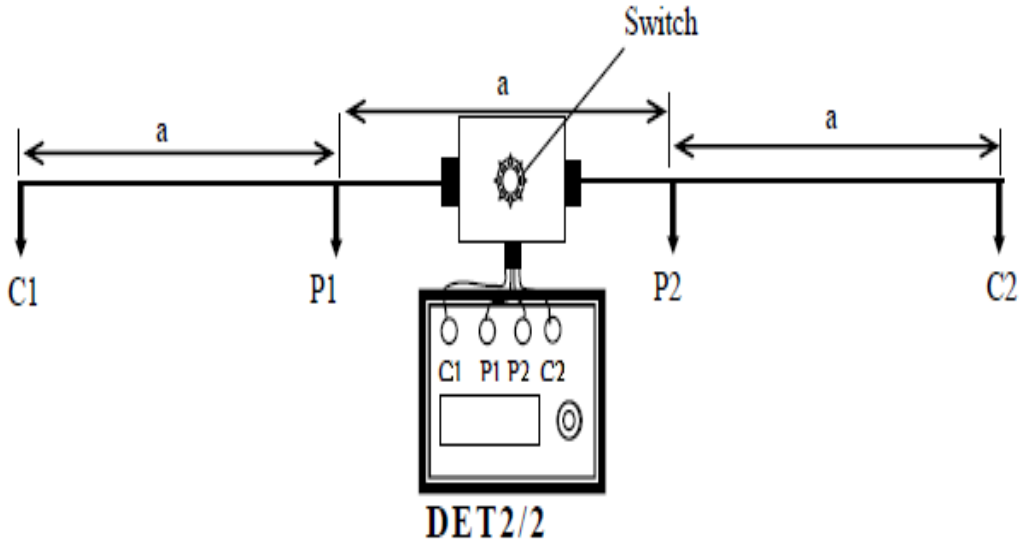

Figure 3.8: Soil resistivity measurement set-up using DET2/2 earth tester

Electrode spacings of 1m, 2m, 3m, 6m, 9m, 14m, 18m, 27m, 42m and 60m were used [3.7]. Figure 3.8 shows the experimental setup of the DET2/2, where the switch box and the measuring instrument are maintained in the middle of the array. The manual switch was used to change between positions. The reading is provided as a ratio of the potential difference to current injected, and then the soil resistivity is calculated using Equation (3.1).

3.5.2 Lund/ Abem SAS 1000 Terrameter

The Abem SAS1000 meter with Lund imaging system is shown in Figure 3.9. The Abem SAS1000 earth tester injects a dc current of up to 1A between the current electrodes, with a voltage of up to 400V. It offers the ability to display values for both earth resistance and soil resistivity. In the field test site, this instrument has been used with the Lund electric imaging system [3.11] which is designed for automatic resistivity profiling. The Lund is a multi electrode device employing a switched sequential measurement process. The system has a built-in microprocessor, which enables an automatic measurement process and data storage [3.11].

High-resolution graphical presentation and depth interpretation can be obtained by means of 2D inversion software. The probes are arranged in a straight line and are equally spaced, establishing an electrical contact with the earth at each point. During the survey, a minimum and a maximum electrode spacing were chosen as 3m and 72m respectively. A total of 61 electrodes were used along each survey line of 240m length. Table 3.2 summarises the number of readings per spacing.

Figure 3.9: Test set-up for the ABEM/LUND imaging system

Table 3.2: Number of readings per spacing

Spacing (m)	Number of reading
3	38
6	55
9	34
12	34
18	32
24	26
36	14
48	3
60	9
72	5
Total number of readings	250

3.6 Test Results

This section describes the test results of soil resistivity at the Llanrumney field test site at different location and date.

3.6.1 Soil Resistivity Results Obtained between at 2002 and 2003

Figure 3.10 shows the apparent resistivity results as a function of Wenner spacing as they were measured in 2002 [3.7]. The measurement results collected along the orthogonal lines are depicted in Figure 3.4. The minimum value of resistivity measured was 70Ωm, along line R_5 to the right of the tower with 60m Wenner spacing. The maximum value of resistivity measured was 165Ωm along line L_8 with the same (60m) Wenner spacing. For the survey, lines parallel to the tower line route (H_1 to H_9) and a 20m separation between survey lines was adopted. Figure 3.11 shows the apparent resistivity results plotted against Wenner spacing. The minimum value of resistivity recorded is 60Ωm at the line H_5 while the maximum value recorded is 314Ωm in the line H_7. For these surveys presented, the minimum inter-electrode spacing was set to 3m and maximum to 6m. 61 electrodes were used along each survey line of length 240m.

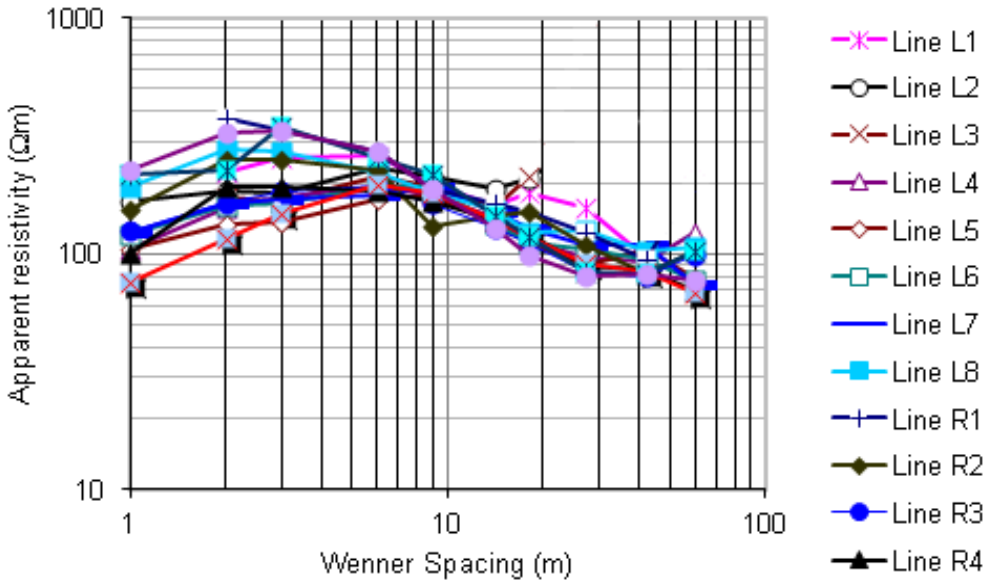

Figure 3.10: Resistivity curve measured at the Llanrumney site (DET 2/2), orthogonal to tower line (reproduced from reference [3.7])

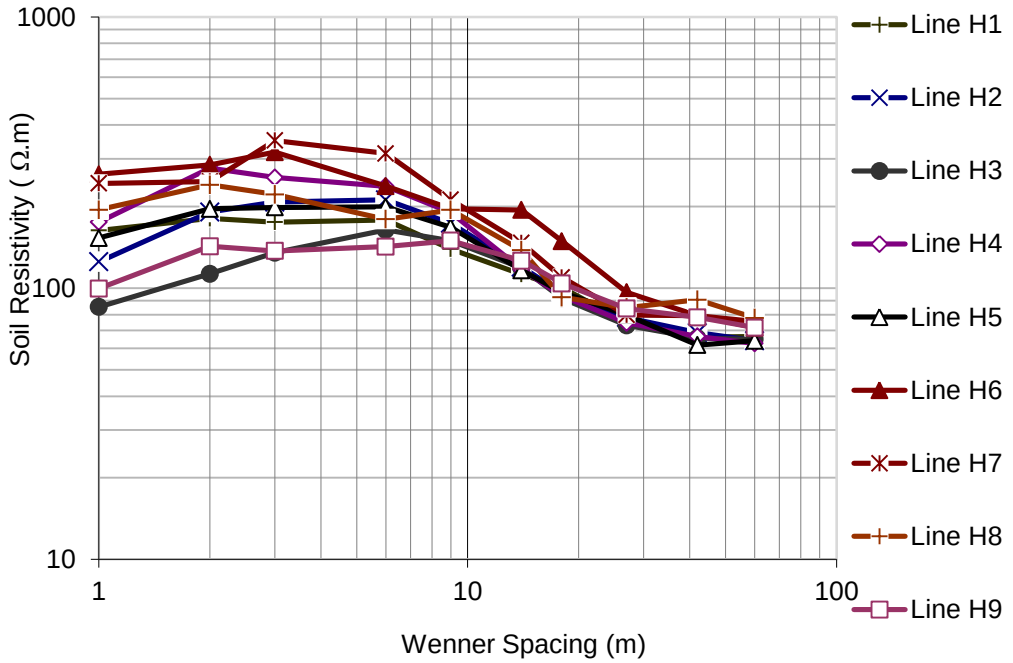

Figure 3.11: Resistivity curve measured in the Llanrumney site (DET 2/2), parallel to tower line (reproduced from reference [3.7])

3.6.2 Comparison of Soil Resistivity at Different Location and Date

Selected results of measured apparent resistivity curves are shown in Figure 3.12, where the average apparent resistivity of lines L_1, L_2 and R_1 are taken and plotted as a function of Wenner spacing. Soil resistivity measurements were performed along two parallel survey lines close to the earth rod location (the rod being located approximately 1.5m from each line) at the third location, as shown in Figure 3.6. Although the two profiles were only 10m apart, the results show that there are differences between the two profiles and that the soil is not strictly uniform within one layer of the same profile. For modelling purposes, the resistivity values measured at each electrode spacing (Wenner spacing) were averaged and a simplified average resistivity curve produced as shown in Figure 3.13.

A fourth location was chosen as per Figure 3.7, and fourteen profiles were measured with the separation between profile lines fixed. As has already been seen, the resistivity of the top layer varies significantly from one point to another, likely reflecting differences in water content in the upper and lower soil layers. The average values of the apparent soil resistivity are shown in Figure 3.14 for this fourth location. From Figure 3.14, the minimum and maximum values for the largest and smallest electrode spacings are 69Ωm and 294Ωm respectively. Generally, all the profiles represent the high value of soil resistivity in the upper layer, reducing with increased depth. From the curves obtained previously with the ABEM Terrameter for lines (13) and (14), a point-wise comparison cannot be considered because of the different profile locations. However, the range of values obtained with the same instrument give similar trends. Figure 3.15 shows the results for parallel lines (13) and (14), spaced 5m apart. Results of the survey lines 1 and 14, with a spacing of 65m, are shown in Figure 3.16. From this plot, it can be seen that the apparent soil resistivity along line 14 is higher than along line 1 with both the shortest and longest electrode spacing, which might be attributed to variation in soil moisture content.

Figure 3.17 shows the results of soil resistivity measurement along line R_1 of Figure 3.1 (at location 1). These measurements were taken at the same location on three separate dates in 2002 and 2003. From this figure, the value of the maximum soil resistivity increases significantly at the shortest electrode spacing, from 185Ωm in March 2002 to 359 Ωm in July 2003. At the largest electrode spacing, the resistivity decreases from 110Ωm in March 2002 to 60Ωm in October 2002 and July 2003. From these results, it is clear that seasonal variation of soil conditions has a significant effect on the observed soil resistivity at any given location. The soil resistivities were surveyed on 23/01/2009 and 01/04/2009 along the line selected for installation of the

88m horizontal electrode (location 2). Although, both measurements were conducted on different dates, there are no significant differences of the resistivities at the shortest electrode (the top layer) and the longest electrode spacing (the bottom layer) [3.12]

For the measurements conducted at Llanrumney test site, minimum and maximum electrode spacings were chosen as 3m and 72m respectively. A total of 61 electrodes were used to survey a line of 240m. For each survey set, 276 voltage and current readings at various positions and spacing were taken using the Wenner configuration. Figure 3.18 shows the average apparent resistivity for both sets of measurements plotted as a function of the Wenner electrode spacing. As can be seen from the figure, the apparent resistivity curves indicate a higher resistivity for shorter spacing (up to 10m) and a gradual fall up to 72m spacing. Such curves indicate the potential to apply a simplified 2-layer soil model with higher resistivity upper layer. The variations in measured soil resistivity with Wenner spacing, at location 3 between 2008-2010, are summarised in Figure 3.19. From the curve, it can be seen that the resistivity associated with the greatest electrode spacing varied between 138Ωm in 2009 to 65Ωm in 2010. The measured resistivity with the smallest electrode spacing varied between 296Ωm in 2008 to 116Ωm in 2009. Table 3.3 illustrates a comparison of the estimated values of the soil resistivity at different locations at Llanrumney test site. As can be seen from the table, the soil resistivity varies with time and location across the site. In addition, soil resistivity varies widely at the top layer due to changes seasonally and variations in the soil's moisture content and temperature.

Table 3.3: Summary of calculated values of soil resistivity from different test dates and locations

Date	Location	Soil Resistivity (Ωm)	
		Longest spacing	Shortest spacing
10/2002	1	300-650	60-70
07/2003	1	320-350	50-90
01/2009	2	160-200	60-80
04/2009	2	160-180	50-70
12/2008	3	200-250	40-65
11/2010	3	150-170	50-60
11 to 01/2011	4	160-250	60-70

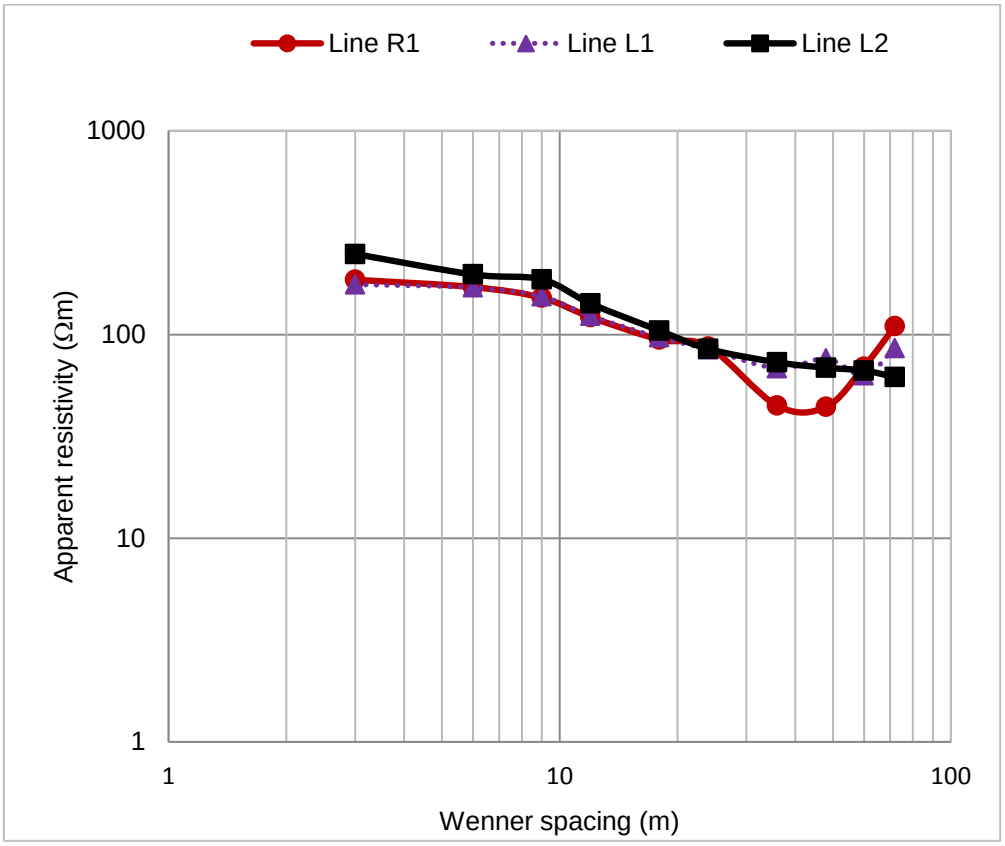

Figure 3.12: Average soil resistivity curves with the Lund imaging system (reproduced from reference [3.7])

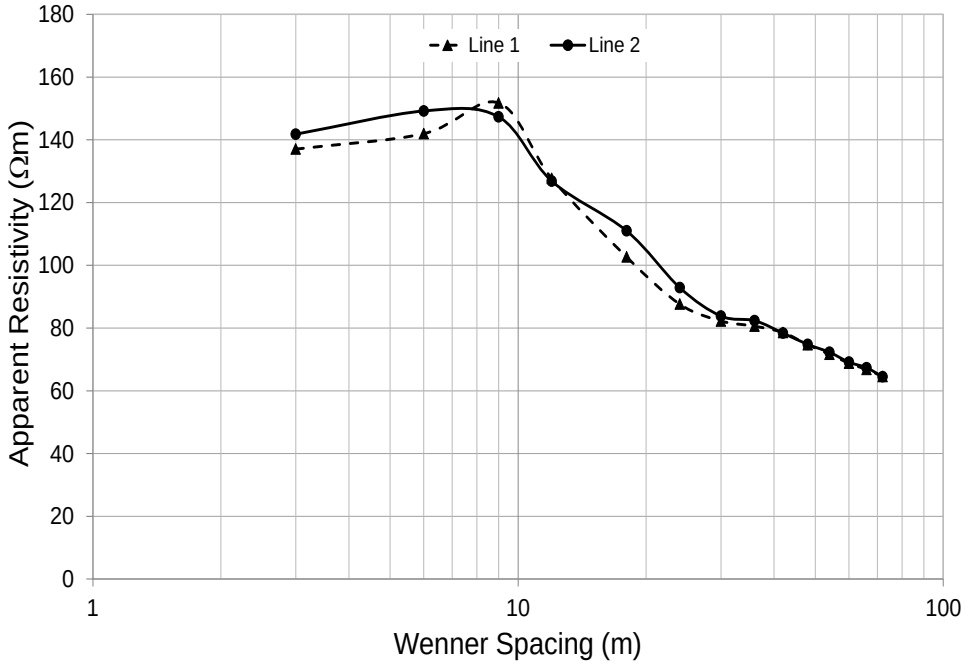

Figure 3.13: Average apparent soil Resistivity

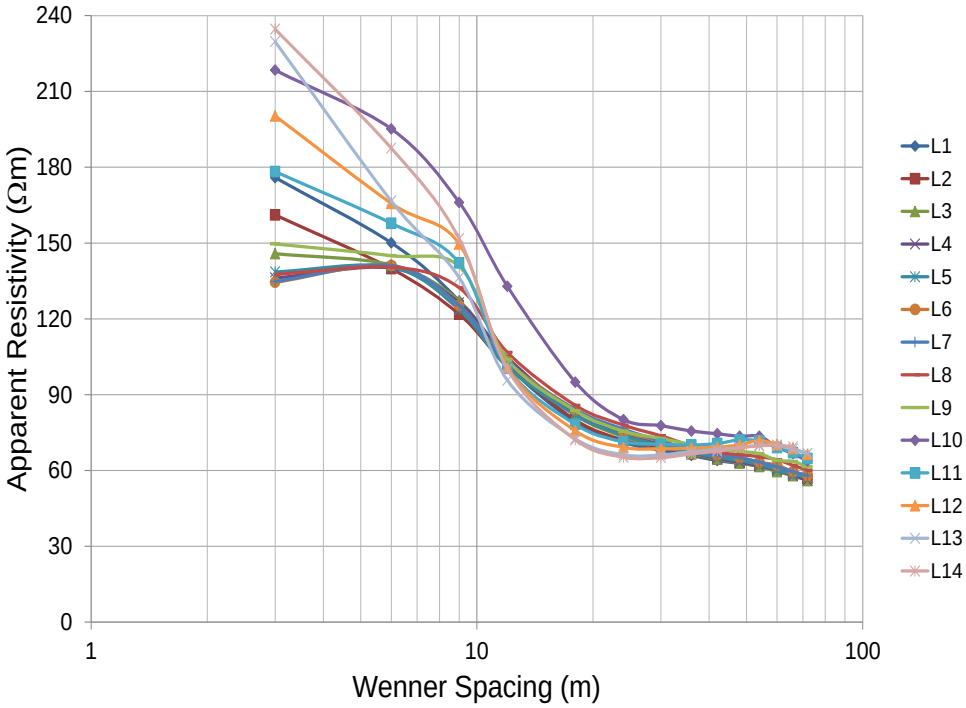

Figure 3.14: Apparent soil resistivity measured by ABEM Terrameter

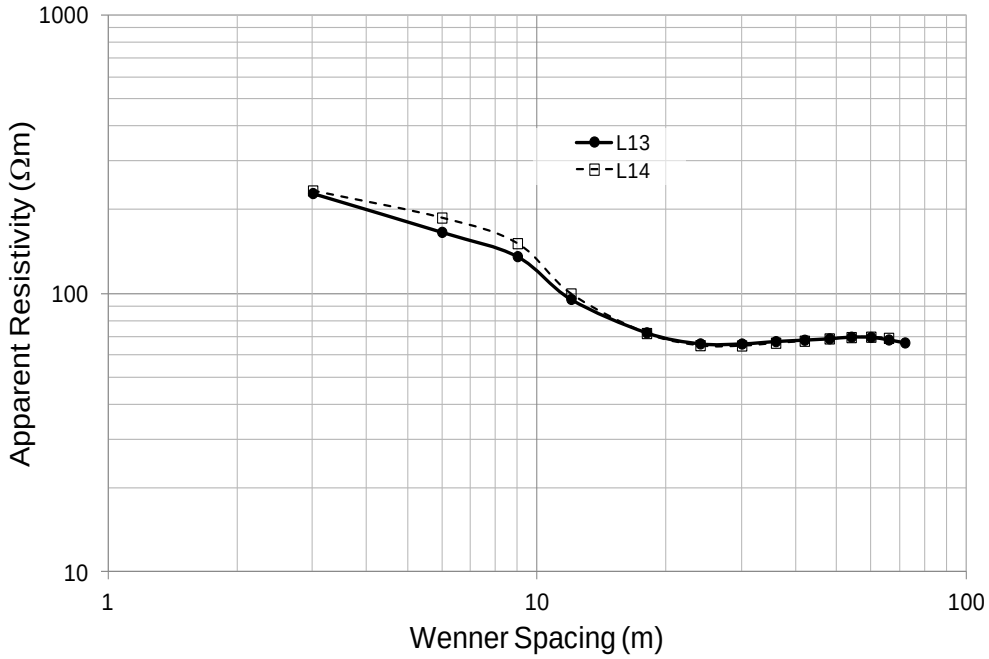

Figure 3.15: Selected results of average apparent resistivity obtained using ABEM meter at the Llanrumney field site

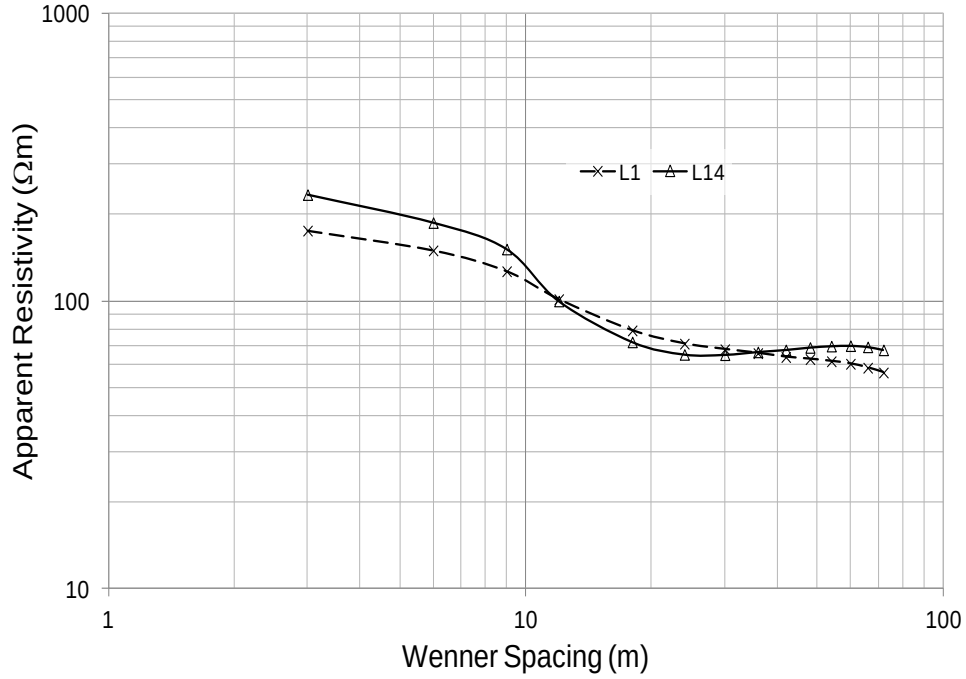

Figure 3.16: Average of apparent soil resistivity for line 1 and line 14 at Llanrumney site

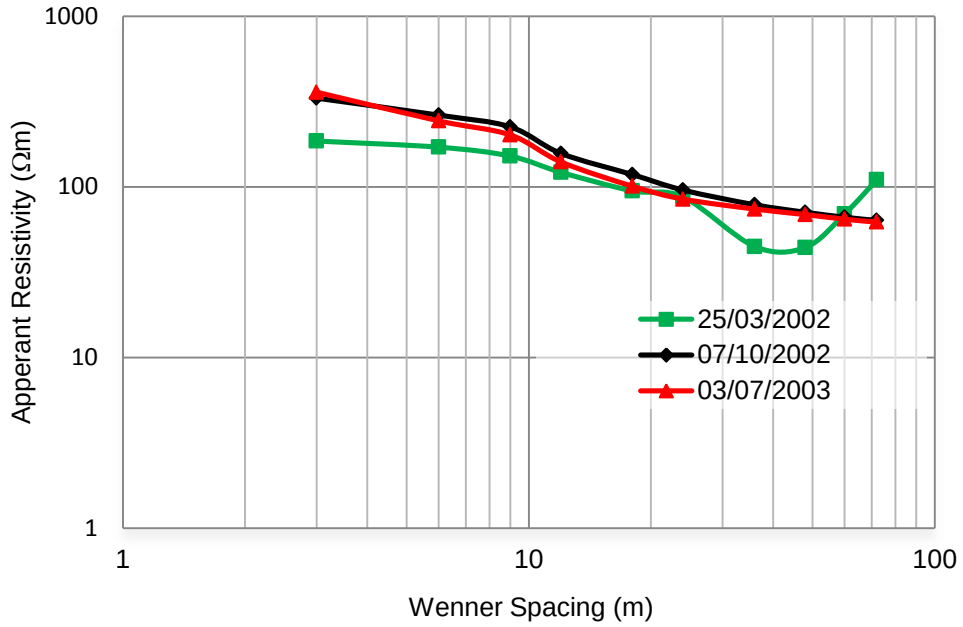

Figure 3.17: Soil resistivity measurements at line R_1 with different date (reproduced from reference [3.7])

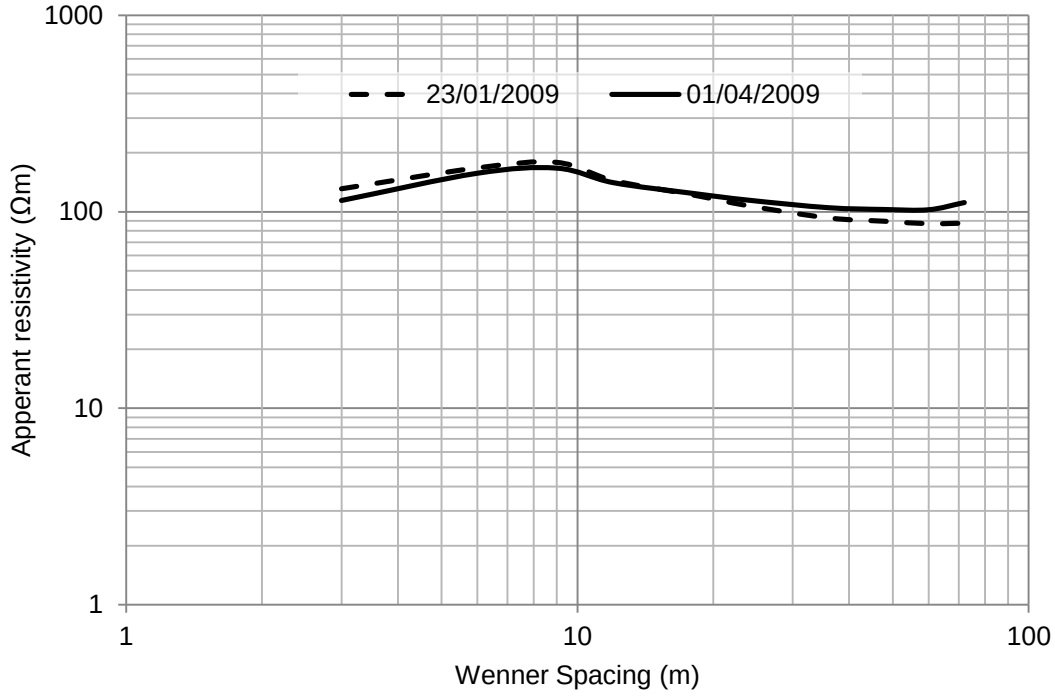

Figure 3.18: Average soil resistivity curves obtained for both lines (reproduced from reference [3.11])

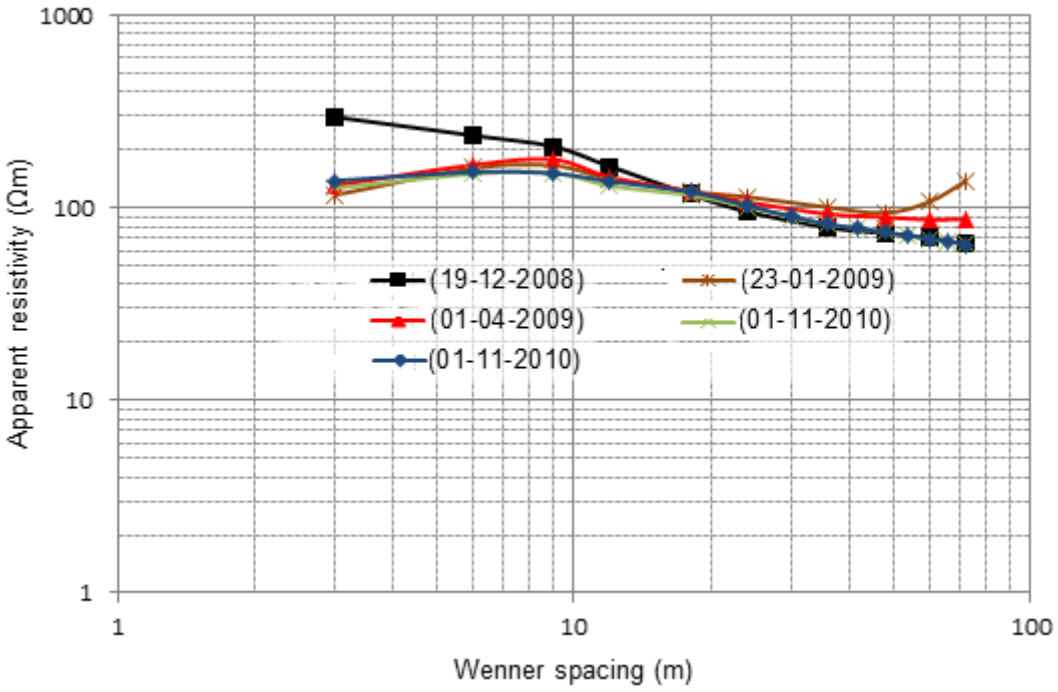

Figure 3.19: Selected results of apparent resistivity surveys obtained by ABEM Terrameter for location 2

The basic test (4 terminal measurements) was carried out 16 times at two different locations in 2010 and 2011. Figure 3.20 shows the examples of the average, minimum and maximum values at two locations, lines L1 to L2 for location one while L3 to L8 for location 4. As can be seen that, variations are due to different test spacing, different positions, changes in soil moisture, temperature and current test magnitude which is not always constant. Also mention that a single repeat test was carried out for one test location to establish repeatability of the commercial test meter and automated survey switching system/rest set up. Mention also that significant effect in variation in values is due to position, spacing and soil moisture which leads to a level of uncertainly in any assumed model. Further, that this helps to justify the adoption of a relatively simplified two layer model.

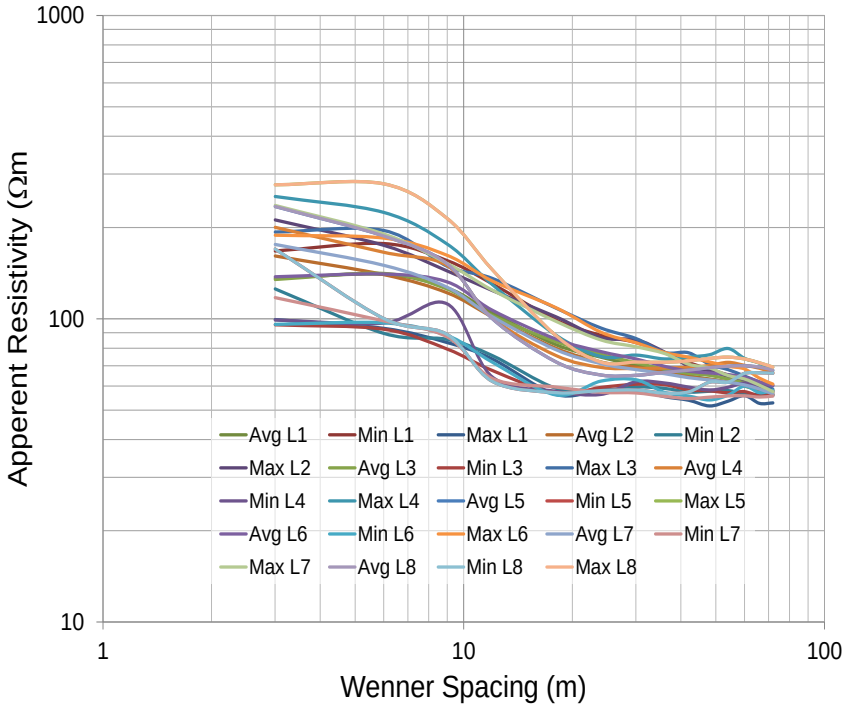

Figure 3.20: Maximum, minimum and average for different lines

3.6.3 Comparison between Results Obtained with Megger DET2/2 and ABEM Terrameter

This section describes a comparison of measured results from two earth testers. In order to compare results obtained by the both the conventional Wenner and the 2-D setup using Wenner technique, average values were calculated for lines H_1 and L_1 in 2002. During the test, a number of readings were taken at each electrode spacing at different locations along the survey lines as shown in the Table 3.2. Therefore, the average values correspond to one reading per spacing for the purpose of comparison. Figure 3.21 shows a comparison of the results obtained for each line with the two test instruments. Although the results obtained with the DET2/2 correspond to single spacing and for a shorter line, the curves generally agree with the subsurface soil structure (two layer soil model).

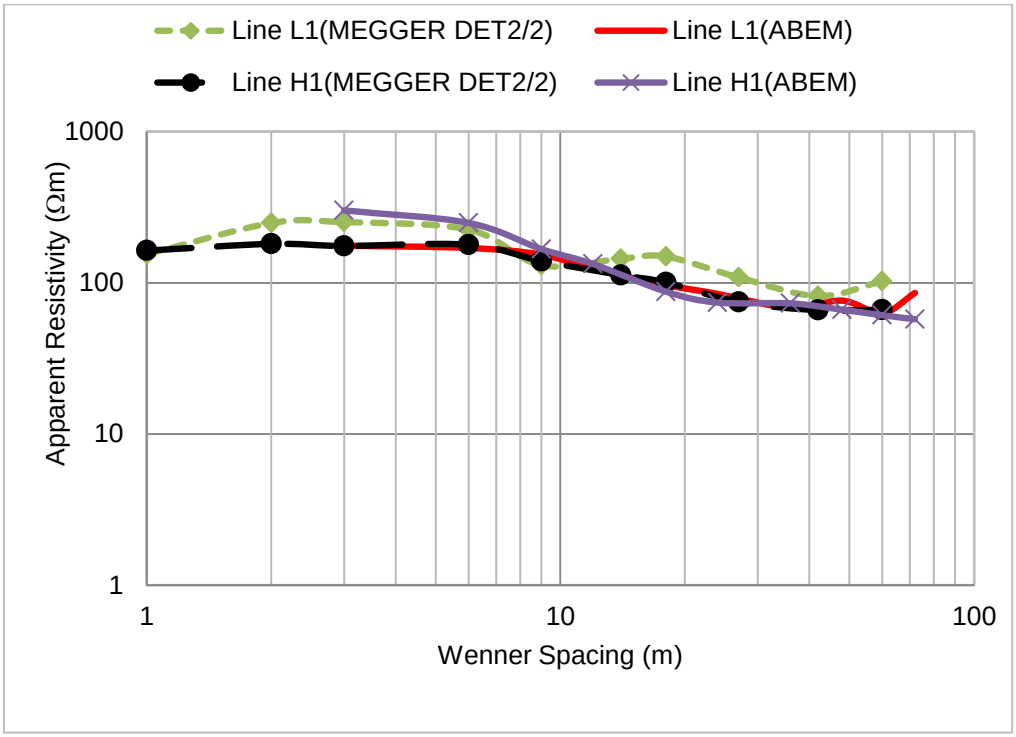

Figure 3.21: Comparisons between ABEM and DET2/2 survey results (reproduced from reference [3.7])

3.6.4 Different Dimensional Resistivity Models

Soil resistivity modelling has developed greatly, from the traditional 1D model which use only horizontal layering to 2D and 3D models which give a more detailed picture of the subsurface resistivity; three models are shown in Figure 3.22.

The major limitation of the 2D geoelectrical resistivity imaging is that measurements made with large electrode spacing are often affected by the deeper sections of the subsurface as well as structures at a larger horizontal distance from the survey line [3.9]. The software uses a least-squares inversion technique to generate a 2D map of the soil structure from the input survey data. Fourteen earth resistivity lines as depicted in Figure 3.7 were surveyed at the Llanrumney field test site.(location 4). For each test profile, the apparent resistivity distribution and the curves of the maximum, minimum

and average apparent resistivity values as well as 2D inverse models were derived. Figure 3.23 a and b show an example of a 2-D resistivity inversion for a test lines (13) and (14). The contours indicate an upper soil layer having a depth of 5m with resistivity values ranging from 230Ωm to 312Ωm, and a bottom layer with a depth of 23m and resistivity around 70Ωm.

The results of soil resistivity inversion at location 3 are shown in Figure 3.24 (a) for line L1 while (b) for line 2. From the 2D soil structure maps, the contours indicate a top soil layer for all the results having different depth with different values of resistivity. Although the top soil layer have values ranging between 120Ωm and 160Ωm and a bottom layer with soil resistivity ranging between 45 Ωm and 60Ωm, the maps give an improved view of the subsurface resistivity stratification.

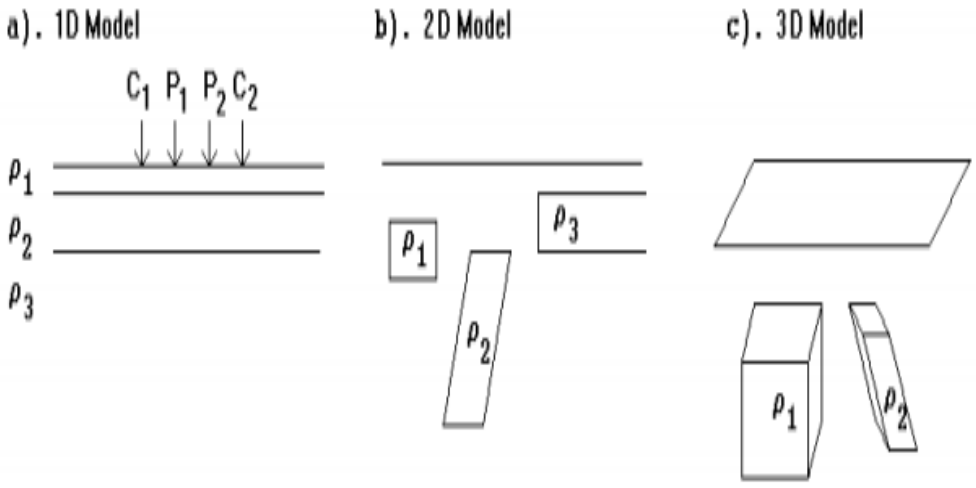

Figure 3.22: Different models used in the investigation of resistivity tests (reproduced from reference [3.13])

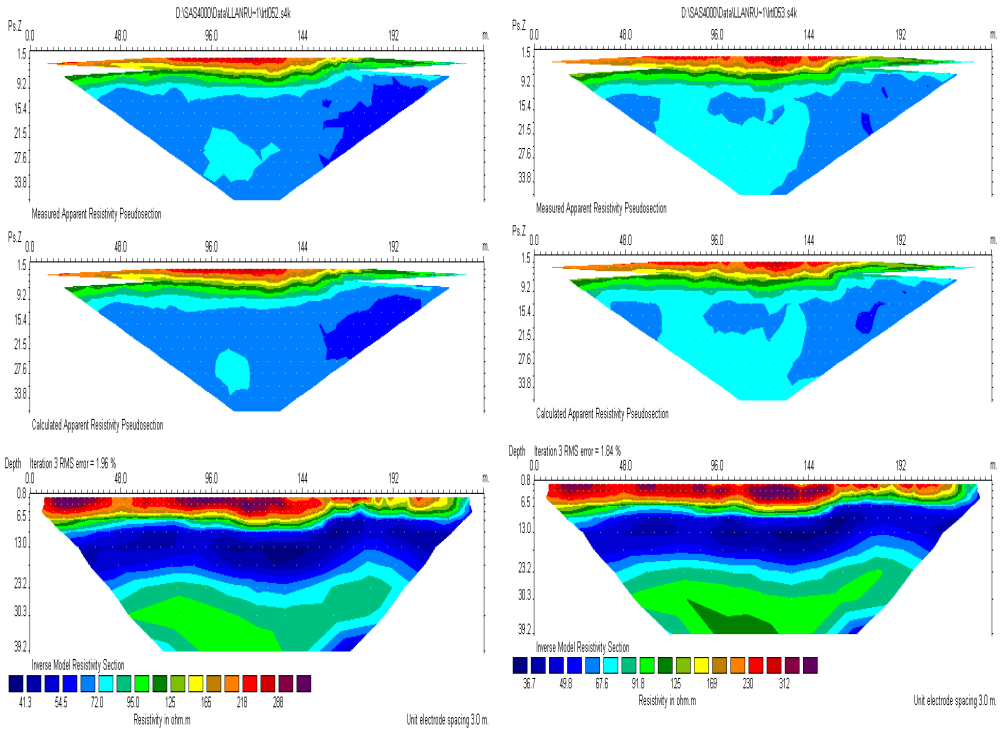

(a) (b)

Figure 3.23 a, b: Selected results of inverse model 2D-plot for two lines of location 3: a) line 13 and a) line 14

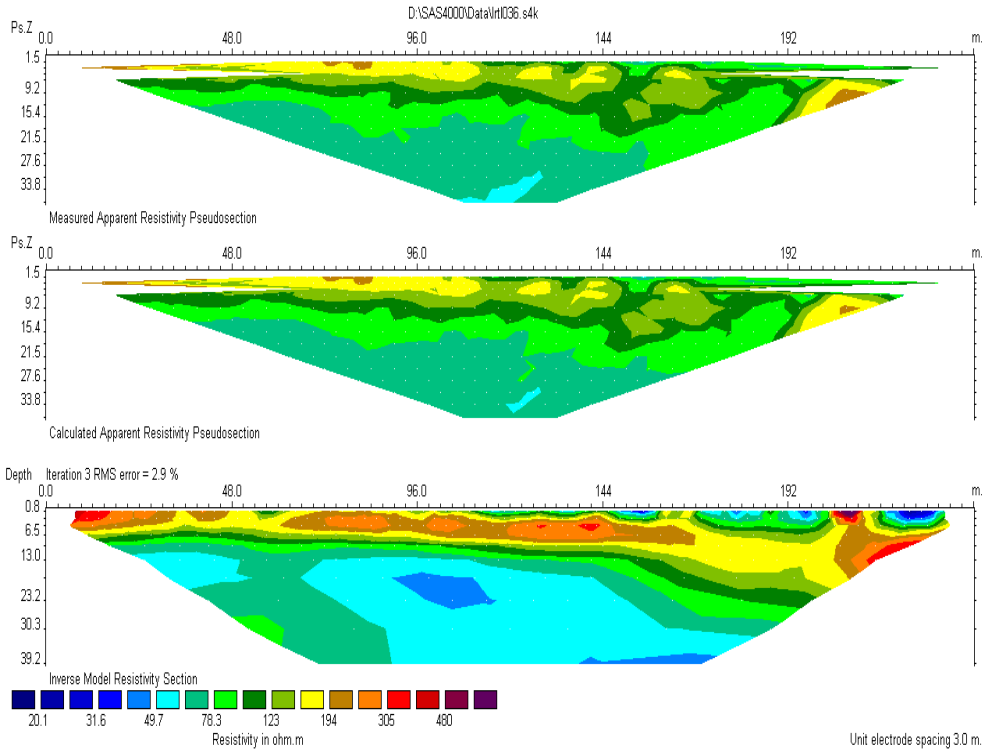

a) Survey line 1

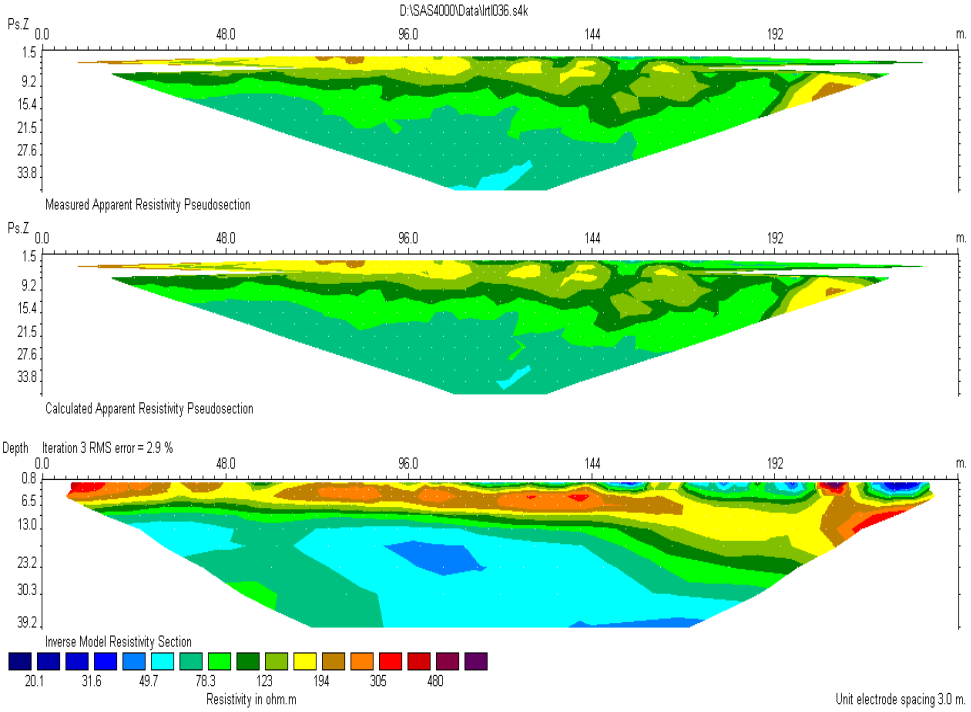

b) Survey line 2

Figure 3.24: Inverse model 2D-plot for line 1and 2 at location3

3.7 Adopted Models for Test Electrode Locations

The soil resistivity was measured prior to installation of vertical and a horizontal electrode at the Cardiff University earthing field test facility at Llanrumney.

Soil resistivity measurements were performed along two parallel survey lines close to the earth rod location (the rod being located approximately 1.5m from each line). High-resolution graphical presentation and depth interpretation can be obtained by 2D inversion software in the form of colour resistivity maps. Figure 3.25 shows an example of 2-D resistivity mapping for the two profiles.

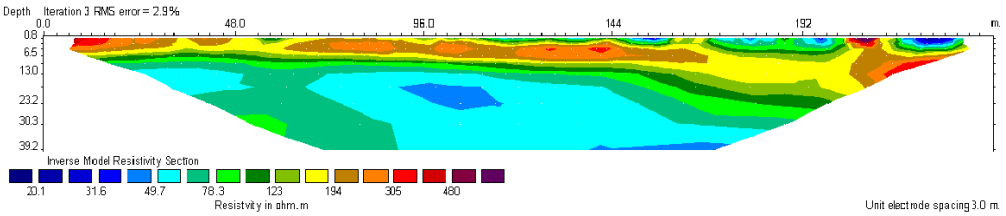

(a) Line 1

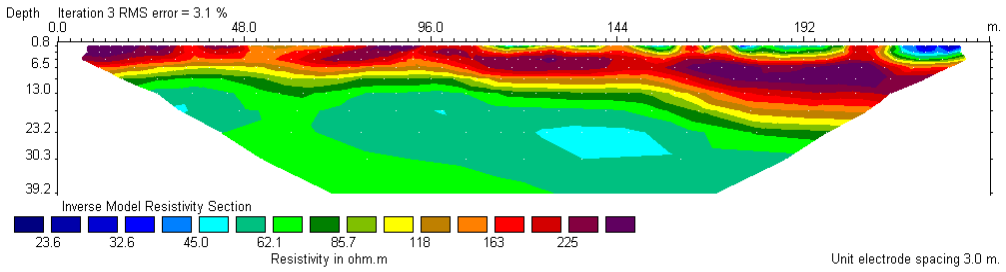

(b) Line 2

Figure 3.25: 2D model for Line 1 and line 2 at the rod location of test site

The contours indicate a top soil layer having a depth of about 10m with resistivity ranging between 120Ωm and 160Ωm, and a bottom layer with soil resistivity ranging between 45 and 60Ωm. Based on actual measurements, a computational soil model was proposed having a top layer resistivity of 150Ωm to a depth of 10m and a bottom layer of infinite depth having a resistivity of 55Ωm

The soil resistivity measurements at the location of the 88m horizontal electrode before installation were conducted on two different dates. Figure 3.26 shows the 2-D apparent resistivity pseudosections obtained for the data measured on 23/01/2009, giving best agreement between measured and calculated apparent resistivity. The figure shows significant lateral variations in the resistivity of the top layer. The distribution of the soil resistivity in the immediate subsurface region shows a range of localised values from 23Ωm to 300Ωm. In general, however, the soil resistivity occupies the range

130Ωm to 200Ωm. A similar observation can be made for the model based on data collected on 01/04/2009. Based on these measurements, a computational soil model was proposed having a top layer resistivity of 180Ωm to a depth of 9m and a bottom layer of infinite depth having a resistivity of 70Ωm [3.12].

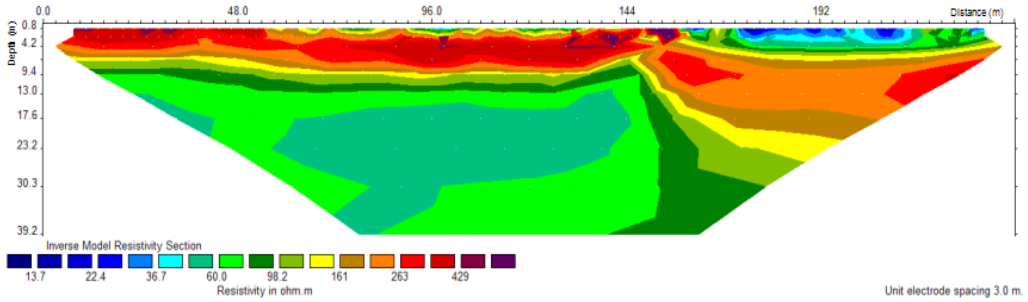

(a)

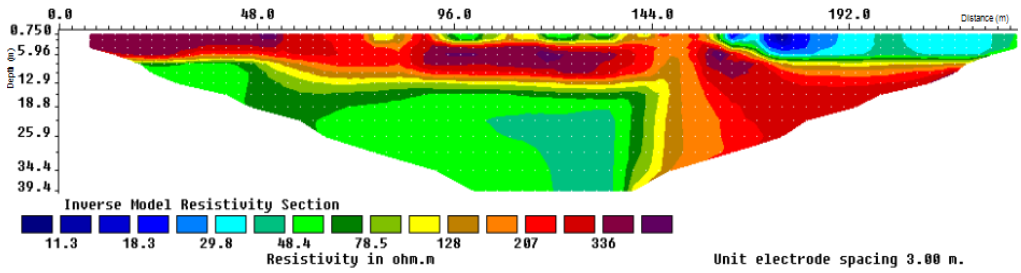

(b)

Figure 3.26: 2D soil resistivity inversion maps: a) 01/04/2009, b) 23/01/2009 (reproduced from reference [3.12])

3.8 Conclusions

Measurements of soil resistivity at the Llanrumney fields university test site are described. Two dc earth testers have been used: the MEGGER DET 2/2 and the ABEM SAS 1000 meter associated with the Lund imaging system. The Wenner technique was adopted for the survey, since it offers both convenience of use and accuracy of results.

Although, a point-to-point comparison cannot be made due to different experimental arrangements and profiling extent. However, the range of values obtained with both instruments is comparable and both curves exhibit similar trends. An apparent soil resistivity was measured at the earth electrode locations before installation. Inversion software to produce the 2D survey images was used, and the estimation value of soil resistivity was suggested. Although, the distance between two profiles was not exceeded 3m, the results showed that the resistivity is non-uniform, and a two soil layer models was obtained.

Considerable lateral variation in soil resistivity was found within the site, as was seen from the results obtained by both testers and the extent of the lateral variation is more easily detected by the 2-D measurement technique. The soil resistivity models have been adopted after actual tests at both locations (vertical and horizontal electrodes) and used in Chapters 4, 5, 6 and 7 in this thesis.

CHAPTER FOUR: LOW VOLTAGE VARIABLE FREQUENCY CHARACTERISATION OF PROPOSED ENHANCED EARTH ELECTRODE SYSTEMS

4.1 Introduction

The high-frequency performance of vertical earth rods is important for designing earthing systems and lightning protection systems. In high voltage substations, buried earth grid, vertical rods and horizontal electrodes in combination provide a low impedance connection to earth [4.1].

As described in Chapter 2, much of the previous experimental work on vertical rod electrodes dealt with experimental and measurement techniques using low magnitude DC, low frequency AC and impulse currents. Besides, experimental work was confined on the whole to small laboratory tests with restricted space and theoretical studies [4.1-4.15].

In this chapter, the DC earth resistance and high-frequency characteristics of vertical rods up to 6m in length buried in a non-uniform soil, with and without proposer enhancements of horizontal electrodes in 4-point cross and 8-points star configurations, are investigated. In addition, the frequency response of 43m and 88m horizontal electrodes, with and without insulated conductor, are measured over the range from DC to 10MHz. The tests were carried out at the Cardiff University outdoor earthing test facility at Llanrumney test field. Simulated results are compared with measured results for vertical earth electrode, and the equivalent two-layer soil model is described in Chapter 3.

4.2 Equivalent Circuit Models Used

The lumped parameter equivalent circuit applied to earth rods was proposed by Rudenberg [4.16] and is shown in Figure 4.1 below.

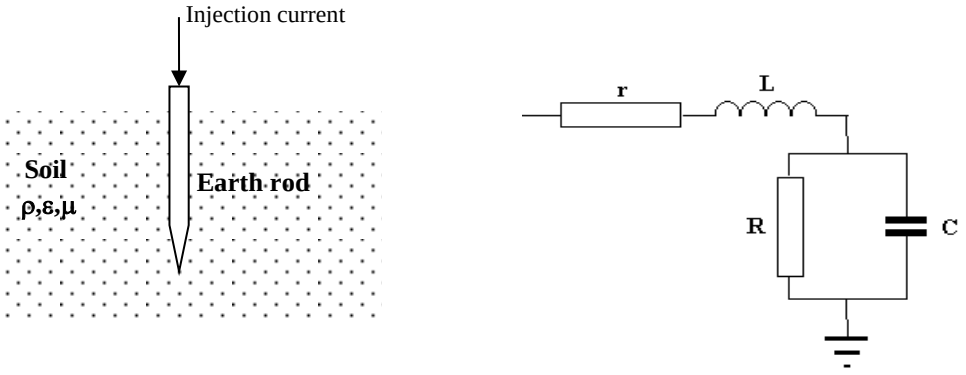

Figure 4.1: The basic arrangement of a vertical earth rod (a) and its equivalent circuit (b)

Where:

r: Series resistance of the earth electrode.

L: Series self-inductance of earth electrode.

R: Shunt earth resistance of the soil.

C: Shunt capacitance of the soil.

Some equations which are relevant to the circuit model parameters for vertical rods have been suggested by Rudenberg [4.16], Tagg [4.17], Sunde [4.18] .Table 4.1 shows the relevant equations for the circuit model elements suggested by these authors.

Table 4.1: Formulae for earth resistance, inductance and capacitance of a vertical earth electrode

	Resistance (R)	Inductance (L)	Capacitance (C)
Tagg	$R = \rho/2\pi l \ln(4l/a) - 1)$	Not calculated	Not calculated
Sunde	$R = \rho/2\pi l \ln(2l/a) - 1)$	$L = l\mu/2\pi \ln(2l/a) - 1)$	$C = \frac{2\pi\epsilon l}{\left(\ln\left(\frac{2l}{a}\right) - 1\right)}$
Rudenberg	$R = \frac{\rho}{2\pi l}\ln\left(\frac{2l}{a}\right)$	$L = \frac{l\mu}{2\pi}\ln\left(\frac{2l}{a}\right)$	$C = \frac{2\pi\epsilon l}{\ln\left(\frac{2l}{a}\right)}$

A distributed circuit model applied to an earth electrode and the impedance of the earth electrode can be determined by combined over the whole length [4.19]. Using this model, the open-circuit impedance of a vertical rod electrode can be calculated by Equation (4.1) [4.20]:

$$Z_{oc} = \sqrt{\frac{Z_c}{Y_c}} coth\left(\ell\sqrt{Z_c Y_c}\right) \qquad (4.1)$$

Where, Z_C: Series impedance (Ω/m), Y_C: Parallel admittance (Ω/m) and ℓ: The length of earth electrode (m).

The horizontal earth electrode can be represented by a ladder network equivalent circuit model, shown in Figure 4.2, as suggested by Velazquez and Mukhedkar [4.21]. Each parameter in this circuit is calculated as per-metre quantities, and the earth electrode is split into n sections, each of length 1m. Each parameter of the circuit model can be calculated by Sunde's equations [4.18] as shown below.

$$\mathrm{R} = \frac{\rho}{2\pi\ell}\left(\ln\left(\frac{2\ell}{\sqrt{2\mathrm{ha}}}\right) - 1\right) \qquad (4.2)$$

$$L = \frac{\mu_0 \ell}{2\pi}\left(\ln\left(\frac{2\ell}{\sqrt{2ha}}\right) - 1\right) \qquad (4.3)$$

$$C = \frac{2\pi\varepsilon\ell}{\left(\ln\left(\frac{2\ell}{\sqrt{2ha}}\right) - 1\right)} \qquad (4.4)$$

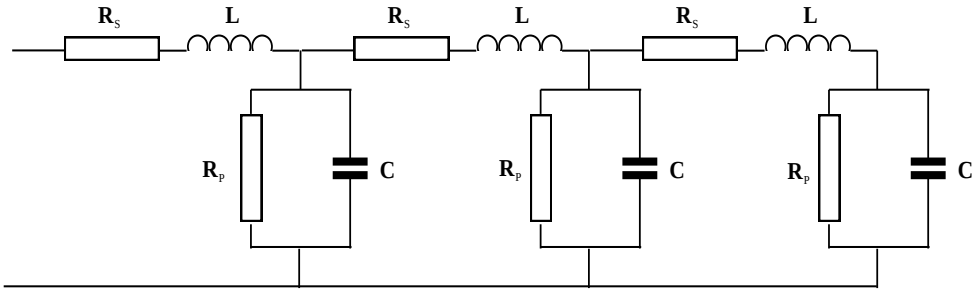

Figure 4.2: Equivalent ladder circuit model of a horizontal earth electrode (Reproduced from reference [4.21])

4.3 Installation of the Earth Electrodes

After the soil resistivity had been measured and modelled in Chapter 3, the horizontal enhancements (cross/star-shaped) and 1.2m rod were installed. Figure 4.3 shows different stages of the installation of the 8-point star and the 1.2m vertical rod at the test field facility at Llanrumney playing fields. A trencher, shown in Figure 4.3(a), was used to dig channels to a depth of 30cm. The angle between electrodes in the star was fixed at 45^0. A further 2.4m rod was installed to act as a return current electrode, situated approximately 150m from the electrode under test. An aluminium ring was used to connect the horizontal enhancements to the rod, as shown in Figure 4.3(b). A vertical rod was connected to either the 4-point cross or the 8-point star electrodes by an aluminium ring. The rod was installed at the centre of the aluminium ring to avoid any contact between the vertical electrodes with horizontal enhancements during the experimental tests for rods only.

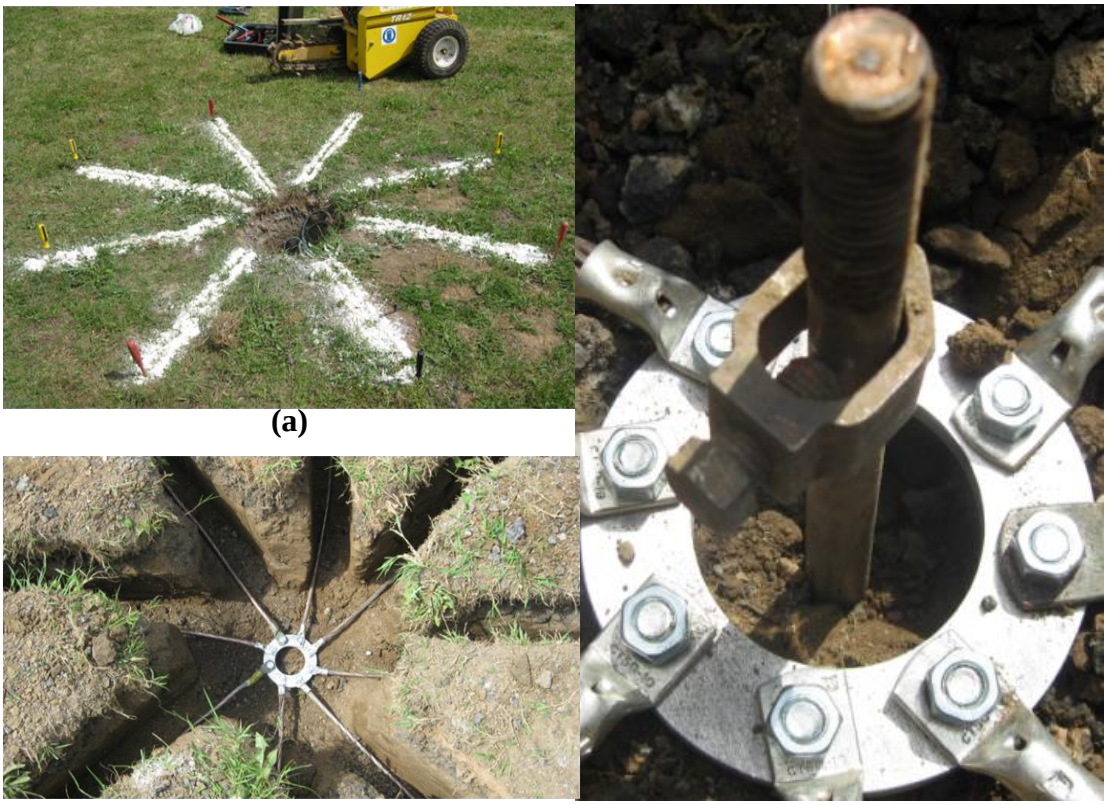

(a)

(b) **(c)**

Figure 4.3: Installation of vertical rod and horizontal enhancements

4.4 Description of Experimental Setups of Test Electrodes

Figure 4.4 shows a schematic diagram of the experimental setup used for DC, high frequency and impulse tests. Because of its high conductivity and withstand to corrosion, earth electrodes made from copper material were selected. The test electrodes used are 1.2m, 2.4m, 3.6m, 4.8m-and 6m rod in length, with a diameter of 14mm are used. The rods were connected, in turn, to ‘cross’ and ‘star’ configured horizontal rod conductors of 1m length and 8mm diameter, buried at a depth of 30 cm. The main reason of connecting the horizontal enhancements at the top of the rods that high frequency content will dissipate into the earth easily. Also, providing multiple paths for current injection into the earth decreases current density at earth electrode

interface which can reduce the over voltages. However, connecting enhancements at the bottom of the rod decreases the earth impedance at low frequency only.

Figure 4.5 shows the second test setup for the 88m horizontal earth electrode, buried in non-uniform soil at the Cardiff University earthing test facility. The horizontal bare electrode under test is 88m in length and has a cross-sectional area of 50mm^2, buried at a depth of 30cm. A recently proposed technique for reducing the impedance of horizontal electrodes is the addition of an insulated parallel conductor, bonded to the bare underground horizontal earth electrode at multiple points to increase the effective length of the electrode [4.22, 4.23].

This conductor is enhanced with new ground surface insulated conductor with cross-sectional area of 25mm^2, and this conductor is bonded to the buried bare conductor at points along its length. The bare conductor is divided into 14 sections of graded lengths such that the section lengths are smallest close to the injection point and increase with distance along the conductor. There are 14 test pits installed above each intersection, to allow measurement of the voltage and current at different electrode positions. The test pits can be used to make and break connections so as to vary the bare conductor length, thus enabling measurement of current and voltage distributions for electrodes of different dimensions. The insulated conductor, sectionalised in the same lengths as the bare buried electrode, was laid on the ground surface for testing purposes and bonded to the bare underground horizontal electrode at section points along its length. If such an enhancement were to be used in a practical installation, it is envisaged that the insulated conductor to be buried just below the ground surface

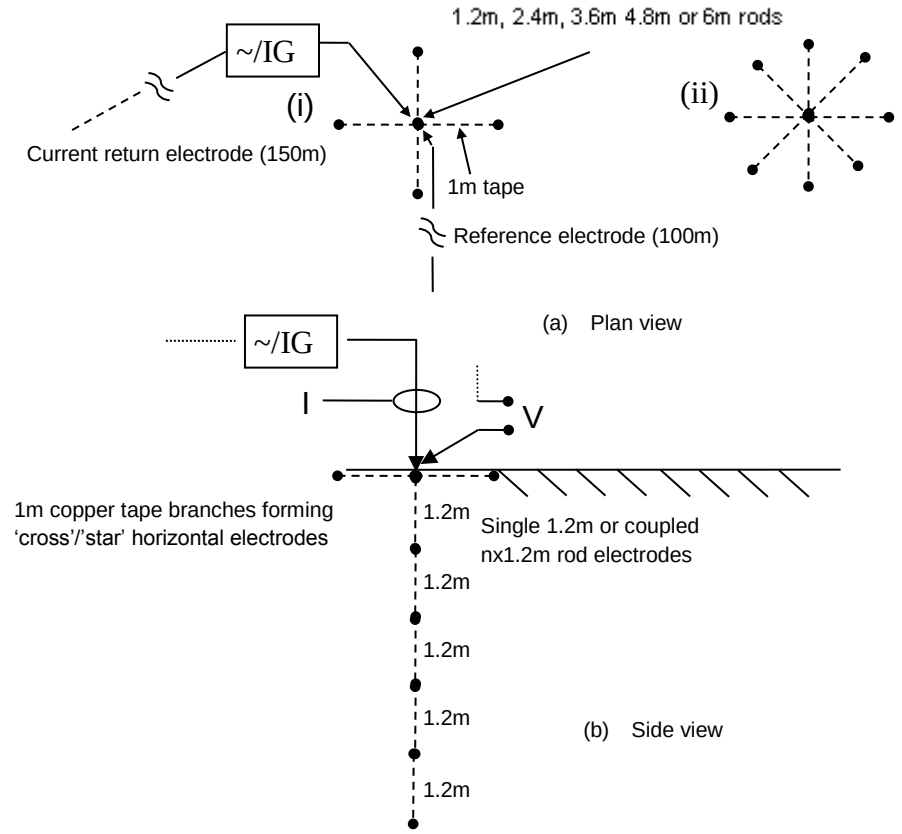

Figure 4.4: Plan and side views of experimental set-up of Installation A: Rods with (i) 4-point cross and (ii) 8-point star enhancements.

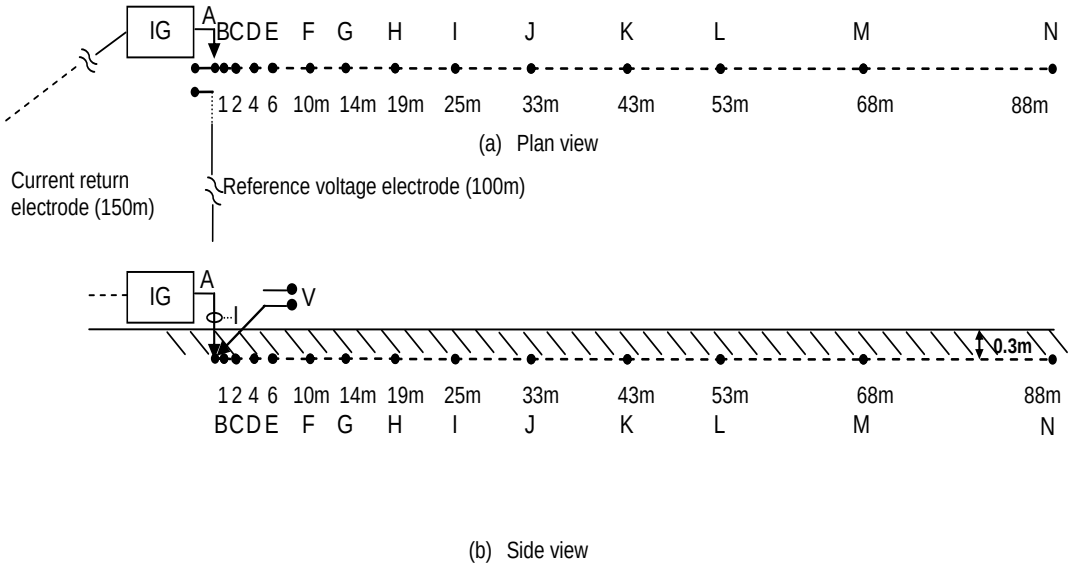

Figure 4.5: Installation B under test: (a) plan view (b) side view

4.4.1 AC Test Sources

Two sources were employed for AC tests over a wide frequency range: A variable frequency impedance measurement system (IMS), which was developed by Cardiff University for this type of test [4.24], and an RF system based on a Marconi 2019A signal generator and power amplifier systems [4.25]. The IMS consists of two EG&G 7260 Lock in Amplifiers and a QSC Audio Power Amplifier. The lock-in amplifier can recover measurement signals in the presence of an overwhelming noise background, or alternatively, it can be used to provide high resolution measurements of relatively clean signals over several orders of magnitude and frequency [4.25]. The applied frequency was varied from the lock-in amplifier in the range 10Hz to 120 kHz. The amplitude and phase angle were recorded for the resistance and readings were taken directly from the IMS. The audio-frequency (AF) and radio frequency (RF) signal generators and corresponding AF and RF power amplifiers (up to 2.4kW) were used to inject AC currents of several hundred milli-amperes for frequencies up to 10MHz frequency. Figure 4.6 shows the picture of the IMS and Marconi instruments. The current return electrode was located 100m from the test object, and the reference potential electrode, fixed 150m away, was connected by a lead placed orthogonal to the current return lead. Current transformers of 0.1V/A sensitivity with a bandwidth of 20MHz, and high-bandwidth differential voltage transducers were used for the current and voltage measurements. An oscilloscope (LeCroy WaveJet 354) with 2GS/s sampling rate and a bandwidth of 500MHz was used to capture the voltage and current waveforms. An isolation transformer was also used in mains supply circuit to eliminate stray earth currents.

Figure 4.6 Pictures of IMS and Marconi instruments at field test site

4.4.2 DC Resistance Tests

The MEGGER DET 2/2 instrument, designed to measure earth electrode resistance and soil resistivity, performs four terminal continuity tests (see Figure 4.7). Preliminary DC resistance measurements were carried out on the vertical rods and horizontal electrodes with a MEGGER DET 2/2 instrument, with and without enhancements. The degree of variation in electrode performance was evaluated by repeating the DC resistance measurements several times over the testing period. Similar test circuits in Figures 4.4 and 4.5 were used to measure the dc earth resistance for both installation electrodes A and B.

Figure 4.7: DET 2/2 earth tester

4.5 Test Results for Installation A

4.5.1 DC Resistance Test Results for Installation A

In order to study the effect of additional horizontal enhancements to the vertical earth electrode on the earthing resistance, the DC resistance of the various earthing configurations was measured and compared with computed results. The test electrode was simulated using the HIFREQ module of the CDEGS software [4.26]. The computer simulation requires the vertical and horizontal electrodes to be simulated as cylindrical conductors, with radii much smaller than their lengths. A two-layer soil model was used, with an upper layer soil resistivity of 150Ωm to a depth of 10m, and bottom layer of soil resistivity is 55Ωm as given in Chapter 3 Section 3.7. The results are summarised in Table 4.2.

Table 4.2: DC resistance of earth rod systems

	DC Resistance(Ω)	
Configuration	**Measured**	**CDEGS**
1.2m rod	131.1	133.8
1.2m rod with cross-shaped electrode	47.4	49.4
1.2m rod with star-shaped electrode	36.6	38.5
2.4m rod	55.7	59.2
2.4m rod with cross-shaped electrode	29.3	33.9
2.4m rod with star-shaped electrode	22.7	25.5
3.6m rod	40.4	44.9
3.6m rod with cross-shaped electrode	27.1	32
3.6m rod with star-shaped electrode	20.4	24
4.8m rod	35.0	39.7
4.8m rod with cross-shaped electrode	25.0	28.6
4.8m rod with star-shaped electrode	18.0	23.9
6m rod	30.6	33.4
6m rod with cross-shaped electrode	18.4	24.7
6m rod with star-shaped electrode	16.4	22

As can be seen from the table, as the length of the earth rod increases, both the earth resistance and its rate of fall-off decrease with length. The addition of the star and cross electrodes reduces significantly the overall DC earth resistance for all rod lengths. The CDEGS computed results, also given in Table 4.2, show some differences with the measured values of the DC earth resistance, which may be attributed to the simple soil resistivity model used. Figure 4.8 shows the results of computation of the DC earth resistance of the rods only and with cross/star enhancements. From Figure 4.8, the computed DC resistances have slightly higher than the measured results.

It is known that there are seasonal variations in soil resistivity and this affects the resistance of earth electrodes and potentials developed in their close vicinity. For example, in raining season, there is a wet surface soil layer with decreased resistivity

while, in the frozen season, the resistivity of the frozen soil increases to several to ten times that in normal season [4.27]. Figure 4.9 shows the variation of the DC resistance of the different length rods of the testing period. The greatest variation in resistance is seen with the 1.2m rod and, although no detailed rainfall measurements were taken at the site, it was noted that the period March-April 2011 was particularly dry, and this corresponded to the highest recorded values of resistance. Also, from the figure, it can be seen that, for the longer rods subsequently installed, there was less variation in measured resistance. This may be explained by the expected lower variation in soil moisture at greater depth.

Calculations of the earthing resistance of different lengths of the vertical electrodes up to 6m, with diameter of 14mm, were carried out using equations of Rudenberg's, Tagg's and Sunde's [4.16-4.18] as given in Table 4.1. An average soil resistivity value of 150 Ωm was compared with the measurement results using the DET2/2 test instrument while a two-layer soil model was used for CDEGS software, with an upper layer soil resistivity of 150Ωm to a depth of 10m, and a bottom layer of soil resistivity is 55Ωm (See Chapter 3 Section 3.7).

Figure 4.10 shows a comparison between the various calculated and measured results. From the figure, it can be seen that the measured dc resistance values show reasonably close agreement with those obtained from different simplified equations, with Sunde's equation giving the closest match. In addition, the CDEGS and Rudenberg computed results are in good agreement. Furthermore, Table 4.2 shows some differences between the measured and calculated values of the DC resistance of the rods.

The numbers of test repetitions for each length of rod at the test site were carried out, as shown in Figure 4.11 a, b. The transducers (voltage and current transformers) used

in this work were calibrated and the measurement error in the results estimated to be ±4%. The results showed that the different potential transducers tested had a measured error of less than ± 3% over a complete frequency range, and the LILCO current transformer showed less than 2% error [4.19]. From the figure it can be seen that the temporal variation in measured DC resistance is far greater than that allowed by the calculated error margin. The conclusion can be drawn that the major factors in the resistance is the resistivity of the bulk of the soil surrounding the electrode is liable to variations with moisture content and temperature.

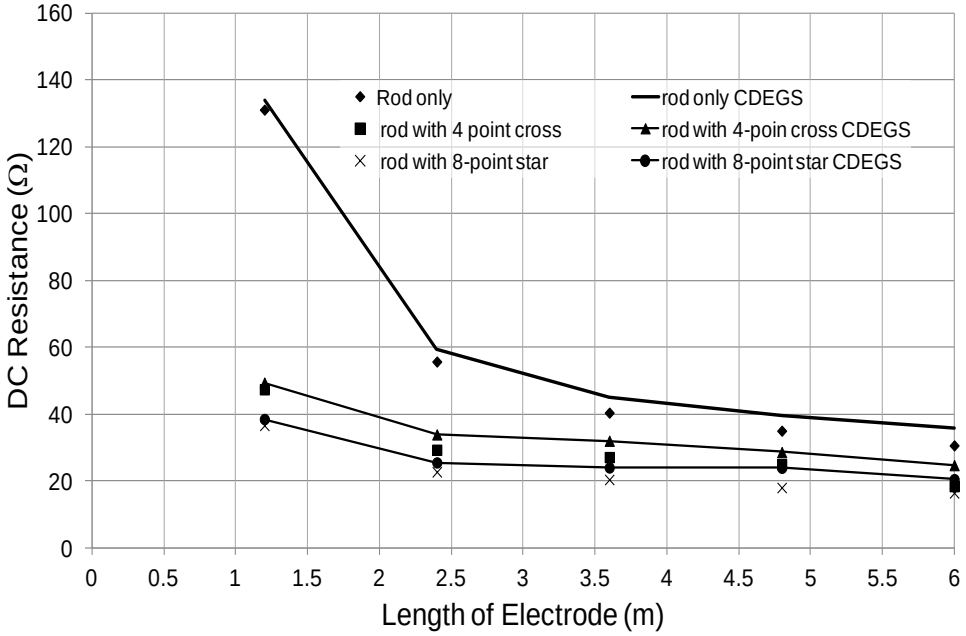

Figure 4.8: Computed and measured DC resistances of rods only and with enhancements

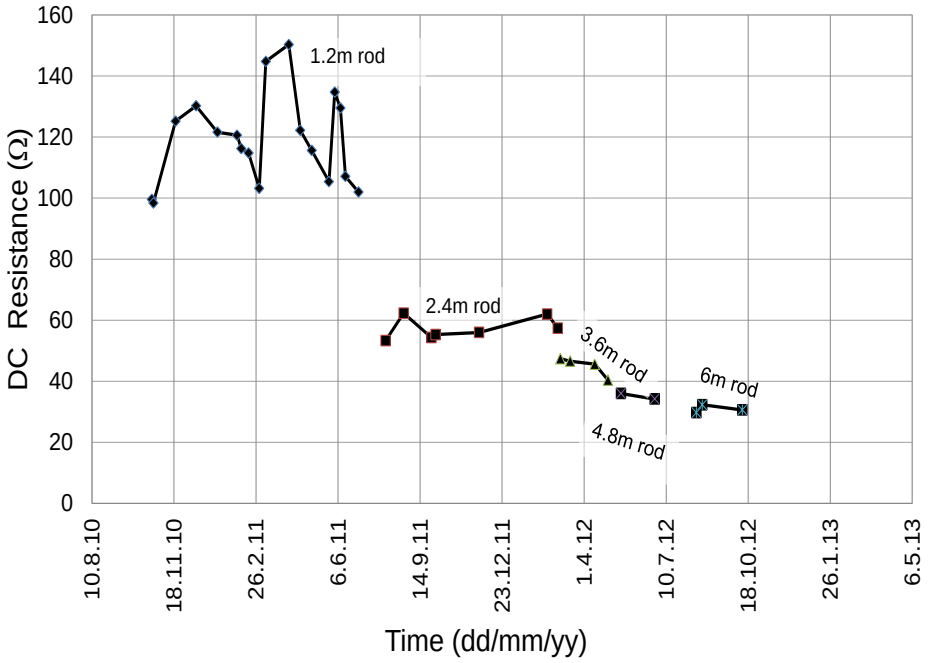

Figure 4.9: Variation in measured DC resistance of rod electrodes

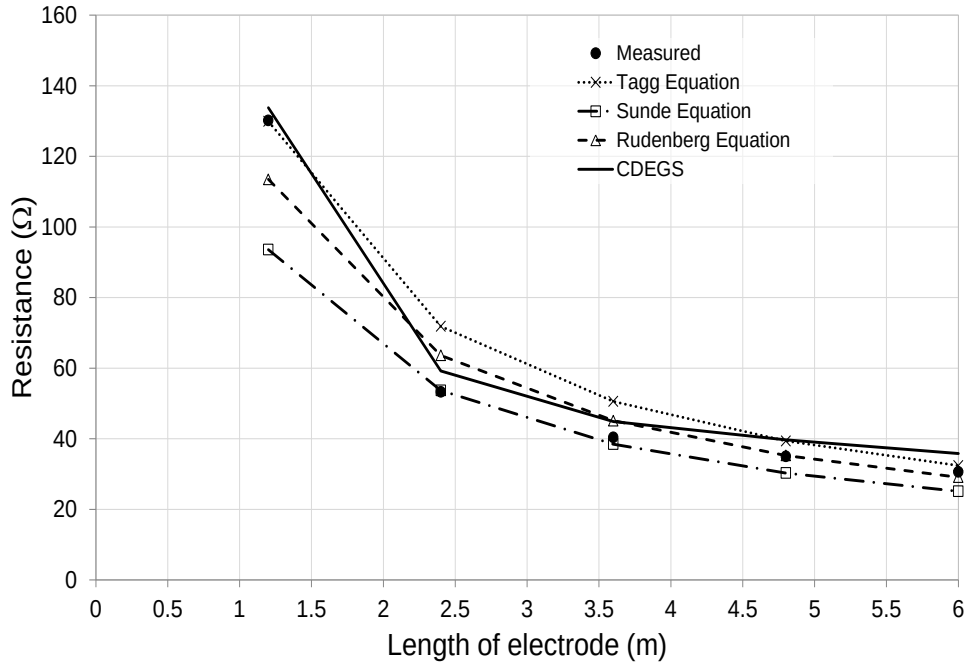

Figure 4.10: Comparison of calculated and measured resistance of rods up to 6m in length using DET2/2 earth tester

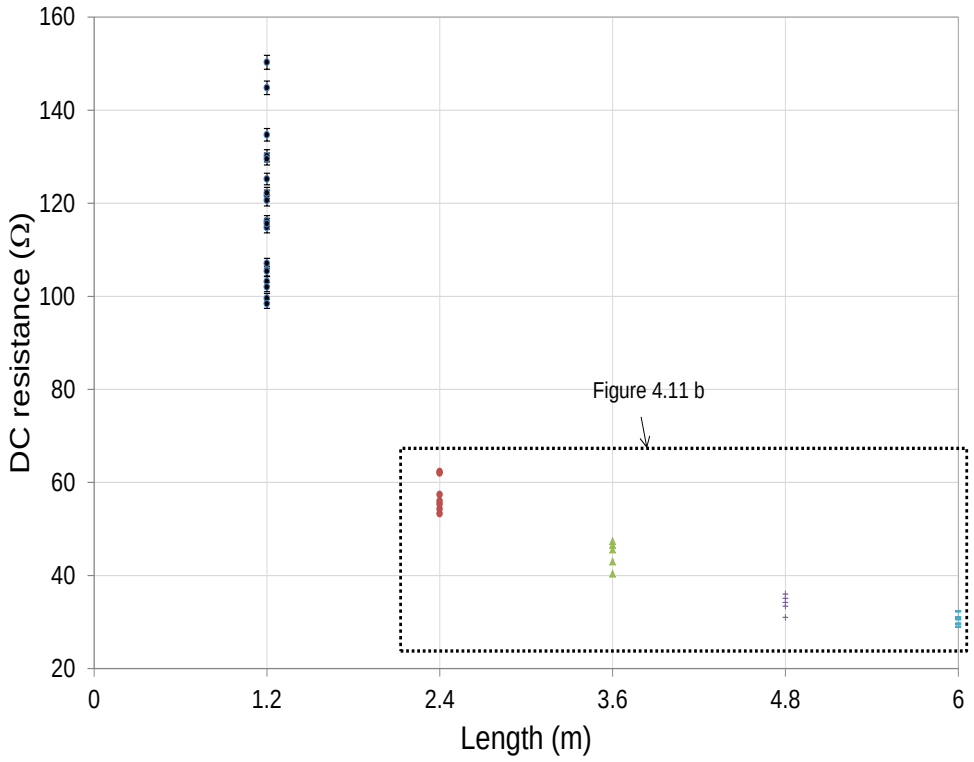

(a)

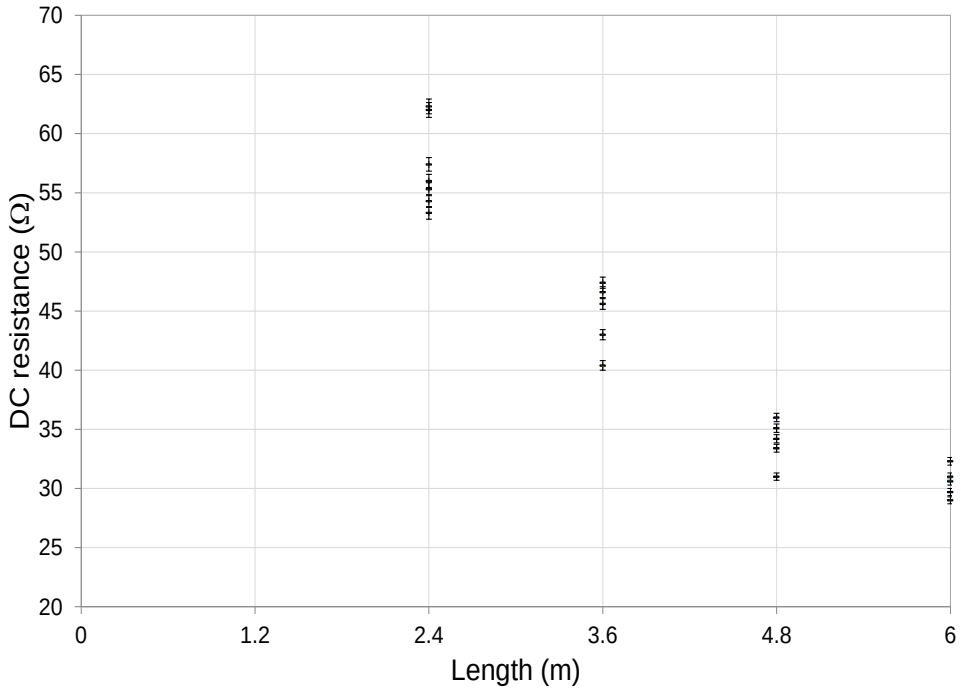

(b)

Figure 4.11: Repetitions of measured DC resistances for: a) 1.2m rod; b) 2.4m, 3.6m, 4.8m and 6m rod

4.5.2 Variable Frequency Test Results for Installation A

The results of the variable frequency tests are shown in Figure 4.12 for the 1.2m and 2.4m rods. The impedance magnitude shown in Figure 4.12 indicates that each curve has, i) a lower frequency response range over which the impedance magnitude is almost constant, indicating that the electrode is predominantly resistive, and ii) a higher frequency range where inductive and capacitive effects can be observed. As can be seen from the figure, over the low frequency range (10-10kHz), extending the earth rod from 1.2m to 2.4m provides a significant reduction in earth impedance which is consistent with the measured DC resistances in Table 4.2. At higher frequencies, above 100 kHz, a slight fall in earth impedance is observed in the case of the 1.2m rod. However, this fall in impedance is not seen in the case of the 2.4m rod. In contrast, the impedance of the longer rod increases over the range 100 kHz to 1 MHz. Above 1MHz, the impedance of the 2.4m rod exceeds that of the 1.2m rod.

Figure 4.13 shows the frequency responses for the 3.6m and 4.8m rods. It is clear that the impedance magnitude for a 6m vertical rod is lower than that for 3.6m and 4.8m rods, up to a particular frequency which depends on the soil resistivity. Generally, at these lengths, the effect of inductance is more pronounced with sharper upturns occurring at a lower frequency (~50 kHz). Following the first maximum (at ~200 kHz), the impedances follow an oscillatory pattern with frequency, and the second peak is considerably higher for the 4.8m rod.

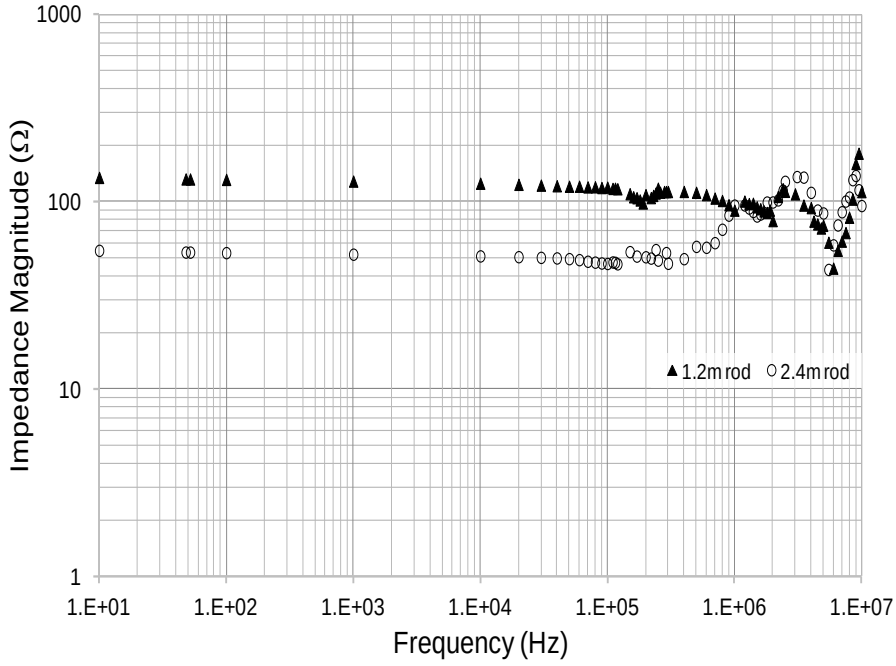

Figure 4.12: Frequency responses of the 1.2m and 2.4m earth rods.

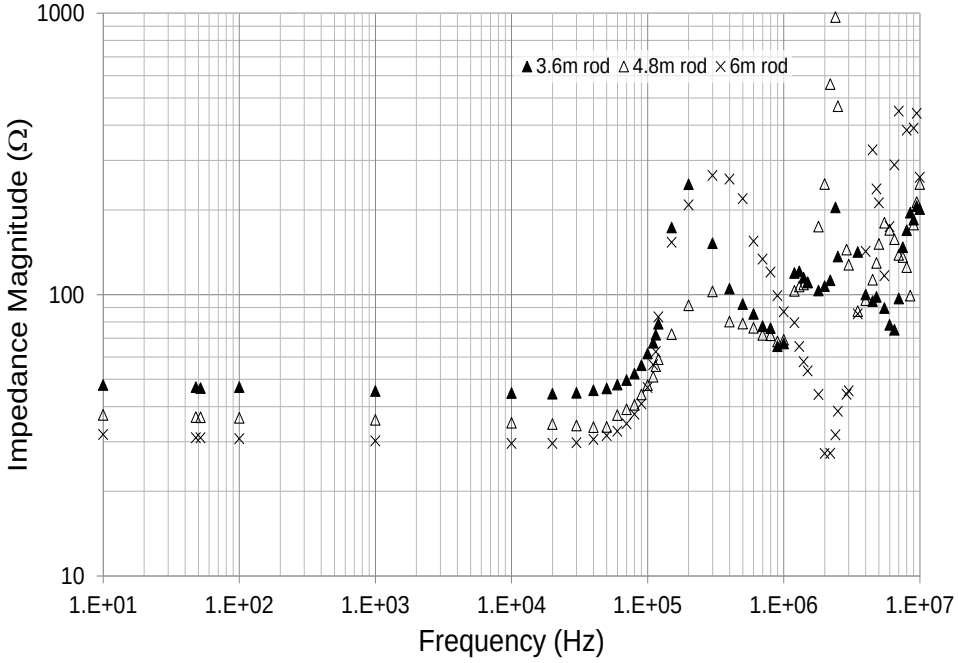

Figure 4.13: Frequency responses of the 3.6m, 4.8m and 6m earth rods

The seasonal effect on earthing resistance has been investigated by many authors [4.28-4.32]. Here, seasonal variation in resistance and impedance magnitude under variable frequency up to 10MHz was investigated for 1.2m vertical rod buried at the test site. Figure 4.14 shows an example of the frequency response of the 1.2m vertical earth electrode measured on different dates. As can be seen, the impedance at low frequency increases by around 11% in the winter season (15/12/2010) compared to that in the summer (02/06/2011). As can be seen from figure, the impedance over the frequency range DC to 2MHz was higher on the winter day compared with the summer day, and this could be attributed to a particularly dry winter period in that year. Over 2MHz, the difference between the measured earth impedance on the two different dates becomes less significant.

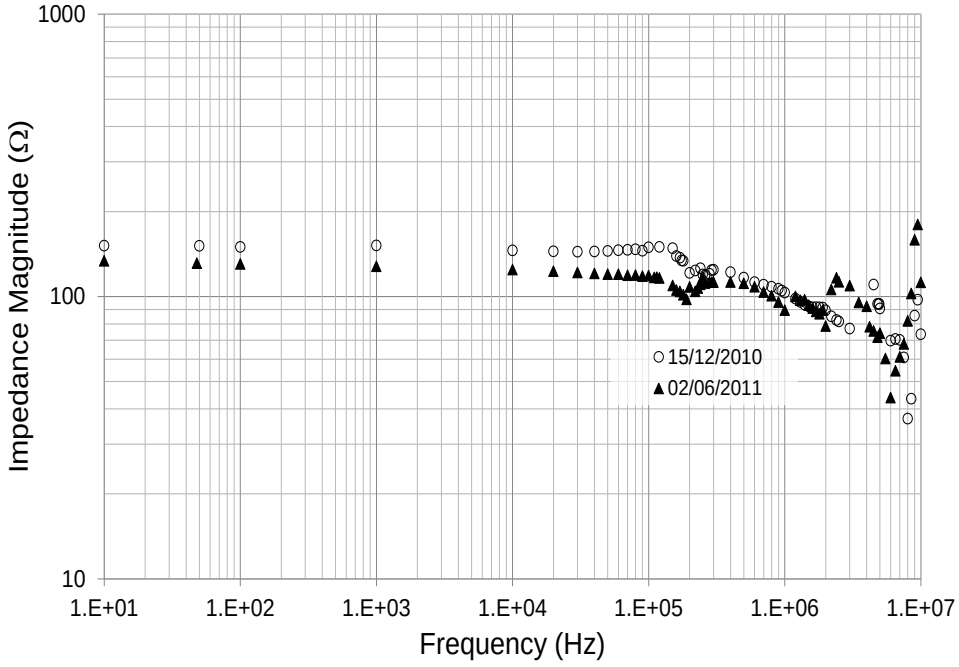

Figure 4.14: Comparison of impedance magnitude of 1.2m rod on two different dates

4.6 Test Results for Installation B

4.6.1 Variable Frequency Test Results for Installation B

The injection frequency was varied from 10 to 10MHz, and the frequency response of the 43m and 88m horizontal electrodes is shown in Figure 4.15. Over low frequency range 10 to 3 kHz**,** the earthing resistance of the 43m horizontal electrodes is twice that of the 88m horizontal electrodes. At high frequency where inductive effects start to appear, a sharp upturn is seen in the earth impedance curve at 30 kHz and 10 kHz for the 43m and 88m horizontal electrode respectively. Above 100 kHz, the earthing impedances for both horizontal electrodes are almost the same.

As for the differences between earthing impedance readings on different dates, further sets of experiments were undertaken on the 29/04/2012 and 01/03/2013. Figure 4.16 shows the effects of the weather on the impedance of the 88m horizontal electrode, showing a reduction in low frequency resistance of approximately 6.4% between tests. Therefore, there is no major variation in impedance at low frequency, and up to 10kHz. Above 10kHz, a significant difference was observed, with this difference itself increasing with frequency. At 1MHz, a maximum percentage reduction in the impedance of 55% was observed. Between 2 and 10MHz, the measured results showed the occurrence of some peaks on the first test, but such behaviour is not seen in the second test.

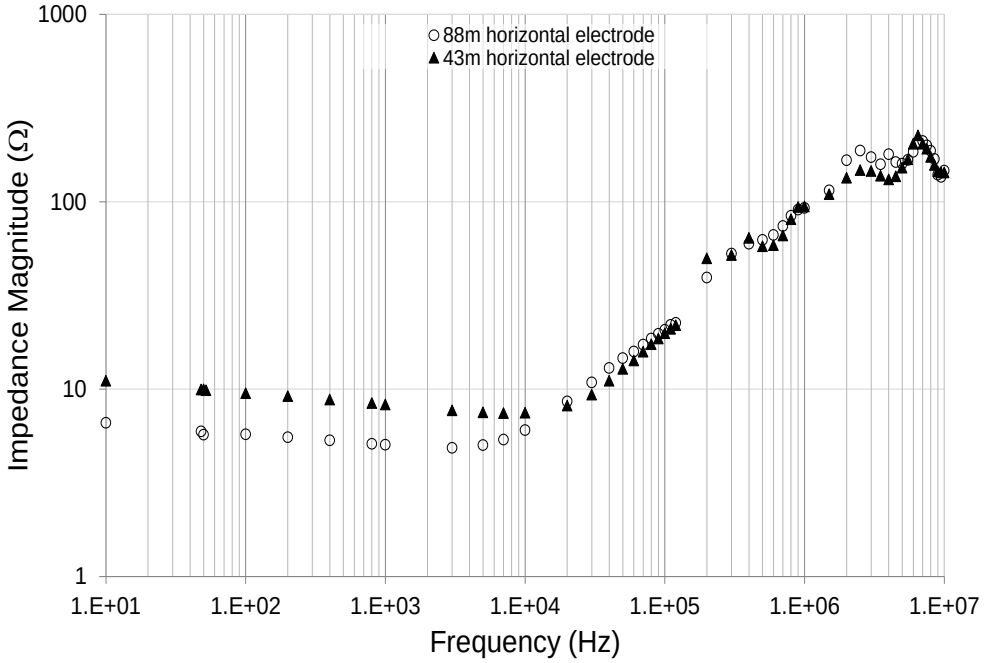

Figure 4.15 Frequency response of different length of the horizontal earth electrode

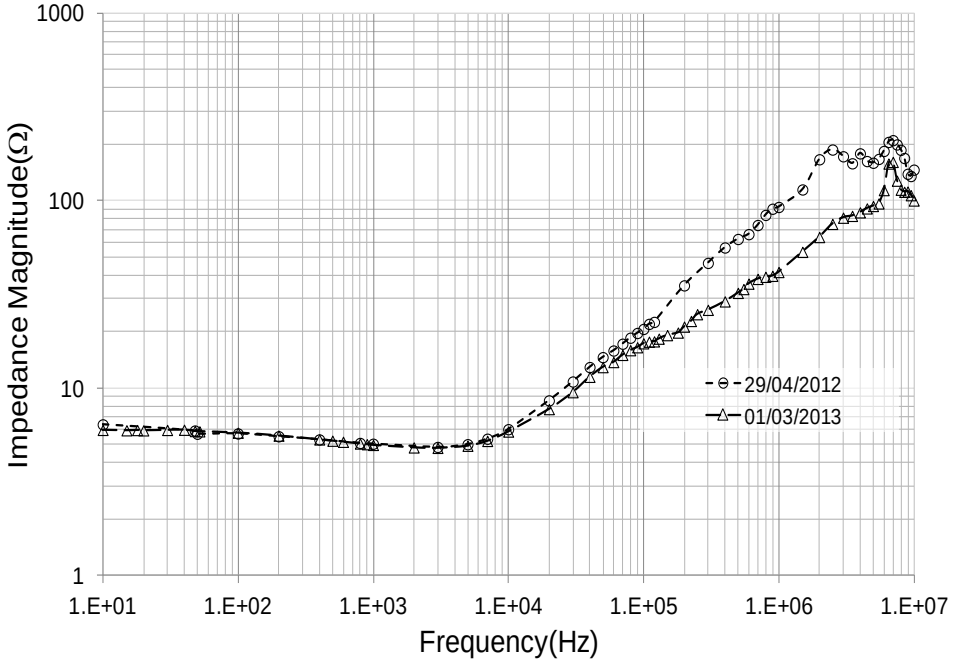

Figure 4.16: Measured of impedance magnitude of the 88m horizontal electrode on two different dates

4.7 Frequency Response of Vertical Electrodes with Enhancements

Tests on the earth electrode (Installation A) were extended to investigate the benefit of adding supplementary electrodes to the individual rods in the form ‘star’ formation horizontal conductors, as shown in Figure 4.4. The addition of the 8-point star enhancements had a beneficial effect on the measured earth impedance, for all rod lengths considered. Figure 4.17 shows the results of an 8-point star enhancement applied to a 1.2m rod. From the figure, it can be seen that there is a considerable reduction in earth resistance/impedance over the entire frequency range.

The frequency response of the 2.4m rod with and without an 8-point star enhancement is shown in Figure 4.18. The results in Figure 4.18 also demonstrate that there is a significant benefit at low and high frequency by adding the additional enhancements.

Figure 4.19 shows the results for the 8-point star applied to the 3.6m rod. As with the short 1.2m rod, benefits are obtained over the entire frequency range, although the average impedance between 100 kHz and 10 MHz is lower for the system with the shortest (1.2m) rod. As can be seen from the figure, the inductive contribution can be also reduced by adding horizontal enhancements with the 3.6m rod at high frequency range.

Figure 4.20 shows the effect of 8-point star enhancements on the 6m rod. It is clear from the figure that a significant reduction in impedance compared to the rod alone occurs only at low frequency (approximately 41%), indicating that horizontal enhancements can reduce the impedance of long vertical electrodes at low frequency. Above 100 kHz, the impedance of rods with horizontal enhancements is still lower than the impedance of the rod alone, up to a frequency of 1MHz. However, above 1MHz, the effect of horizontal enhancements decreases due to the increase in inductive

effects, dominating the impedance at high frequency. Horizontal enhancements can be said to offer some reduction in impedance up to 1MHz for the 6m rod, but beyond this frequency, the beneficial is not clear.

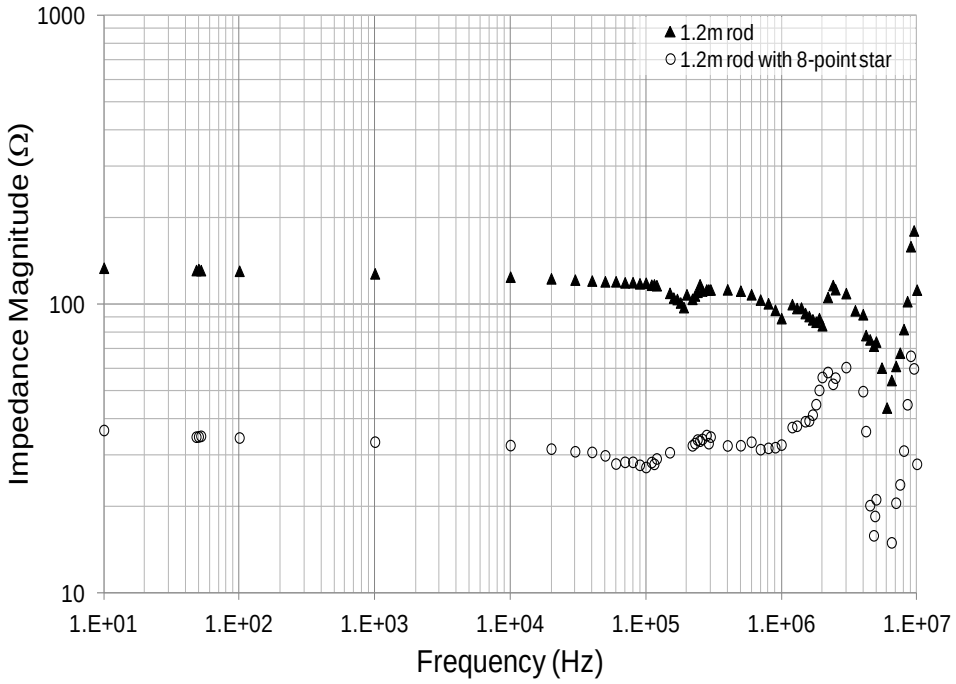

Figure 4.17: Effect of 8-point star enhancement on the impedance of a 1.2m rod

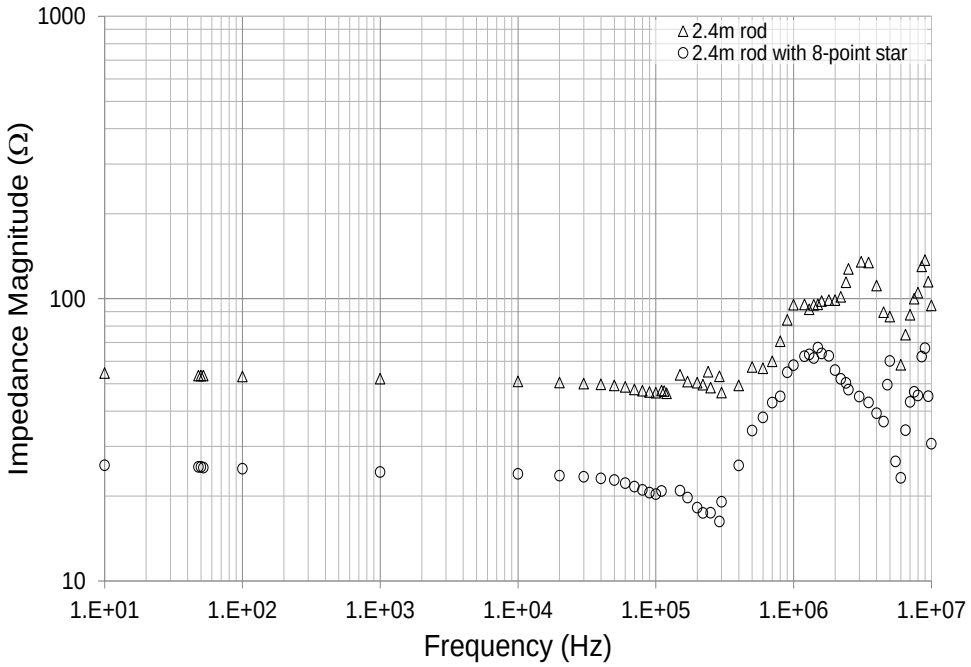

Figure 4.18: Effect of 8-point star enhancement on the impedance of a 2.4m rod

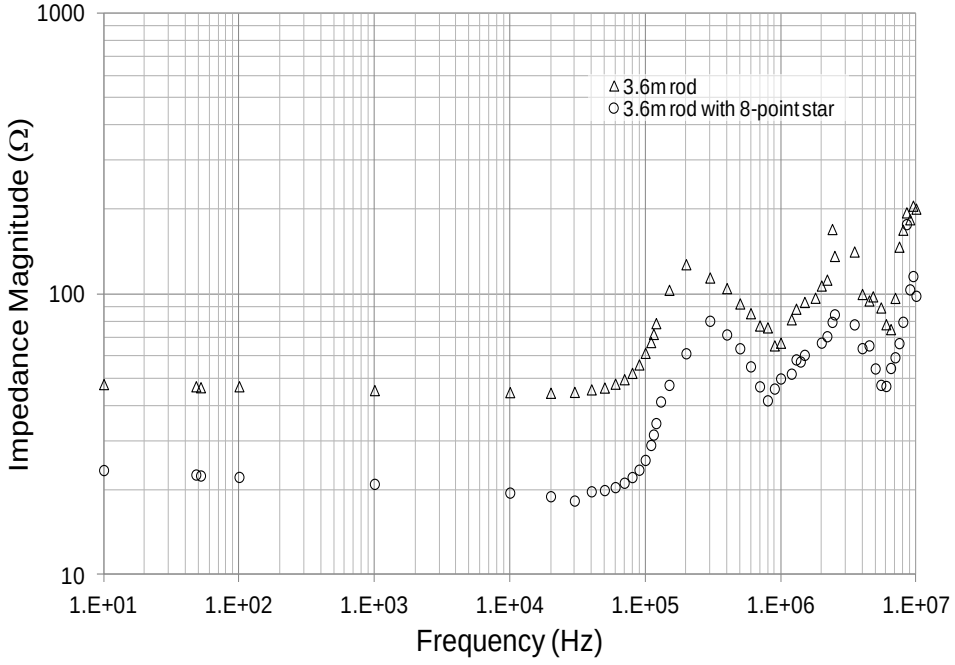

Figure 4.19: Effect of 8-point star enhancement on the impedance of a 3.6m rod

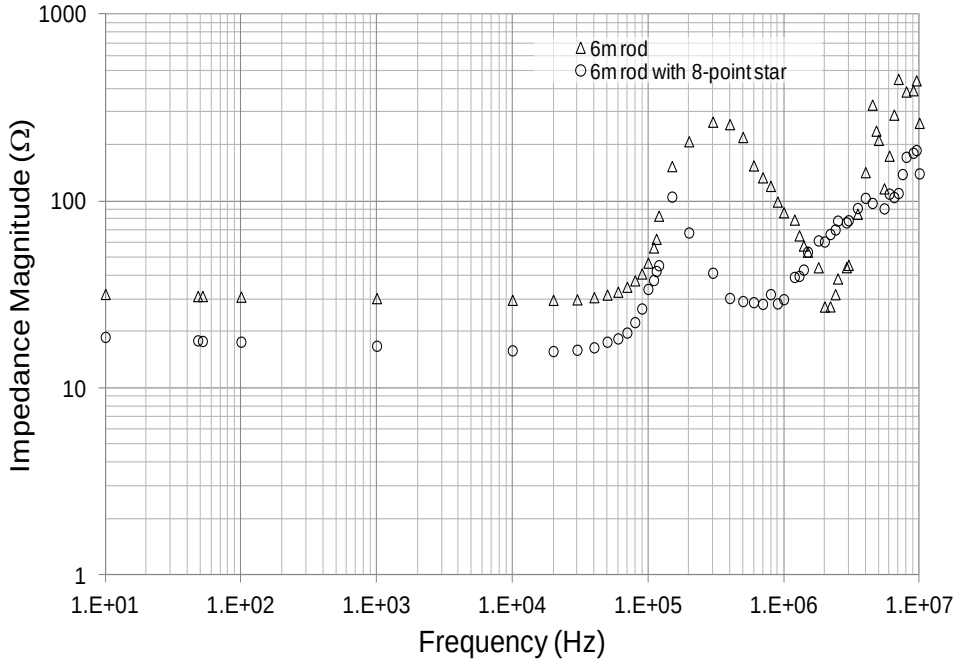

Figure 4.20: Effect of 8-point star enhancement on the impedance of a 6m rod

4.8 Frequency Response of Horizontal Electrodes with Enhancements

The frequency-dependent earthing impedance measured for different lengths of horizontal electrodes (installation earth electrode B) in two-layered soils, with and without insulated conductor, are shown in Figure 4.21. The earth resistance of the 43m counterpoise was found to be 12Ω, reducing to 11Ω with the addition of an above ground insulated conductor. The DC earth resistances of the 88m counterpoise only and with insulated conductor were 7Ω and 6Ω respectively. From the figure, a slight reduction in earthing impedances is observed for frequencies from 10Hz up to 10 kHz for 43m and 88m horizontal earth electrodes, both with and without above-ground insulated conductors. Above 10 kHz, the impedance increases significantly, indicating an inductive behaviour. The upturn frequency is lowered with an increase in the length of the horizontal electrode, due to the increased influence of self-inductance in the longer electrode.

In general, the addition of a parallel insulated conductor has no major effect on the impedance of the earth electrode at low frequency. However, at high frequencies, a reduction in impedance becomes apparent, starting at 300 kHz for a 43m horizontal electrode, and at 400 kHz for the 88m electrode. This can be attributed to the connections between the buried bare earth conductor and the above-ground-insulated conductor. It is thought that the drop in earth impedance occurs due to a reduction in electrode inductance compared to that of the bare conductor alone.

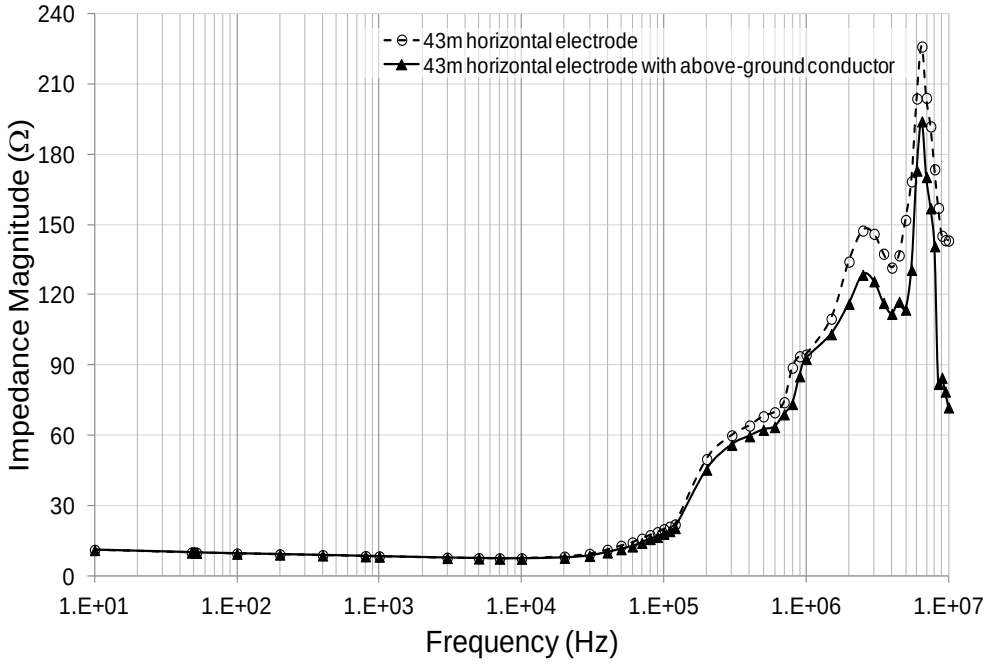

(a)

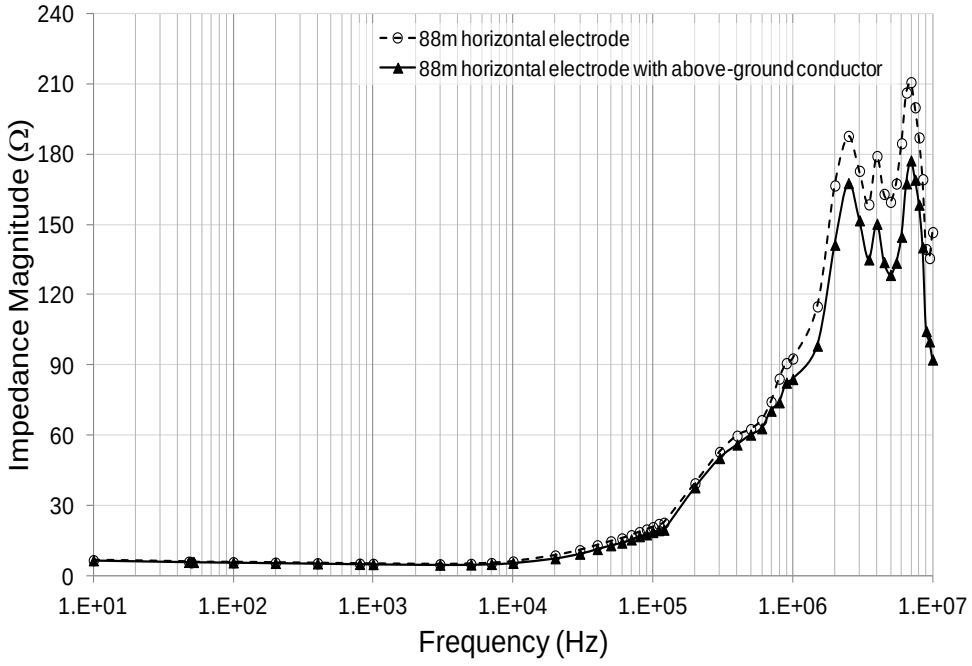

(b)

Figure 4.21: Frequency response of the horizontal earth electrode with and without above-ground insulated conductor: (a) 43m, (b) 88m

4.9 Computer Models of Tested Electrodes

The earthing systems shown in Figure 4.4 were also simulated using CDEGS-HIFREQ software [4.27], as shown in Figure 4.22. In the software, a detailed geometric model of the test electrodes was established including the current return electrode, remote potential electrode and the current and voltage leads. Based on the detailed soil resistivity measurements carried out at the location prior to the earth electrode installation, a two-layer soil model was adopted (See Chapter 3 Section 3.7) for the simulations with a top layer having a depth of 10m and resistivity 150Ωm and bottom layer with a resistivity of 55Ωm. The variable frequency simulations were carried out at each of the test frequencies.

Figure 4.23 shows the results of variable frequency simulations of the 1.2 m vertical rod and the same rod with the 8-point star enhancement. From the figure, it can be seen that there is very close agreement at low frequencies. In addition, the oscillating trends seen in the measured impedance magnitude at high frequencies are reproduced by the computer model, although there are differences between the measured and simulated peak and trough values. In addition, the slight fall off in impedance, seen in the mid-frequency range (10 kHz-1MHz) with the measured values, is not reproduced by the computer model. This difference may be attributed to the assumed constant medium parameters (resistivity and permittivity).

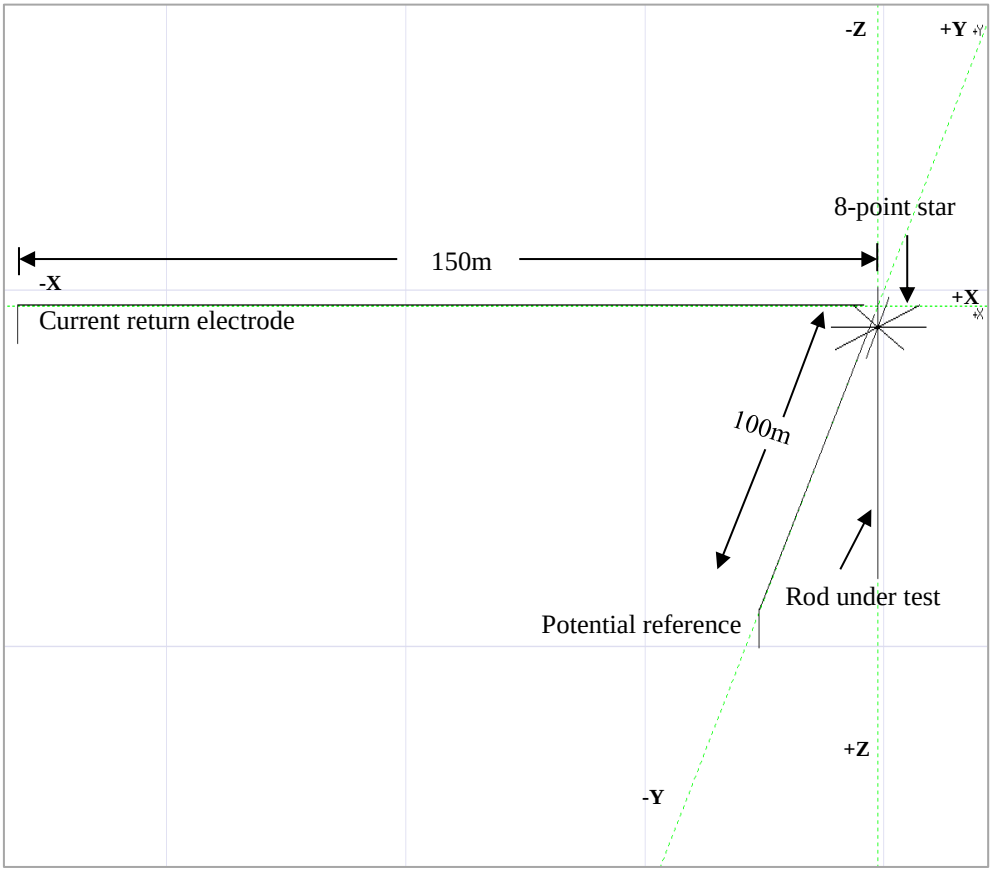

Figure 4.22: CDEGS model of test circuit

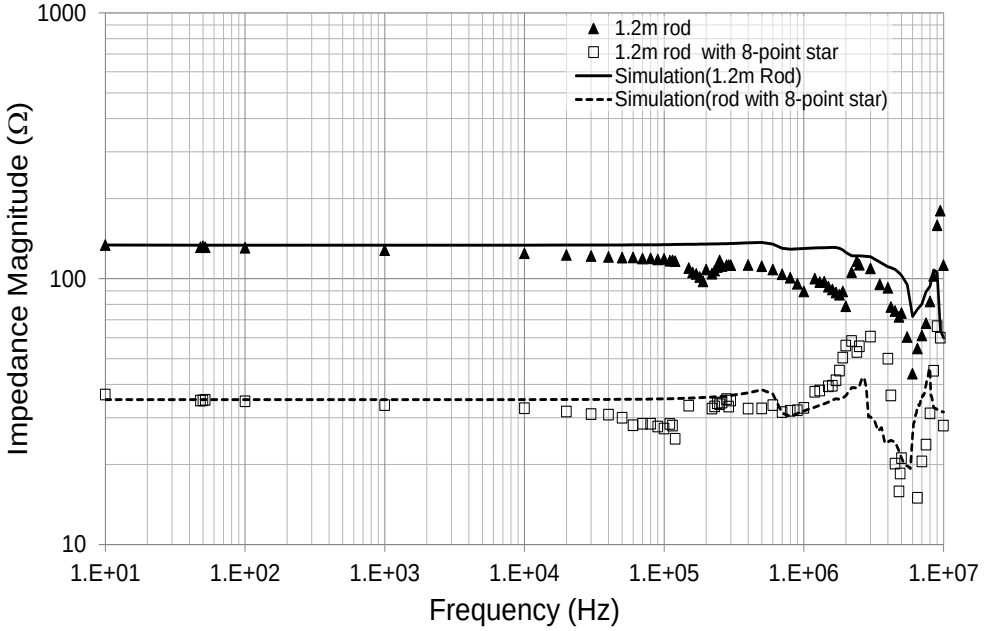

Figure 4.23: Frequency response of the 1.2m vertical rod with and without 8-point star enhancement: Computed and measured values.

A comparison between measured and computed results using a lumped-parameter circuit model and a distributed-parameter representation for the 2.4m rod was carried out. The impedance magnitudes computed with the distributed-parameter model and the lumped-parameter model agree with measurements up to 30 kHz, as shown in Figure 4.24. However, at high frequencies, despite showing an increase in impedance at a frequency of about 1 MHz for the lumped parameter model, while around 3MHz and 6MHz for the distributed parameter model, respectively. It can be said from these results that these circuit models are not valid for predicting the high-frequency behaviour of short vertical rods, especially when buried in a non-uniform soil.

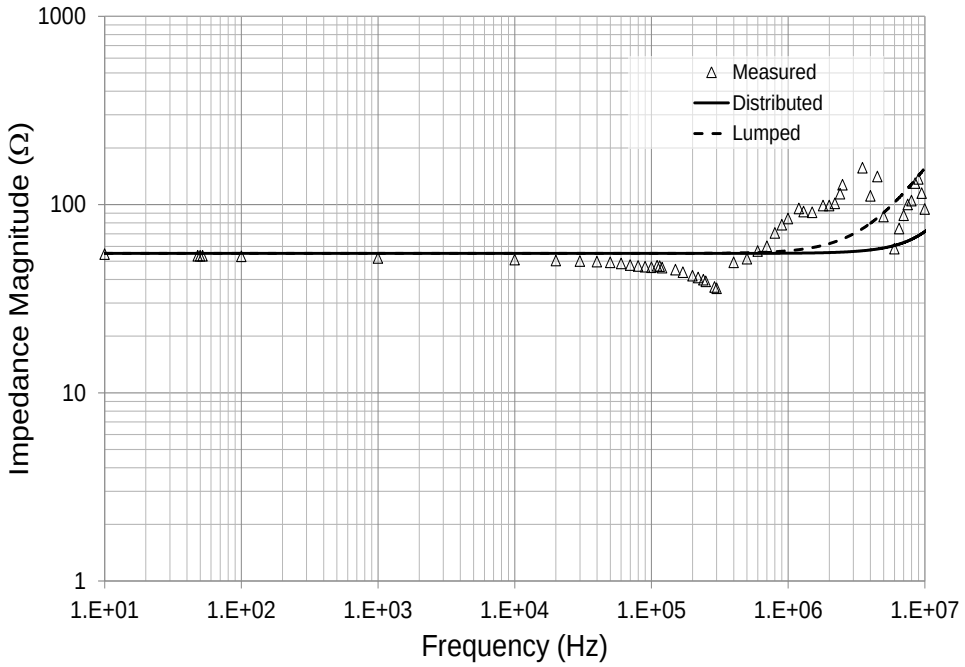

Figure 4.24: Comparison between measurement results and computation for a 2.4m vertical rod

4.11 Conclusions

Experimental results of DC earth resistance tests on different lengths of vertical rods were reported. The results show that the DC resistance of vertical rods decreases with increasing length of the conductor. The measured DC resistance of the short vertical rod was found to vary seasonally due to soil resistivity variations over the period of the study.

Variable frequency field tests (DC to 10MHz) on different lengths of earth rod reveal the benefits to low frequency performance of extending the rod length, although these gains are less significant with longer rods. In addition, the tests indicate that, at higher frequencies, rod length extension may be counterproductive, with higher values of impedance recorded for the longer rods.

A new technique to reduce the earth resistance/ impedance of the earth electrode was demonstrated. This technique involves the installation of horizontal enhancements at the top of vertical earth electrodes of increasing length. The results show that a significant reduction in impedance is achieved over both low and high frequency ranges.

The measurement results indicated that an insulated conductor did not give a significant reduction in the earthing impedance at low frequency. However, at high frequency, the reduction in the impedance is noticeable and can be explained by a reduction in the inductive effect due to the additional parallel current paths. Good agreement between experimental and simulation results is obtained.

Although, the standard recommended that effectiveness of the arrester can be improved by connecting it to an earth electrode in the immediate vicinity, for example an earth rod (normally 5m long) [4.33], the rod with horizontal enhancements presented a significant reduction in impedance magnitude at low frequency and high frequency compared with rods only. Therefore, this technique presents a reliable earthing system by dissipating high frequency contents into the earth compared with the vertical rod only. In addition, from the test results, the vertical rod with horizontal electrode enhancement is recommended as the best earth configuration to improve the behaviour of earth electrode under low and high frequency response.

CHAPTER FIVE: PORPOSED ENHANCED EARTH ELECTRODE SYSTEMS UNDER IMPULSE ENERGISATION

5.1 Introduction

In the previous chapter, different lengths of vertical rods were tested under DC and AC over a range of frequencies. The effects of additional horizontal enhancements with different lengths of vertical earth electrode were measured and investigated. The results showed that using horizontal enhancements with the rods gave significant reduction of earth resistance at low frequency and served to reduce the earth impedance at high frequencies.

The response of earth electrode systems to impulse currents has been published in theoretical [5.1-5.22] and experimental studies [5.23-5.30]. In these studies, a variety of impulse currents were investigated, and particular quantities were determined, such as the rise in potential of the earth electrode system, the electromagnetic field near the earth electrode, and current distribution and dispersion. According to the reviewed literature, it appears that a detailed study of the application of '4-point cross' and '8-point star' enhancements to single rod electrodes has not been attempted before.

In this chapter, an experimental investigation on the impulse response of vertical earth rods up to 6m with and without horizontal enhancements (4-point star and 8-point star-shaped) is described. In addition, the effects of an additional above-ground insulated conductor bonded to the 43 and 88m horizontal earth electrodes are also investigated. Moreover, the experimental results are compared with simulations using CDEGS HIFREQ and FFT software [5.31].

5.2 Impulse Tests

In Chapter 4, the experimental setup at Cardiff University's earthing test facility was described (see Figure 4.4). A Haefely recurrent surge generator was used to produce double exponential impulse currents of different shapes, with amplitudes up to a few amperes. The current return electrode was located 150m from the test object and the reference potential electrode, fixed 100m away, was connected by an insulated lead arranged orthogonally to the current return lead to avoid ac mutual coupling [5.32]. Lilco current transformers of 0.1V/A sensitivity with a bandwidth of 20MHz were used for current measurements. Voltage measurement was achieved using a differential voltage transducer of 25MHz bandwidth and ratio of 1/20, 1/50 and 1/200 attenuation.

5.3 Vertical Earth Electrode

As described previously, vertical earth electrodes are widely used in earthing and lightning protection systems, either as main earth electrodes or as reinforcing electrodes to help reduce the earth impedance and improve the system's high frequency and transient performance.

Figure 5.1 shows the transient earth potential rise (TEPR) for different lengths of vertical rod electrode for a fixed peak current injection of 1.2A and of 11/36 μs shape. From the figure, it can be seen that, for this value of current impulse rise-time, the voltage and current peaks occur at the same time for all rod lengths, indicating a predominantly resistive response. The peak voltage falls as the electrode length increases and, with a similar trend to that seen with the DC resistance measurements. The decrease in the peak voltage also reduces with rod length.

Two different definitions of calculating the impulse resistance were used. Equation (5.1) defines the impulse resistance as the ratio of voltage peak to current peak, and is

valid when the earth electrodes have negligible inductance, and thus impulse voltage and current maxima occur at the same time. Equation (5.2) is used where the time of the impulse voltage peak and current peaks do not coincide, so as to eliminate any inductive effect in the test results [5.33].

$$R_{imp_1} = \frac{V_p}{I_p} \qquad (5.1)$$

$$R_{imp2} = \frac{V_{@I_p}}{I_p} \qquad (5.2)$$

Table 5.1 shows the calculated impulse resistance as defined by Equations (5.1) and (5.2) from the test results. The DC resistances were tested by a standard earth tester (DET 2/2). From the table, it can be seen that, due to the close coincidence of all voltage peaks with the current peak, the values of V_p/I_p (R_{imp1}) and R_{imp2} are very similar. The values of impulse resistance are also very close to the measured DC resistance values.

Table 5.1: Performance indices of different length earth rods (10/36 current impulse)

Rod length (m)	$R_{im1}(\Omega)$	$R_{imp2}(\Omega)$	R_{dc} (Ω)
1.2	119.5	118.4	113
2.4	52.7	51.8	55.7
3.6	42.4	42.4	40.4
4.8	35.2	34.7	35.0
6	32.1	32	30.6

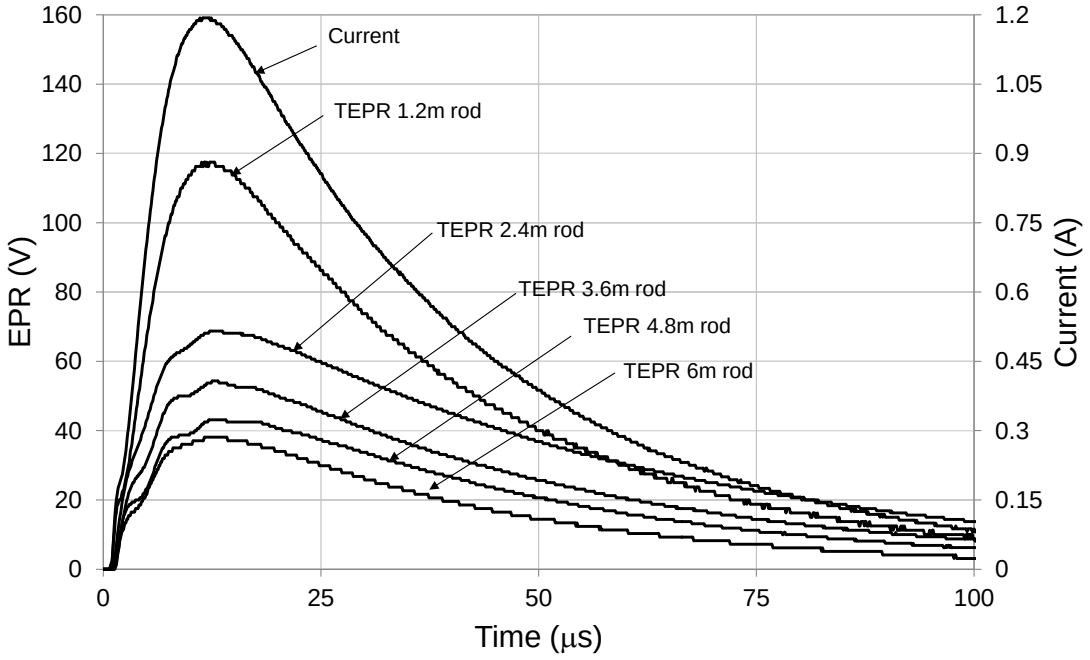

Figure 5.1: Responses of earth rods of different lengths to a 10/36 current impulse

5.4 Vertical Earth Electrode with Horizontal Enhancements

The transient response of the 1.2m vertical rod with additional 'cross' and 'star' formation horizontal conductors is shown in Figure 5.2. In the figure, it can be seen that significant gains are achieved through reduction in peak TEPR. These gains are in direct proportion to the reduction in impulse resistance.

Figure 5.3 shows the effect of horizontal enhancements on the earth potential rise of a 2.4m rod. The peak injected current was 1.44A with 3.2μs rise time at the injection point, and was shown in Figure 4.4 in Chapter 4. From the waveforms presented in Figure 5.3, it can be seen that the percentage reduction in the voltage of a rod with cross and star enhancements is 40.8% and 54.9% compared to the rod only.

In order to investigate the effect of increasing the length of the vertical electrode with additional horizontal enhancements, the earth potential rise (EPR) of the 6m rod with

and without cross/star-shaped electrodes was measured. Figure 5.4 shows the EPR of the regular and enhanced 6m rod for an impulse current of 5.5A peak with rise-time of around 1.8/4.5μs. As can be seen from the figure, significant reduction of the peak voltage was obtained in the case of rods with horizontal enhancements, and is in agreement with the DC earth resistance shown in Table 4.2 of Chapter 4. The impulse resistance for the 6m rod, rod with cross and rod with 8-point star obtained from the Equation (5.2) are 28.6Ω, 18.6,Ω and 16Ω respectively.

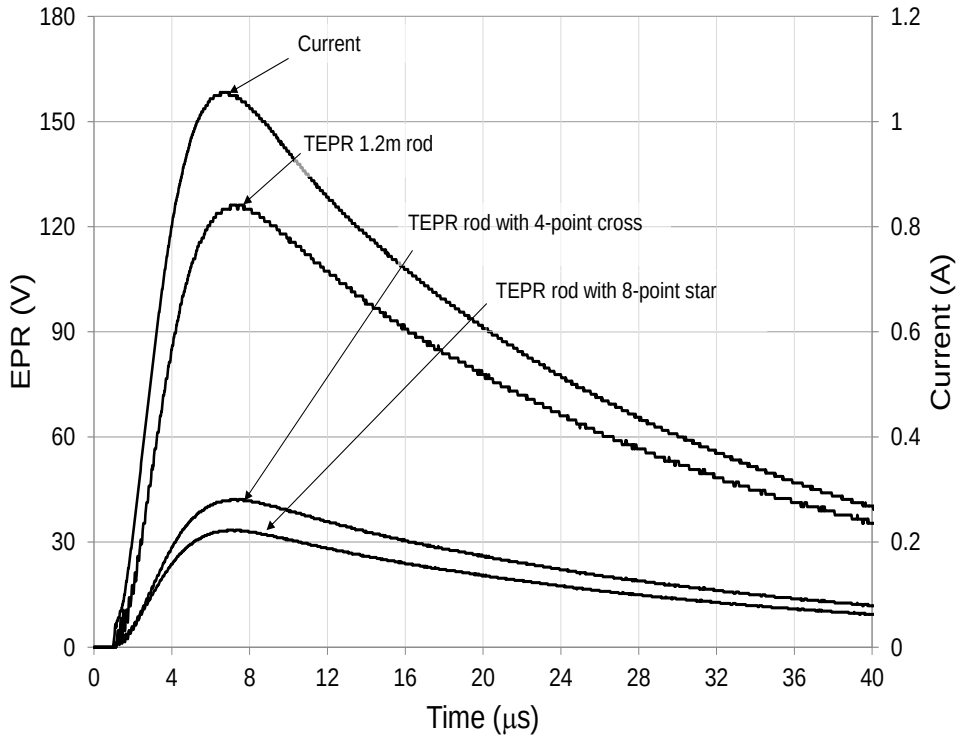

Figure 5.2: Voltages and current shapes at injection point for the 1.2m rod with cross and star-shaped enhancements

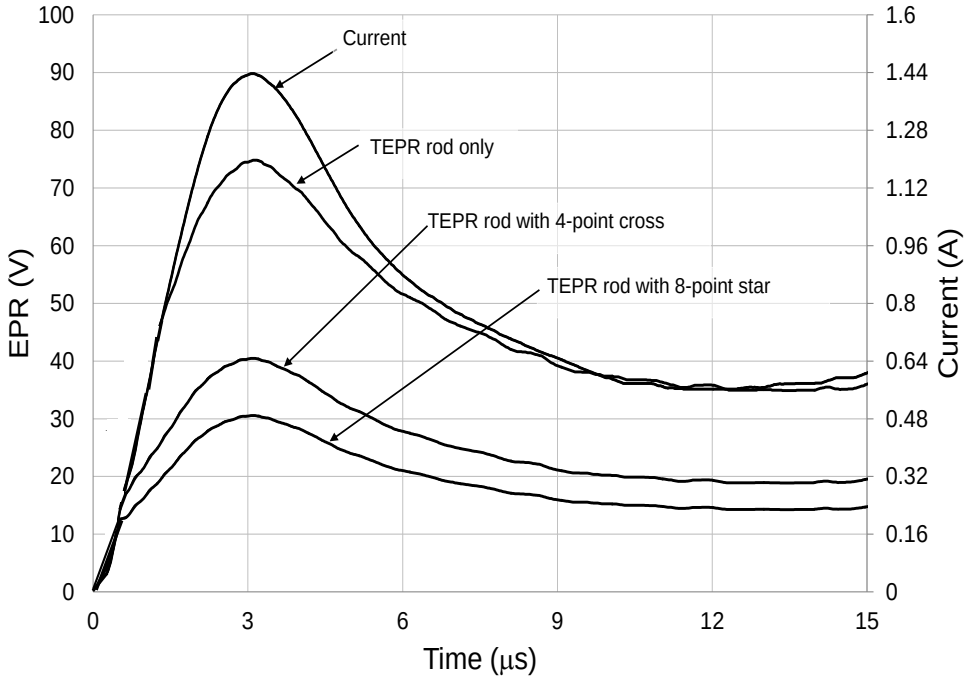

Figure 5.3: Voltages and current shapes at injection point for the 2.4m rod with cross and star-shaped enhancements

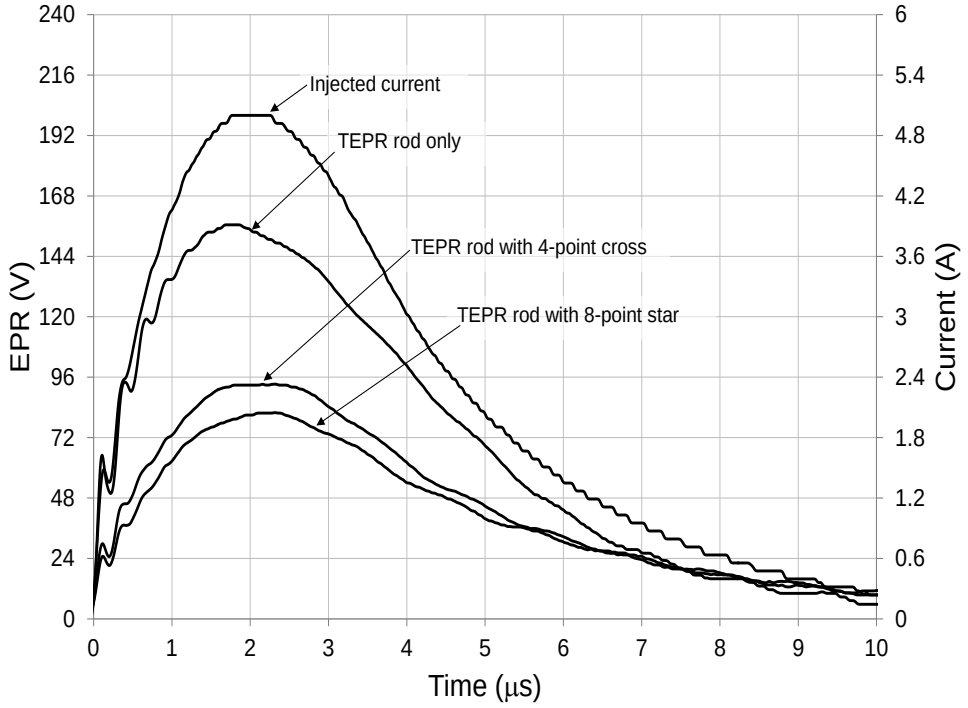

Figure 5.4: Voltages and current shapes at injection point for the 6m rod with cross and star-shaped enhancements

5.5 Horizontal Earth Electrode

The experimental test circuit which was described in Figure 4.5 in Chapter 4 shows the current source, the 88m bare conductor under consideration, the current return electrode (2.4m rod) and the remote reference potential electrode and cable. A current impulse of magnitude 2.375A with rise time of 5.2μs is injected into 14m, 19m, 33, 53 and 88m horizontal earth electrodes and the waveforms of earth potential rise (EPR) measured with the same injected current and rise-time values. Figure 5.5 shows a sample of the resulting waveforms which illustrates the impulse applied to different lengths of the horizontal earth electrode. It is clear from the figure that increasing the length of electrode reduces the maximum earth potential rise (EPR). For example, the measured voltage peak values at the injection point were 38.7, 32.8, 26.8, 26.8 and 26.9V for 14m, 19m, 33, 53 and 88m respectively.

However, it is clear that the peak voltages for all lengths of the horizontal electrode occur before the peak injected current, which indicates that the inductive behaviour is dominant. Therefore, a longer horizontal earth electrode leads to lower earth resistance but larger inductance of the test circuit. Furthermore, when the length of the horizontal electrode is increased from 33m to 88m, with no further reduction in the peak voltages is observed as the length increases, as explained in Chapter 2 at Section 2.6. This might be attributed to the effective length, and it can be verified by comparison with Equation (5.3) [5.34].

$$\iota_{eff} = A(\rho\tau)^{0.5} \qquad (5.3)$$

Where:

ρ: is the soil resistivity in Ωm

τ: is the wave front time in sec

A is a constant factor which depends on the location of the injection current point and is equal to 1.4 for current injected at one end.

A value of the 43m horizontal electrode was calculated the effective length using Equation (5.3) with a uniform soil resistivity of 180Ωm and front time of 5.3μs is 43m. Table 5.2 illustrates the peak values of current (A) and the voltage at the instant of current peak ($V_{(@Ip)}$) at the injection point, for an injected current at all electrode lengths of 2.375A. The impulse resistance was calculated to be 9.2Ω for the 88m electrode by the ratio of $V_{@Ip}/I_p$. This ratio remains roughly constant for all electrode lengths greater than 33m. Further shortening of the electrode causes an increase of the ratio. This means that the impulse resistance is limited by the effective length and no further reduction in the impulse resistance may be obtained by extending the electrode. Similar results have been reported by [5.35, 5.36].

Table 5.2: Measured peak current and voltage at injected point

Length of electrode(m)	**I_p(A)**	**$V_{(@Ip)}$(V)**	**$V_{@Ip}/I_p$**
14	2.375	38.14	16.1
19	2.375	31.6	13.3
33	2.375	23.11	9.7
53	2.375	22.5	9.5
88	2.375	21.9	9.2

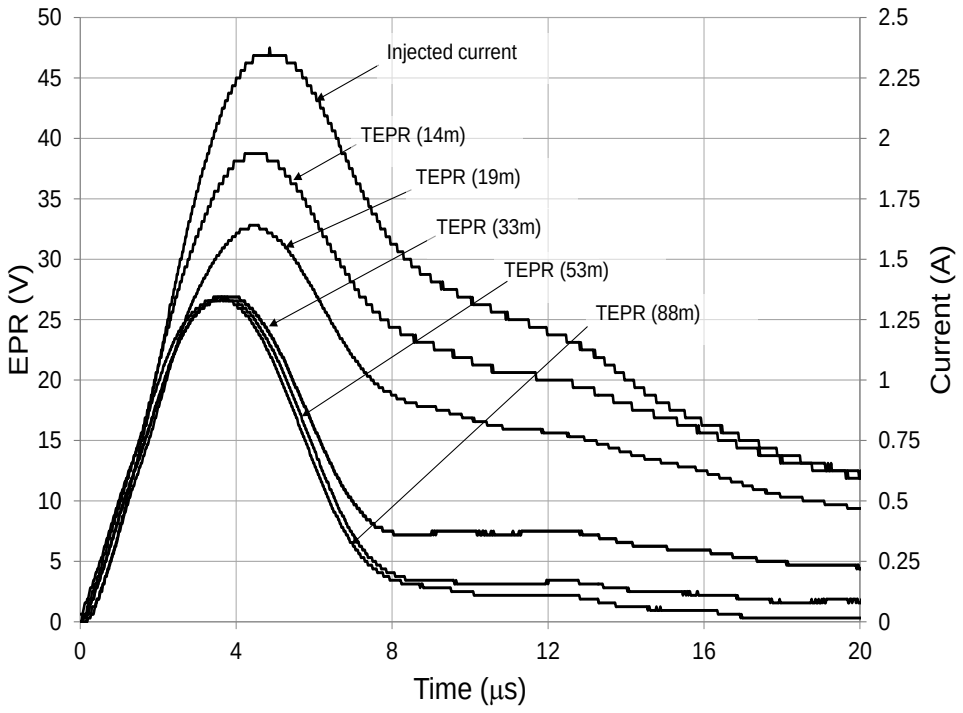

Figure 5.5: Responses of horizontal electrodes of different lengths to a 5/12 μs current impulse

5.6 Horizontal Electrode with Above Insulated Parallel Conductor Enhancement

Figure 5.6 shows the EPR and current traces for a 2.76/9μs injected current with 2.47A magnitude for the 43m and 88m bare conductor with and without above-ground insulated conductor. From the figure, the effect of the electrode inductance is indicated in the rising edge by a sharp rise in electrode potential for both the 43m and 88m electrodes with and without above-ground conductor. However, using the above ground conductor can reduce the EPR of both horizontal electrodes and, it was found that the percentage reductions in the EPR are 12% for the 43m horizontal electrode, while there was a 14% reduction for the 88m bare conductor. Hence, the developed earth impulse impedance of the horizontal electrode is reduced.

Table 5.3 gives the data obtained from the test of the 43m and 88m horizontal with and without insulated conductor. The DC resistance was measured by DET 2/2 earth tester

and the impulse resistance was calculated by Equation (5.2). From this table, it is clear that an additional above-ground insulated conductor presents a small reduction for both the DC and impulse resistances.

Table 5.3: DC and Impulse Resistance of Horizontal Electrodes

Configuration	DC resistance(Ω)	Impulse resistance(Ω)
43m bare only	8.4	9.5
43m with above conductor	8.1	8
88m bare only	4.73	7.5
88m with above conductor	4.2	6.2

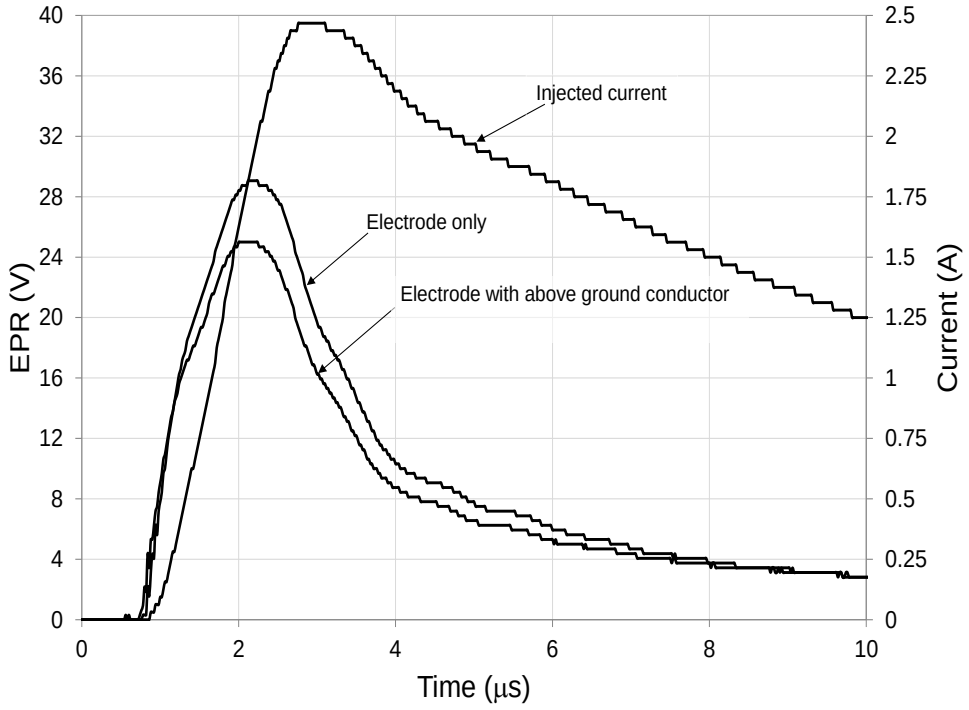

(a)

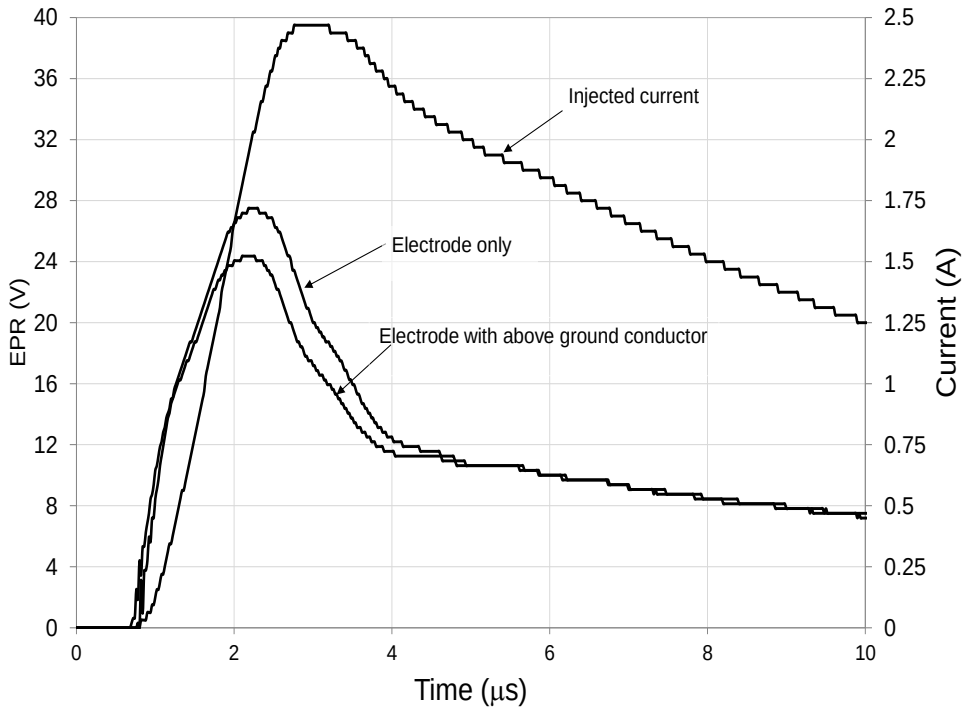

(b)

Figure 5.6: Impulse responses of horizontal electrodes with and without above-ground insulated conductors: (a) 43m length (b) 88m length

5.7 Computer Models of Earth Electrodes

The actual geometrical test configuration was modelled using CDEGS program [5.31]. A two-layer soil model was used and both the current injection and voltage measuring leads were simulated. The computation was achieved by energising the electrode using the measured time-domain current data. The frequency spectrum of the impulse current is then calculated using an FFT routine before processing in the HIFREQ module which calculated the earthing system response in the frequency domain. An inverse FFT routine is then performed to compute the time domain response of the electrode.

The transient behaviour of the 3.6m vertical rod with and without 4-point star cross and 8-point star enhancements was measured, and compared with the CDEGS computations. Figure 5.7 shows an example of results obtained from computer

simulations of the 3.6m rod with 4-point cross and 8-point star enhancements. Considering the 3.6m rod only, the computed transient voltage impulse has a slightly lower peak magnitude compared with the measured value. However, for the 3.6m with enhancements, slightly higher magnitudes are predicted by the simulations. Overall, there is very good agreement between computed and measured values, and the small differences may be due to the uniformity of the stratified soil model used in the simulation model.

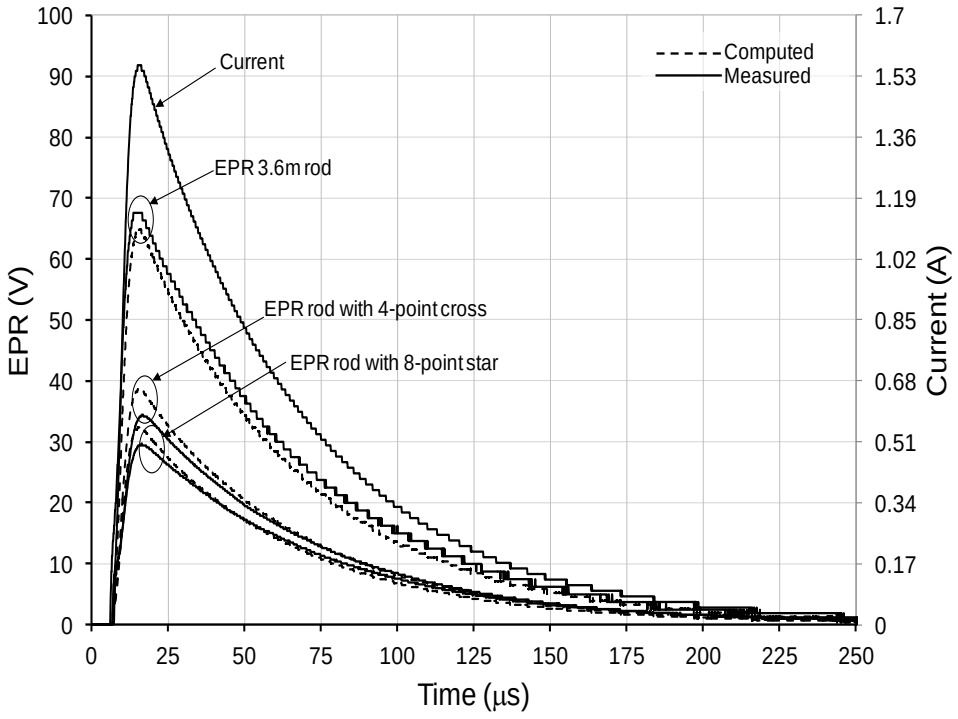

Figure 5.7: Transient response of the 3.6m vertical rod to an 11/36 current impulse with 'cross' and 'star' enhancements: Computed and measured values.

5.8 Conclusions

Different lengths of simple vertical earth electrodes up to 6m have been measured under impulse conditions with various rise times. Low voltage impulse tests with 11/36μs current injection reveal a similar trend to that seen for low frequency and DC

resistance tests with the longer rod. This results in lower earth potential rise (EPR) as discussed in Chapter 4. For the relatively slow-front current shape used in the tests, a predominantly resistive behaviour was obtained.

Furthermore, the earth potential rise (EPR) of vertical rods with additional horizontal enhancements was measured. Significant reduction in earth potential rise (EPR) at the injection point is obtained when a 4-point cross or 8-point star is connected to the vertical rods. Further reduction in TEPR was realised with additional vertical rods installed at each ends of the horizontal enhancements, with a 6m vertical rod at the centre point.

In addition, impulse tests on horizontal electrode of different lengths were conducted. The results showed that the EPR reduces when the length of electrode increases until it reaches a certain value which is attributed to the effective length.

Experimental tests under impulse injection on the 43m and 88m horizontal earth electrodes with and without the above ground-insulated conductor were carried out. The results showed that the impulse resistance reduced when the horizontal earth electrode was enhanced with an above ground insulated conductor.

Thus design given above is optimal because it presents minimal earth potential rise (EPR) for all length of rods close to the injection point compared to the rod only. In addition, reducing the earth potential rise means decrease the step and touch voltages near the injection point. Therefore, from the results in Chapter 4 and 5, using the rod with enhancements can be recommended to improve the behaviour of the earthing system at low, high frequency and impulse response.

Computed results for the impulse response showed good agreement with measurement results.

CHAPTER SIX: IMPROVED VOLTAGE AND CURRENT DISTRIBUTIONS IN ENHANCED EARTH ELECTRODE SYSTEMS

6.1 Introduction

As reviewed in Chapter 2, many papers have attempted to analyse the current distribution of earthing electrodes by computer simulation [6.1-6.5] and in the laboratory [6.6, 6.7]. However, these analyses do not fully reflect the results of experimental investigations in the field, due to the complex current dispersal processes involved. This limits the suitability of computation and laboratory studies for validation purposes, because precise modelling of the earthing system in representative field conditions requires knowledge of both voltage and current distributions in non-uniform soils. On the other hand, a few researchers have conducted current distribution experiments under impulse conditions in the field [6.8, 6.9]. However, these authors have studied the current distribution under impulse response for horizontal earth electrodes only. To the author's knowledge, the current distribution in vertical and horizontal earth electrodes with enhancements under low/high-frequency and impulse conditions was not attempted before.

In Chapters 4 and 5, a new technique to improve the performance of earthing system under high frequency and impulse response was proposed and investigated both experimentally and analytically.

This chapter undertakes an investigation of the voltage and current distributions for two electrode systems installed at Cardiff University's earthing test facility under high frequency/transient conditions compared with that at power frequency: (i) vertical earth rods of different lengths with horizontal electrode enhancements in cross formation, (ii) the long horizontal earth electrode with a parallel interconnected

insulated conductor. The measurement results obtained are compared with those obtained by computations.

6.2 Experimental Setup

Figure 6.1 shows a diagram of the experimental setup used for the first electrode system which comprises 1.2m, 2.4m, 3.6m and 4.8m-long vertical rod conductors.

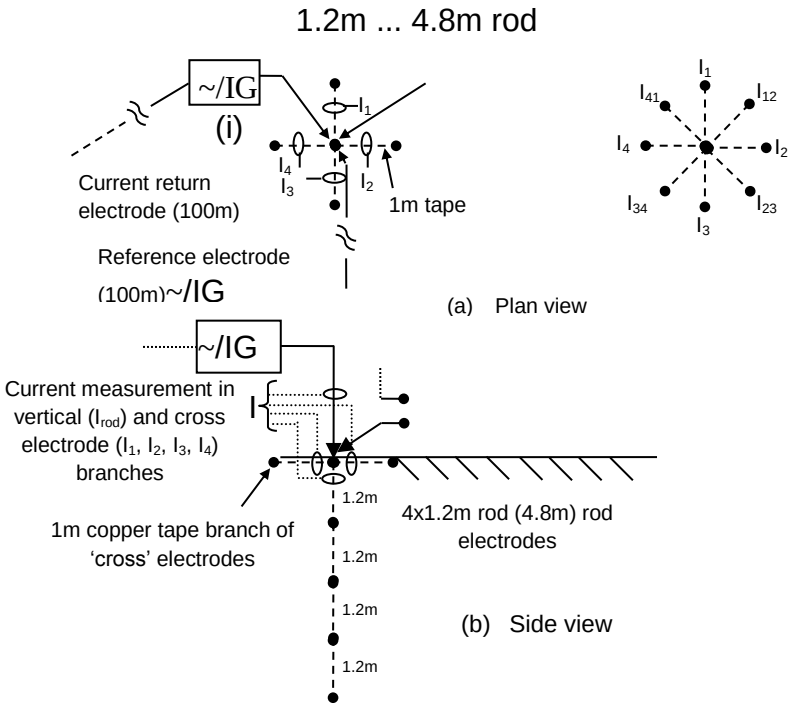

Figure 6.1: Plan and side views of experimental set-up: Rods with horizontal enhancements.

Five Lilco-58MH100 current transformers were installed at the junction point between the vertical and horizontal electrodes, as shown in Figure 6.1, to achieve current measurement for the complete electrode system, the rod component and each of the branches (I_1-I_4) for the cross configuration. The electrode was energised using (i) a variable frequency source and (ii) a recurrent surge generator with the current return electrode located 100m away. The second earth electrode under test is a horizontal bare electrode, 88m long as shown in Figure 6.2. This conductor is enhanced with an

additional above-ground insulated conductor For this electrode system, 5 Lilco-58MH100 current transformers were installed, in turn, at each junction point (A to N) in order to obtain a picture of current distribution in the above-ground insulated sections and from this conductor to the bare underground conductor. A similar energisation and reference electrode arrangement was used for this electrode. The EPR (vertical rod or horizontal electrode) was measured with respect to a remote potential reference electrode installed at a distance of 100m from the injection point. To eliminate interference including mutual coupling effects, a Nicolet Isobe 3000 fibre-optic system was used to transmit the measurement signals to the recording instruments. This Nicolet fibre-optic (Isobe 3000) links have an input resistance of 1 MΩ, and the transmitter has a selectable input range from 0.1 V, 1 V, and 10 V.

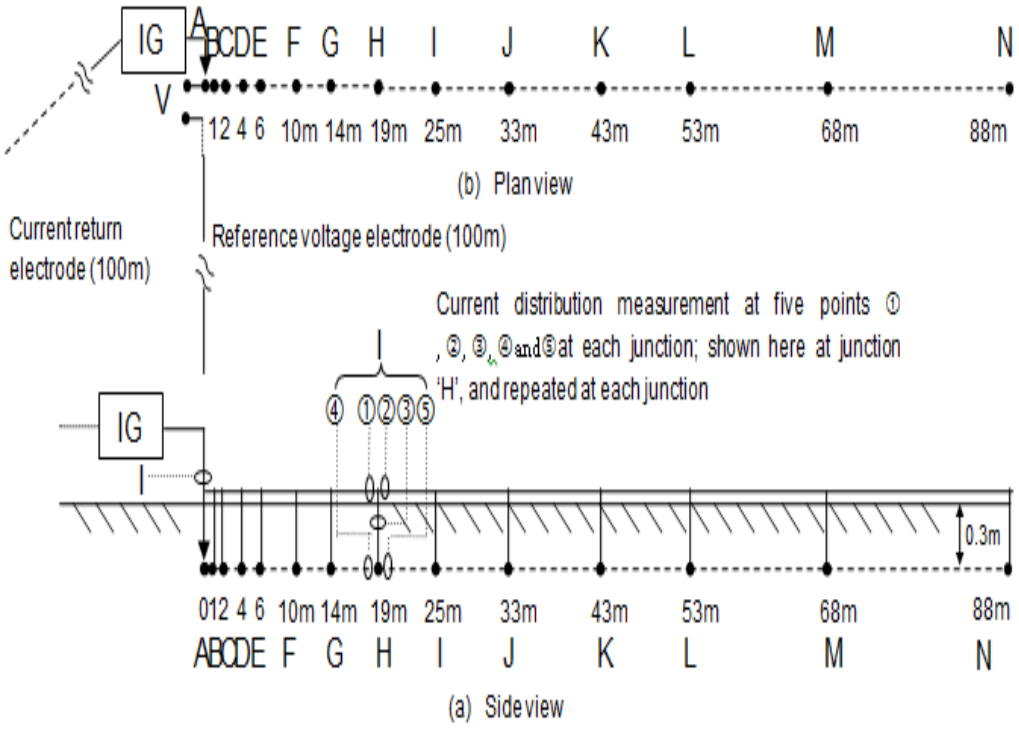

Figure 6.2: Plan and side views of horizontal test earth electrode with parallel insulated interconnected conductor: (a) plan view (b) side view

6.3 Test Results

In this part, results from experimental tests to investigate the voltage and current distribution of different structure earth electrode under different low/high frequency and transient performance are presented.

6.3.1 Frequency Response

6.3.1.1 Vertical Earth Rod Systems

Current distribution in the 2.4m-rod/4-point star earth electrode system is shown in Figure 6.3. With reference to the figure, it can be seen that the rod carries a very high proportion (220mA) of the total current (530mA) at low frequency with the horizontal electrode sharing the remainder in unequal portions. However, as the frequency is increased, the magnitude of the current flowing in the rod decreases quite significantly, while there is a general increase in magnitude of current in all the horizontal electrodes (note that the total injected current was maintained constant over the entire frequency range). Figure 6.4 shows the waveforms of current measured at the top of the rod and at the beginning of each horizontal enhancement under low and high- frequency. It is clear from the figure that the current waveforms at 52Hz and 1MHz are in agreement with the results in Figure 6.3. The measured DC earth resistance of the combined electrode system together with the values of the resistances of the individual elements are shown in Table 6.1. Table 6.1 confirms that, as expected, the majority of current flows through the rod at low frequency due to the rod's much lower resistance compared with an individual branch of the cross electrodes. However, the reduced proportion of current flowing in the rod at high frequency is not as expected from a 'high-frequency earth electrode' which is recommended to enhance horizontal

electrodes or earth grids [6.10]. These present tests indicate that the rod is more effective in distributing current at lower frequencies.

Table 6.1 Measured earthing resistance of different configurations

Configuration	DC Resistance(Ω)	
	2.4m rod	4.8m rod
Rod with cross	25	23
Rod only	58	35
Cross only	34	38
Cross branch 1(R_1)	104	115.4
Cross branch 2(R_2)	103	113.2
Cross branch 3(R_3)	93	92.5
Cross branch 4(R_4)	98	104.3

Current distribution in the 4.8m-rod/4-point star earth electrode was also measured, with results as shown in Figure 6.5. A current of 553mA was injected at all frequencies. As can be seen from the figure, roughly 60% of injected current flows into the 4.8m rod, which is higher than the current which flowed into the 2.4m rod at low frequency 10Hz, while 9%, 8%, 12% and 11% of injected current value flows into cross branches R_1, R_2, R_3 and R_4, respectively. However, at 1MHz, only about 38% of the injected current flows into the rod, with between 12% and 20% in cross branches.

The measured DC earth resistance of the 4.8m-rod/4-point star earth electrode, the values of the resistances of the individual elements and 4-point cross are also shown in Table 6.1. As expected, when the resistance of the rod decreases, most of the current flows through the rod at low frequency compared with an individual branch of the

cross electrodes. Despite a doubling of the rod length, a higher current was still shown to flow in the cross branches compared with the rod at high frequency.

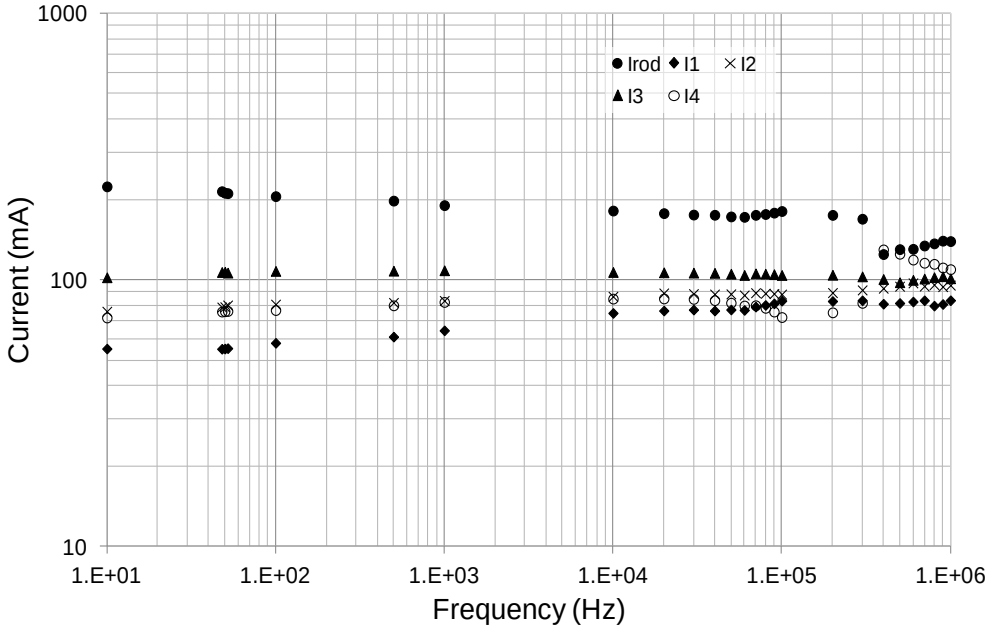

Figure 6.3: Current distribution in the 2.4m rod-horizontal cross electrode formation

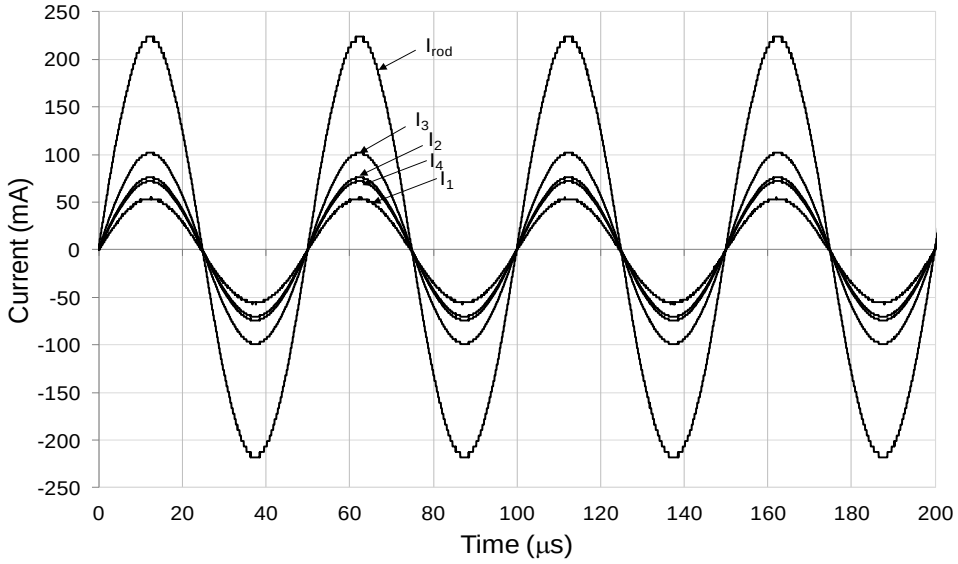

(a)

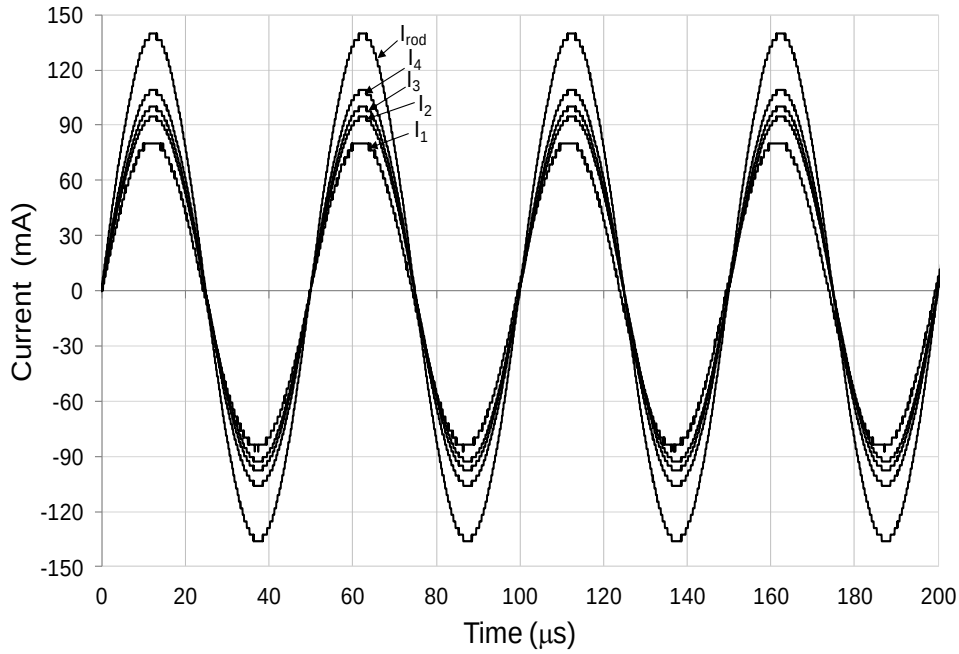

(b)

Figure 6.4: Alternative current distribution between individual 2.4m rod and horizontal cross electrode formation at: 10Hz; b) 1MHz

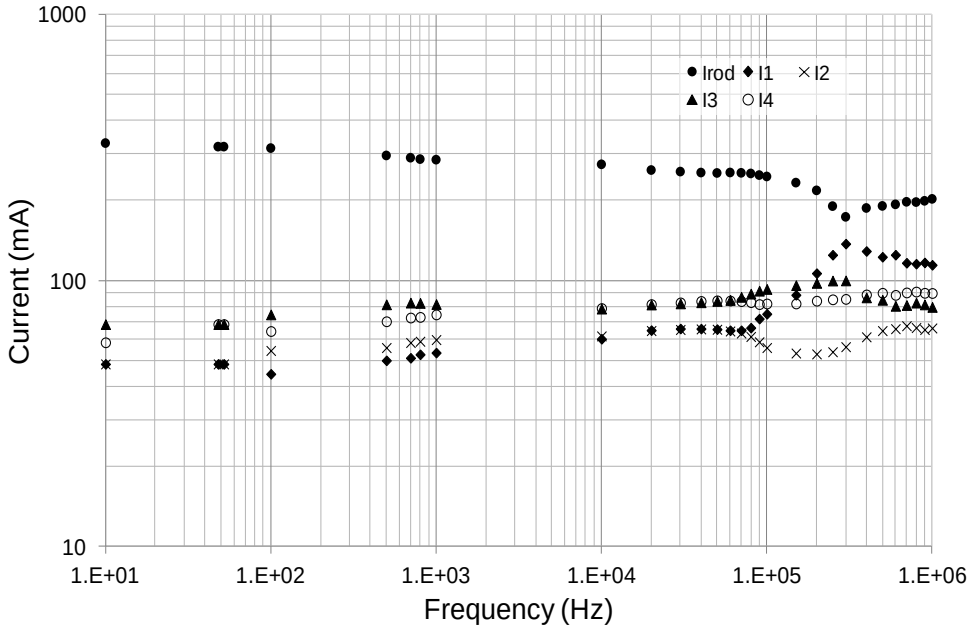

Figure 6.5: Current distribution in the 4.8m rod-horizontal cross electrode formation

6.3.1.2 Horizontal Earth Electrode Systems

Simulations were carried out using CDEGS-HIFREQ software [6.11] based on the actual dimensions of the test electrode and an equivalent two-layer soil model (top layer 180Ωm to 9m, bottom layer 70Ωm), as shown in Figure 6.6.

In order to investigate the current distribution in the insulated and bare sections of the horizontal electrode system shown in Figure 6.2, reference test was first carried out on only the bare horizontal conductor. Several test frequencies were used ranging from 52Hz to 100 kHz. Different currents were injected under low frequency (52Hz) and high frequency (100 kHz) at one end with 642mA and 109mA respectively. The current and voltage distributions along the electrode are shown in Figure 6.7 and Figure 6.8 at 52Hz and 100 kHz respectively.

As can be seen from the figure, the current dissipates more rapidly with conductor length at high frequency compared with power frequency. Moreover, regarding the voltage distribution, the voltage is constant for power frequency (52Hz), as shown in Figure 6.7, and this might be due to the relatively low series inductive reactance at this frequency. On the other hand, reducing exponentially in magnitude along the length of the earth electrodes for the high frequency (100 kHz) due to the inductive effect of the horizontal electrode (see Figure 6.8). As can be seen from the Figure 6.7 and 6.8, quite close agreement are obtained between measured and simulated current and voltage distributions (see).

The variable frequency test was repeated for the complete electrode system shown in Figure 6.2 which includes the additional insulated parallel conductor bonded to the bare underground horizontal earth electrode. The test results reported in Figure 6.9 correspond to a 52Hz current injection. From the figure, it can be seen that the

potential distribution along the horizontal electrode is constant due to the relatively low inductive reactance at this frequency and the current flowing from the insulated conductor to the buried bare conductor, (I_3), which is distributed reasonably evenly over the length. Variations in section length and soil resistivity along the conductor will, however, influence the distribution.

The test results corresponding to an injection frequency of 100 kHz are shown in Figure 6.10. At this higher frequency, it can be observed that both the voltage and current distributions in the insulated conductor show a fall in magnitude along the length of the conductor. However, the magnitude of the current flowing from the insulated conductor to the bare conductor, I_3, is of the same order at each intersection. The test circuit in Figure 6.2 was simulated by CDEGS software, as shown in Figure 6.11.

Figure 6.12 shows the schematic circuit diagram for the 88m horizontal electrode under 100kHz and compared with the computed results. Here, the percentages of current flowing into the above ground conductor are roughly 59% and 58% of the measured and computed results, respectively. In general, the addition of an above ground conductor changes the current distribution with respect to that of the bare electrode alone (see Figure 6.8), resulting in a reduced current concentration close to the point of injection. In addition, the computed values are reasonably close to the measured values, with some difference between measured and computed results which might be attributed to the soil resistivity estimate used in the simulation. Moreover, the variations in the current dissipation over the length of the 88m horizontal electrode might be due to the variations in the soil resistivity along the bare conductor.

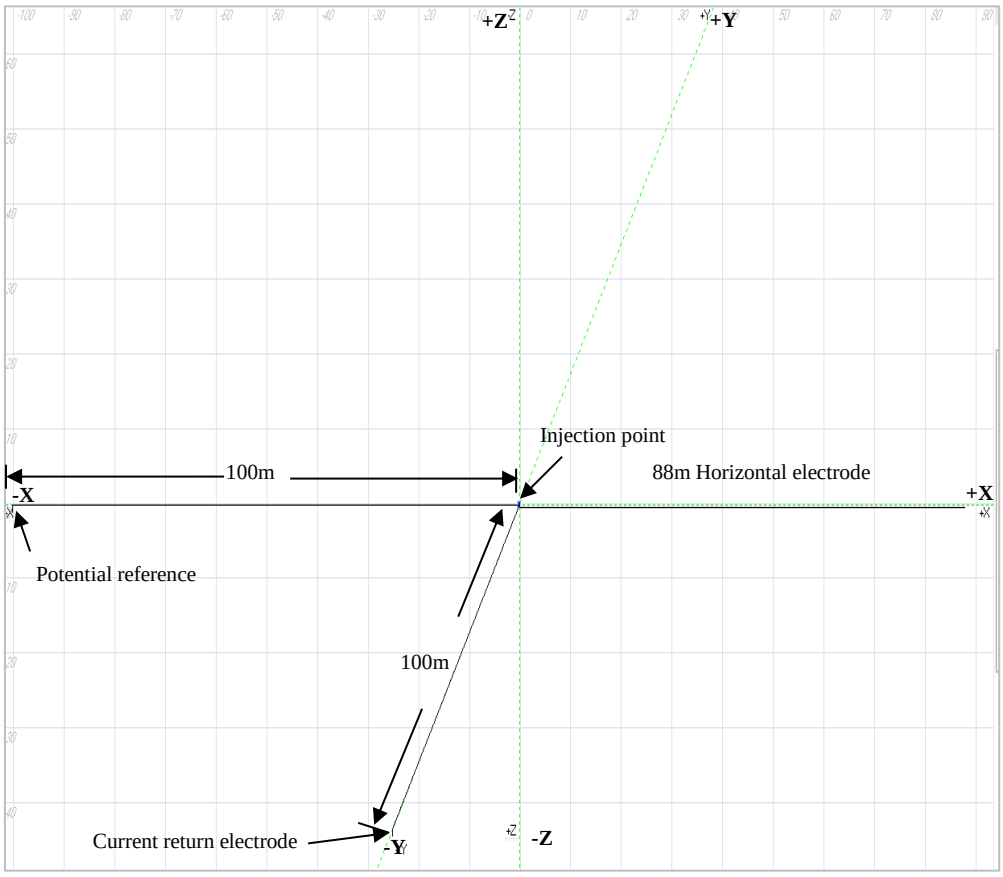

Figure 6.6: CDEGS simulation for the 88m horizontal earth electrode

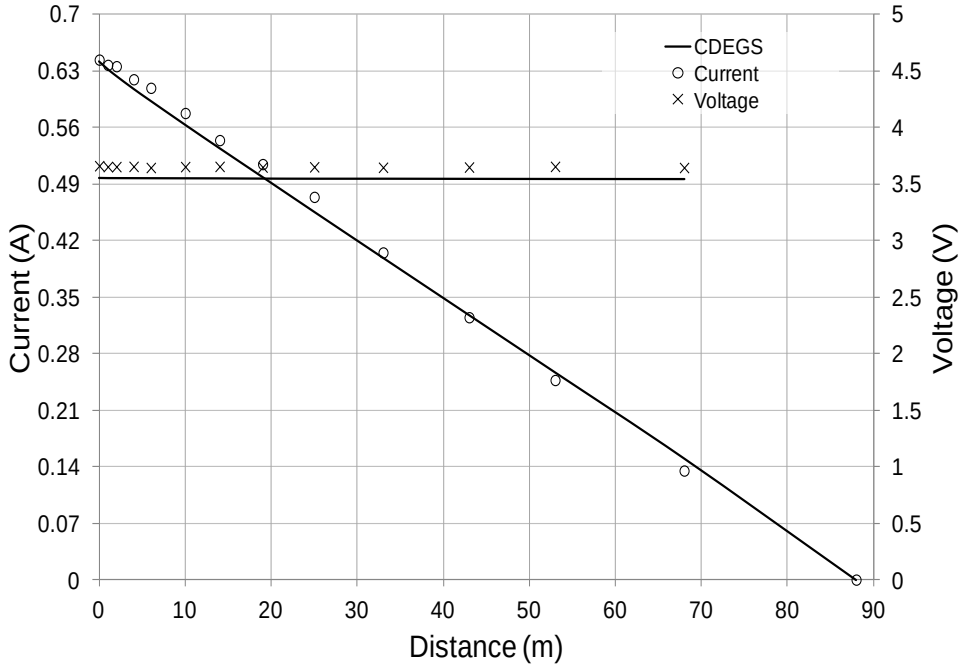

Figure 6.7: Current and voltage distributions at 52Hz along 88m bare electrode

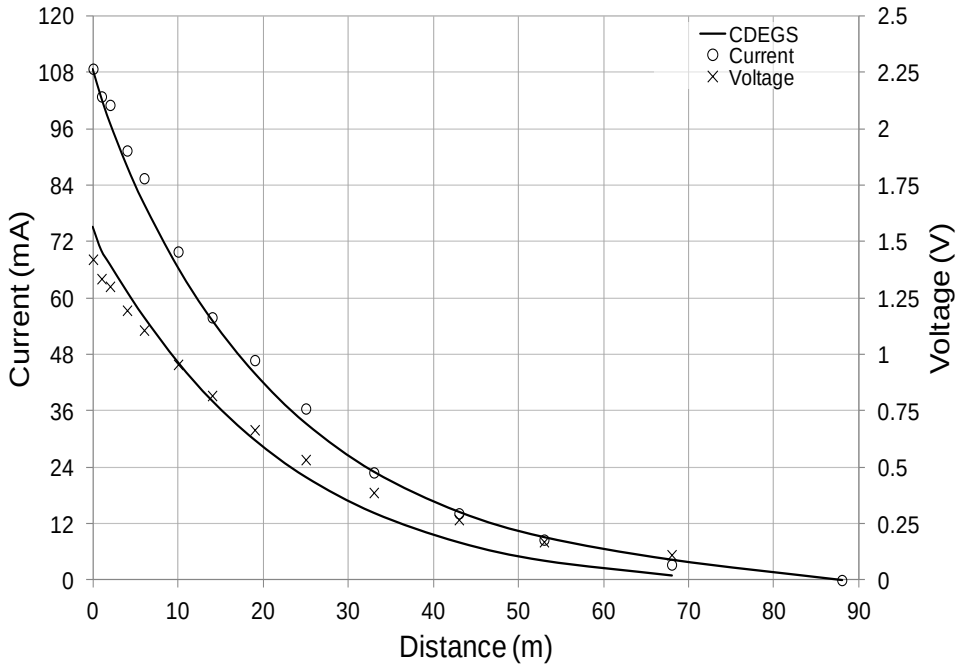

Figure 6.8: Current and voltage distributions at 100 kHz over 88m bare electrode length

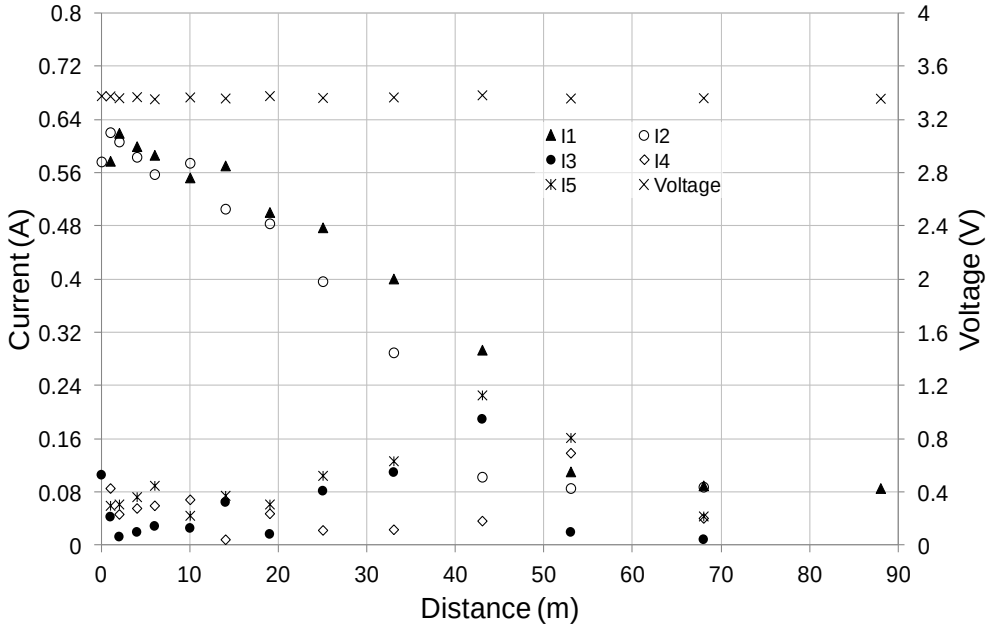

Figure 6.9: Current and voltage distributions at 52Hz along 88m electrode with parallel insulated conductor

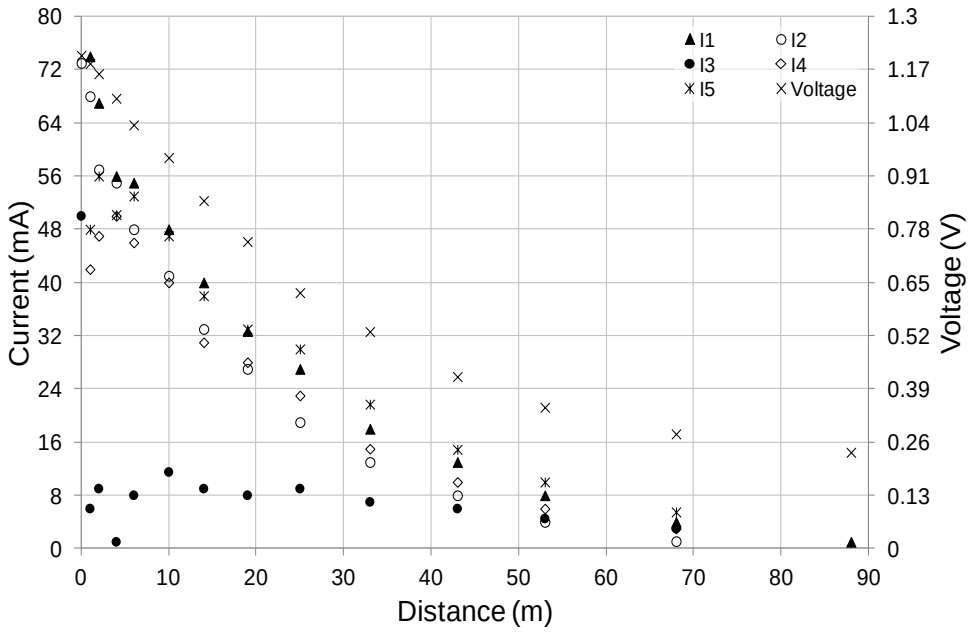

Figure 6.10: Current and voltage distributions at 100 kHz along 88m electrode with parallel insulated conductor

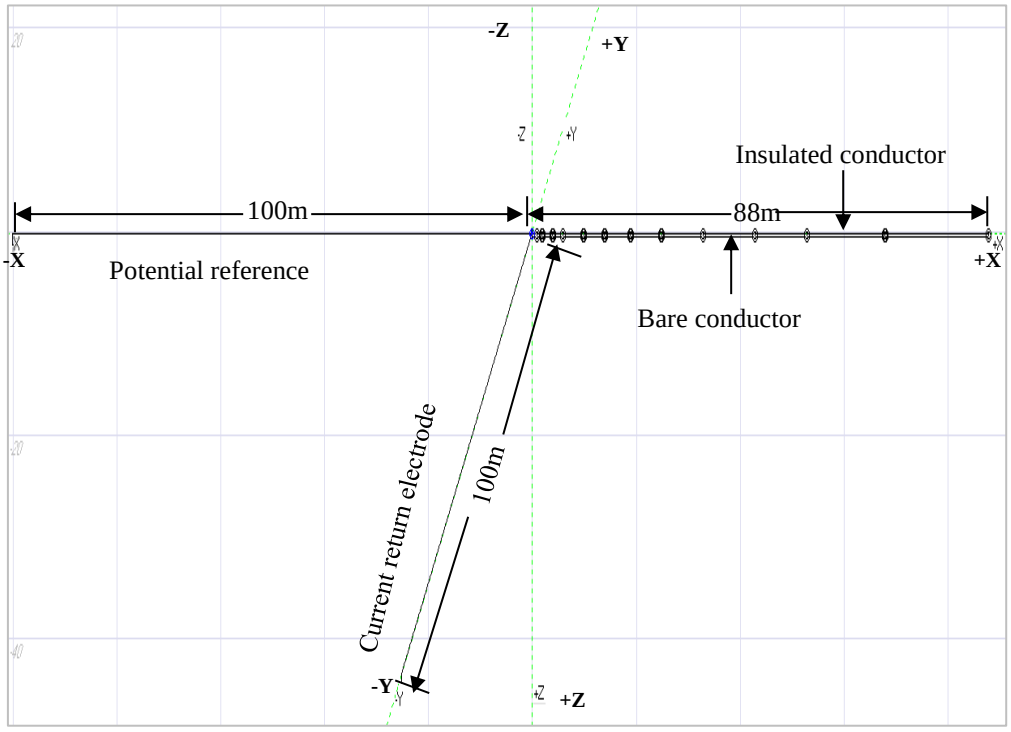

Figure 6.11: CDEGS simulation for the 88m bare with insulated conductor

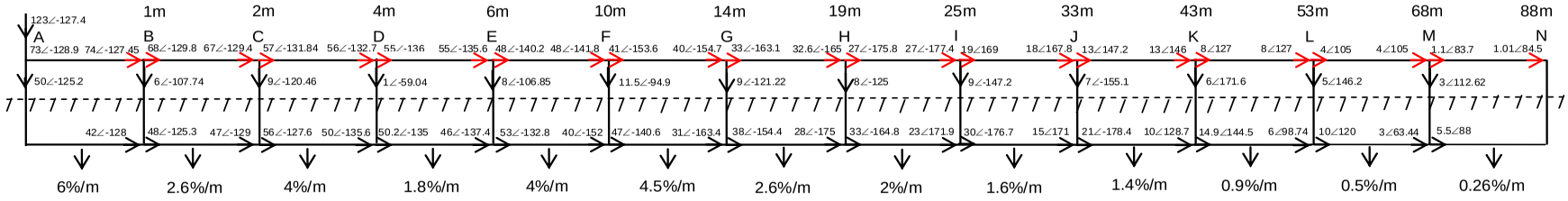

a) Measured results (currents in mA)

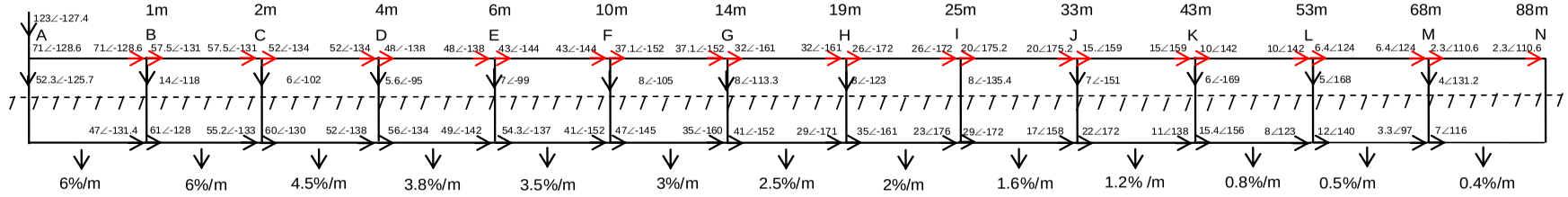

b) Computed results (currents in mA)

Figure 6.12: Schematic flow diagram of the current distribution under 100 kHz for the 88m horizontal electrode with above ground conductor: a) Measured results; b) Computed results

6.3.2 Impulse Response

6.3.2.1 Vertical Rods /4-Point Star Earth Electrode System

Low voltage impulse tests were carried out on the rod electrode with the horizontal cross as shown in Figure 6.1. The measured peak total injected current was 0.81A with a rise time of 4.7μs, and the peak EPR was measured at 20.9V. Figure 6.13 shows the current distribution at each arm of the 4-point cross and in the 2.4m vertical rod. The measured impulse response is closer to that measured under variable frequency tests with the majority of current flowing in the rod and remainder shared reasonably equally between the horizontal conductors. The proportion of peak current flowing in the rod is approximately 35% of the total current.

The current distribution of the 3.6m-rod/4-point star earth electrode is shown in Figure 6.14. As can be seen from figure, the largest proportion of injected current disperses into the path of least resistance, with the rod exhibiting the lowest resistance of all the electrode components. Roughly, 40% flows into the rod, while 13.6%, 14.8%, 13.8% and 18.3% of the injected current flows into the other four cross branches.

Figure 6.15 shows the current distribution of the 4.8m-rod/4-point star earth electrode. The measured peak current magnitude was 1.02A with a rise time of 3.7μs, and the peak EPR was measured at 21.4V. As expected, increasing the length of the rod electrode caused a reduction in the earth resistance, which was reflected in an increase of the current flowing into the 4.8m rod. Approximately, 46% of the injected current value flows into the 4.8m rod, while between 15% to 19% flows into cross branches.

Table 6.3 illustrates the comparison between the computed and measured results of the impulse current distribution for the 2.4m-rod/4-point star earth electrode. It can be observed that, for the simulation results, the current is the same in all four arms of the

star. However, the measured currents in each conductor of the rod-cross configuration exhibit an imbalance, which indicates that the numerical simulation does not fully model the localised current dispersal processes in the soil.

Table 6.3 Comparison between measurement and simulation results

		Current (A)	
Configuration	**Current**	**Measured**	**CDEGS**
2.4mrod with4-point star	I_{Rod}	0.27	0.36
	I_1	0.12	0.11
	I_2	0.13	0.11
	I_3	0.15	0.11
	I_4	0.13	0.11

Figure 6.16 shows the current distribution of the 2.4m-rod/8-point star. The test setup was shown in Figure 6.1. The impulse current has a rise time of 15 μs and a time to half value of 36 μs, with a peak value of 1.5A. A current of 0.23A (23% of the injected value) was found to flow into the 2.4m rod, while 1.27A flowed into the 8 horizontal electrode enhancements. Generally, the currents measured in the star branches were not equal and they are dependent on the value of the soil resistivity immediately surrounding each branch of the 8-point star.

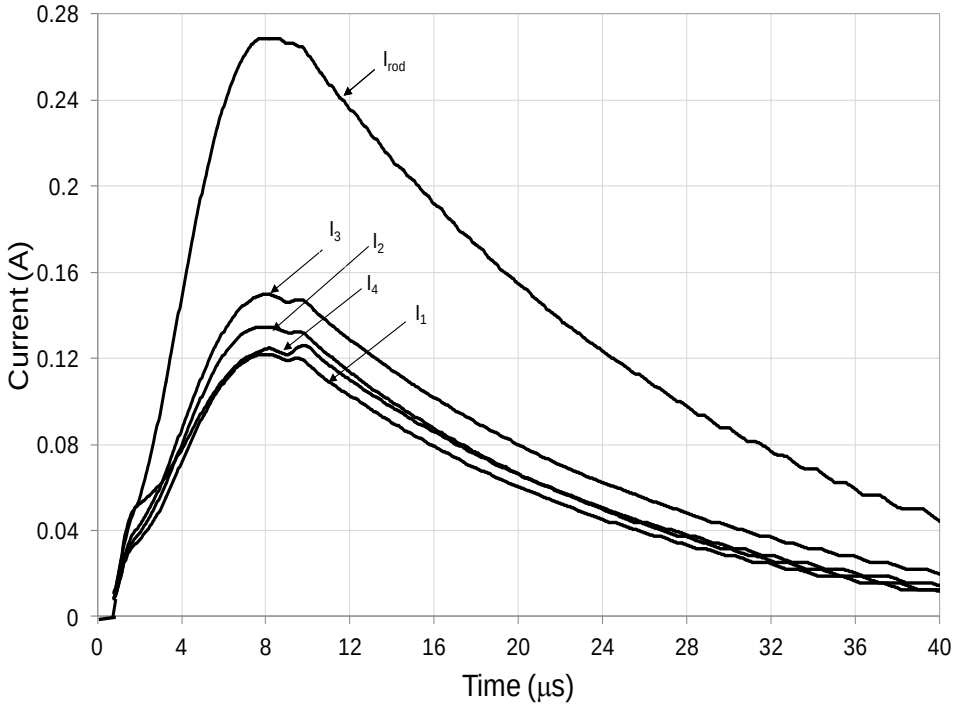

Figure 6.13: Current distribution in the 2.4m rod-horizontal cross electrode formation under impulse

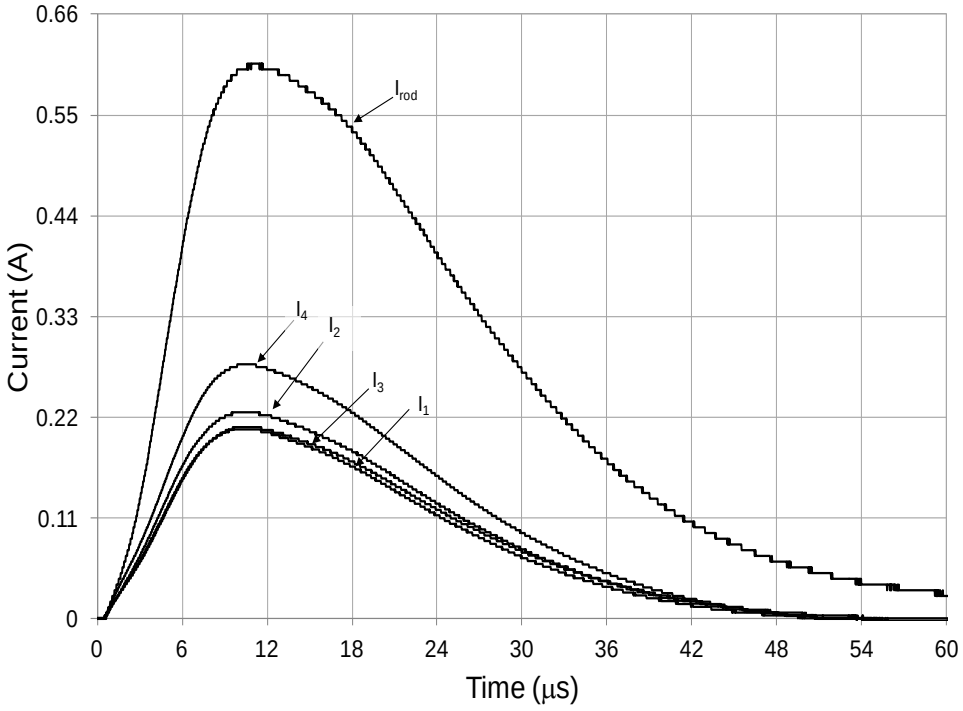

Figure 6.14: Current distribution in the 3.6m rod-horizontal cross electrode formation under impulse

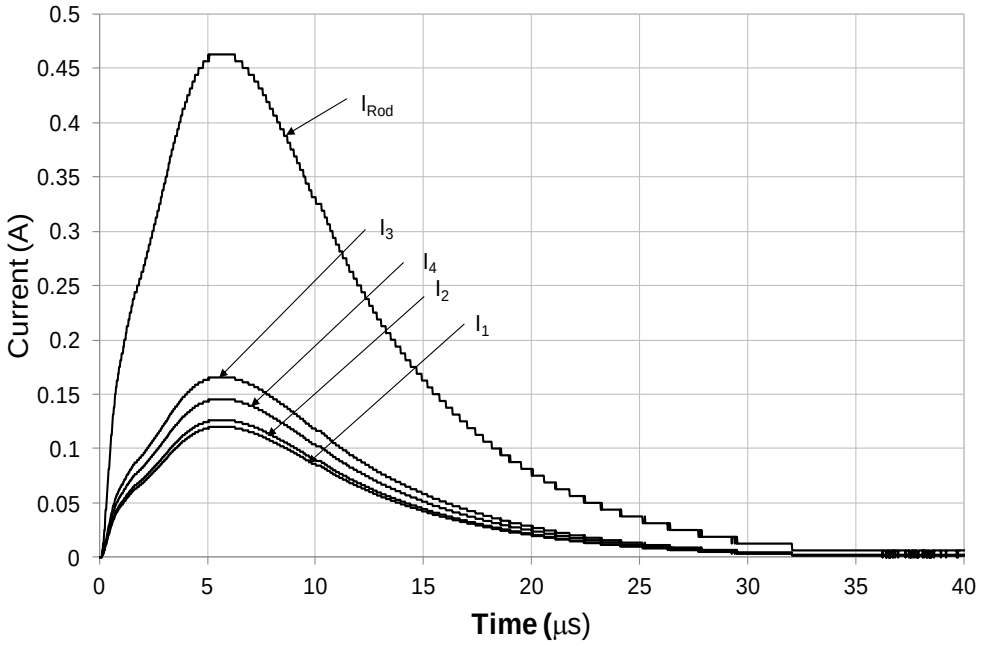

Figure 6.15: Current distribution in the 4.8m rod-horizontal cross electrode formation under impulse

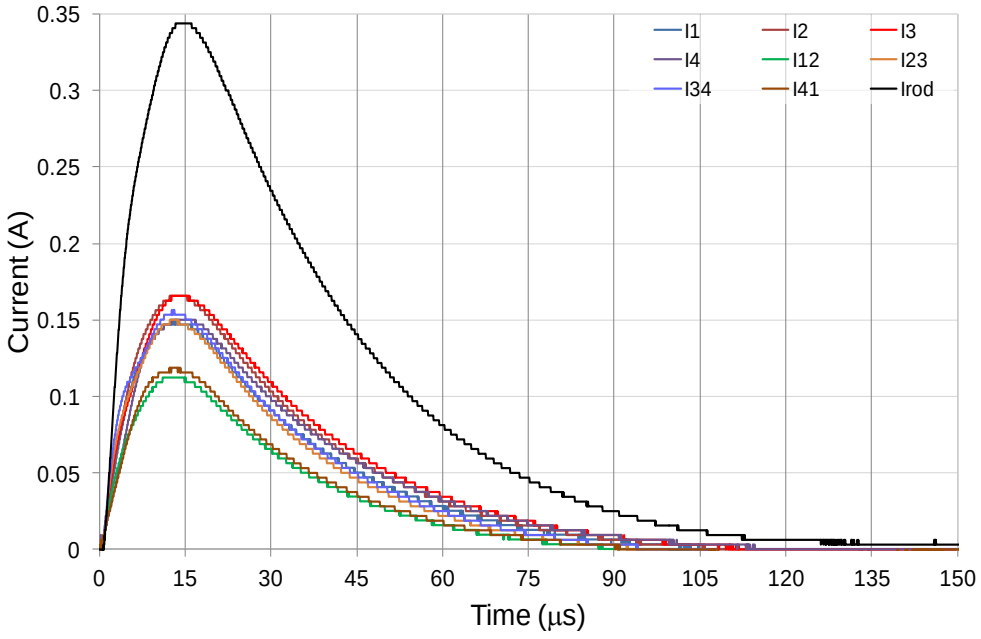

Figure 6.16: Current distribution in the 2.4m rod-horizontal star electrode formation under impulse

6.3.2.2 Horizontal Earth Electrode with and without Enhancement

Impulse tests were carried out on the 88m counterpoise at the test site. A current impulse of magnitude of 4.7A and a wave shape of 7.8/24 μs was injected into the 88m horizontal electrode. Typical applied impulse current and resulting EPR waveforms at the injection point (point A) are shown in Figure 6.17. The significant influence of the electrode inductance is indicated during the front of the impulse by a sharp rise in electrode voltage. The impulse resistance ($V@I_p/I_p$) of the 88m horizontal electrode was calculated to be 7.5Ω.

The impulse currents and voltages were measured at 12 points along the 88m horizontal electrode, but only 7 points are shown in Figure 6.18. From Figure 6.18, it can be seen that the current impulse magnitude is attenuated and a change in the rate of rise occurs. This is due to the current being dispersed into the ground as the impulse propagates along the electrode. The time delay in the current wave front at 1m, 10m, 33m, 43m, 53m, and 68m is attributed to the surge travel time.

The current is seen to disperse over those electrode sections nearest the point of injection. Moreover, in the first 10m of the 88m bare horizontal, 14.7% of the injected current is dispersed into the ground, whereas in 33m, 43m, 53m and 68m long, the amounts of current dissipated are 50.7%, 61.34%, 69.3%, and 82.7%, respectively. It was found that the current dispersed into the ground is not equal, the majority of the current being dispersed in the first 10m of the horizontal electrode.

Similarly, the amplitude of the voltage transient along the electrode shows a reduction with increasing length, and there is a change in the wave shape at both front and tail, as shown in Figure 6.19. The percentage reductions in EPR are 3.44% at length 1m,

20.7% at length 10m, 44.82% at length 33m, 50% at length 43m, 56.9% at length 53m and 61.2% at length 68m. It was shown that the reductions in EPR are non-uniform.

Figure 6.20 shows the distribution of peak current, measured using CTs at different locations along the 88m horizontal electrode. The currents are normalised to the peak current at the injection point (I_{inj}), for injected impulse currents having amplitudes 1.31A and 9.4A, with rise times of 2.5μs and 17.25μs respectively. The results indicate that for a horizontal electrode alone, a greater proportion of the total current is dissipated over those sections of the electrode closest to the injection point. In addition, the results obtained with a current rise time of 2.5μs showed a sharper decrease when compared with having slower rise-times. Similar trends were reported by Ahmeda [6.8].

In order to understand how the shape of the impulse current affects its dissipation into the ground, the current distribution rate as a function of different rise times is shown in Figure 6.21. The average current dispersion was computed from the peak current at each junction of the 88m horizontal electrode. For example, the magnitude of the current dispersed in the 0-10m section was calculated using the difference between the current peak at the injection point and that measured at the 10m node. As can be seen from Figure 6.21, for the fastest rise time, the maximum value of the dispersed current at section 0-10m is 0.54A, approximately 37% larger than the dispersed current at sections 10-19m and 19-33m, and 63.43% larger than the remaining sections. It is likely that the lateral variation of the soil resistivity along the 88m horizontal electrode gave rise to different peak currents and dispersal of currents into the soil, as explained in section 3.7 which showed that the localised soil resistivity is different with vicinity where the horizontal electrode is buried. For the slow rise time, most current was dispersed near the injection point, and the highest current was dissipated between node

0 and 10m with a magnitude of around 1.26A, while the last section extending between nodes 53 and 68m was only 0.9434 and approximately 75% less than the current dissipated at the first section.

Impulse tests were carried out on the 88m counterpoise with the insulated conductor enhancement for an injected current magnitude of 3.71A and a rise time of 5.7μs as shown in Figure 6.22. From the figure, the peak voltage rises sharply and occurs before the current peak, which indicates the influence of the electrode inductance. The impulse resistance ($V@I_p/I_p$) was reduced from 7.1Ω to 6Ω through the introduction of the enhancement.

Figure 6.23 shows the voltage and current distributions for the 88m bare conductor with the above-ground insulated conductor. As can be seen in Figure 6.23, the voltage and the current in the insulated conductor reduce with distance along the conductor. The current flowing from the insulated conductor to the bare conductor, I_3, is well distributed along the conductor length. The results indicate that, the voltage and current distributions are similar to those seen with the variable frequency injection at 100 kHz. Therefore, the addition of an above ground insulated conductor to the bare horizontal conductor can reduce the current dissipation near the injection point, compared with using the horizontal electrode alone.

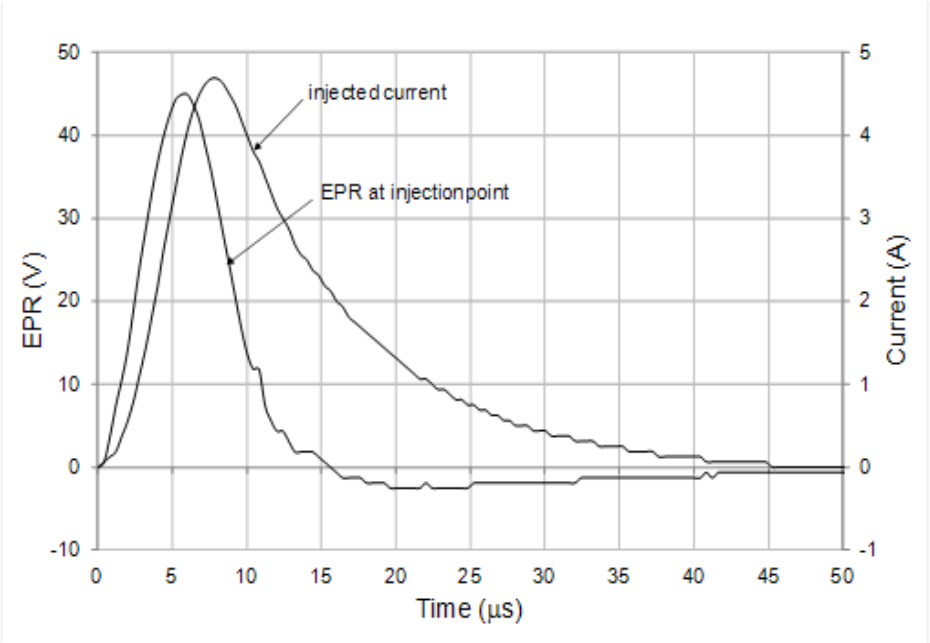

Figure 6.17: Measured voltage and current at injection point of the 88m conductor length

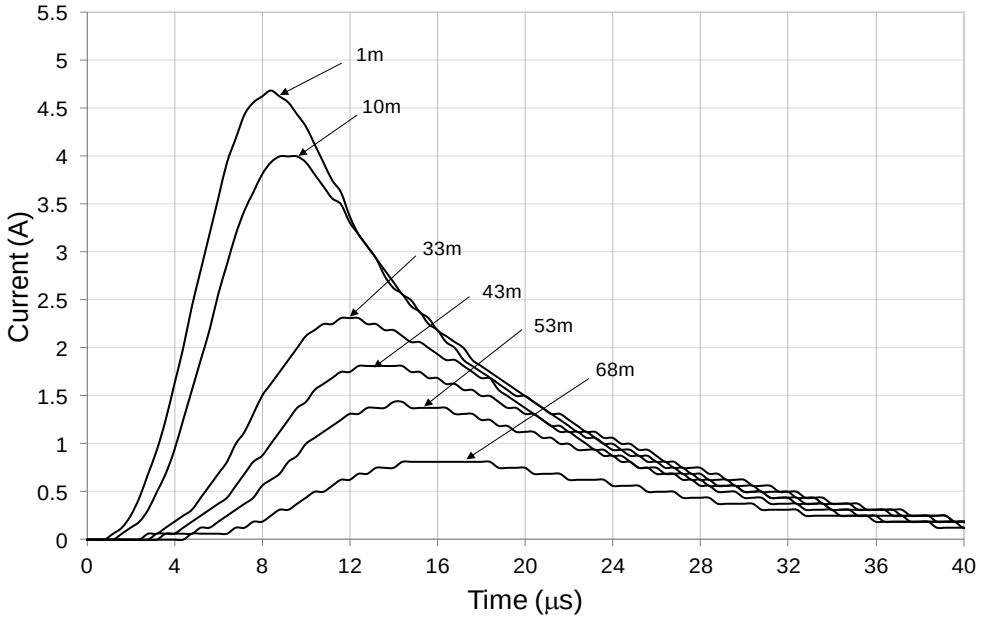

Figure 6.18: Examples of impulse current waveforms measured at points 1m, 10m, 33m, 43m, 53m and 68m

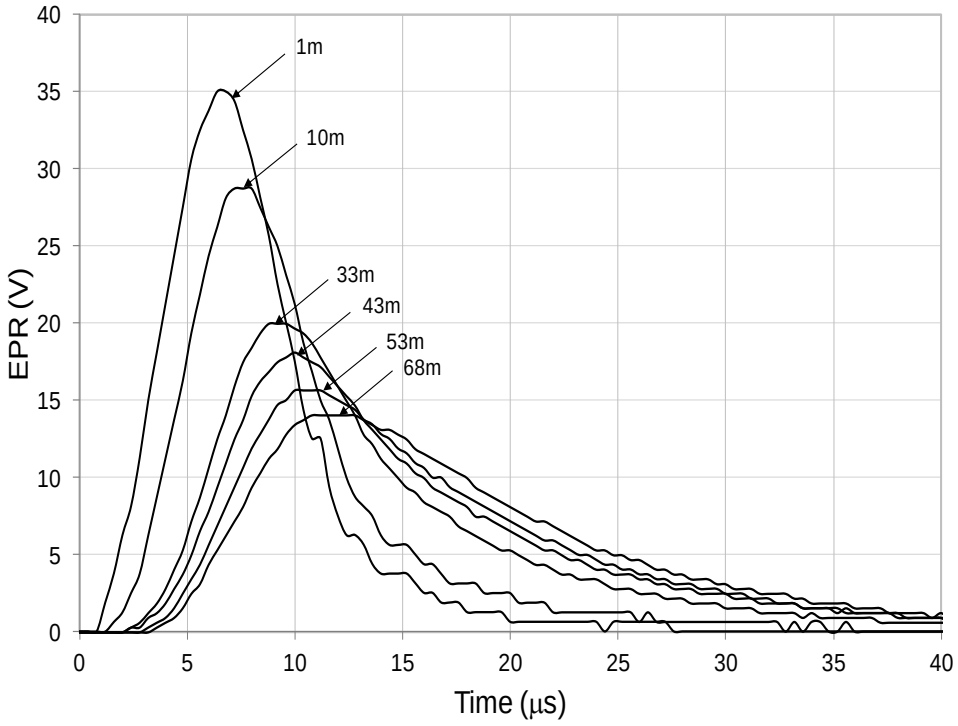

Figure 6.19: Examples of voltage waveforms measured at points 1m, 10m, 33m, 43m, 53m and 68m

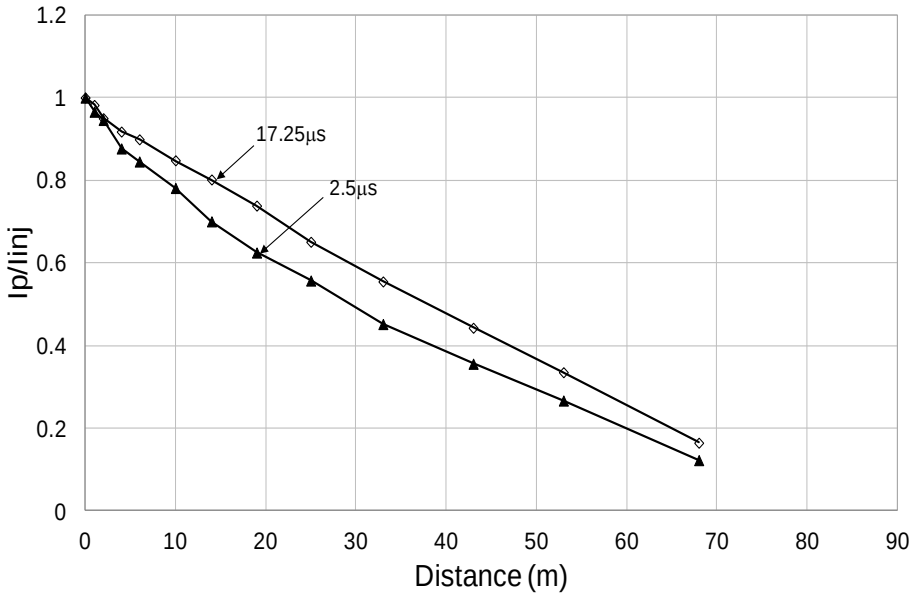

Figure 6.20: Normalised peak current distribution over the 88m electrode length

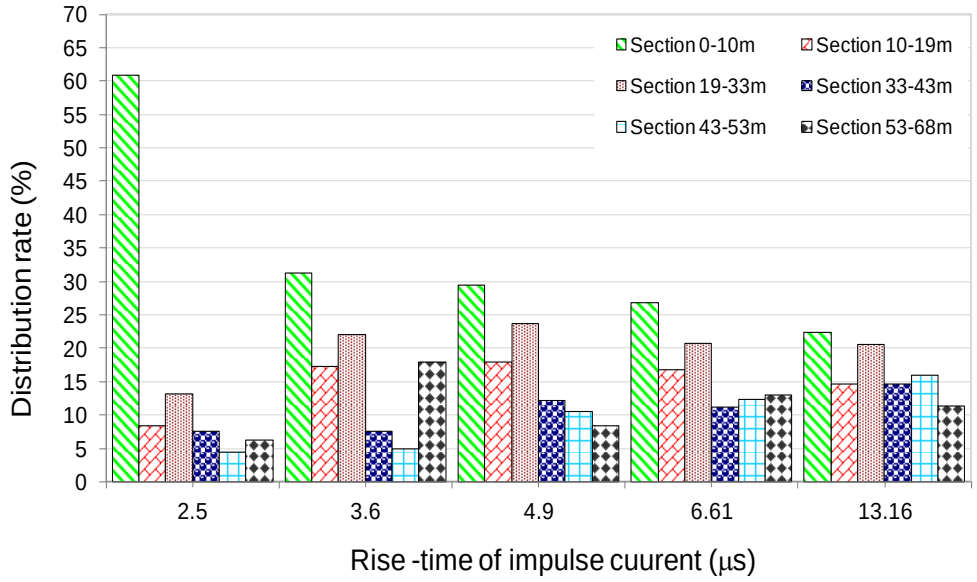

Figure 6.21: Current distribution as function of various rise times of the injected impulse current in six sections of the 88m horizontal electrode

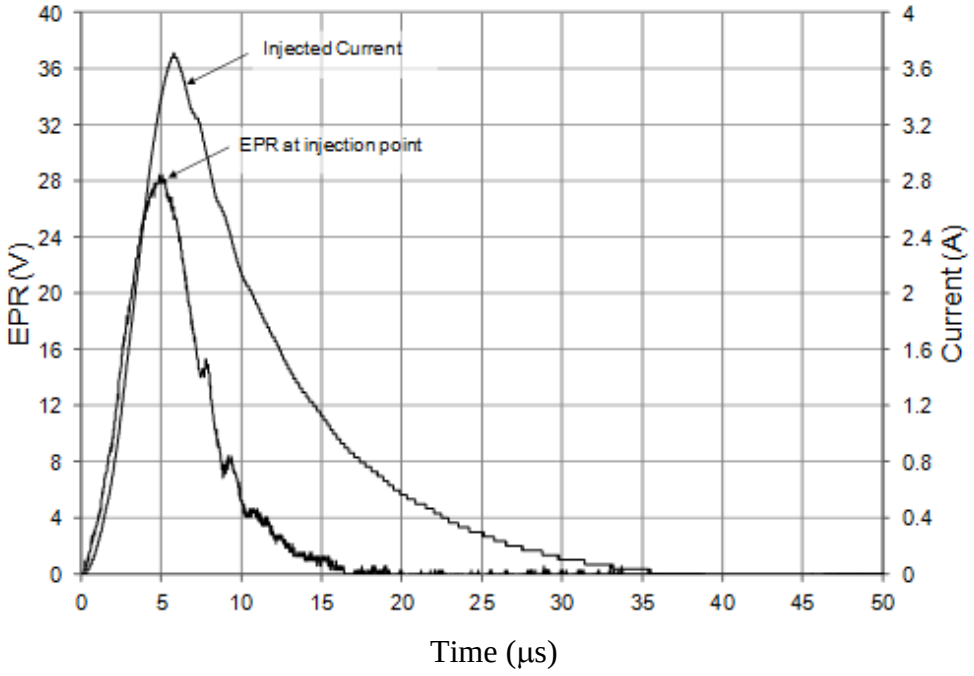

Figure 6.22: Measured voltage and current shapes at the point of injection (88m horizontal electrode with parallel insulated conductor)

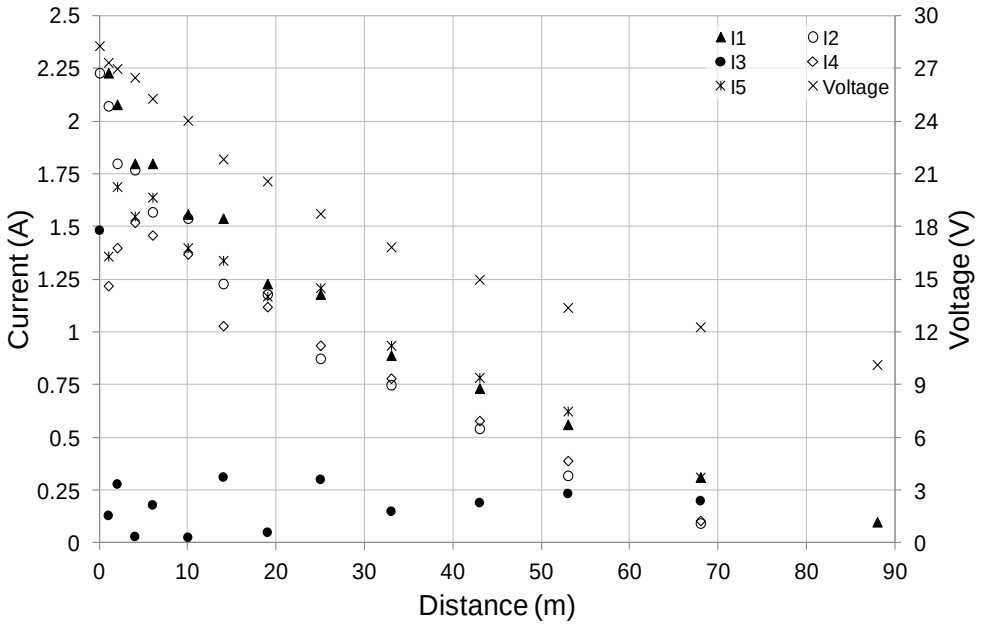

Figure 6.23: Peak current and voltage distributions along 88m horizontal electrode with insulated conductor enhancement

The measured and computed for the circuit arrangement given in Figure 6.11 results of the current distribution under low current impulse for the 88m horizontal electrode are shown in Figure 6.24. The results indicate that the current flowing in the above ground conductor is almost 60% of the injected current, which means that the above ground conductor had a significant effect on the current distribution, and helps the current to disperse away from the point of injection. Therefore, the main benefit of an additional above ground conductor is that the current dispersed near the injection point is much lower than the current dissipation for the bare conductor only, which in turn serves to minimise the EPR at the injection point. Also, the current dispersed per metre along the 88m horizontal electrode was calculated, and the results showed that the current dispersed into the soil depends on the value of the soil resistivity surrounding the conductor. As can be seen, the computed results show a reasonable agreement with the measured results.

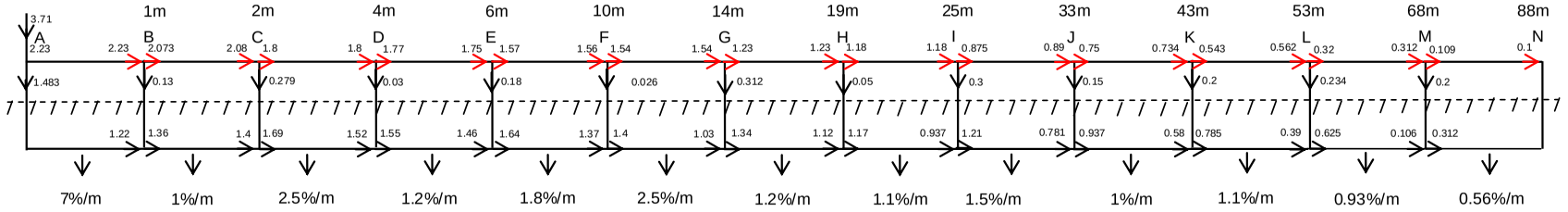

a) Measured results (currents in A)

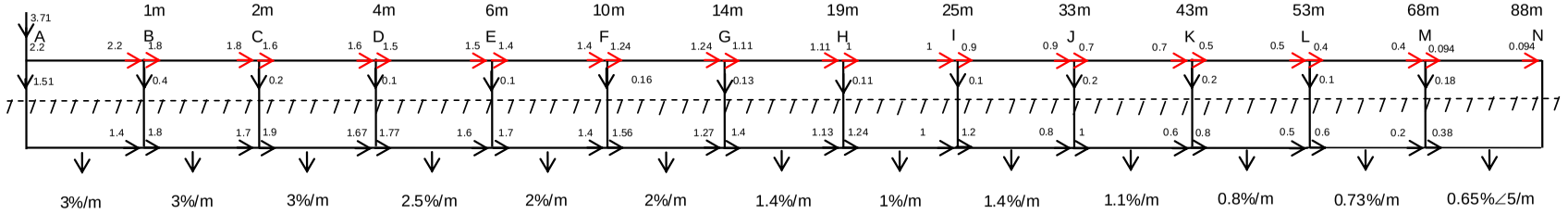

b) Computed results (currents in A)

Figure 6.24: Schematic flow diagram of the current distribution under Impulse for the 88m horizontal electrode with above ground conductor: a) Measured results; b) Computed results

6.4 Conclusions

Experimental tests were carried out to investigate current distribution in three earth electrode systems. In the case of the 2.4m rod with an added '4-cross' horizontal conductor enhancement, it was shown that the rod carries the majority of the current at low frequency, but this proportion decreases significantly as frequency increases. Accordingly, the addition of horizontal enchantments was found to be optimum design of earthing systems due to the dissipation current improved at low and high frequency ranges compared with the rod only. Therefore, the author recommends using the rod with enhancements to avoid any obstruction of the current to dissipate in to the ground under high frequency and impulse performance.

The low voltage impulse test results show similar trends of current distribution to those seen under high frequency. The results presented are not in agreement with the industrial standard reference of the rod satisfying the role of a 'high-frequency earth electrode'.

Current distributions tests on an 88m horizontal earth electrode with the insulated conductor enhancement reveal that current distribution is modified by the presence of the insulated conductor. As expected, the insulated conductor allows a uniform distribution of current from the insulated conductor to the bare conductor at low frequency. However, the voltage distributions along the horizontal electrode were constant due to the resistive nature of the electrode. At high frequency (100kHz) and under current impulse injection, the current magnitude in the intersections between the insulated conductor and the bare conductor is well distributed along the conductor length although the voltage and current in the insulated conductor falls with distance due to the inductive effect.

The best earthing system designs minimise the current dissipation at low/high frequency and transient conditions near the injection point. This can be achieved by increasing a current path by installing the insulated parallel conductor with bare conductor.

The comparison between the measurement and simulation results software carried out in this chapter, the computed showed that the currents were uniform for all cross branches. However, there were unsymmetrical values in the measurements results of the 2.4m rod/ 4-point star electrode. For the 88m horizontal electrode, it was shown that the measurement results are in good agreement with the simulated results. However, some disparities between the measurement and simulation results are expected due to the use of a simplified soil model**.**

CHAPTER SEVEN: HIGH CURRENT IMPULSE CHARACTERSTICS OF ENHANCED ELECTRODE SYSTEMS

7.1 Introduction

A comprehensive review of the frequency and transient response was presented in Chapter 2. Many authors have investigated the behaviour of earthing systems subjected to high impulse current, using both field measurements [7.1-7.4] and laboratory tests [7.5-7.9]. However, field tests are commonly performed in non-uniform soil structures with both lateral and vertical variations in resistivity, and these conditions are difficult to reproduce in the laboratory. In general, the conclusions of these investigations attribute the reduction in electrode earth resistance at high impulse current magnitudes to soil ionisation. While the high current impulse performance of vertical rod electrodes has been widely explored and documented, comparative tests on rods with horizontal enhancements have not been performed to date.

In Chapters 4 and 5, the frequency and transient performances of earthing systems were studied both experimentally and analytically, and new developments were suggested to improve their performance.

In this chapter, extensive simulations using computer software to investigate the touch and step voltages prior to field tests are presented. Moreover, high impulse current tests have been performed, in which currents up to 7kA were injected into vertical electrodes with and without additional horizontal enhancements. Non-linear soil conduction effects are obtained, and some soil ionisation breakdown phenomena are explored and compared with other work.

7.2 Computer Simulations

To ensure the safety of test personnel, site employees and members of the public in the vicinity of the test location, computer simulations were performed using CDEGS software [7.10] prior to high voltage tests to determine the worst-case EPR and step voltage contours, and to identify any hazardous touch potentials developed by exposed metalwork at the site perimeter. Figure 7.1 shows the CDEGS models of the test circuit using horizontal and ring current return electrodes.

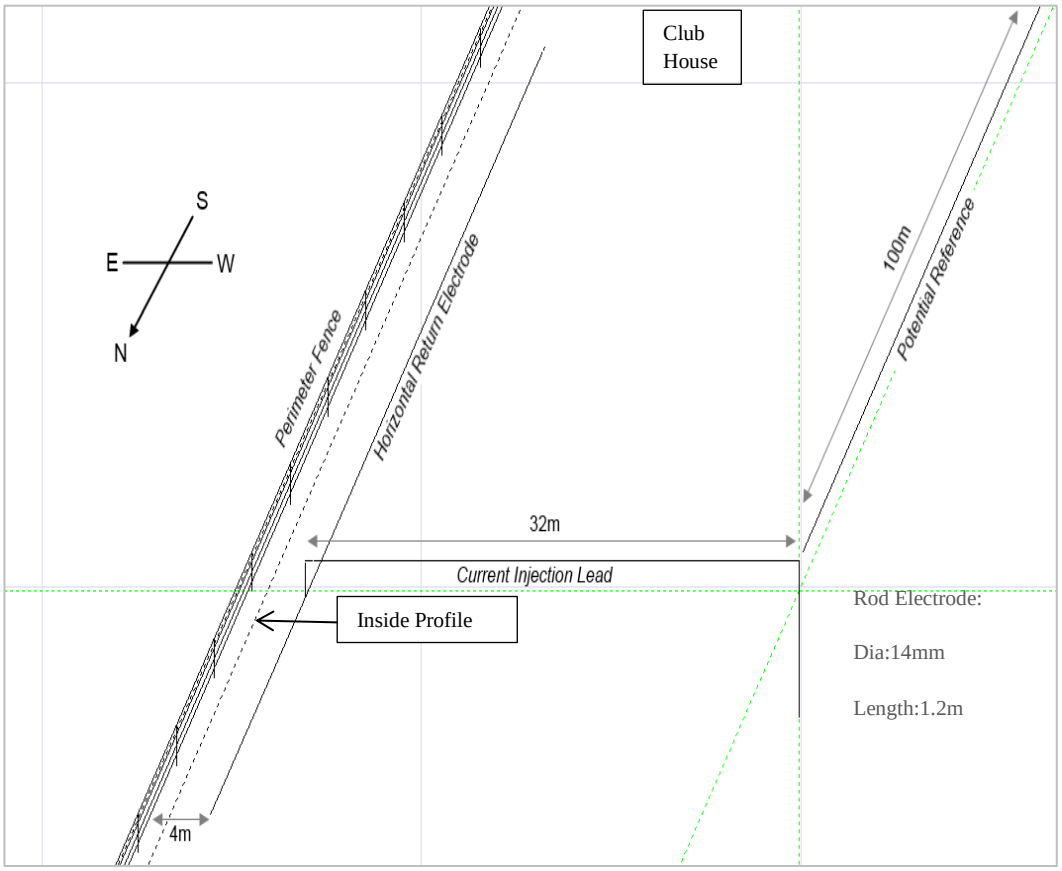

(a) Horizontal current return electrode

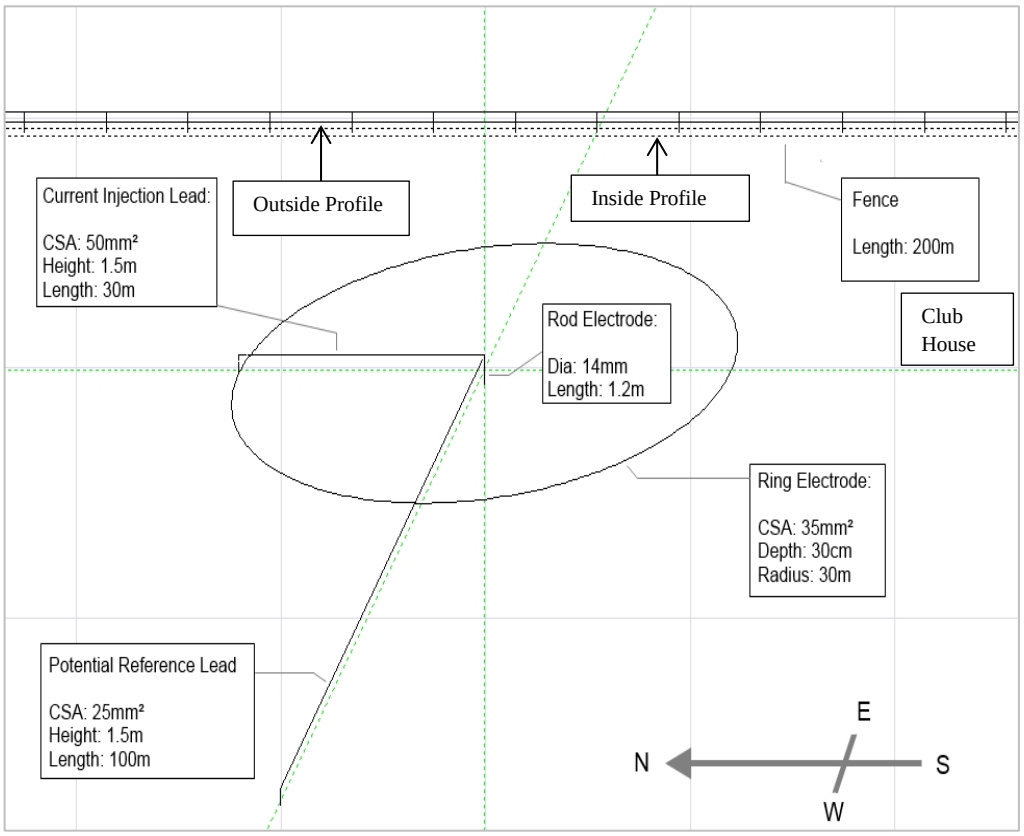

(b) Ring current return electrode

Figure 7.1: Physical layout of the simulated test configurations

7.2.1 Fence Touch Voltages

Figure 7.2 illustrates the computed transient peak touch voltages for persons standing 1m from the perimeter fence (both inside and outside the field), for a 200kV, 1.2/50 impulse. Use of the ring electrode reduces the worst case touch voltages from 4.5kV to 600V for persons inside the perimeter, and from 2.2kV to 600V for persons outside, which is acceptable according to BS EN 50522-2010[7.11], as shown in Figure 7.3. The touch voltage profiles are depicted in Figure 7.2. The magnitude of transferred potentials towards the clubhouse is also reduced.

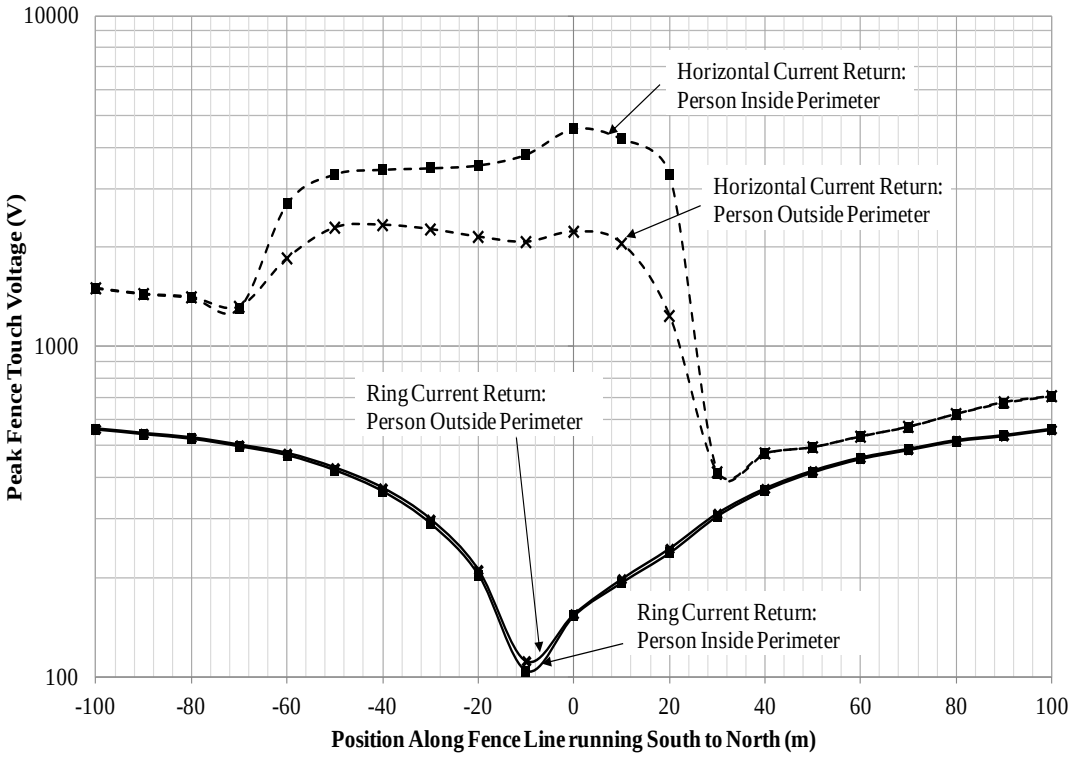

Figure 7.2: Peak Touch voltage profiles at 1m either side of perimeter fence line for both return electrode arrangements

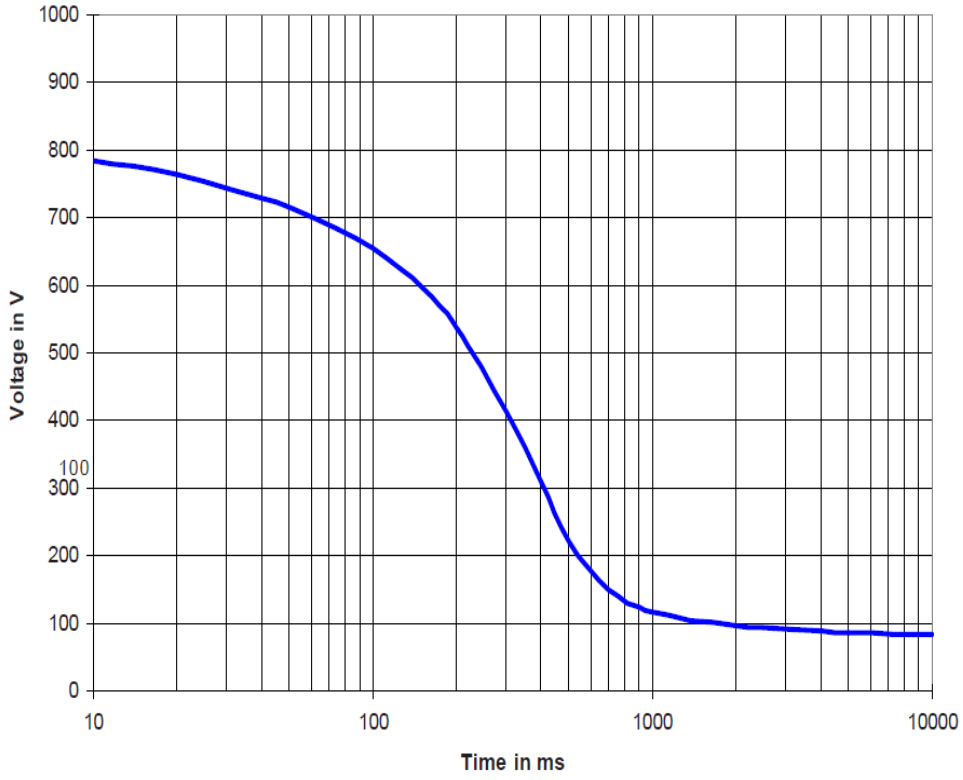

Figure: 7.3 Tolerable touch voltages (Reproduced from reference [7.11])

7.2.2 Step Voltage and EPR Contour Maps

Figure 7.4 shows the step voltage maps for both circuit configurations. It can be observed from the figure that, using the installed linear horizontal electrode, transient step voltages in excess of 2kV peak are developed beyond the boundary fence, rising to 4kV at the location of the source. However, using the ring electrode, positioned 20m from the fence line at its closest point, step voltages beyond the perimeter are limited to a peak value of less than 200V. Figure 7.5 shows the simulated earth potential rise (EPR) (relative to remote earth) for both test configurations. Using the existing horizontal electrode, the 5kV EPR contour near to the source extends beyond the fence line, giving rise to the large transfer touch potentials computed in section 7.2.1. By installing a ring electrode as far away as possible from the boundary, the EPR at the fence and transferred touch potentials can be minimised. It is observed that a distortion of the equipotential contours occurs due to the position of the source on the ring. The EPR can be seen to roll off most rapidly in the direction perpendicular to the current injection lead. It is suggested that the current injection lead should be arranged perpendicular to the fence line where possible. From the simulation results using CDEGS software, it can be said that, using the ring electrode as the current earth electrode, a reduction in the earth potential rise (EPR), step and touch voltages is obtained at the fence compare with the case when a horizontal earth electrode is used.

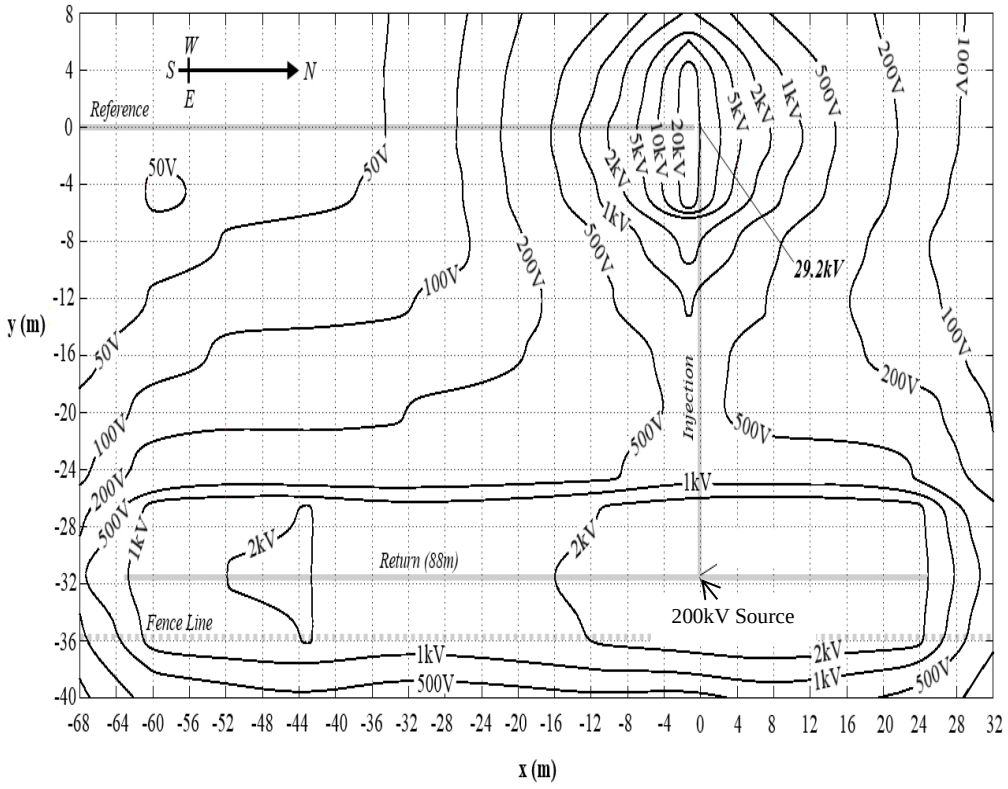

(a) Horizontal current return

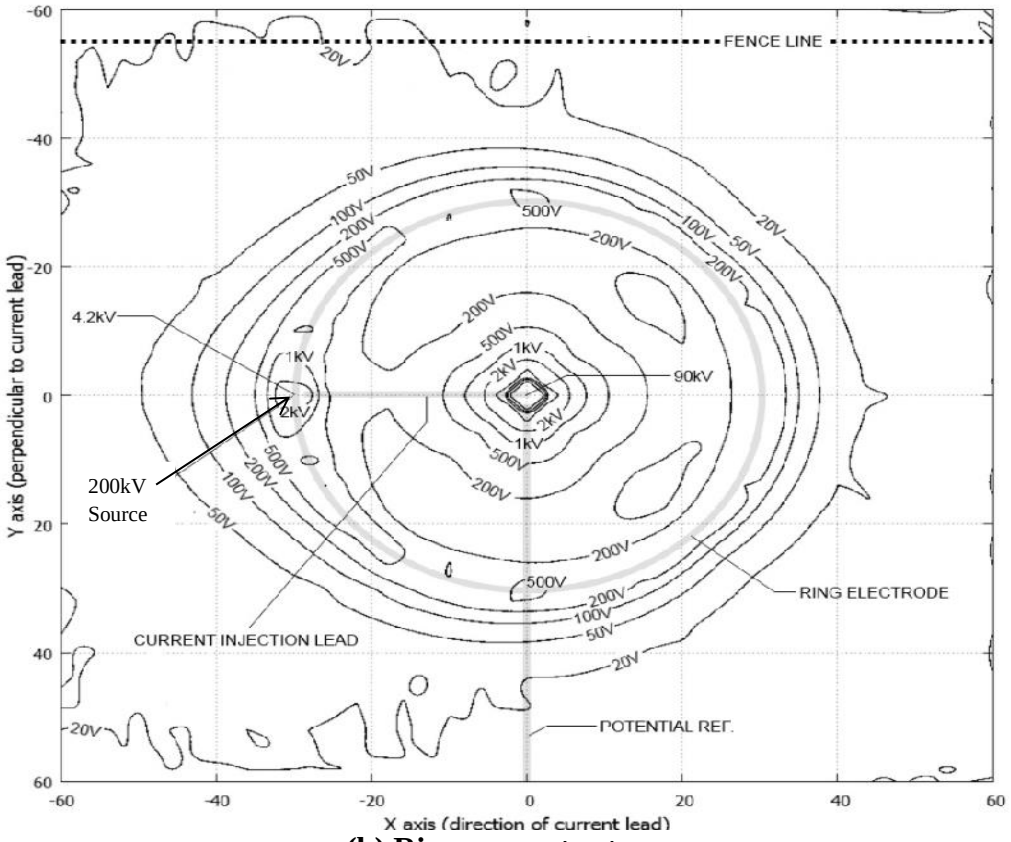

(b) Ring current return

Figure 7. 4: Step Voltage Contour Plots for 200kV impulse test

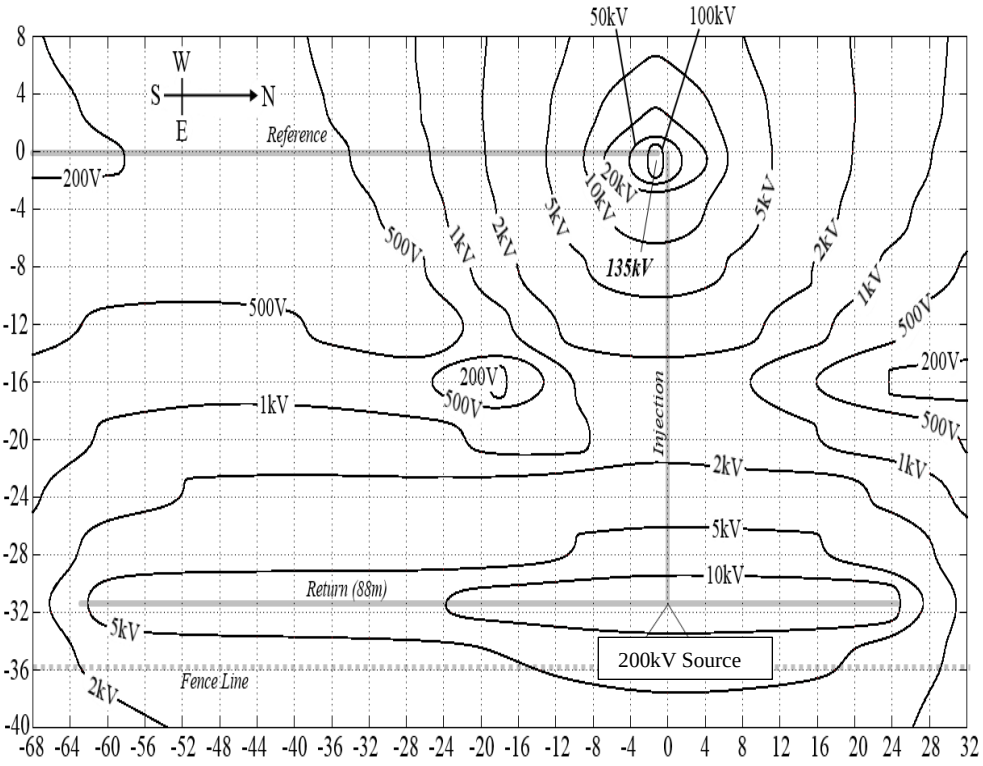

(a) Horizontal current return

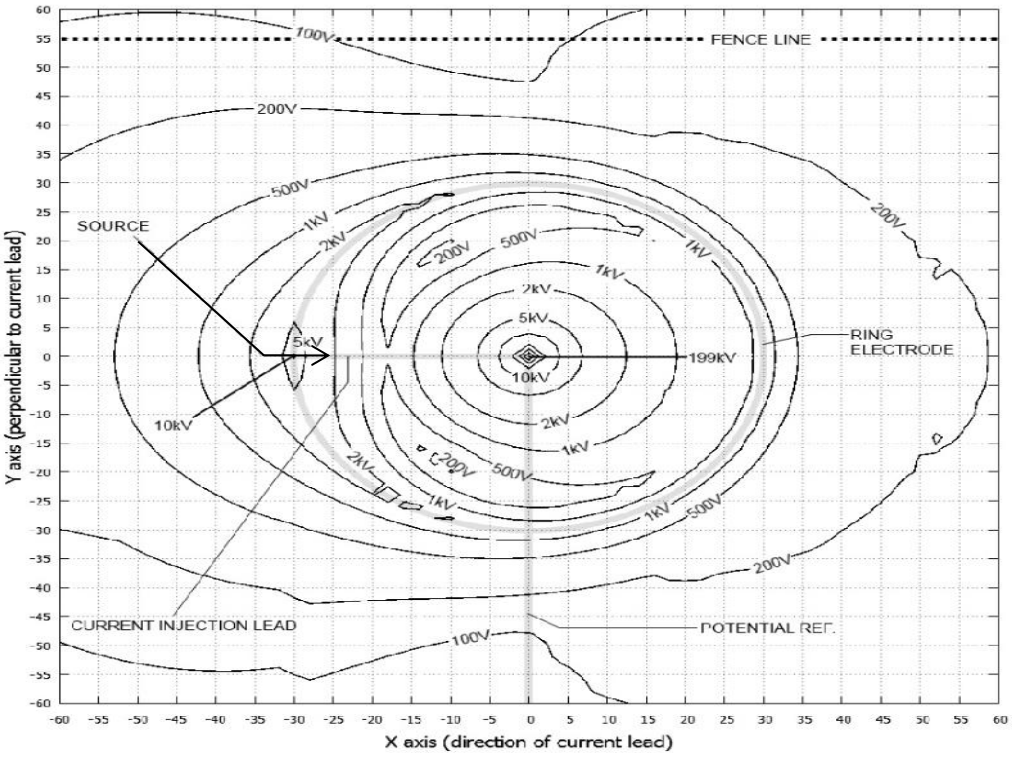

(b) Ring current return

Figure 7.5: EPR Contour plots for 200kV impulse test

7.3 Test Setup

The experimental setup consists of an impulse voltage generator (IG) with maximum output of 200kV, used to generate a high impulse current up to 10kA, its charging unit is supplied from a 25kVA diesel generator. The high impulse current was generated by connecting the two, low inductance (0.25μH), resistor in parallel. A 4.8kΩ tail resistor was used to obtain the required waveform tails. A 30m current injection line connects the impulse generator to the electrode under test, suspended from wood poles to a height of 1.6m as shown in Figures 7.6 and 7.7. The earth potential rise (EPR) at the top of the 1.2m, 2.4m, 3.6m and 4.8m vertical rod earth electrodes were measured with reference to a remote potential imported via a second transmission line using a capacitive divider having a ratio of 2000:1. The remote potential reference lead was arranged orthogonal to the current injection path so as to minimise circuit coupling. The current was measured using a current transformer (CT) (Lilco) with a 50MHz bandwidth, 0.01V/sensitivity and a peak impulse current rating of 50 kA. Following the initial safety simulation studies in Section 7.2, a bare copper ring earth electrode was installed to act as a concentric current return electrode. The ring conductor has a length of 188.5m and a cross sectional area of 20mm^2, and is buried to a depth of 30 cm, with eight junction boxes allowing reconfiguration and current measurement in the electrode segments. Figure 7.7 shows the excavation work undertaken prior to laying the ring electrode at Cardiff University test site in Llanrumney.

A developed wireless data transmission system was used and located at the electrode under test with data acquisition achieved using a real-time PC integrated digital storage oscilloscope. A PC-based oscilloscope was configured with a wireless LAN adapter and antenna for communication via a point-to-point link with a control laptop/PC located inside the equipotential working zone established in the equipment trailer. A

remote desktop server (Tight VNC) was installed on the oscilloscope, and remote control of the scope and established by means of the associated client running on the control PC.

To accommodate the relatively long distances, and based on preliminary on-site tests, long range wireless LAN adapters were adopted at both ends to achieve high-reliability data transfer. The main advantage of this system is the inherent electrical isolation achieved between equipment at the test electrode and the control desk at the test trailer [7.12].

Prior to commencing the high current tests, the DC resistance of the rod and ring electrodes was measured using the four pole method by means of a MEGGER DET2/2 resistance meter. The equivalent low-current impulse resistance was determined using a Haefely recurrent surge generator. These measurements are summarised in Table 7.1. It can be observed that from the table, the dc resistance decreases with an increase in rod length, and only slight differences between the impulse and the dc resistances of each earth rod. Could be seen the readings of the dc resistance values of the vertical rods in Chapter 4 are found to be significantly lower at this location, which was attributed to localised variation in the soil structure and resistivity, changes in soil moisture content and temperature. According to [7.13, 7.14], the earth resistance of the current return electrode must be significantly lower than the earthing electrode under test. The ring electrode was found to have a dc resistance at least an order of magnitude smaller than that of the test electrode, which helps to minimise the EPR occurring at the chassis of the impulse generator.

Table 7.1: Measured DC and Impulse resistances of rod electrodes

Rod length (m)	1.2	2.4	3.6	4.8	Ring
DC resistance (Ω)	184.4	106.2	74.4	58.6	3.85
R_{imp} (Ω)	183	104.4	69	54.2	4.73

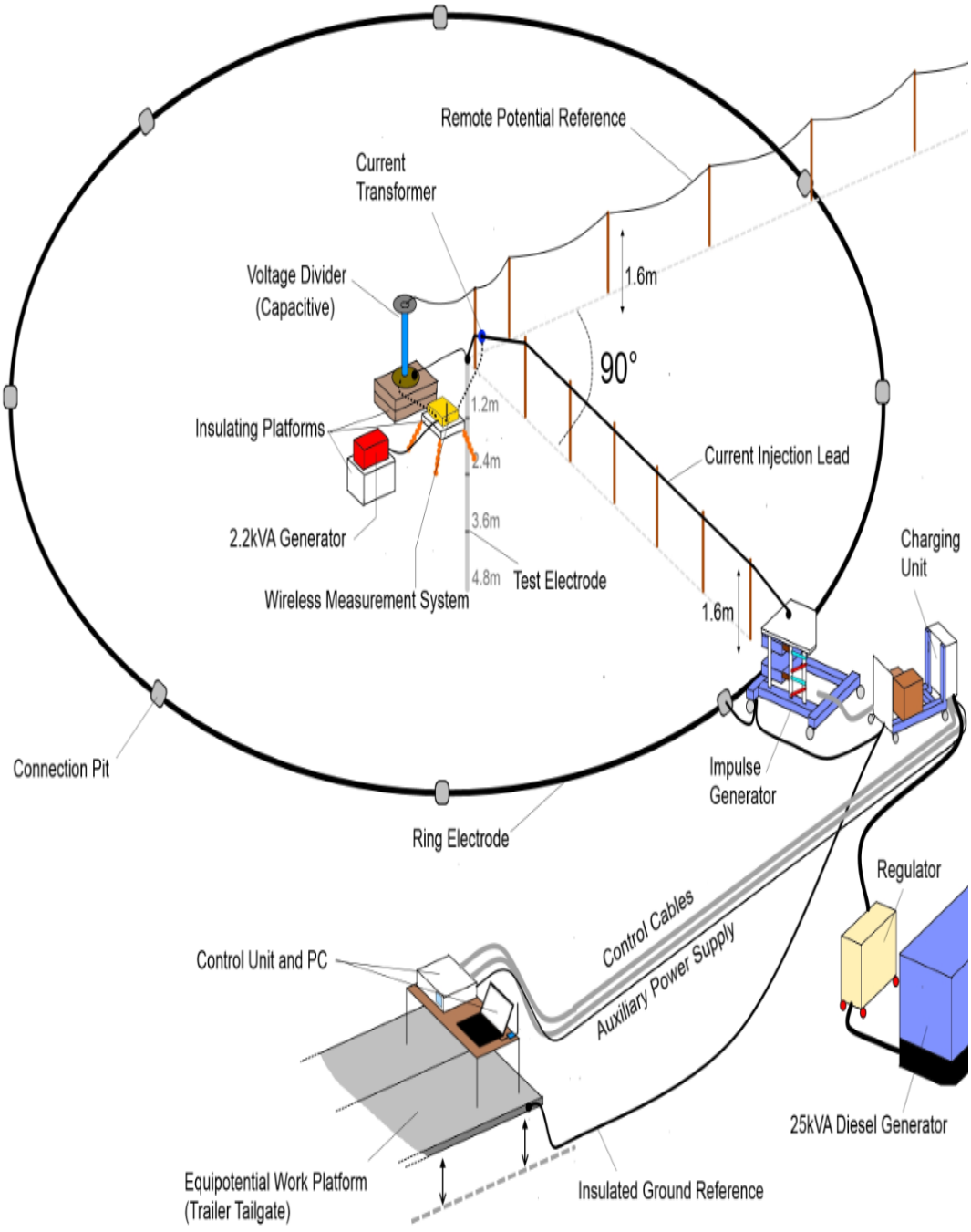

Figure 7.6: High-current field test configuration

Figure 7.7: High current impulse generator at the field site

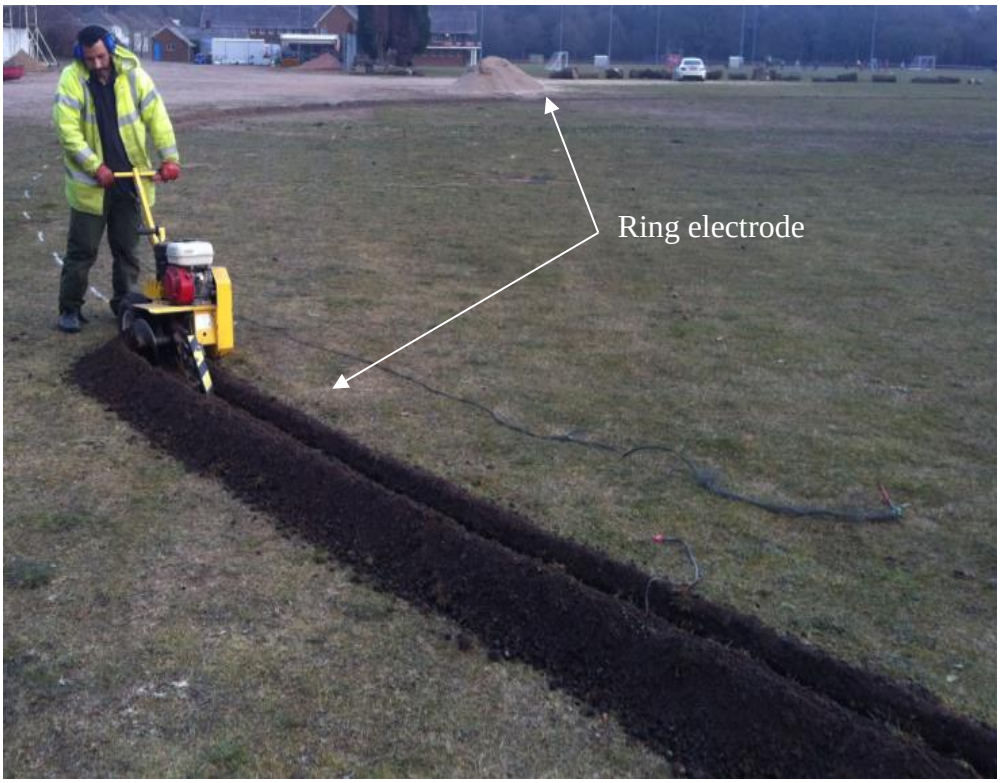

Figure 7.8: Installation of the 188.5m ring electrode at Llanrumney test site

7.4 Investigation of Soil Ionisation Under Impulse Conditions

Impulse tests were conducted for increasing current magnitudes on 1.2m, 2.4m, 3.6m, 4.8m rod electrodes, and up to 3.6m rod with 8-point star at Cardiff University earthing test facility.

7.4.1 Impulse Tests on Vertical Rods

Extensive measurements were carried out on 1.2m, 2.4m, 3.6m and 4.8m vertical electrodes at the field test site: firstly, for low current DC and impulse, and then for high impulse currents up to 7kA. Each rod has a diameter of 14mm and installed into two layer soil resistivity at Cardiff University earthing facilities.

Figure 7.9 shows the voltage and current recordings for the tests on the 4.8m rod. Impulse test result for the rod electrode shows that a second current peak occurs after a short time delay, due to the breakdown of soil in the ionised region surrounding the electrode. Therefore, it is important to investigate the aspect of inception time (T_i) and introduce another new value, time to second peak [7.15], as shown in Figure 7.9. As can be seen from the figure, the indication of the soil ionisation occur at the inception time (T_i) corresponding to inception current I_{pi} and voltage V_{pi}. After ionisation starts, current increases and is accompanied by a sharp fall in voltage. Table 7.2 presents the comparison of amplitude of voltage reduction (ΔV), the ionisation times and earth resistance magnitudes obtained at low and high voltage for the 4.8m vertical electrode.

There are two different current peaks which can be used to define two different resistances. The pre-ionisation resistance (R_1) corresponds to the soil properties prior to the influence of soil ionisation [7.16]. It represents the pre- breakdown behaviour of the electrode resistance and is subject to thermal effects. Additionally, the pre-ionisation resistance decreases with increasing current magnitude, which may be due

to non-linear thermal effects in the soil. The post-ionisation resistance (R_2) is a measure of the effective electrode resistance following soil breakdown [7.16]. The resistances R_1 and R_2 can be calculated by using the following equations [7.17]:

$$R_1 = \frac{V@I_{p1}}{I_{p1}} \qquad (7.1)$$

$$R_2 = \frac{V@I_{p2}}{I_{p2}} \qquad (7.2)$$

Where, $V_{@Ip1}$ is the voltage at the instant of the first current peak and $V_{@Ip2}$ is the instant of the voltage at the second current peak. From theses equations, the inductive effect is eliminated in these results at the instant of peak current, di/dt=0. As can be seen from Table 7.2, the pre-ionisation resistance R_1 falls slightly in comparison to the dc resistance. By contrast, a significant reduction in R_2 is observed, which may be attributed to a fully developed and highly conductive ionised region in soil.

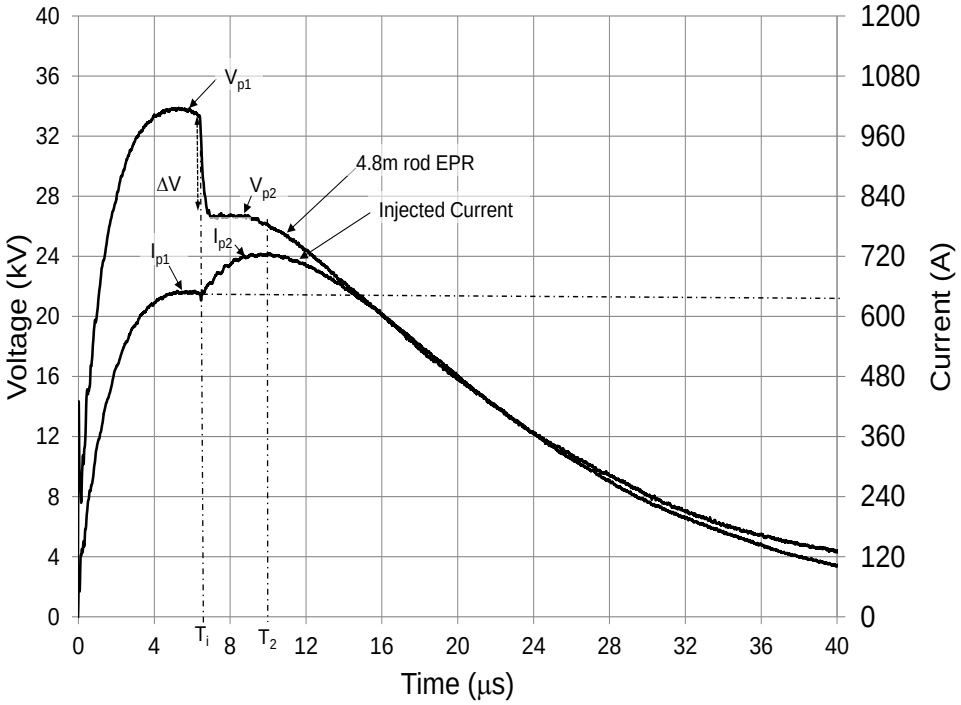

Figure 7.9: Measured results of voltages and applied currents of the 4.8m earth rod electrode

Table 7.2: Measured the time of ionisations, ΔV, R_{dc} and $R_{impulse}$ of test 4.8m electrode

Rod length (m)	4.8
R_{DC} (Ω)	58.6
ΔV (kV)	8
T_i(μs)	6
T_2(μs)	10
I_{p1} (A)	640.7
I_{p2}(A)	722.6
$V_{1@Ip1}$ (kV)	33.4
$V_{2@Ip2}$ (kV)	25.7
R_1(Ω)	52.1
R_2(Ω)	35.6
Difference between R_{DC} and R_1 (%)	11.1
Difference between R_{DC} and R_2 (%)	56.3

7.4.2 Impulse Resistance Characteristics

Figure 7.10 shows the impulse resistance values obtained for different applied voltages. As can be seen from the figure, the impulse resistance values (R_1) are close to the dc earth resistances at the lowest applied voltage. However, the earth resistance values were found to decrease slowly when the current magnitudes increased which might be due to the soil ionisation behaviour of the earthing system under high impulse current. This reduction of the impulse resistance was also reported in the literature [7.14-7.21]. The authors [7.8, 7.19] attribute this reduction to thermal processes, where the temperature of the soil is increased by I^2R (heating the soil), reducing the soil resistivity and hence the overall earth resistance. However, the post-impulse resistance R_2 decreases gradually to an asymptotic value as the current increases, eventually becoming independent of the current. This trend in the relationship between impulse resistance (R_2) and current may be due to the formation of an increasingly uniform hemispheric at ionisation region. As the current increases from 125A to 6.8kA, the impulse resistance falls by 94% for a 1.2m rod, 91% for a 2.4m rod, 87% for a 3.6m rod and 81% for a 4.8m rod, thus exhibiting similar results to those observed in previous research work [7.18- 7.22].

The impulse resistance was calculated as the percentage of the DC resistance of earth electrodes up to 4.8m as shown in Figure 7.11. It was observed that the percentage reduction of the resistance R_1 values, were found to decrease slightly with increasing length of earth electrodes at current magnitudes up to 641A. However, this fall in resistance R_2, increases markedly for the earth rod which has the highest R_{dc} (1.2m rod) which indicates that the fall of earth resistance can be linked to its DC earth resistance.

Figure 7.12 shows the time variation of the ratio of instantaneous voltage and current (dynamic resistance) $R_{imp}(t)$ ($V_i(t)/I_i(t)$) for the 4.8m rod. Prior to the non-linear region, the dynamic resistance presents a value of around 53Ω, which is nearby equal to the DC resistance shown in Table 7.2 for the 4.8m rod. Following ionisation, the resistance sharply drops from its DC resistance value with strong dependence on the applied current. After the first peak of impulse current, the new lower resistance is obtained for most of the duration of the impulse, indicating that the ionisation region as expanded to its maximum and then decaying at much slower rate as the current magnitudes falls to zero.

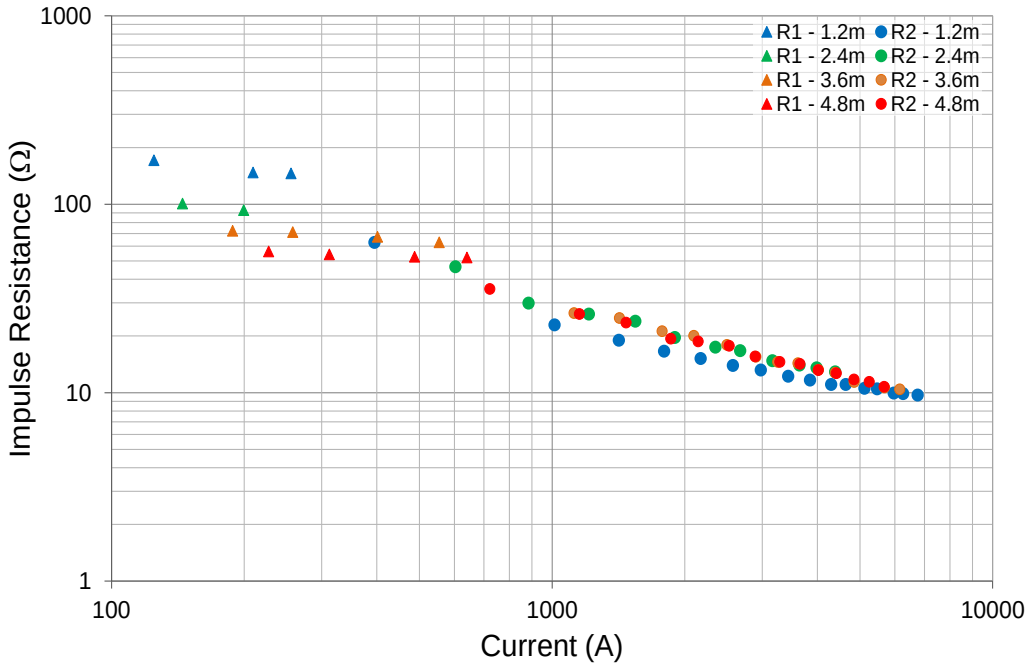

Figure 7.10: Measured impulse resistances of 1.2m, 2.4m, 3.6m and 4.8m rod

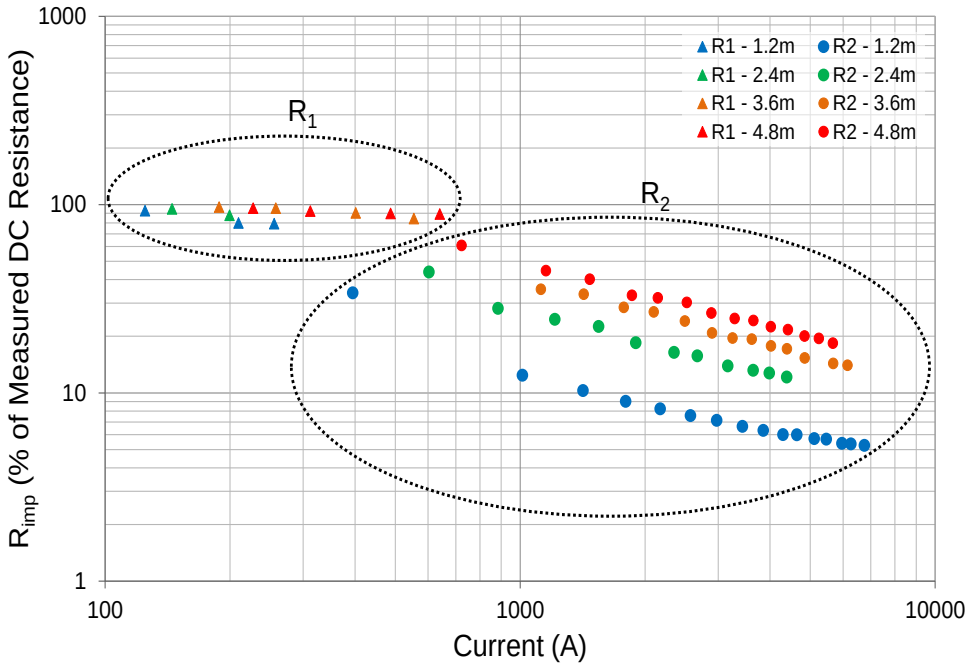

Figure 7.11: Measured impulse resistances of 1.2m, 2.4m, 3.6m and 4.8m rod with current magnitude

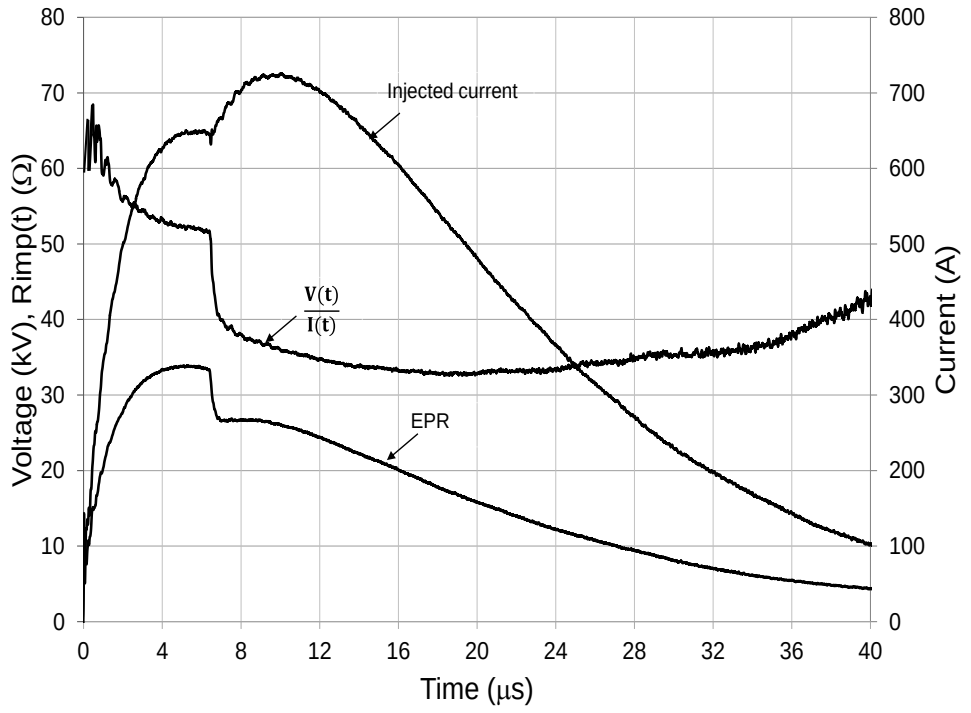

Figure 7.12 Time variations of the 4.8m vertical electrode impulse resistance

7.4.3 Vertical Earth Electrodes with Horizontal Enhancements

The horizontal enhancements were bonded with the vertical earth electrodes to reduce the earth potential rise (EPR) and investigate the behaviour of the soil ionisation. The horizontal enhancements were buried at a depth of 30cm; each horizontal electrode has length of 1m and diameter of 8 mm. Impulse currents up to 2.4A magnitude with different rise times were injected into rods with 8-point star enhancement. Table 7.3 shows the DC and impulse resistances of the enhanced vertical electrodes. The impulse resistances of the electrodes were calculated by Equation (7.3) [7.15]:

$$R_{imp} = \frac{V_{@I_p}}{I_p} \qquad (7.3)$$

As can be seen from the table, the dc resistances for all configurations are close to the impulse values. Figure 7.13 shows the effect of additional horizontal enhancements on the impulse resistance of the vertical rods. It is clear from the figure that the percentage decrease in impulse resistance in comparison with the rod alone is small. This small reduction is due to current division between the horizontal enhancements and the rod. As can be calculated from Equations (7.4) and (7.5) [7.18], due to the increased surface area of earth electrode, a lower current density (J_c) is developed which reduces the critical field intensity (E_c), and hence, no non-linear behaviour was observed in the electrode resistance. Soil ionisation can thus be said to have the greatest effect with short electrodes having small surface area.

$$E_c = \rho J_c \qquad (7.4)$$

$$J_c = \frac{I_c}{A} \qquad (7.5)$$

Table 7.3: Measured the dc resistance of the vertical rods with additional horizontal enhancements

Configuration	DC resistance (Ω)	Impulse resistance R_{imp}(Ω)
1.2m rod with 8-point star	56.6	53.3
2.4m rod with 8-point star	51.3	51.4
3.6m rod with 8-point star	42.6	42.1

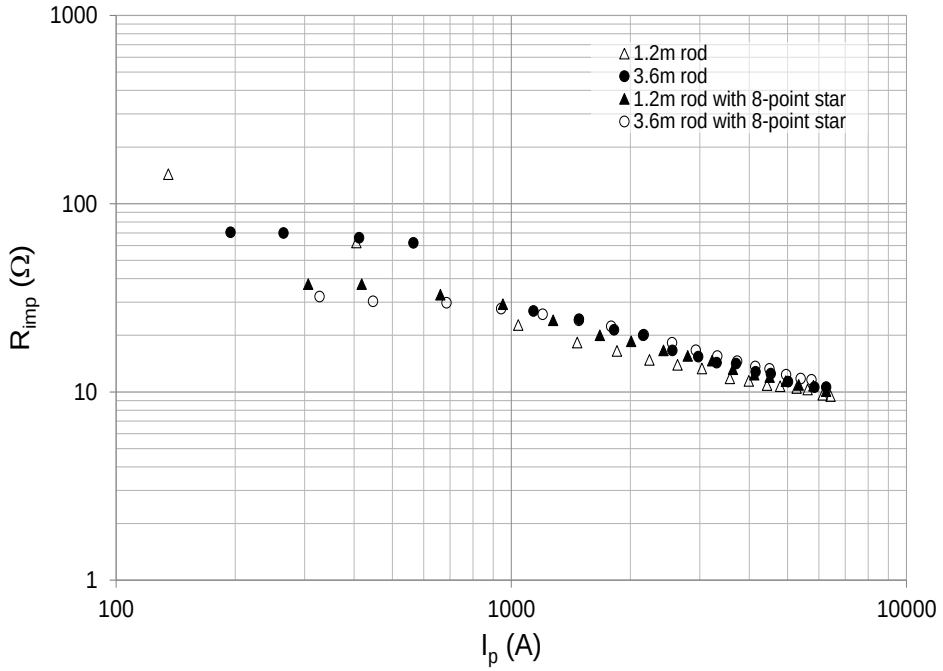

Figure 7.13: Variation of impulse resistance with current magnitude for 1.2m and 3.6m rod with and without horizontal enhancements

7.5 Conclusions

High current tests on practical grounding electrodes have been performed at the Cardiff University earthing test facility. As a precursor to the field tests, extensive computer simulations using CDEGS were undertaken which showed that, by employing a ring current return electrode, step and touch voltages in the vicinity of the test electrode area could be kept to a safe level. The characteristics of full scale vertical

rod electrodes up to 4.8m in length subjected to impulse currents of low and high-magnitude have been studied. At low current magnitude, the impulse and DC resistances of vertical electrodes were found to have slightly different values. Generally, the impulse resistance of all vertical electrodes decreases with increasing current magnitudes. This fall in impulse resistance was attributed to two different factors affecting the soil medium. When the impulse current increases, the conductivity of the soil increases, therefore, the resistivity of the soil reduces. Above a certain level of voltage applied, the ionisation process starts to take place leading to a further reduction of the impulse resistance as the ionisation region expands. The largest fall in impulse resistance was obtained for the shortest vertical rod having the largest low-current DC resistance, as only a relatively small current is required to initiate soil ionisation. Vertical electrodes with horizontal enhancements, by contrast, showed only small reduction due to their large surface area. Finally, to demonstrate a reduction in the impulse resistance of enhanced vertical electrodes for both low and high current magnitudes, the addition of horizontal enhancements is recommended as the best earthing design.

CHAPTER EIGHT: GENERAL DISCUSSION AND CONCLUSIONS

8.1 CONCLUSIONS

An extensive review of the behaviour of earth electrode systems under high frequency and transient conditions has been carried out; revealing that at low frequencies, the earth impedance of electrodes is broadly frequency independent, and practically equal to the power frequency resistance. At high frequencies, the earthing impedance is entirely frequency dependent. Much of the previous experimental work has been based on laboratory tests with restricted space requirements, and no established technique is as yet available for investigating experimentally the performance of the different lengths of vertical earth electrodes with 4-point/8-point star enhancements under variable high frequency and impulse conditions. Published works have determined that the behaviour of earth electrodes subjected to transients is different to that observed at power frequency, high lightning that the impulse resistance of an earth electrode differs from its power frequency resistance. The impulse resistance of an earth electrode depends on a number of factors, such as electrode geometry, peak value and of rise time of impulse current.

An extensive soil resistivity survey has been performed at the Llanrumney test facility, and results exhibiting similar trends were obtained using different instrument types. The soil resistivities in the vicinity of vertical and horizontal earth electrodes were investigated prior to installations, and 2D inversion software used to obtain the soil resistivity sections.

The measured DC resistance of vertical rods was found to decrease with increasing of rod length. The measured DC resistance of the short vertical rod was also found to vary seasonally due to soil resistivity variations over the period of the study. Thus,

changes in the earth resistance/impedance should be taken into account when designing an earthing system for use at a particular location.

The measured earth impedance characteristics of vertical rods up to 6m in length indicated that short earth electrodes present a small reduction in the earth impedance at low frequency. It was found that, at high frequencies, the capacitive effect is dominant for short electrodes while the inductive effect dominates for the long earth electrode. The computed results show a good agreement with the measurements in low frequency range, but they overestimate the resistance/impedance at high frequency. This was attributed to the uniform single-valued estimate of the soil resistivity used in the simulation, which does not fully represent the localised variations in soil resistivity at the test site.

Work was carried out to improve the earth electrode performance under high frequencies up to 10MHz. The field tests reveal that the addition of horizontal enhancements to vertical earth electrodes can be an effective way to reduce the earthing resistance/impedance across the entire frequency spectrum.

In addition, the effective length of the 88m horizontal electrode was determined by an empirical formula reported in literature. The impulse results show that increasing the length of the electrode to 6m leads to a reduction in the earth potential rise (EPR). Coincidence of the instants of voltage and current peaks for all rod lengths indicates a predominantly resistive behaviour.

A significant reduction in the earth potential rise (EPR) at the injection point was achieved with the addition of horizontal enhancements to vertical ground rods buried in non-uniform soil at the field test site. The measured impulse response of vertical electrodes configurations with and without 4-point/8-point star electrodes were

compared with computations, and found to be in satisfactory agreement. It was also experimentally demonstrated that the impulse resistance of a horizontal earth electrode decreased in the presence of an interconnected insulated above-ground conductor.

It was shown that significant current flows into a rod at low frequency due to the rod's resistance being much lower than that of the individual branches of the cross enhancement. Conversely, only a small proportion of the current flows in the rod at high frequency, indicating that results may not be in agreement with the industrial standard reference of the rod satisfying the role of a 'high-frequency earth electrode'. In addition, the current and voltage distributions of the 88m horizontal electrode at high frequency show that the majority of the current is dissipated close to the injection point, and that the voltage falls with distance away from this injection point. Test results on the 88m horizontal earth electrode with the insulated conductor enhancement reveal that the current distribution is modified by the presence of the insulated conductor. The comparison between measurements and computations using CDEGS of the rod/4-point star electrode showed an asymmetry in the four branch currents that is not predicted by the simulations, though reasonable agreement is still achieved.

A full safety simulation study was performed to determine the most appropriate current return arrangement for carrying out high current tests. In this study, 88m bare horizontal and 188.5m diameter ring conductors were selected to act as current return electrodes. The simulation results showed that using the ring electrode as current return gave a significant reduction in the earth potential rise (EPR), step and touch voltages throughout the test area compared to those arising from using a horizontal earth electrode. Accordingly, a 188.5m ring earth electrode was installed at Llanrumney test site. High voltage tests on the vertical electrodes with and without horizontal enhancements were conducted to examine nonlinear behaviour under high impulse

current magnitudes. A test method was employed in which a wireless system was used to transfer the current and voltage measurements to a local computer in order to minimise the effect of coupling between current injection and measurement circuits. The test results showed that the measured impulse resistance decreases with increasing impulse current, the greatest reduction in impulse resistance occurring with a vertical electrode having the highest initial DC resistance. However, vertical electrodes with horizontal enhancements exhibited only a small reduction in comparison due to the low current density at the electrode-soil interface. The pre-ionisation resistance R_1 was found to be less dependent on current magnitude compared with the post-ionisation resistance R_2 was found to decrease with increasing impulse current magnitude.

Finally, the test results of rods with enhancements under DC, high frequency, low impulse injected current value, high impulse injected current magnitudes showed that significant reduction in earthing impedance, DC earth resistance and impulse resistance was obtained. Also, using the rods with enhancements modified the current distribution behaviour. Therefore, this technique is a good design when one requires reliable earthing systems.

8.2 FUTURE WORK

The following suggestions are proposed for future work:

i) Further experimental investigations on the soil resistivity survey using different types of array such as pole-pole, pole-dipole and dipole-dipole electrode arrays to produce 3D images (xyz coordinates) by using 3D inversion software might be useful for the field test site.

ii) Experimental studies could be conducted at the field test site and comparing results between various configurations and resistivity of earthing systems, in order to develop a greater understanding of the characteristics of earthing systems under high frequency and low /high current impulse with various rise-times.

REFERENCES

Chapter One

[1.1]M. Davies, ‘‘High frequency and transient performance of earthing systems,’’ Ph.D., dissertation, Cardiff University, 1999

[1.2]ENA-TS 41-24 ‘‘Guidelines for the design, installation, testing and maintenance of main earthing systems in substations, ’’ Energy Networks Association, Issue 1, UK, 1992

[1.3]IEEE guide for safety in AC substation grounding, ANS/IEEE standard 80, 2000.

[1.4]BS 7430:2011: ‘‘Code of practice for protective earthing of electrical installations,’’ British Standard Institution, 2011

[1.5]BS EN 62305-3:2011: ‘‘Protection against lightning: part3: Physical damage and life hazard to structures,’’ European Committee for Electrotechnical Standardisation (CENELEC), 2011

[1.6]L. Grcev and V. Arnautovski, ‘‘Comparison between simulation and measurement of frequency dependent and transient characteristics of power transmission line grounding,’’ proceedings on 24th International Conference on Lightning Protection (ICLP), pp. 524-529, Birmingham, UK, 1998

[1.7]L. Grcev, “High frequency performance of ground rods in highly resistivity soil’’ Proceedings on International Conference on Grounding and Earthing , pp. 1-4, Belo Horizonte , Brazil, Jun. 2000

[1.8]A. Rousseau and P. Gruet, ‘‘Practical high frequency measurement of a lightning earthing system,’’ Proceedings of the 27th International Conference on Lightning Protection (ICLP), Avignon, France, September 2004

[1.9]S. Mousa, N. Harid, H. Griffiths, and A. Haddad, ‘‘Experimental investigation of high frequency and transient performance of a vertical earth electrode,’’ Proceedings of the 46th International Universities Power Engineering Conference (UPEC), pp. 4, September 2011

[1.10]S. Mousa, H. Griffiths, N. Harid and A. Haddad, ‘‘Experimental investigation of high frequency and transient performance earth rod systems,’’ Proceedings of the 31st International Conference on Lightning Protection (ICLP), pp. 4, Vienna, Austria, September 2012.

[1.11]L. Grcev and D. Heimbach ‘‘Frequency dependent and transient characteristics of substation grounding system,’’ IEEE Transaction on Power Delivery, vol. 12, no. 1, 1997

[1.12]A. Davies, and H. Griffiths, “High frequency and transient performance of a vertical earth electrode,” Proceedings of the 24th International Conference on Lightning Protection (ICLP), Birmingham UK, pp. 536-540, 1998

[1.13]A. Otero, J. Cidras, and J. L. Del Alamo, “Frequency-dependent grounding system calculation by means of a conventional nodal analysis technique,” IEEE Transactions on Power Delivery, vol. 14, no.3, pp.873-878, 1999.

[1.14]B. Zedan, H. Griffiths, and A. Haddad, “Frequency response of earthing systems”, Proceedings on 28th International Universities Power Engineering Conference (UPEC), Vol. 2, pp. 717-720, Thessaloniki, Greece, 2003.

[1.15]L. Grcev and M. Popov, ‘‘On High-frequency circuit equivalents of a vertical ground rod,’’ IEEE Transactions on Power Delivery, vol. 20, no. 2, April 2005

[1.16]M. Lorentzou and N. Hatziargyriou‘‘EMTP modelling of grounding electrodes,’’ Proceedings on 32nd International Universities Power Engineering Conference (UPEC), pp. 351-354, Manchester, UK, September 1997

[1.17]A. Davies, ‘‘High frequency and transient performance of earthing systems,’’ PhD Thesis, Cardiff University, 1999

[1.18]H. Griffiths, ‘‘Aspects of earthing system under variable and impulse conditions,’’ PhD Thesis, Cardiff University, 2008

[1.19]H. Towne, ‘‘Impulse characteristics of driven grounds,’’ General Electric Review, vol.31, no.11, pp.605, Nov., 1928

[1.20]E. Sunde, ‘‘Earth conduction effects in transmission systems,’’ New York, Dover publications Inc., 1968

[1.21]H. Dwight, ‘‘Calculation of resistances to ground,’’ AIEE Transactions, pp. 1319-1328, December 1936

[1.22]P. Bellaschi, ‘‘Impulse and 60-Cycle Characteristics of Driven Grounds’’, AIEE Transactions, Vol.60, p.123, March 1941

[1.23]P. Bellaschi, P.L., R.E. Armington and A. E. Snowden, ‘‘Impulse and 60-cycle characteristics of driven grounds-II,’’ AIEE Transactions, vol.61, pp. 349-363, 1942

[1.24]C. Pritindra, ‘‘Impulse impedance tests on laboratory model ground electrodes,” IEE Proceedings on Generation, Transmission and Distribution, vol. 150, no. 4, pp. 427-433, 2003

[1.25]N. Mohamed Nor, A. Haddad and H. Griffiths, ‘‘Characteristics of ionisation phenomena in soil under high impulse currents,” IEEE Transaction of Power Delivery, vol. 21, no. 95, pp. 353-361, 2006

[1.26]ITU-T (International Telecommunication Union): ‘Calculating Induced Voltage and Currents in Practical Cases.’ Volume II, 1999

[1.27]BS EN 50522:2010, ‘‘Earthing of power installations exceeding 1 kV a.c. ’’, October 2010

[1.28]Effects of Current on Human Beings and Livestock-Part1:General Aspects, IEC/TS 60479-1:2005, 2005

[1.29]BS EN 50522:2010: ‘‘ Earthing of power installations exceeding 1kV ac,’’ European Committee for Electrotechnical Standardisation (CENELEC), 2010

[1.30]BS 7430:2011: ‘‘Code of practice for protective earthing of electrical installations,’’ British Standard Institution, 2011

Chapter Two

[2.1]D. Sunde., Earth conduction Effects in Transmission line Systems, Dover Publications Inc., 1968

[2.2]J. Schon, ‘‘Physical properties of rocks: Fundamental and principles of petrophysics,’’ In: K. Helbig, S. Treitel eds., ‘‘Handbook of geophysical exploration,’’ Section Exploration, vol. 18, Elsevier Science Ltd., Oxford, 1998.

[2.3]IEEE guide for safety in AC substation grounding. ANSI/IEEE standard 80- 2000

[2.4]D. Griffiths, R. King, ‘‘Applied geophysical for geologists and engineers-The elements of geophysical prospecting,’’ 2nd Ed., Permagon Press, Oxford, 1981.

[2.5]G. Bell, ‘‘Ground engineers reference book,’’ Butterworth, London, 1987.

[2.6]G. Tagg: ‘Earth resistances,’ G. Newnes Ltd., England, 1964

[2.7]The electricity association: ‘‘Engineering recommendation S.34-A guide for assessing the rise of earth potential at substation site,’’ The electricity association, 1986.p23

[2.8]F. Wenner, ‘‘A method for measuring earth resistivity,’’ Bureau of Standards Scientific Paper, 1915, no. 258

[2.9]R. Van Nostrand and K. L. Cook, ‘‘Interpretation of resistivity data,’’ Geological Survey Professional Paper no. 499, US Dept. Of the Interior, Washington, 1966

[2.10]British Electricity International, ‘‘Modern power station practice,’’ Pergamon, London, 1992, 3rd ed

[2.11]B. Thapar and E. Gross, ‘‘Grounding grids for high voltage systems,’’ IEEE Trans. PAS, 1963, pp. 782-788

[2.12]J. Endrenyi, ‘‘Evaluation of resistivity tests for design of station grounds in non-uniform soil,’’ AIEE Transactions, 1963, vol. 82, pp. 782-788

[2.13]N. Mohamad, ‘‘Effect of enhancement material when mixed with sand under high impulse conditions,’’ International Conference on Properties and Applications of Dielectric Materials, pp. 916-919, 2006.

[2.14]W. Jones, ‘‘Benotnite rods assure ground installation in problem soils,’’ IEEE Transactions on Power Apparatus and System, vol.PAS-99, no. 4, pp. 1343-1346, 1980

[2.15]H. Yamane, T. Ideguchi, N. Tokuda and H. Koga, ‘‘Long-term stability of reducing ground resistance with water-absorbent polymers,’’ IEEE International Symposium on Electromagnetic Compatibility, pp.678-682, 1990

[2.16]L. Yan, ‘‘Research on the mechanism of grounding resistance-reduction agent and the used quantity,’’ Proceedings of the 3rd International Conference on Properties and Applications of Dielectric Materials, vol. 2, pp.1230-1233, Tokyo, Japan, 1991.

[2.17]M. Kostic, Z. Radakovic, N. Radakovic and M.Canovic, ‘‘ Improvement of electrical properties of grounding loops by using bentonite and waste drilling mud,’’ IEE Proceedings on Generation, Transmission and Distribution, vol. 146, pp. 1-6,1999.

[2.18]Q. Meng, J. He, F. Dawalibi and J. Ma, ‘‘A new method to decrease ground resistances of substation grounding systems in high resistivity regions, ’’IEEE Transaction on Power Delivery, vol. 14, no. 3, 1999

[2.19]J. He, G. Yu, R. Zeng, B. Zhang and J. Zou, ‘‘ Decreasing resistance of substation by deep-ground-well method,’’ IEE Transaction on Power Delivery, vol. 20, no. 2,pp. 738-744, 2005.

[2.20]A. Al-Arainy, Y. Khan, N. Malik and M. Qureshi, ‘‘Grounding pit optimization for uses in high resistivity areas,’’ Proceedings on GCC-CIGRE, Doha, 2010

[2.21]A. Al-Arainy, Y. Khan, M. Qureshi, N. Malik and F. Pazheri, ‘‘ Optimized pit configuration for efficient grounding of the power system in high resistivity soils using low resistivity materials ,’’ Proceedings of 4th International Conference on Modelling, Simulation and Applied Optimization (ICMSAO), pp.1-5, Kuala Lumpur, Malaysia, April, 2011.

[2.22]ANSI/IEEE Std 80-1986, ‘‘IEEE guide for safety in AC substation grounding’’

[2.23]H.Towne, ‘‘Impulse characteristics of driven grounds,’’ General Electric Review, vol.31, no.11, pp.605, Nov., 1928

[2.24]P. Bellaschi, ‘‘Impulse and 60-Cycle Characteristics of Driven Grounds’’, AIEE Transactions, Vol.60, p.123-128, March 1941

[2.25]P. Bellaschi, P.L., R.E. Armington and A. E. Snowden, ‘‘Impulse and 60-cycle characteristics of driven grounds-II,’’ AIEE Transactions, vol.61, pp. 349-363, 1942

[2.26]A. Vainer, ‘‘Impulse characteristics of complex earth grid’’, Elektrichestvo, no. 3, pp.107-117, 1965

[2.27]A. Liew and M. Darveniza, ‘‘Dynamic model of impulse characteristics of concentrated earths’’, Proc. IEE, vol.121, no.2, p.122, February 1974

[2.28]W. Dick and H. R. Holliday, ‘‘Impulse and alternating current tests on grounding electrodes in soil environment,’’ IEEE Transactions on Power Apparatus and Systems, vol. PAS-97, no.1, pp.102-108, January/February 1978

[2.29]S. Sekioka, T. Hara, A. Amatani, ‘‘Development of a nonlinear model of a concrete pole grounding resistance,’’ International Conference on Power Systems Transients, pp. 463-468, Lisbon, 3-7 September, 1995

[2.30]M. Almeida, M.T. Correia de Barros, “Accurate modelling of Rod Driven Tower Footing Resistance,” IEEE Transaction on Power Delivery, vol.11, no.3, pp.1606-1609., Jul. 1996

[2.31]L. Bewley, “The counterpoise,” General Electric Review, vol.37, no.2, pp. 73,Feb, 1934

[2.32]L.Bewley, “Theory and tests of the counterpoise,” Electrical Engineering, no.53, p 1163, Aug., 1934

[2.33]R. Gupta, and B. Thapar, ‘‘Impulse impedance of grounding grids,’’ IEEE Transactions on Power Apparatus and Systems, vol.PAS-99, no.6, p.2357 Nov/Dec 1980

[2.34]R. Gupta,V. Singh,’’ Impulse impedance of rectangular grounding grid, Impulse impedance of grounding grids, ‘‘ IEEE Transactions on Power Delivery, vol.7, no.1, pp.214-218,Jan. 1991.

[2.35]S. Toshio, H. Takesus and S. Sekioka,’’Measurement on surge characteristics of grounding resistance of counterpoise for impulse currents, ‘‘International Conference on Lightning Protection (ICLP), Rhodes, Greece, September 2000

[2.36]G. Yanqing, H. Jinliang, Z. Rong and L. Xidong, “Impulse transient characteristic of grounding grids’’ Proceedings on 3rd International Electromagnetic compatibility, pp. 276-280, Beijing, China, May 2002

[2.37]E. Oettle and H. Geldenhuys, “Results of impulse test on practical electrodes at the high-voltage laboratory of the national electrical engineering research institute’’ , The Transactions of the South Africa Institute of Electrical Engineers, vol. 79, no.2, pp. 71-78, 1988

[2.38]A. Geri, M. G Veca., E.Garbagnati ,G.Sartori,'' Non-linear behaviour of ground electrodes under lightning surge currents: computer modelling and comparison with experimental results, '' IEEE Transactions on Magnetics, Vol.28, No.2, March, 1992.

[2.39]S. Skioka, H. Hayashida, T. Hara and A. Ametani, "Measurement of grounding resistance for high impulse currents,'' IEE proceedings Generation, Transmission and Distribution, vol. 145, pp. 693-699, 1998

[2.40]F. Vander, B. Zedan, H. Griffiths and A. Hadadd,'' Impulse response of earth grid,'' Proceedings on 13th International Symposium on High Voltage, Greece, 2003

[2.41]SES (Safe Engineering Services), Current distribution electromagnetic grounding analysis software (CDEGS), available: htt://www.sestech.com/products/spftpackages/cdegs.htm

[2.42]K. Berger, ''The Behaviour of earth connections under high intensity impulse currents,'' CIGRE Paper No.215, 1946

[2.43]G. Petropoulos, ''The High-Voltage Characteristics of Earth Resistances,'' Journal of the IEE, Part 11, vol.95, pp. 172-174, Feb. 1948

[2.44]S. Brourg and B. Sacepe, "Deep earth electrodes in highly resistive ground frequency behaviour,'' IEEE International Symposium on Electromagnetic Compatibility, pp. 584-589, 1995

[2.45]L. Grcev, "High frequency performance of ground rods in highly resistivity soil'' Proceedings on International Conference on Grounding and Earthing , pp. 1-4, Belo Horizonte , Brazil, Jun. 2000

[2.46]J. Choi, Y. AHN, S. Goo, K. Park, J. Yoon and G. Jung, " Direct measurements of frequency domain impedance characteristics of grounding system,'' Proc. International Conference on Power System Technology (Power Con 2002), vol.4, 2002, pp.2218-2221

[2.47]F. Visacro and A. Soares, " Simplified models for tower-footing grounding of transmission lines for the evaluation of lightning performance,'' Proceedings of the 23rd International Conference in Lightning Protection (ICLP), Firenze, Italy, 1996, pp. 574-578

[2.48]B. Nekhoul, P. Labie, F. Zgainski and G. Meunier, "Calculating the impedance of a grounding system,'' IEEE Transaction on Magnetics, pp. 1509-1512, no. 3, 1996

[2.49]A. Papalexopoulos and A. Meliopoulos, "Frequency dependent characteristics of grounding systems,'' IEEE Transaction on Power Delivery, vol.2, no.4, pp.1073-1081, 1987

[2.50]A. Davies, H. Griffiths and T. Charlton, "High frequency performance of a vertical earth rod,'' Proceedings on 24th International Conference on Lightning Protection (ICLP), pp. 536-540, Birmingham UK, 1998

[2.51]B. Zedan, H. Griffiths and A. Haddad, "Frequency response of earthing systems,'' Proceedings on 28th International Universities Power Engineering Conference, pp. 717-720,vol.2, Thessaloniki, Greece, 2003

[2.52]L. Grecev and M. Popov, "On High-frequency circuit equivalents of a vertical ground rod,'' IEEE Transactions on Power Delivery, vol. 20, no.2, April 2005

[2.53]P. Llovera, J. Antonio, A. Quijano and V. Fuster, “High frequency measurements of grounding impedance on resistive soils,’’ Proceedings on 28th International Conference on Lightning Protection (ICLP), Kanazawa, Japan, Sep. 2006

[2.54]H. Griffiths, “Aspects of earthing system under variable and impulse conditions,’’ PhD thesis, Cardiff University, 2008

[2.55]J. Choi and B. Lee, ‘‘An analysis of the frequency-dependent grounding impedance based on the ground current dissipation of counterpoises in the two-layered soils,’’ Electric Power Systems Research, April 2012, Vol. 70, no. 2, pp.184-191

[2.56]R. Alipio and S. Visacro, “How the frequency dependence of soil parameters affects the lightning response of grounding electrodes,’’ Proceedings on 31st International Conference on Lightning Protection (ICLP), Vienna, Austria, 2012

[2.57]H. Griffiths, N. Harid and A. Haddad, “Modelling the effective length of earthing systems under variable frequency,’’ Proceedings on CIGRE Paper, The Japanese National Committee of CIGRE, Hakodate, Japan, 2012

[2.58]A. Farag, T. Cheng and D. Penn, “Grounding terminations of lightning protective systems”, IEEE Trans. Dielectrics Elect. Insul. 5 (6) 869–877, 1998.

[2.59]M. Lorentzou and N. Hatziargyriou, “Effective dimensioning of extended grounding systems for lightning protection”, Proceedings of the 25th International Conference on Lightning Protection, Greece, p.435-439 September 2000.

[2.60]Y. Liu., N. Theethayi and R. Thottappillil, “An engineering model for transient analysis of grounding system under lightning strikes: non uniform transmission-line approach,’’ Power Delivery, IEEE Transactions on , vol.20, no.2, pp. 722-730, April 2005

[2.61]C . Mazetti and G. M Veca, “Impulse behaviour of .grounding electrodes,’’ IEEE Trans. Power App. Syst., vol 102, no. PAS-9, 3148-3154, 1983.

[2.62]S. Ghosh, S. Munshi. and . J. Biswas, “Computer aided analysis of surge behaviour of an earthing counterpoise discharging impulse current to ground,” Journal of the Institution of Engineers India, vol. 77, pp. 128-132, November 1996.

[2.63]H. Griffiths and A. Davies, “Effective length of earth electrodes under high frequency and transient conditions,’’ International Conference on Lightning Protection, Vol. 1, Rhodos Greece, pp 536-540, 2000.

[2.64]L. Chonghui, J. He , Y. Gao, R. Zeng and J. Zou, “Effective length of extended earthing electrode under lightning impulse,’’ 13th International Symposium on High Voltage Engineering, Netherlands 2003

[2.65]H. Griffiths, N. Harid and A. Haddad, “Modelling the effective length of earthing systems under variable frequency," Proceedings of the CIGRE Symposium, October 2012, Hakodate, Japan no.2, pp. 722- 730, April 2005

[2.66]A. Elmghairbi, N. Harid, H. Griffiths, and A. Haddad, “A new method to increase the effective length of horizontal earth electrodes,’’, Proceedings on 45th International Universities Power Engineering Conference (UPEC), 2010, Cardiff, UK, pp. 4

[2.67]A. Elmghairbi, M. AhmedaN. Harid, H. Griffiths, and A. Haddad, “A technique to increase the effective length of horizontal earth electrodes and its application to a practical earth electrode system," Lightning (APL), 2011 7th Asia-Pacific International Conference pp.690-693, 1-4 Nov. 2011

[2.68]L. Grcev and D. Heimbach, “Frequency dependant and transient characteristics of substation grounding systems’’, IEEE Transactions on Power Delivery, vol.-12, No.1, Jan 1997.

[2.69]L. Grcev, “Lightning surge efficiency of grounding grids’’, IEEE Transactions on Power Delivery, vol.-26, No.3, pp. 1692-1699, July 2011.

[2.70]W. Xishan, Z. Zhengguo, W. Yi and C. Jiangbo, “Measurement on current distribution of grounding grid,’’, Proceedings of 13th International Symposium on High Voltage Engineering, vol. 1, Rotterdam, Netherlands, 2003

[2.71]Y. Tao, S. Wen-xia, Y. Cai-wei and Y. Qing, ‘‘Experimental investigation on the impulse-current distribution of grounding electrodes with varies structures’’, Proceeding of International Conference on High Voltage and Application (ICHVE), Chongqing, China, pp.269-272, Nov.2008

[2.72]M. Ahmeda, N. Ullah, N. Harid, H. Griffiths and A. Haddad, ‘‘Current and voltage distribution in a horizontal earth electrode under impulse conditions,’’ Proceedings of the 44th International Universities Power Engineering Conference (UPEC), 2009, Glasgow, UK, pp. 1-4

[2.73]J. Choi, J. Kim, B. Lee and Y. Chung, ‘‘An analysis of conventional grounding impedance based on the impulsive current distribution of a counterpoise,’’

Proceeding of 30th International Conference On Lightning Protection (ICLP), 2009, Cagliari, Italy, pp. 1179-1185

[2.74]J. Choi, and B. Lee, ‘‘An analysis of conventional grounding impedance based on the impulsive current distribution of a horizontal electrode,’’ Electric Power Systems Research, vol. 85, pp.30-37, April 2012

Chapter Three

[3.1]F. Tagg “Earth resistance,’’ George Newnes Ltd, England, 1964

[3.2]BS 7430, “Code of practice for earthing,’’ British Standards Institution, 1991

[3.3]R. Ryder “Earthing principles and practice,’’ Sir Isaac Pitman, Sons Ltd., 1952

[3.4]IEEE guide for safety in AC substation grounding, ANSI/IEEE standard 80-2000

[3.5]F. Wenner,” A method of measuring earth resistivity,’’ Scientific papers of the bureau of standards, no. 258, pp. 469-478, Washington, October, 1915.

[3.6]A. Haddad and D. Warne, “Advances in high voltage engineering, ’’IEE Power &Energy Series 40, 2004

[3.7]Cardiff University, “Understanding of earthing associated with transmission tower bases, ’’ A project sponsored by NGC Ltd., Progress Report No 3, 14 March, 2002

[3.8]ABEM Terrameter, Instruction manual and user guide, ABEM Instrument AB, Sweden

[3.9]RES2DINV, Geoelectrical Imaging 2D, Geotomo Software, Nov. 2011

[3.10]Megger DET2/2, Auto earth tester specification

[3.11]Lund Imaging System, Instruction Manual, ABEM Instrumnet AB, Sundbyberg, Sweden

[3.12]A. Elmghairbi, "Assessment of earthing systems and enhancement of their performance,'' PhD thesis, Cardiff University, 2012

[3.13]M. Loke, "Electrical imaging surveys for environmental and engineering studies,' 'A practical Guide to 2D and 3-D Surveys, 1999

[3.14]RES3DINV manual, ver. 3.04, Geotomo Software, Nov. 2011

Chapter Four

[4.1]S. Mousa, N. Harid, H. Griffiths, and A. Haddad, ''Experimental investigation of high frequency and transient performance of a vertical earth electrode,'' Proceedings of the 46th International Universities Power Engineering Conference (UPEC), pp. 4, September 2011

[4.2]H. Griffiths, "Aspects of eathing system under variable and impulse conditions,''Ph.D. dissertation, Cardiff University, 2008

[4.3]A. Davies, and H. Griffiths, "High frequency and transient performance of a vertical earth electrode," Proceedings of the 24th International Conference on Lightning Protection (ICLP), Birmingham UK, pp. 536-540, 1998

[4.4]B. Zedan, H. Griffiths, and A. Haddad, "Frequency response of earthing systems", Proceedings on 28th International Universities Power Engineering Conference (UPEC), Vol. 2, pp. 717-720, Thessaloniki, Greece, 2003.

[4.5]M. Davies, ‘‘High frequency and transient performance of earthing systems,’’ Ph.D., dissertation, Cardiff University, 1999

[4.6]S. Mousa, H. Griffiths, N. Harid and A. Haddad, ‘‘Experimental investigation of high frequency and transient performance earth rod systems,’’ Proceedings of the 31st International Conference on Lightning Protection (ICLP), pp. 4, Vienna, Austria, September 2012.

[4.7]L. Grcev and D. Heimbach ‘‘Frequency dependent and transient characteristics of substation grounding system,’’ IEEE Transaction on Power Delivery, vol. 12, no. 1, 1997

[4.8]A. Otero, J. Cidras, and J. Del Alamo, “Frequency-dependent grounding system calculation by means of a conventional nodal analysis technique,” IEEE Transactions on Power Delivery, vol. 14, no.3, pp.873-878, 1999.

[4.9]B. Zedan,” Characterisation of substation earth grid under high frequency and transient conditions,’’ Ph.D. dissertation, Cardiff University, 2005

[4.10]A. Mghairbi,” Assessment of earthing systems and enhancements of their performance,’’ Ph.D. dissertation, Cardiff University, 2012

[4.11]A. Rousseau and P. Gruet, ‘‘Practical high frequency measurement of a lightning earthing system,’’ Proceedings of the 27th International Conference on Lightning Protection (ICLP), Avignon, France, September 2004

[4.12]L. Grcev and M. Popov, ‘‘On High-frequency circuit equivalents of a vertical ground rod,’’ IEEE Transactions on Power Delivery, vol. 20, no. 2, April 2005

[4.13]L. Grcev and V. Arnautovski, ‘‘Comparison between simulation and measurement of frequency dependent and transient characteristics of power

transmission line grounding,'' proceedings on 24th International Conference on Lightning Protection (ICLP), pp. 524-529, Birmingham, UK, 1998

[4.14]R. Alipio and S. Visacro ''Frequency dependence of soil parameters: effect on the lightning response of grounding electrodes,'' IEEE Transactions on Electromagnetic Compatibility, vol55, no. 1, pp.132-139, 2013.

[4.15]M. Lorentzou and N. Hatziargyriou''EMTP modelling of grounding electrodes,'' Proceedings on 32nd International Universities Power Engineering Conference (UPEC), pp. 351-354, Manchester, UK, September 1997

[4.16]R. Rudenberg: 'Electrical shock Waves in Power Systems – Travelling Waves in lumped and distributed circuit elements,' Harvard University Press, Cambridge, Massachusetts, ISBN 011281, 1968.

[4.17]G. Tagg: 'Earth Resistance,' Gorge Newnes Limited. (London), 1964

[4.18]E. Sunde: 'Earth conduction effects in transmission line systems,' Dover Publications Inc., 1968.

[4.19]D. Lathi,'' Impulse measurements in earthing systems'', Ph.D. dissertation, Cardiff University, 2012

[4.20]W. Johnson: 'Transmission lines and networks,' International Student Edition, McGraw-Hill Kogakusha Ltd., Tokyo, Japan.

[4.21]J. Endrenyi, ''Analysis of transmission tower potentials during ground faults,'' IEEE Transactions on Power Apparatus and Systems, vol. PAS-86, no. 10, pp.1274-1283, Jun. 1984

[4.22]R. Velazquez and D. Mukhedkar ‘‘Analytical modelling of grounding electrodes transient behaviour,’’ IEEE Transactions on Power Apparatus and Systems, vol. PAS-103, no. 6, pp.1314-1322, Oct. 1967

[4.23]A. El Mghairbi, N. Harid, H. Griffiths and A. Haddad, ‘‘A new method to increase the effective length of horizontal earth electrode,’’ Proceedings on 45th International Universities Power Engineering Conference (UPEC), Vol. 2, pp. 1-4, Cardiff University, Cardiff, UK, 2010.

[4.24]A. El Mghairbi, M. Ahmeda, N. Harid, H. Griffiths, A. Haddad, (2012, May), ‘‘Technique to increase the effective length of practical earth electrodes: Simulation and field test results,’’ Electric Power Systems Research [Online]. Available http://dx.doi.org/0.1016/j.epsr.2012.04.015

[4.25]P. Jones, ‘‘Electrical measurement of large area substation earth grids,’’ PhD thesis, Electrical Division, Cardiff University, 2001

[4.26]Operating manual for Single Generators 2018&2019A, Marconi Instruments Ltd., April 1994

[4.27]SES (Safe engineering services). Current distribution electromagnetic grounding analysis software (CDEGS), Available http://www.sestech.com/products/softpackages/cdegs.htm

[4.28]J. He, , Y. Gao, R. Zeng, W. Sun, J. Zou and Z. Guan , ‘‘Optimal design of grounding system considering the influence of seasonal frozen soil layer,’’ IEEE Transactions on Power Delivery, vol. 20, no. 1, pp.107-115, 2005

[4.29]R. Gustafson, R. Pursley and V. Albertson, ‘‘Seasonal grounding resistance variations on distribution systems,’’ IEEE Transactions on Power Delivery, vol. 5, no. 2, pp.1013-1018, 1990

[4.30]J. He, R. Zeng, Y. Gao,Y. Tu, W. Sun, J. Zou and Z. Guan , ‘‘Seasonal influences on safety of substation grounding system,’’ IEEE Transactions on Power Delivery, vol. 18, no. 3, pp.788-795, 2003

[4.31]J. Tarilanyo, and C. Anaele, ‘‘Seasonal variation of soil resistivity and soil temperature in Bayelsa state,’’ American J. of Engineering and Applied Sciences, vol. 4, pp. 704-709, 2010

[4.32]N. Abdullah, A. Marcian, M. Osman, N. and AbdulRahman ‘‘Case study on impact of seasonal variations of soil resistivities on substation grounding systems safety in tropical country,’’ Proceedings on 7th Asia- Pacific International Conference on Lightning, pp.150-154, 2011, Chengdu, China

[4.33]ENA-TS 41-24 ‘‘Guidelines for the design, installation, testing and maintenance of main earthing systems in substations, ’’ Energy Networks Association, Issue 1, UK, 1992

Chapter Five

[5.1]P. Bellaschi and R. Armington, ‘‘Impulse and 60-cycle characteristics of driven grounds-III: Effect of lead in ground Installation,’’ AIEE Transactions on Electrical Engineering, vol.62, pp. 335-345, 1943.

[5.2]A. Davies, ‘‘High frequency and transient performance of an earthing system,’’ Ph.D dissertation, University of Wales, Cardiff, 1999

[5.3]F. Dawalibi, W. Ruan and S. Fortine, ‘‘Lightning transient of communication tower and associated ground networks,’’ Malaysia paper from CDEGS: Getting started manual, Safe Engineering Service and Technologies Ltd, Canada, 1998.

[5.4]F. Dawalibi, W. Xiong and J. Ma, ‘‘Transient performance of substation structures and associated grounding system,’’ IEEE Transactions on Industrial Applications, vol.31, no. 3,pp. 520-527,1995.

[5.5]A. Geri, ‘‘Practical design criteria of grounding systems under surge conditions,’’ Proceedings of 25th International Conference Lightning Protection (ICLP), 2000, pp.458-463

[5.6]L. Grecv, ‘‘Computer analysis of transient voltages in large grounding systems,’’ IEEE Transactions on Power Delivery, vol.11,no. 2, pp.815-823, April 1996.

[5.7]L. Grecv and M. Heimbach, ‘‘ Frequency dependent and transient characteristics of substation grounding systems,’’ IEEE Transactions on Power Delivery, vol. 12, no. 1, pp. 172-178, January 1997.

[5.8]L. Grecv and F. Menter, ‘‘ Transient electromagnetic field near large earthing systems,’’ IEEE Transactions on Magnetics, vol. 32, no. 3, pp. 1525-1528, May 1996.

[5.9]B. Gupta and B. Thapar, ‘‘ Impulse impedance of grounding grids,’’ IEEE Transactions on Power Apparatus and Systems, vol. PAS-99, no. 6, pp. 469-473, December 1980.

[5.10]B. Gupta and V. Singh, ‘‘ Inductance of rectangular grids,’’ IEEE Transactions on Power Delivery, vol. 7, no. 3, pp. 1218-1222, July 1992.

[5.11]B. Gupta and V. Singh, ‘‘ Impulse impedance of rectangular grounding grids,’’ IEEE Transactions on Power Delivery, vol. 7, no. 1, pp. 214-218, January 1992.

[5.12]M. Heimbach and L. Grecv, ‘‘Grounding system analysis in transient programs applying electromagnetic field approach,’’ IEEE Transactions on Power Delivery, vol. 12, no. 1, pp. 186-193, January 1997.

[5.13]A. Meliopoulos and M. Moharam, ‘‘Transient analysis of grounding systems,’’ IEEE Transactions on Power Apparatus and Systems, vol. 9, no. 4, pp. 389-399, February 1983

[5.14]F. Menter and L. Grecv, ‘‘ EMTP-Based model for grounding systems analysis,’’ IEEE Transactions on Power Delivery, vol. 9, no. 4, pp. 1838-1849, October 1994.

[5.15]F. Van der Linde, B. Zedan, H. Griffiths and A. Haddad, ‘‘Impulse response of earth grid,’’ Proceedings of 13th International Symposium on High Voltage Engineering, Greece, 1992

[5.16]F. Van der Linde, B. Zedan, H. Griffiths and A. Haddad, “Impulse response of earth electrode systems”, Proceedings of 37th International Universities Power Engineering Conference (UPEC), pp.827-831, Thessaloniki, Greece, 2003

[5.17]R. Velazquea and D. Mukhedkar, ‘‘ Analytical model of grounding electrodes transient behaviour,’’ IEEE Transactions on Power Apparatus, vol. PAS 103, no. 3, pp. 1314-1322, June 1984

[5.18]W. Xiong and F. Dawalibi, ‘‘Transient performance of substation grounding systems subjected to lightning and similar surge currents,’’ IEEE Transactions on Power Delivery, vol. 60, pp. 123-128, March 1941.

[5.19]B. Zidan, ‘‘Characterisation of substation earth grid under high frequency and transient conditions,’’ Ph.D dissertation, University of Wales, Cardiff, 2005

[5.20]G. Yanqing, H. Jinliang, Z. Rong and L. Xidong, “Impulse transient characteristics of grounding grids,” Proceedings of 3rd Symposium on Electromagnetic Compatibility Conference, 276-280, Beijing, China, May 2002

[5.21]L. Grcev, ‘‘Lightning surge efficiency of grounding grids,’’ IEEE Transactions on Power Delivery, vol. 26, no. 3, pp. 1692 - 1699, July 2011.

[5.22]X. Han, Y. Lu, C. Xia, J. Yu, Y. Huang, W. Zhou, B. Xu and H. Li, ‘‘Simulation research on impulse characteristics of horizontal grounding conductor,’’ Proceedings of Power Engineering and Automation Conference(PEAM), vol.2, pp. 31-35, September, 2011

[5.23]P. Bellashi, ‘‘Impulse and 60-cycle characteristics of driven grounds,’’ AIEE Transaction on Electrical Engineering, vol. 60, pp. 123-128, March 1941

[5.24]P. Bellashi and R. Armington, ‘‘Impulse and 60-cycle characteristics of driven grounds-II,’’ AIEE Transaction on Electrical Engineering, vol. 61, pp. 349-363, 1942

[5.25]L. Bewley, ‘‘Theory and tests of counterpoise,’’ AIEE Transaction on Electrical Engineering, vol. 53, pp. 1163-1172, 1934

[5.26]R. Kosztaluk, M. Loboda and D. Mukhedkar, ‘‘Experimental study of transient ground impedance,’’ IEEE Transactions of Power Apparatus and Systems, vol. PAS-100, pp. 4653-4660, 1981

[5.27]P. Chowdhuri, ‘‘Impulse impedance tests on laboratory model grounding electrodes,’’ IEE Proceedings of Transmission and Distribution Generation, vol. 150, pp. 427-433, July 2003

[5.28]A. Haddad, H. Griffiths, M. Ahmeda and N. Harid, ‘‘Experimental investigation of the impulse characteristics of practical ground electrodes,’’ Proceedings of International Conference on High Voltage Engineering and Application (ICHVE), pp. 469-472, October 2010

[5.29]S. Mousa, N. Harid, H. Griffiths, and A. Haddad, ‘‘Experimental investigation of high frequency and transient performance of a vertical earth electrode,’’ Proceedings of the 46th International Universities Power Engineering Conference (UPEC), pp. 4, September 2011

[5.30]S. Mousa, H. Griffiths, N. Harid and A. Haddad, ‘‘Experimental investigation of high frequency and transient performance earth rod systems,’’ Proceedings of the 31st International Conference on Lightning Protection (ICLP), pp. 4, Vienna, Austria, September 2012.

[5.31]SES (Safe engineering services). Current distribution electromagnetic grounding analysis software (CDEGS), Available http://www.sestech.com/products/softpackages/cdegs.htm

[5.32]IEEE guide for safety in AC substation grounding. ANSI/IEEE standard 80-2000

[5.33]N. Harid, H. Griffiths and A. Haddad, ‘‘Effect of return path of on impulse characteristics of earth electrodes,’’ Proceedings on 7th Asia-Pacific International Conference on Lightning, pp. 1-4, Chengdu, China, 2011

[5.34]B. Gupta and B. Thapar, ‘‘Impulse characteristics of grounding electrodes,’’ Journal of the Institute of Engineers India, vol. 1, pp. 156-162, August 1998

[5.35]A. Haddad, H. Griffiths, M. Ahmeda and N. Harid, ‘‘Experimental investigation of the impulse characteristics practical electrode systems ,’’ International Conference on High Voltage Engineering and Application (ICHVE), pp. 469-472, New Orleans, US, 2010

[5.36]A. Elmghairbi, M. AhmedaN. Harid, H. Griffiths, and A. Haddad, “A technique to increase the effective length of horizontal earth electrodes and its application to a practical earth electrode system," Lightning (APL), 2011 7th Asia-Pacific International Conference pp.690-693, 1-4 Nov. 2011

Chapter Six

[6.1]A. Toseva and L. Grecev, ‘‘High frequency current distribution in horizontal grounding systems in two-layer soil,’’ Proceedings of International Symposium on Electromagnetic Compatibility, vol.1, pp. 205-208, May 2003

[6.2]B. Zhang, J. He and J. Lee, ‘‘Numerical analysis of transient performance of grounding systems considering soil ionization by coupling moment method with circuit theory ,’’ IEEE Transaction on Magnetics , vol.41, no. 5, pp. 1440-1443, May 2005

[6.3]T. Takashima T. Nakae and R. Ishibashi, ‘‘High frequency characteristics of impedances to ground and field distribution of ground electrodes,” IEEE Transactions on Power Apparatus and Systems, vol. PAS-100, no. 4, April 1981

[6.4]C. Buccella, ‘‘Calculation of current distribution in a lightning stroked metal structure considering the non-linear ground impedance,” Proceedings of Industry Applications Conference, vol. 4, pp. 2703 – 2708, October 2001

[6.5]B. Johnson, W. Price and A. Schultz, ‘‘Lightning-current distribution in towers and ground wire,” Transactions of the American Institute of Electrical, vol. 77, pp.1414-1417, April 1958

[6.6]Y. Tao, S. Wen-xia and Y. Cai-wei, YANG Qing, ‘‘Experimental investigation on the impulse-current distribution of grounding electrodes with varies structures’’, in Proceedings of International Conference on High Voltage and Application, Chongqing, China, pp.269-272, November 2008

[6.7]W. Xishan, Z. Zhengguo, W. Yi, L. Lei and C. Jaingbo, “Measurement on current distribution of grounding grid,’’ in Proceedings of 13th International Symposium on High Voltage Engineering, Rotterdam, Netherlands, 2003.

[6.8]M. Ahmeda, N. Ullah, N. Harid, H. Griffiths and A. Haddad, “ Current and voltage distribution in a horizontal earth electrode under impulse conditions,’’ in Proceedings of the 44th International Universities Power Engineering Conference (UPEC) ,Glasgow, Scotland, pp. 1-4, September 2009.

[6.9]J. Choi, H. Shin, D. Kim and B. Lee, “Grounding impedance based on the current distribution for the horizontal ground electrode installed in two-layer soil structure,’’ in proceedings of 7th Asia-pacific international conference on lightning ,Chengdu, China, pp. 112-116, November 2011.

[6.10]ENA TS-41-24-1: '' Guidelines for the design, installation, testing and maintenance of main earthing systems in substations,'' Energy Networks Association, Issus 1,UK, 1992.

[6.11]Safe engineering services, "Current distribution electromagnetic grounding analysis software (CDEGS),'' Canada, 2010

[6.12]A. Elmghairbi, "Assessment of earthing systems and enhancement of their performance,'' Ph.D. dissertation, Cardiff University, 2012

[6.13]S. Kurz, Recurrent surge generator RSG 481, High Voltage, Test, Manual

Chapter Seven

[7.1]P. Bellaschi, ''Impulse and 60-Cycle Characteristics of Driven Grounds'', AIEE Transactions, Vol.60, pp.123-128, March 1941

[7.2]P. Bellaschi, R. Armington and A. Snowden ''Impulse and 60-Cycle characteristics of driven grounds-II'', AIEE Transactions, pp.349-363, 1942

[7.3]G. Petropoulos, ''The high-voltage characteristics of earth resistances,'' Journal of the institution of Electrical Engineers Part II: Power Engineering, Vol. 95, pp. 59-70, February 1948

[7.4]M. Victor, M. Cabrera, S. Lundquist and V. Cooray, ''On the physical properties of discharges in sand under lightning impulses,'' Journal of Electrostatics, pp. 17-28, 1993.

[7.5]I. Cotton, ''The soil ionization process,'' ERA Conference, pp. 4.4.1-4.4.11, 2000

[7.6]C. Pritindra, ‘‘Impulse impedance tests on laboratory model ground electrodes,” IEE Proceedings on Generation, Transmission and Distribution, vol. 150, no. 4, pp. 427-433, 2003

[7.7]Y. Chen and C. Pritindra, ‘‘Correlation between laboratory and field tests on impulse impedance of rod-type ground electrodes,” IEE Proceedings on Generation, Transmission and Distribution, vol. 150, no. 4, pp. 420-426, 2003

[7.8]N. Mohamed Nor, A. Haddad and H. Griffiths, ‘‘Characteristics of ionisation phenomena in soil under high impulse currents,” IEEE Transaction of Power Delivery, vol. 21, no. 95, pp. 353-361, 2006

[7.9]N. Mohamed Nor, S. Abdullah, R. Rajab and K. Ramar, ‘‘Field tests: performances of practical earthing systems under lightning impulses’’, Electric Power Systems Research, Vol. 45, pp. 223-228, 2013.

[7.10]SES (Safe engineering services). Current distribution electromagnetic grounding analysis software (CDEGS), Available http://www.sestech.com/products/softpackages/cdegs.htm

[7.11]BS EN 50522:2010, ‘‘Earthing of power installations exceeding 1 kV a.c. ’’, October 2010

[7.12]D. Clark, H. Griffiths, N. Harid, D. Guo and A. Haddad, ‘‘Wireless measurement system for a large-scale grounding electrode test facility,’’ in Proceedings of the 48th International Universities Power Engineering Conference (UPEC), Dublin, Ireland, September 2013.

[7.13]IEEE guide for safety in AC substation grounding. ANSI/IEEE standard 80-2000

[7.14]IEEE guide for measuring earth resistivity, ground impedance, and earth surface potentials of aground system. ANSI/IEEE standard 81- 1983

[7.15]N. Harid, N. Ullah, M. Ahmeda, H. Griffiths and A. Haddad: ‘‘Experimental Evaluation of Potential Rise and Step and Touch Voltages at High Voltage Towers under Lightning Impulse’’ 16th International Symposium on High Voltage Engineering (ISH), pp. 1651-1656, Cape town South Africa, 24-28 August 2009.

[7.16]B. Zedan,” Characterisation of substation earth grid under high frequency and transient conditions,’’ Ph.D. dissertation, Cardiff University, 2005

[7.17]N. Mohamad Nor, S. Srisakot, H. Griffiths and A. Haddad, ‘‘Characterisation of soil ionisation under fast impulse,’’ in Proceedings of the 25th International Conference on Lightning Protection (ICLP) ,Rhodes, Greece, pp. 417-422 September 2000

[7.18]S. Skioka, H. Hayashida, T. Hara and A. Ametani, “Measurement of grounding resistance for high impulse currents,’’ IEE proceedings Generation, Transmission and Distribution, vol. 145, pp. 693-699, 1998

[7.19]N. Mohamad Nor, A. Haddad and H. Griffiths, “Determination of threshold electric field Ec under high impulse currents,’’ IEEE Transactions on Power Delivery, vol. 20, pp. 2108-2113, 2005

[7.20]B. Hee Lee, G. Hun Park, H. Gu Kim and K. Sun Lee, ‘‘Analysis of soil ionization behaviours under impulse currents,’’ Journal of Electrical Engineering& Technology, vol. 4, pp. 98-105, 2009

[7.21]N. Harid, H. Griffiths, N. Ullah, M. Ahmeda and A. Haddad, ‘‘Experimental investigation of impulse characteristics of transmission line tower footings,’’ Journal of Lighting Research, vol. 4, pp. 36-44, 2012

[7.22]N. Mohamad Nor, S. Abdullah, R. Rajab and K. Ramar, “Field tests: Performance of practical earthing systems under lightning impulses,’’ Electric Power System Research, vol. 45, pp. 223-228, February 2013